

**The effect of dissolved hydrogen
on the dissolution of ^{233}U doped
 $\text{UO}_2(\text{s})$, high burn-up spent fuel
and MOX fuel**

P Carbol, J Cobos-Sabate, J-P Glatz, C Ronchi, V Rondinella,
D H Wegen, T Wiss
ITU

A Loida, V Metz, B Kienzler
FZK-INE

K Spahiu, Svensk Kärnbränslehantering AB

B Grambow, ARMINES-SUBATECH

J Quiñones, CIEMAT

A Martinez Esparza Valiente, ENRESA

Edited by: K Spahiu

March 2005

Svensk Kärnbränslehantering AB

Swedish Nuclear Fuel
and Waste Management Co
Box 5864

SE-102 40 Stockholm Sweden

Tel 08-459 84 00

+46 8 459 84 00

Fax 08-661 57 19

+46 8 661 57 19



The effect of dissolved hydrogen on the dissolution of ^{233}U doped $\text{UO}_2(\text{s})$, high burn-up spent fuel and MOX fuel

P Carbol, J Cobos-Sabate, J-P Glatz, C Ronchi, V Rondinella,
D H Wegen, T Wiss
ITU

A Loida, V Metz, B Kienzler
FZK-INE

K Spahiu, Svensk Kärnbränslehantering AB

B Grambow, ARMINES-SUBATECH

J Quiñones, CIEMAT

A Martinez Esparza Valiente, ENRESA

Edited by: K Spahiu

March 2005

Abstract

In this report the results of the experimental work carried out in a large EU-research project (SFS, 2001–2004) on spent fuel stability in the presence of various amounts of near field hydrogen are presented. Studies of the dissolution of ^{233}U doped $\text{UO}_2(\text{s})$ simulating “old” spent fuel were carried out as static leaching tests, autoclave tests with various hydrogen concentrations and electrochemical tests. The results of the leaching behaviour of a high burn-up spent fuel pellet in 5 M NaCl solutions in the presence of 3.2 bar H_2 pressure and of MOX fuel in dilute synthetic groundwater under 53 bar H_2 pressure are also presented. In all the experimental studies carried out in this project, a considerable effect of hydrogen in the dissolution rates of radioactive materials was observed. The experimental results obtained in this project with α -doped UO_2 , high burn-up spent fuel and MOX fuel together with literature data give a reliable background to use fractional alteration/dissolution rates for spent fuel of the order of $10^{-6}/\text{yr}$ – $10^{-8}/\text{yr}$ with a recommended value of $4 \times 10^{-7}/\text{yr}$ for dissolved hydrogen concentrations above 10^{-3} M and Fe(II) concentrations typical for European repository concepts. Finally, based on a review of the experimental data and available literature data, potential mechanisms of the hydrogen effect are also discussed.

The work reported in this document was performed as part of the Project SFS of the European Commission 5th Framework Programme under contract no FIKW-CT-2001-20192 SFS. It represents the deliverable D10 of the experimental work package “Key experiments using α -doped UO_2 and real spent fuel”, coordinated by SKB with the participation of ITU, FZK-INE, ENRESA, CIEMAT, ARMINES-SUBATECH and SKB.

Contents

1	Introduction	7
2	Corrosion of α-doped UO₂ pellets under Ar and H₂ atmospheres	11
2.1	Experimental	12
2.1.1	Fabrication and characterisation of ²³³ U doped UO ₂ pellets	12
2.1.2	Preparation and characterisation of α -doped UO ₂ electrodes	14
2.1.3	Leach test description	17
2.2	Experimental results from leaching tests with α -doped UO ₂ (s)	27
2.2.1	Static leaching of α -doped pellets under Ar + 6% H ₂ (ITU/CIEMAT/ENRESA)	27
2.2.2	Results from static leaching under anoxic conditions	28
2.2.3	Conclusions on static leaching of α -doped UO ₂ (s).	32
2.2.4	Results from autoclave leaching of a 10% ²³³ U doped pellet under various H ₂ pressures (ITU/SKB).	33
2.2.5	Results from electrochemical testing of α -doped UO ₂ (ITU)	59
2.2.6	Dissolved hydrogen and redox conditions	69
2.2.7	Discussion of the results obtained with ²³³ U doped UO ₂ pellets in the presence of dissolved hydrogen and comparison with literature data	70
3	Corrosion of spent fuel in the presence of dissolved H₂	75
3.1	Experimental	76
3.1.1	Spent fuel characterization	76
3.1.2	Leach test description	79
3.1.3	Analytical procedures	84
3.2	Results and discussion on spent fuel leaching	86
3.2.1	Leaching of high burn-up spent fuel in 5 M NaCl solution under 40 bar Ar / 8% H ₂ overpressure (FZK-INE)	86
3.2.2	Results of MOX fuel leaching under 50 bar H ₂ (ITU/SKB)	105
3.2.3	Discussion of the results on spent fuel leaching in the presence of dissolved H ₂ and comparison with literature data	111
3.2.4	Mechanism of the hydrogen effect	120
3.2.5	Summary and conclusions	124
	Acknowledgements	129
	Literature	131

1 Introduction

The direct disposal of spent nuclear fuel as a waste form is currently under consideration in many countries of the European Union. In most disposal concepts for high level waste, spent nuclear fuel will be encapsulated in canisters made of or containing large amounts of iron. The canisters will then be placed in deep repositories built at several hundred meters depth in granitic, clay or salt bedrocks. Each canister will be surrounded by compacted bentonite clay or salt gravels in the case of salt bedrock. This arrangement constitutes a multiple barrier system, including the engineered or technical barrier (waste form and container = waste package), the geotechnical barrier (backfill materials, borehole sealing etc) and the geologic barrier (the host rock formation itself and its overburden). All barriers contribute to isolate the radionuclides from the biosphere by (i) retardation of groundwater access and by (ii) their retention on solid surfaces present in the repository. Additionally, an engineered barrier may affect the geochemical environment to provide favorable conditions with respect to low radionuclide solubilities and waste form dissolution rates.

The chemical form of the uranium in light-water reactors (LWR) fuel is nearly stoichiometric uranium dioxide both before and after irradiation, with only a small fraction of other actinides and fission products. The majority of these radionuclides are dispersed or in solid solution in the $\text{UO}_2(\text{s})$ matrix [KLE 1988]. Transport by groundwater is the only credible mechanism for the migration of radionuclides contained in the spent fuel to the biosphere. Migration is only possible in the case of a damaged canister; it is then important to evaluate the rate of dissolution of the spent fuel matrix and the rate of release of the various radionuclides, the so-called source term. The rate of dissolution of spent fuel matrix depends on a variety of factors such as the composition of the spent fuel itself and of the groundwater, as well as the redox conditions under which the dissolution takes place. Besides LWR fuel, other types of UO_2 materials tested during this project will be discussed, as well as the specific redox conditions created by the presence of dissolved hydrogen.

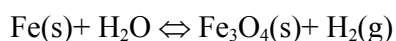
Another type of nuclear fuel is the Mixed OXide (MOX) fuel, containing 3%–10% of $\text{PuO}_2(\text{s})$ mixed with $\text{UO}_2(\text{s})$. The mixed oxide fuel consists of Pu-rich grains, composed of ~ 25 wt-% Pu in natural UO_2 , embedded in a UO_2 matrix. This implies that most of the fissions, during the reactor irradiation, occur in the U-Pu grains resulting in an uneven distribution of the fission products in the fuel matrix. Additionally, high local α -radiation fields exist in the U-Pu grains, since most of the α -emitting isotopes are contained there. Reactors can be loaded with up to 30% MOX fuel. About 35 commercial nuclear power reactors are currently loaded with MOX fuel in Europe and up to 70 reactors world-wide are scheduled to be using this fuel by 2010 including Japan, Russia and the United States. The operational and safety record of MOX use is excellent and comparable to UO_2 fuel. MOX fuel is manufactured in Europe in specialized fabrication plants located and operated in France, Belgium and England.

The spent nuclear fuel in a geologic repository is not expected to be exposed to groundwater before storage times of the order of thousand years have elapsed. From this point of view, the spent nuclear fuel available today is in fact not representative of aged fuel after hundreds or thousands years of storage under two aspects. Firstly, the decay of fission products and actinides will result in a change of the fuel composition; the α -decays will produce increasing amounts of He, and also cause the accumulation of microstructural defects at low temperature, at which less defect recovery occurs than during reactor irradiation.

This will alter properties of the fuel such as thermal conductivity, lattice parameter, or hardness over long time intervals. Secondly, another consequence of the decay process will be the disappearance of the short-lived radionuclides which account for almost all of the β - and γ -decays dominating the activity of the “young” spent fuel available nowadays. As a result, already after a few hundred years of storage, α -decays will dominate the radiation field in and around the spent nuclear fuel. UO_2 containing different fractions of short-lived α -emitters, the so-called α -doped UO_2 , simulates the level of activity of spent fuel after different storage times, and can be used to study the effects of radiolysis on the corrosion behaviour of aged spent fuel exposed to groundwater in a geologic repository.

When the spent fuel comes into contact with water, the release of the actinides and most of the fission products will depend on the $\text{UO}_2(\text{s})$ matrix dissolution and corrosion processes. Both, the dissolution rate of the spent fuel itself, and the release/retention of radionuclides are expected to be governed more by geochemical constraints encountered in the near field of the waste package, rather than by inherent material properties of the fuel. Conditions such as the redox potential and the pH of the solution as well as the availability of oxidative radiolysis products are key parameters controlling the overall alteration behavior of spent fuel. Within a few years after closure of the repository, all the oxygen present will be consumed by reducing minerals and bacteria, resulting in oxygen free and reducing environment. Under these conditions $\text{UO}_2(\text{s})$ is stable and the release of actinides and the majority of fission products will be controlled by its low solubility. The reducing conditions can change as a result of the α -, β - and γ - radiolysis caused by the radioactivity of the spent nuclear fuel, and resulting in the production of free radicals and molecular oxidants such as O_2 and H_2O_2 . Although oxidizing and reducing species are produced in equivalent amounts, the lower reactivity and the higher diffusivity of the reducing species (mainly hydrogen) will lead to locally oxidizing conditions near the fuel surface. In order to understand and model spent fuel alteration/dissolution it is necessary to take these oxidants into account in the mathematical models used to describe the near field. The effects of α -radiolysis are considered as dominating, both because of the much longer time periods of its presence, and because of the relatively short range from the fuel surface in which the energy is deposited.

In the description of the environmental boundary conditions for the evaluation of spent fuel matrix dissolution within this project, it is discussed that relatively large amounts of dissolved hydrogen will be present in all European disposal concepts during long time periods. A major hydrogen source is the anoxic corrosion of the massive iron containers:



The equilibrium pressure of hydrogen for this reaction is very high, of the order of several hundred atmospheres [GAR/CHR 1965]. Another hydrogen source is the α -, β - and γ -radiolysis of the groundwater by the spent fuel radiation.

In the German disposal concept spent nuclear fuel has to be canistered in heavy weight steel packages and to be disposed off in a deep geological repository. Disposal in a salt formation such as the Gorleben salt dome is the most investigated option. Assuming that saline solutions in the vicinity of the waste package would find access to these packages, they will corrode, and after breaching of the container and the cladding the brine will interact with the spent fuel matrix. The container corrosion rate may be high ($\sim 100 \mu\text{m}/\text{yr}$), thus hydrogen will be produced at considerable rate. The loss rate of the container material may be high initially but will decrease within approximately 1,000 years as convergence occurs in a repository situated in a salt host rock. As a consequence the hydrogen pressures will increase to some tens of MPa.

In the Swedish and Finnish concepts for disposal of high level waste, the spent nuclear fuel will be encapsulated in copper canisters with a massive cast-iron insert. In the case of a limited container defect and groundwater intrusion, the anoxic corrosion of iron gives rise to the production of dissolved hydrogen at a higher rate than its diffusive mass transport away from the canister. The concentration of dissolved H₂ in the solution inside the canister is expected to quickly exceed its solubility in groundwater [LIU/NER 2002, SEL 2001]. Gas phase formation occurs when the pressure of the hydrogen equals at least the hydrostatic pressure, around 5 MPa at 500 meters depth. For this reason, it is considered relevant to study spent UOX or MOX fuel leaching in the presence of hydrogen at pressures of the order of 5 MPa.

At the range of temperatures expected in a repository (< 100°C) dissolved hydrogen should be quite inert [JON/SHO 1988] and is not expected to contribute in the redox capacity of the deep groundwaters. However, there are some first indications in the literature that the radiolytic fuel oxidation/dissolution may be suppressed effectively by the presence of dissolved hydrogen. In a study of UO₂(s) electrodes under γ -radiation and 5 MPa H₂ [KIN/QUI 1999] very low corrosion potentials were measured and the data indicated a potential reduction of the UO₂ surface under the experimental conditions. Very low and practically constant concentrations of all radionuclides were observed in studies of spent fuel powder [SPA/WER 2000, SPA/EKL 2002] under 5 MPa hydrogen pressure. In particular, very strong effects on reducing the matrix dissolution rates and re-immobilizing important radionuclides were observed during a long-term test corroding spent fuel in the presence of metallic Fe powder in 5 M NaCl brine, where a final partial pressure of 2.7 bar H₂ built up in the autoclave [GRA/LOI 2000]. Decreasing rates of radionuclide releases were observed in 5 M NaCl [LOI/GRA 2001] under 3.2 bar H₂ and in synthetic groundwater under 0.5 MPa H₂ [SPA/CUI 2004]. In another study [RÖL/SPA 2001] of spent fuel dissolution using a flow-through technique in solutions saturated with hydrogen at 1 atm, a decrease of the dissolution rates of the spent fuel by 3–4 orders of magnitude as compared to dissolution under oxidizing conditions was observed.

These experimental data were obtained in systems where radical rich radiations such as γ -radiation contribute strongly in the activation of molecular hydrogen through reactions with radiolytic radicals. The effect was expected to be smaller in the case of homogeneous α -radiation, which produces mainly molecular radiolytic products such as H₂O₂. However, an experimental study of the effect of α -radiolysis on the oxidation of UO₂(s) surfaces under 0.1–1 bar H₂ [SUN/BOY 1990] and 100°C indicated that the surface became more reduced with increased α -dose, while a clear oxidation was observed under Ar atmosphere. Extremely low uranium concentrations were reported from tests with α -doped UO₂ in the presence of an actively corroding Fe strip in the EU-project INCAN [OLL/ALB 2003].

In the framework of this project, further experimental studies on the effect of the dissolved hydrogen on the dissolution of spent fuel were performed within the SFS project by ITU, FZK-INE, CIEMAT/ENRESA and SKB both with high burn-up spent fuel and MOX fuel as well as with UO₂(s) doped with different quantities of α -emitters to simulate the much lower dose rates expected in spent fuel after long disposal times. Detailed experimental studies of the effect of α -radiolysis on UO₂(s) matrix oxidation/dissolution were carried out by different methods and under different conditions. Methods include static leaching and electrochemical tests using different gas compositions to vary redox conditions and autoclave leaching under higher than atmospheric pressure. New analytical methods were developed for measurements of very low radionuclide concentrations and, besides intensive parameters such as pH and Eh, radiolytic product concentrations and other parameters were measured as well. The experiments were combined with a detailed pre- and post-leaching characterization of the solid specimens. In general, tests of a relatively high degree of complexity, mainly due to the extreme reducing conditions realized in some of the systems, were completed with good reproducibility and with a large number of test parameters varied and properties measured.

This report contains experimental data obtained in tests with different types of spent fuels and ^{233}U -doped pellets in water solutions containing various amounts of dissolved hydrogen, as well as a discussion of the results and some conclusions. All these data will be subsequently integrated and coupled in a time-dependent radiolytic model describing the dissolution of the spent fuel matrix.

The experimental data obtained during the study of the following systems are included:

- a) Leaching of $\text{UO}_2(\text{s})$ pellets containing 1% and 10% ^{233}U as well as undoped $\text{UO}_2(\text{s})$ in synthetic groundwaters under Ar and Ar+ 6% H_2 flushing.
- b) Dissolution of a $\text{UO}_2(\text{s})$ pellet containing 10% ^{233}U under 16, 1.6, 0.16 bar H_2 and Ar.
- c) Electrochemical tests of $\text{UO}_2(\text{s})$ pellets containing 1% and 10% ^{233}U under N_2 +8% H_2 purging.
- c) Leaching of a high burn-up spent fuel pellet in 5 M NaCl solutions under 40 bar (Ar+8% H_2) pressure.
- d) Leaching of MOX fuel fragments in dilute chloride and bicarbonate containing solutions under 50 bar H_2 pressure.

In all the experimental studies presented here a considerable effect of hydrogen in the dissolution rates of radioactive materials was observed. All the experimental information gathered within the SFS project has contributed to an improved experimental basis for a reliable evaluation of long term dissolution rates of spent fuel and an increased credibility in its stability as a waste form.

The work reported in this document was performed as part of the Project SFS of the European Commission 5th Framework Programme under contract no FIKW-CT-2001-20192 SFS.

2 Corrosion of α -doped UO_2 pellets under Ar and H_2 atmospheres

The spent nuclear fuel in a geologic repository is not expected to be exposed to groundwater before storage times of the order of thousand years have elapsed. A key factor in determining the dissolution behaviour of spent fuel exposed to groundwater might be then the radiolysis of the water in a film approximately 50 μm thick [GRA/CAC 2005] surrounding the surface of the fuel caused by the α -decays. Radicals and molecular species radiolytically produced near the fuel surface could oxidize the fuel matrix, thus enhancing its dissolution, in spite of the nominally reducing conditions, which characterize the repository.

UO_2 containing different fractions of short-lived α -emitters, the so-called α -doped UO_2 , simulates the level of activity of spent fuel after different storage times, and can be used to study the effects of radiolysis on the corrosion behaviour of aged spent fuel exposed to groundwater in a geologic repository. Figure 2-1 (from [RON/MAT 2000]) shows the α -activity as a function of storage time for different types of spent fuel. In the frame of the present project three materials were tested under anoxic and reducing conditions: α -doped UO_2 containing 10 w/o and 1 w/o of $^{233}\text{UO}_2$, and undoped UO_2 . The work has been performed by ITU in collaboration with CIEMAT/ENRESA for the static leaching tests and with SKB for the autoclave test. To provide a comprehensive picture of the effects of different α -activities on the leaching behaviour of UO_2 , previously obtained data from experiments under anoxic conditions using higher activity α -doped UO_2 containing ^{238}Pu are also shown [RON/COB 2001, 2003]. In Figure 2-1 the activity levels of the four α -doped UO_2 materials used for these studies are indicated as horizontal dashed lines (see also next sections).

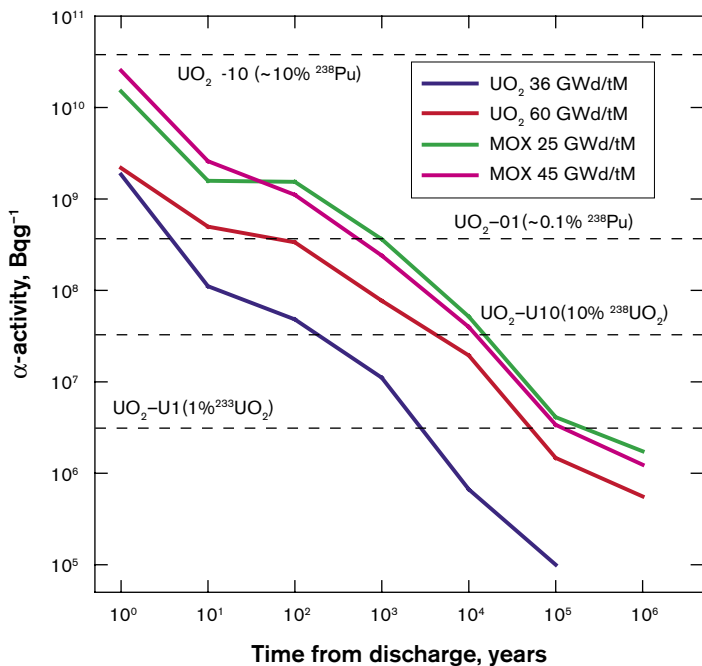


Figure 2-1. α -activity of spent LWR fuel as a function of time (from [RON/MAT 2000]). The horizontal lines indicate the activity of the α -doped UO_2 used for these studies (this activity can be assumed to be constant during the timeframe of this project).

Furthermore, the integral over time of the α -decay in α -doped UO_2 can simulate the decay damage accumulated in spent fuel during storage. This allows investigations of property modifications occurring to the fuel during storage periods of interest (e.g. in view of spent fuel retrieval or in view of final disposal) within a laboratory-acceptable timescale.

Electrochemical studies carried out at ITU with UO_2 electrodes doped 10 w/o and 1 w/o ^{233}U under $\text{N}_2 + 8\% \text{H}_2$ atmosphere are reported as well in this section.

2.1 Experimental

2.1.1 Fabrication and characterisation of ^{233}U doped UO_2 pellets

^{238}Pu and ^{233}U doped UO_2 samples were produced at ITU by the sol-gel method with an α -activity simulating large ranges of fuel ages after discharge. Sample names, doping levels, target fuel ages, dose rates [JEG 2004], organisations using the samples and the test method are summarized in Table 2-1.

The $^{233}\text{U}_3\text{O}_8$ powder (enrichment 99.99 wt-% in ^{233}U) used to fabricate the pellets was analysed for impurities [CAR/SOL 2000]. The mixed U-solution containing ^{233}U and depleted U (0.335 wt-% ^{235}U) was analysed by ICP-MS before the actual pellet fabrication. The ^{233}U doped UO_2 pellets (1% and 10 wt-% ^{233}U) were fabricated by the sol-gel method [SOM/VOE 2002, FER/RIC 1999]. At the end of the fabrication the pellets were sintered at 1,700°C for 6 hours in an Ar/6 vol-% H_2 atmosphere. Some of the pellets were used for characterisation, using optical microscopy, density measurements, ceramographic examinations (cracks and grain structures), SEM, XRD, α -autoradiography, α -track analysis of the surface and an analysis of the isotopic composition was made by radiometric methods and ICP-MS. The result of the characterisation is given elsewhere [CAR/COB 2003].

Table 2-1. Summary of some properties of the α -doped materials used for the leaching tests.

Material	Additive weight fraction %	α -activity of mixture $\text{Bq}\times\text{g}^{-1}$	Target fuel age for 45 MWd / kgU (burn-up dependent int.) yr	Dose rate Gy/h (40 μm)	Organisations Method
UO_2 -10 (^{238}Pu)	^{238}Pu : 10.0	3.8×10^{10}	Activity higher than expected	62,000	ITU/ENRESA Static
UO_2 -01 (^{238}Pu)	^{238}Pu : 0.1	3.8×10^8	300 (5–1,000)	620	ITU/ENRESA Static
UO_2 -U10 (^{233}U)	^{233}U : 10.0	3.3×10^7	3,000 (200–20,000)	82.8	ITU/SKB Autoclave
UO_2 -U10 (^{233}U)	^{233}U : 10.0	3.3×10^7	3,000 (200–20,000)	82.8	ITU Electrochemical
UO_2 -U10 (^{233}U)	^{233}U : 10.0	3.3×10^7	3,000 (200–20,000)	82.8	ITU/ENRESA Static
UO_2 -U1 (^{233}U)	^{233}U : 1.0	3.5×10^6	100,000 (3000–200,000)	10.2	ITU/ENRESA Static
UO_2 -U1 (^{233}U)	^{233}U : 1.0	3.5×10^6	100,000 (3,000–200,000)	10.2	ITU Electrochemical
UO_2 -0	0	1.1×10^4	$> 10^6$	0.033	ITU/ENRESA Static

The weight of the pellets varied in a small interval of 2.2–2.3 g and 2.8–2.9 g for UO₂–U1 and UO₂–U10, respectively. The height of the pellets was ~6.5 mm (UO₂–U1) and ~8.3 mm (UO₂–U10) respectively. The diameter of both ²³³U-doped compositions was approximately 6.6 mm. The geometrical density of the material was measured to be approximately 10.3 g/cm³ corresponding to ~95% theoretical density (TD). The optical microscopy revealed a homogenous UO₂ matrix with little or no evidence of microcracks or defects at the pellet surfaces, in both UO₂–U1 and UO₂–U10.

The isotopic composition of the fabricated pellet used in the autoclave experiment is given in Table 2-2. The composition of the mixed U-solution analysed before pellet fabrication and the composition of U in the fabricated pellet was compared and the results confirmed the ²³³U-dopant level. It could be concluded that the fabricated pellets had two activity vectors, the dominating U-isotopes with their decay daughters and the traces of plutonium and americium originating from the fabrication line. Etched samples exhibited a relatively homogenous grain size distribution of ~10 µm. α -autoradiography indicated an accumulation of few spots with higher α -activity. An average surface α -activity of 1,090 Bq/mm² was found using 56 background areas. Only six significant spots 2–5 times above the background level were found on a 55.6 mm² area. Approximately 0.4% of the total surface α -activity was located in these spots. The average diameter of a α -spots was ~30 µm giving an area of 730 µm².

Table 2-2. Composition of the 10.116 wt-% ²³³U doped UO₂-pellet.

Radionuclide	Decay mode	t _{1/2}	A, 10% (Bq/g UO ₂ -pellet)
²³² U-chain			
²³² U	α	69.85 yr	7.898×10 ⁴
²²⁸ Th	α	1.914 yr	8.120×10 ⁴
²²⁴ Ra	α	3.62 d	8.122×10 ⁴
²²⁰ Rn	α	55.6 s	8.122×10 ⁴
²¹⁶ Po	α	145 ms	8.122×10 ⁴
²¹² Pb	β	10.64 h	8.122×10 ⁴
²¹² Bi	$\beta(\alpha)$	1.009 h	8.122×10 ⁴
²¹² Po	α	300 ns	8.122×10 ⁴
²⁰⁸ Tl	β	3.055 min	29,190
²³³ U-chain			
²³³ U	α	1.594×10 ⁵ yr	3.605×10 ⁷
²²⁹ Th	α	7.345×10 ³ yr	1.291×10 ⁵
²²⁵ Ra	β	14.80 d	1.289×10 ⁵
²²⁵ Ac	α	10.0 d	1.287×10 ⁵
²²¹ Fr	α	4.9 min	1.287×10 ⁵
²¹⁷ At	$\alpha(\beta)$	32.3 ms	1.287×10 ⁵
²¹⁷ Rn	α	540 µs	1.287×10 ⁵
²¹³ Po	α	4.2 µs	1.287×10 ⁵
²¹³ Bi	$\beta(\alpha)$	45.59 min	1.287×10 ⁵
²⁰⁹ Pb	β	3.253 min	1.287×10 ⁵
²⁰⁹ Tl	β	2.2 min	2,780
²³⁴ U	α	2.484×10 ⁵ yr	6.22×10 ⁴
²³⁵ U	α	7.038×10 ⁸ yr	263
²³⁶ U	α	2.34×10 ⁷ yr	411
²³⁸ U	α	4.699×10 ⁹ yr	1.06×10 ⁴

Radionuclide	Decay mode	$t_{1/2}$	A, 10% (Bq/g UO ₂ -pellet)
²³⁸ Pu	α	87.744 y	5.2×10 ⁵
²³⁹ Pu	α	2.413×10 ⁴ yr	4.15×10 ⁵
²⁴⁰ Pu	α	6.537×10 ³ yr	2.32×10 ⁵
^{239,240} Pu	α		4.6×10 ⁵
²⁴¹ Pu	β	15.16 y	6.9×10 ⁶
²⁴² Pu	α	3.869×10 ⁵ yr	436
²⁴¹ Am	α	433.176 yr	4.3×10 ⁵

2.1.2 Preparation and characterisation of α-doped UO₂ electrodes

For the electrochemical tests electrodes from different materials have been prepared, Figure 2-2. Slices of ~ 1 mm thickness were cut from ²³³U doped UO₂ pellets. These were then cut into 2 halves, Figure 2-3. After annealing to maintain UO₂ at stoichiometry the half slices were mounted upright with conductive resin on the gold coated electrode holder. Then they were impregnated under vacuum in epoxy resin (EPOTHIN), Figure 2-4. The electrodes were mechanically polished after curing.

Electrochemical long-term testing under static conditions was carried out on vacuum impregnated and polished 10% ²³³U doped UO₂ (94.6% TD) and 1% ²³³U doped UO₂ (92.4% TD) at room temperature. The electrode parameters are given in Figure 2-5 and Figure 2-6.

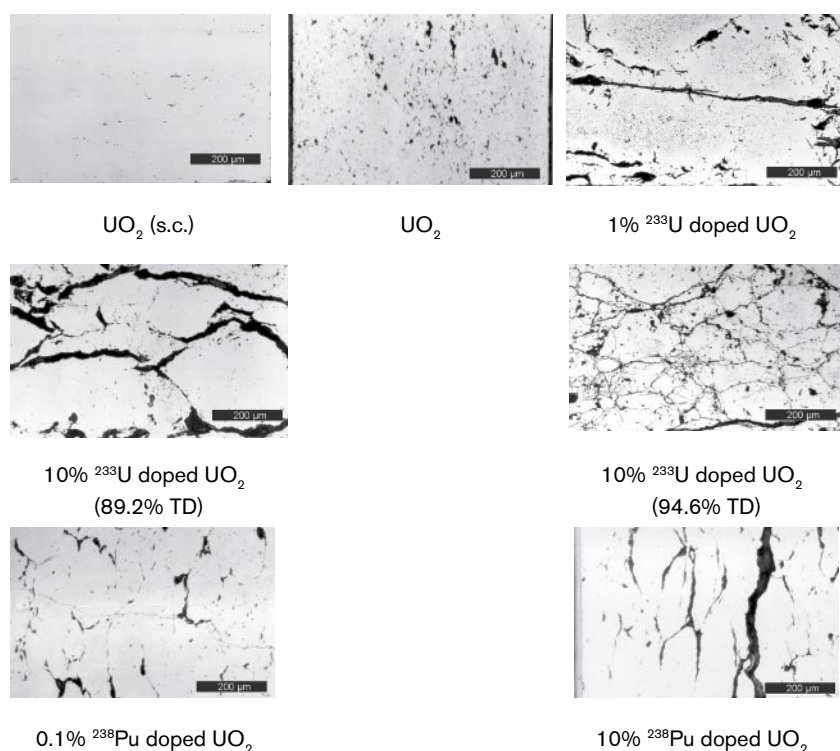


Figure 2-2. Macro- and micrographs of electrodes prepared from different UO₂ materials showing different surface characteristics.

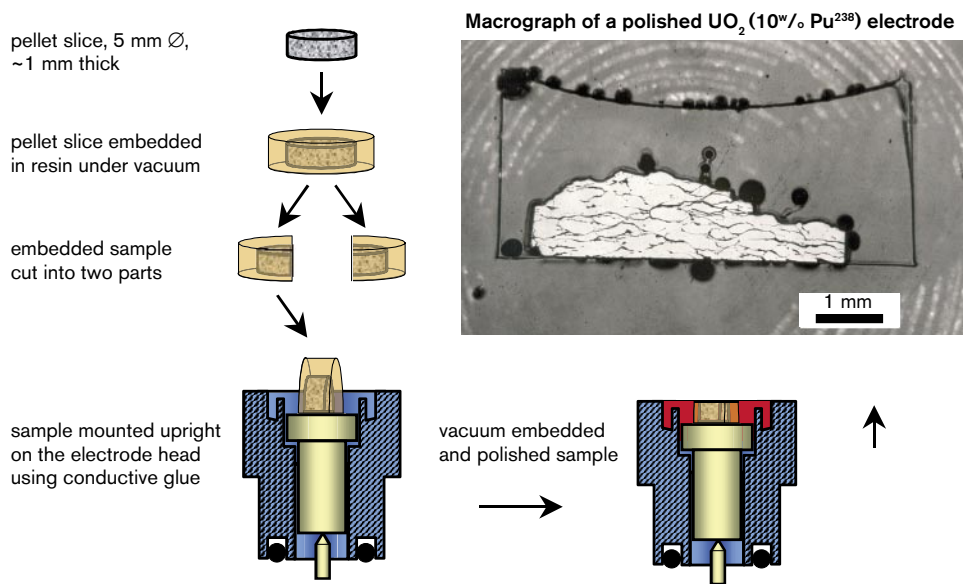


Figure 2-3. Preparation of α -doped UO_2 samples for electrochemical experiments.

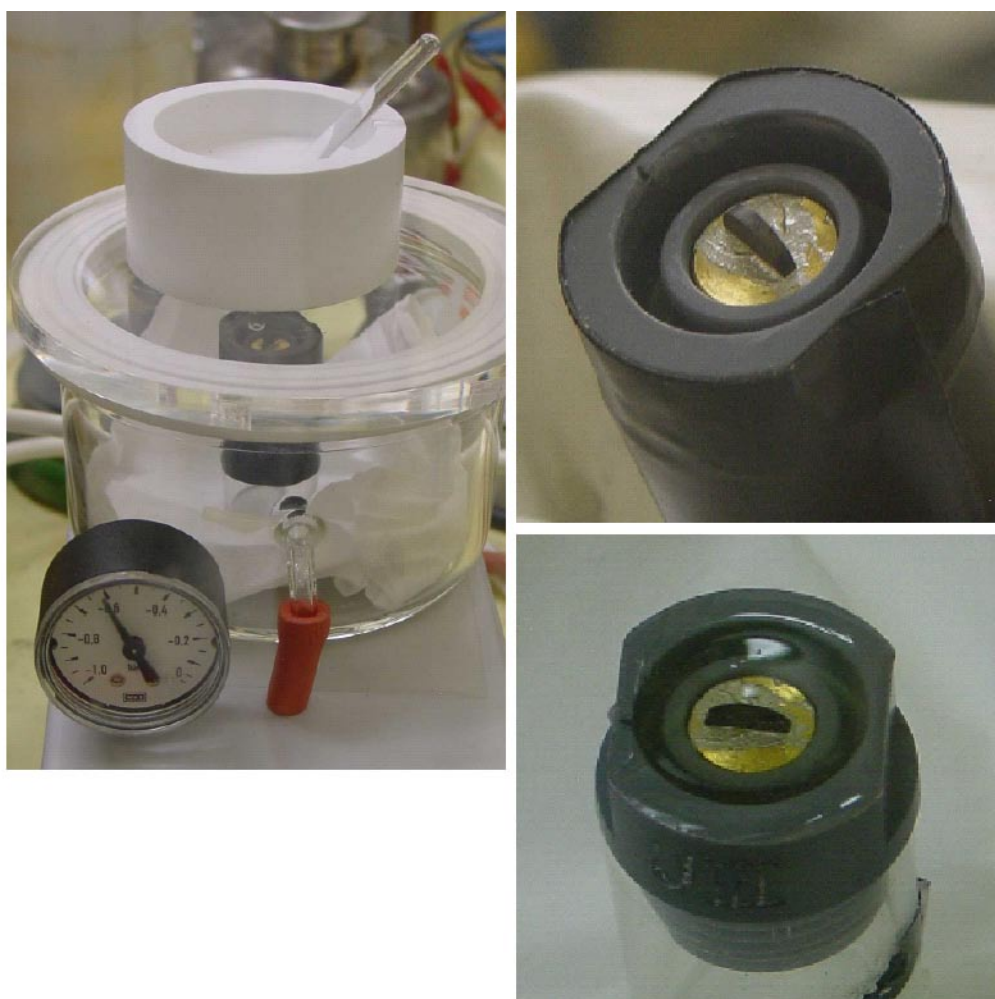


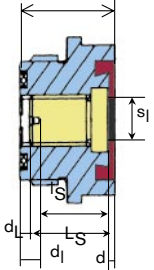
Figure 2-4. Mounting and embedding of electrochemical samples. Left: Vacuum impregnation chamber for resin embedding. Top right: sample mounted in holder. Bottom right: sample mounted and embedded.

material: depleted UO_2 10% U-233 mat.code: SG106
description: PVC(grey), advanced design 1/2 slice mounted perpendicular on Au coated brass

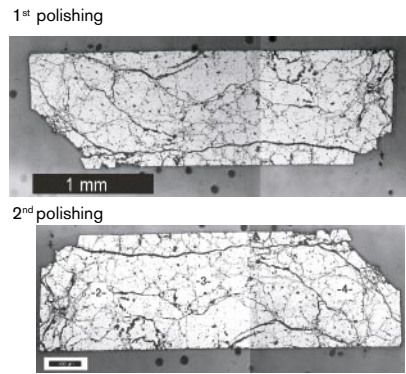
density: ρ : 10,37 g/cm³
 ρ : 94,60 %

pellet diameter: D_p : 6,58 ± 0,10 mm
slice thickness: s_d : 1,30 ± 0,10 mm

geometry:



L_s : 16,65 ± 0,10 mm
 l_s : 14,80 ± 0,10 mm
 d_L : 0,50 ± 0,01 mm
 d_I : 2,67 ± 0,11 mm



d_H / mm	d_L / mm	d_I / mm	sample thickness		s_I / mm	surface area			A_{opt} taken from	sample mass	
			1) d / mm ($d_H - L_s - d_L$)	2) d / mm ($d_H - l_s - d$)		A_{gp} / cm^2 (rectangle)	A_{opt} / cm^2	$\frac{A_{crack}}{A_{opt}}$		estimated m / g (sample)	
input	input	input			input				1)	2)	
19,18 ± 0,02	0,50 ± 0,01	2,67 ± 0,11	2,03 ± 0,10	1,72 ± 0,15	4,52 ± 0,20	0,059 ± 0,005	0,053 ± 0,003	0,212 ± 0,02	A742	0,203	0,212

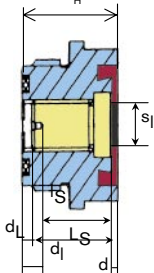
Figure 2-5. Geometric parameters of electrode U-I (10% ^{233}U doped UO_2). A_{crack} is the area of cracks on the electrode surface obtained from optical examination.

material: depleted UO_2 1% U-233 mat.code: SG101
description: PVC(grey), advanced design 1/2 slice mounted perpendicular on Au coated brass

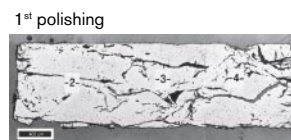
density: ρ : 10,13 g/cm³
 ρ : 92,40 %

pellet diameter: D_p : 5,54 ± 0,10 mm
slice thickness: s_d : 0,96 ± 0,10 mm

geometry:



L_s : 16,83 ± 0,10 mm
 l_s : 15,00 ± 0,10 mm
 d_L : 0,78 ± 0,02 mm
 d_I : 2,82 ± 0,06 mm



d_H / mm	d_L / mm	d_I / mm	sample thickness		s_I / mm	surface area			A_{opt} taken from pic	sample mass	
			1) d / mm ($d_H - L_s - d_L$)	2) d / mm ($d_H - l_s - d$)		A_{gp} / cm^2 (rectangle estimate)	A_{opt} / cm^2	$\frac{A_{crack}}{A_{opt}}$		estimated m / g (sample)	
input	input	input			input				1)	2)	
19,33 ± 0,04	0,78 ± 0,02	2,82 ± 0,06	1,72 ± 0,11	1,52 ± 0,12	3,46 ± 0,10	0,033 ± 0,004	0,033 ± 0,00	0,117 ± 0,02	A739	0,104	0,108

Figure 2-6. Geometric parameters of electrode U-V (1% ^{233}U doped UO_2). A_{crack} is the area of cracks on the electrode surface obtained from optical examination.

2.1.3 Leach test description

Sample pre-treatment before leaching

Static leach tests: The specimens used in the static tests of ITU-CIEMAT-ENRESA were discs approximately 1 mm thick cut from sintered pellets. Fines produced during sample preparation before leaching were removed by appropriately washing the samples. The handling of the samples and the experimental procedures and setup were similar for all the materials.

Before the leaching tests, all the samples (α -doped and undoped UO_2) were annealed for six hours at 1,200°C in Ar/(4%) H_2 to reduce the specimens to stoichiometry and to recover α -decay damage and mechanical stresses accumulated during the sample preparation.

Although some degree of preoxidation cannot be excluded at the start of the contact period with water for the experiments at low S/V, the annealing was performed at the same time for all samples of a given batch of tests, so that the initial condition for all the samples was the same. Therefore, possible differences between α -doped and undoped in terms of pre-oxidized surface layer forming before contacting the water must be ascribed to the different α -activities of the samples.

Autoclave test: The pellet used in the autoclave leaching of ITU/SKB was cut in two parts and the part used in the experiments had a height of 3.75 mm, a diameter of 6.58 mm, a weight of 1.2643 g and a geometric surface area of $1.5 \times 10^{-4} \text{ m}^2$. The pellet was annealed one day before start of the leaching experiment. The annealing was performed at 1,200°C in a gas mixture of 4 vol.-% H_2/Ar at a flow rate of 2 ml/min for 12 hours. In order to verify the efficiency of the annealing process a piece of an annealed UO_2 -pellet was analysed before and after the annealing. Thermo-gravimetric analysis was used to check the oxidation state of the U in the UO_2 -pellets according to the method outlined in ASTM [AST 1980]. The pellet was only slightly oxidised ($\text{O}/\text{U} = 2.002 \pm 0.010$) before the annealing process and the annealing process yielded a ^{233}U doped UO_2 -pellets with a composition of $\text{UO}_{2.000 \pm 0.007}$. Direct after the annealing the pellet was washed with H_2 -purged 10 mM NaCl solution for 20 min and thereafter placed in the autoclave. The leaching solution in the autoclave was also pre-purged with H_2 and consisted of 10 mM NaCl solution.

Electrochemical tests: To reduce higher uranium oxides which may have formed at the sample surface during polishing the electrode was cathodically polarised for 10 min at -2.5 V at the beginning of the experiment. In case of 10% ^{233}U doped UO_2 this treatment was done in the same solution as the experiment. In the second experiment the solution was exchanged after precathodisation to avoid contamination of the liquid during the polarisation. To follow the ongoing corrosion processes solution samples (3–5 ml each) were taken for analysis and impedance spectra were measured during the experiment.

Leach solutions

Commercial carbonated water (CW) was used for the static leaching tests of ITU/CIEMAT/ENRESA and its compositions in equilibrium with air at room temperature and after purging with Ar are given in Table 2-3. Deionized water (MQ) was used in the leaching of ^{238}Pu doped pellets under anoxic conditions [RON/COB 2001, 2003] and the results are reported here for comparison.

Table 2-3. Composition of the commercial carbonate water CW in equilibrium with air at room temperature (data supplied by the manufacturing company) and under conditions representative of the beginning of the experiments (results of in-house analysis).

Concentration	Air conditions (mol/kg H ₂ O)	Anoxic conditions* (mol/kg H ₂ O)
Na ⁺	4.09×10 ⁻⁴	5.05×10 ⁻⁴
K ⁺	1.46×10 ⁻⁴	1.74×10 ⁻⁴
Mg ²⁺	2.51×10 ⁻⁴	2.94×10 ⁻⁴
Ca ²⁺	2.47×10 ⁻⁴	2.72×10 ⁻⁴
Cl ⁻	2.37×10 ⁻⁴	3.53×10 ⁻⁴
Si	4.99×10 ⁻⁴	(4.99×10 ⁻⁴) [°]
SO ₄ ²⁻	7.19×10 ⁻⁵	8.15×10 ⁻⁵
HCO ₃ ⁻	1.07×10 ⁻³	1.68×10 ⁻³
F ⁻	1.05×10 ⁻⁵	1.40×10 ⁻⁵
PO ₄ ³⁻	1.04×10 ⁻⁷	1.04×10 ⁻⁷
Al ³⁺	1.85×10 ⁻⁷	3.00×10 ⁻⁹
U _{total}	2.32×10 ⁻⁹	2.00×10 ⁻¹⁰

*Measured after purging with Ar.

°Si could not be measured in-house.

The initial leachate in the autoclave test of ITU/SKB consisted of 10 mM NaCl and its composition was changed after 113 days to 10 mM NaCl, 2 mM NaHCO₃ by addition of a NaHCO₃ solution. Only ultra pure milliQ-water and pro analysis grade chemicals (Merck, supra pure) were used in solution preparation. The pH of the leachate after the introduction of the 10 mM NaCl, 2 mM NaHCO₃ solution in the autoclave was measured to be 8.4. The same solution was added to the autoclave to compensate for extractions of leachate for sampling.

A 10 mM NaCl solution was used in the electrochemical tests.

Test description for static leaching experiments with α -doped UO₂

In order to investigate the influence of a radiolysis on spent fuel dissolution mechanisms, α -doped UO₂ containing 10 w/o and 1 w/o of ²³³UO₂, (labelled UO₂-U10 and UO₂-U1 respectively) were leached under reducing and anoxic conditions. To provide a comprehensive picture of the effects of different α -activities on the dissolution of UO₂, the results on the leaching behaviour of undoped UO₂ under similar conditions as well as previously obtained data from experiments using higher activity ²³⁸Pu-doped UO₂ under anoxic conditions are also shown [RON/COB 2001, 2003].

All tests were performed at room temperature, using borosilicate or Pyrex glass vessels, in gloveboxes with N₂ atmosphere under static conditions (no water flow). A nominal O₂ concentration value of ~ 8% was provided by the centralized gas supply service. However, direct measurements using O₂-sensors (Orbisphere) determined that the concentration of oxygen in the gloveboxes where the tests took place was typically of ~ 1.2% (~ 12 mbar) O₂. The values of the S/V ratio were calculated using the geometric surface and counting both faces of the fuel discs or pellet. In general “low S/V” tests are discussed here, “high S/V” tests under deaerated conditions are reported elsewhere [GRA/CAC 2005]. The discs used in the experiments were of similar shape and size. Detailed information on each experiment is available in the tables included in the results section for the static tests.

All leachates were filtered through 450 nm membrane filters.

The dissolution rates were calculated by dividing the amount of U released in solution during a contact period by the corresponding leaching time and by the geometrical surface area of the pellet.

a. Static leaching in reactors flushed with Ar + 6% H₂

Static batch (with same leachant and same vessel for each leaching time) leaching experiments were performed on UO₂ discs. Pyrex glass leaching reactors with a total volume of 500 ml and a volume of leachant (CW) of 400 ml were used. A pH and a redox glass electrode were immersed in the leachant: this allowed logging of these parameters every 30 min during the experiments. The E_h electrodes were provided by Mettler-Toledo (InLab®302, InLab®501). During the experiment the gas volume above the electrolyte was purged with N₂. A constant flow of ~ 1.7 l·h⁻¹ of Ar/(6%)H₂ was bubbled in the water during the experiments. Preliminary tests performed to check the tightness of the vessels before introducing the fuel samples showed that the redox potential values of the solutions decreased to levels corresponding to anoxic conditions (E_h (SHE) < 0 mV) in times of the order of a few days, depending on the flow rate of the purging inert gas used, and on the effectiveness of the sealing of the leaching vessel. After switching from inert N₂ to Ar/(6%)H₂, the E_h rapidly decreased to values between -400 and -500 mV_{SHE}. During these initial reduction stages the fuel sample remained suspended in a quartz sample holder above the water. The leaching experiments started when the sample holder was immersed to the center of the water volume. This procedure prevented the sample from contacting the water until the water reached low E_h values (-400 mV_{SHE}).

Sampling of ~ 8 ml of leachate using a tight four-valve system was performed, see Table 2-5. The system consisted of three needle valves and one on/off valve that minimized the ingress of air inside the reactor. At the end of the experiment, the vessels were rinsed with 50 ml 2 M HNO₃ for 3 hours.

b. Static leaching under anoxic conditions

Static batch (with same leachant and same vessel for each leaching time) leaching experiments are performed on UO₂ discs. Similar glass vessels and water volumes are used as in the leaching experiments performed in presence of H₂. A constant flow of ~ 1.5 l·h⁻¹ of Ar/(0.02%)CO₂ is bubbled in the leaching vessel. The sample, suspended in a quartz sample holder, was immersed in the water after reaching the nominal redox values in the water. For comparison, results obtained on α -doped UO₂ discs with ²³⁸Pu are also presented [RON/COB 2001,2003]. These tests were performed using setups and procedures similar to the ones described above in 160 ml of MQ water. Specific experimental conditions are mentioned in the figure captions.

c. Errors

The overall error for each single data point can be estimated to be in the range of 15–20%, including deviations caused by the solution analysis procedure and leaching equipment. A certain degree of scatter is typical for leaching experiments on these materials especially when trying to achieve/maintain anoxic conditions. Whenever possible, outliers or datapoints in need of verification have been discarded or labelled as such; moreover, possible factors interfering with the quantities to be measured have been accounted for.

However, the overall trends and the indications resulting from the experiments are supported by a good reproducibility among multiple, independent experimental campaigns carried out adopting similar conditions often after time intervals of months or years.

Test description for autoclave leaching under various H₂ pressures

The study of the influence of dissolved molecular hydrogen on the leaching rate of UO₂ was performed using α -doped UO₂ doped with 10 wt-% ²³³U to simulate an old fuel. The activity emitted by such an old fuel is dominated by α -decay.

This type of UO₂-leaching study necessitates a set-up that is completely airtight. We have chosen to work with autoclaves placed in an N₂-purged glove box. Shortly before the leaching experiment the pellet was annealed to obtain a stoichiometric UO₂ pellet. Directly after the annealing the pellet was washed with H₂-purged 10 mM NaCl solution for 20 min and then placed in the autoclave. The leaching solution in the autoclave was also pre-purged with H₂ and consisted of 10 mM NaCl solution. The pellet was loaded into the autoclave and the autoclave was sealed. The H₂-pressure was applied and the stirring was started. The pressure of H₂, O₂ and temperature was measured intermittently during the whole experiment. The E_h was measured on-line during the sampling of leachate. The leachate was analysed by different techniques. The leaching of the UO₂ was run for 823 days. A post-characterisation of the pellet and the deposits in the autoclave was performed.

a. Autoclave set-up

The experimental set-up consisted of two autoclaves installed in a glove box. The main autoclave with a total volume of 620 ml (Parr Instruments Co, USA) was used for the actual leaching while the second smaller autoclave with a volume of 50 ml was used to load the leaching solution into the main autoclave, Figure 2-7. This was done by applying a ~ 3 bar higher pressure to the small autoclave compared to the main autoclave thereby forcing the solution from one autoclave to the other. The solution in the small autoclave was, before the transfer, purged for hours and since the gas composition was the same in the two autoclaves, it was possible to avoid intrusion of oxygen into the main autoclave. All wetted surfaces of the autoclaves were made of titanium (grade II to be able to be welded) including valves, security valves, tubing's, E_h-measuring cell, pellet holder and magnetic stirrer.

The reason to use titanium is that Ti in contact with humid air or water immediately reacts and forms a thin layer of TiO₂ on top of the Ti-metal according to the overall reaction:

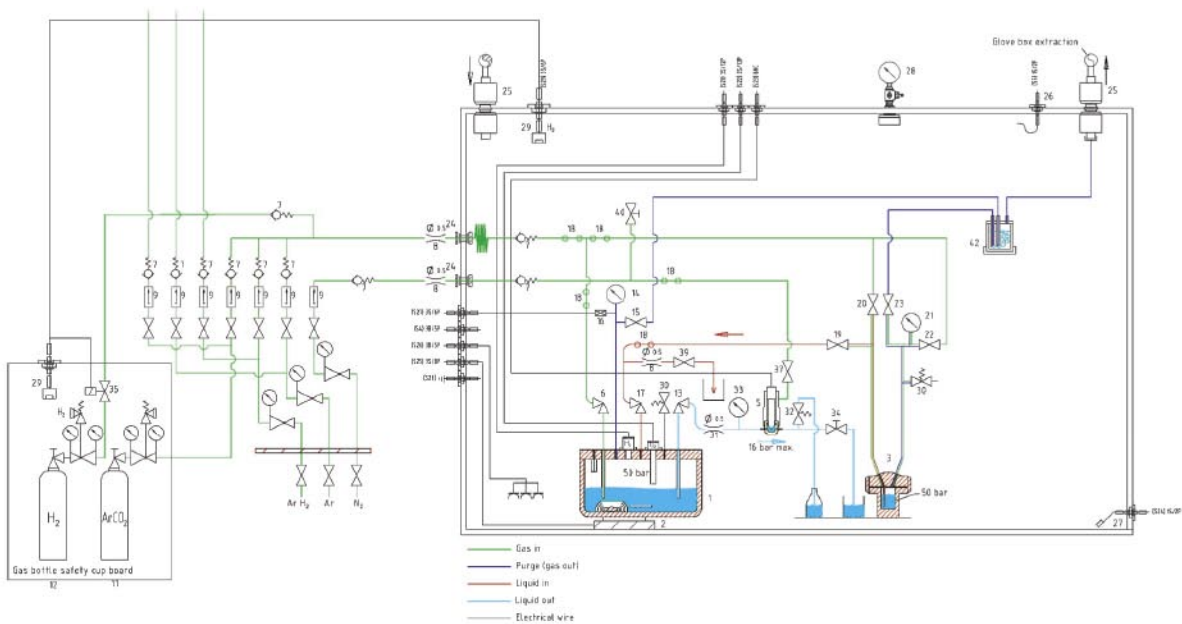
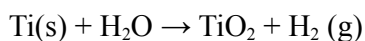


Figure 2-7. Autoclave setup.



The titanium dioxide layer is approximately 100 nm thick and presents a good barrier to penetration by hydrogen. The TiO_2 resists corrosion from diluted salt solution in the pH interval of 3–12 and temperatures below 80°C. The titanium dioxide is a passive surface having a point of zero charge close to 6 making it a poor surface for sorption of U.

On the other hand, manufacturing all wetted parts in Ti one experience the problem of abrasion of the stirrer and the autoclave since both items are made of the same material. Taking into account that the stirrer made 100 rotations per minute, the total number of revolutions was ~ 118 millions during the experiment. No materials resists magnetic stirrer abrasion and therefore small fragments of titanium released from the autoclave or the stirrer will enter into the solution. The titanium fragments will directly react with water forming small fragments covered with TiO_2 .

Pressure test of the welding joints up to 800 bar were made to certify the autoclave for use at 50 bar hydrogen pressure in the glove box [MCG/STU 2002]. Graphite seals were used to avoid metallic or organic seals that exhibit either a high sorption tendency for actinides or poor radiation resistance. The autoclaves were certified for a pressure of 70 bar. The part for extraction of the leachate could only be pressurised to 16 bar due to the presence of a gel-based E_h -electrode (Xerolyt®, Mettler-Toledo AG, Switzerland) connected to an analyser (pH 340/ION, WTW GmbH, Germany). A fully acceptable pressure leak rate of < 14 Pa/h, at 16 bar H_2 pressure, was measured during the experiment. The gases, of highest purity grade (Linde/AGA, Scientific 6.0), used to pressurise the autoclaves and for purging were delivered from a stand-alone gas tube.

Two electro-chemical sensors for measurements of O_2 (made of titanium, Orbisphere, Switzerland) and H_2 (stainless steel was selected due to corrosion between titanium and the electrolyte in the sensor, Orbisphere) were fitted in the main autoclave and couple to two analysers (MOCA 3600, Orbisphere). A calibration and control of the sensors stability was made prior the experiment according to the instructions from the manufacturer. The H_2 and O_2 -sensors also measured the temperature of the leachate. The leachate in the main autoclave was homogeneously distributed using a magnetic stirrer made in titanium. The stirring of the solution is necessary for the proper function of the oxygen sensor and contributes additionally to a homogeneous distribution of the dissolved uranium.

The leachate was collected using the pressure inside the autoclave pushing the solution from the bottom of the autoclave through a 1 cm^3 -cell equipped with a redox-electrode (described above) and into a sampling PE-vial (50 ml).

b. Loading of the pellet

Before the start of the experiment the autoclave was washed several times with milliQ-water and 10 mM NaCl solution. The annealed pellet was placed on top of a Ti-holder situated 8 mm above the bottom of the autoclave. The holder consisted of a tube, open in the top and with a flat bottom with fifteen 0.5 mm holes drilled in it to ensure a flow of solution past the whole pellet surface. The space below the pellet was needed for the magnetic stirrer manufactured in Titanium. A volume of 500 ml of a 10 mM NaCl solution was introduced into the autoclave. The NaCl-solution was bubbled with wetted Ar-gas (Linde/AGA Scientific 6.0) for > 48 h before being added to the autoclave. Immediately after the mounting of the lid the autoclave was pressurised to 16 bar pure H_2 . The S/V-ratio at the start of the experiment was 0.281 m^{-1} .

c. Autoclave test description

The static corrosion experiment of the 10 wt-% ^{233}U doped UO_2 pellet was run in total for a period of 823 days without opening the autoclave. In principal, two variables were studied: the composition of the leachate and the concentration of dissolved H_2 in the leachate. Additionally the oxygen concentration in the autoclave was monitored. The leaching of an annealed UO_2 -10 pellet was started by first determining the baseline for UO_2 dissolution in 10 mM NaCl-solution under 16 bar H_2 -pressure. In order to accelerate dissolution of all oxidized uranium from the pellet, a 10 mM NaCl + 2 mM HCO_3^- -solution was added to the autoclave after 117 days and this solution composition was used during all the rest of the experiment. In order to avoid high dissolution rate of UO_2 and, consequently high concentration of U in the leachate, the experiment was run backwards. This means that we started the experiment by applying a high H_2 pressure (expecting a small dissolution of UO_2) and decreasing the pressure assuming that the amount of radiolytically produced $\text{H}_2\text{O}_2/(\text{O}_2)$ would increase the dissolution rate and the U concentration in the leachate. The H_2 -pressure in the autoclave was decreased in steps of one order of magnitude: with start at 16 bar pure H_2 for 140 days then 1.6 bar pure H_2 during 178 days and 0.16 bar H_2 (6.08 vol-% H_2/Ar at 3.06 bar) for a period of 141 days. The last part of the experiment was run under pure Ar-gas (Linde/AGA Scientific 6.0) with the composition shown in Table 2-4. In order to verify the H_2 concentration in the autoclave a gas sample was taken after 670 days of experiment and analysed by gas mass spectrometry. The results of the analysis are shown in Table 2-4. The MS-analysis of the sampled gas and the in situ H_2 sensor measurements deviated by 30%. The results of the analysis are shown in Table 2-4. It could therefore be concluded that the sensor worked correctly for a period of at least 22 months.

The control of the functionality of the Orbisphere O_2 -sensor was made after the end of the experiment, when the autoclave was opened. At this time, the O_2 -sensor used in the autoclave was compared against an independent second Orbisphere O_2 -sensor, also that one present inside the N_2 -glovebox. The second O_2 -sensor had been calibrated against air. The comparison showed that the autoclave O_2 -sensor registered a 40% too high O_2 concentration.

The temperature in the autoclave was $\sim 23^\circ\text{C}$, as measured by Pt100 sensors built-in in the H_2 and O_2 -sensors. The solution in the autoclave was continuously stirred with a speed of 100 r/min. The concentration of H_2 and O_2 in the autoclave was recorded intermittently. This was done to minimise the consumption of the electrolyte in the electro-chemical sensors making it possible to measure for a time up to two years and to minimise consumption of H_2 and O_2 during the measurements.

Table 2-4. Composition of the pure Ar-gas (Linde/AGA scientific grade 6.0) added to the autoclave and the composition of the sampled gas from the autoclave after 670 days of experimental time, Table 2-8. The ratio $\text{O}_2/(\text{O}_2+\text{N}_2) = 0.15$ measured by gas mass spectrometry of the gas sample collected in the autoclave indicate a contamination of oxygen during the sampling. The oxygen originates from the glove box and air.

Components	Concentration, Gas bottle Linde/AGA (mass-ppm)	Concentration, Autoclave Mass spectrometry (mass-ppm)	Concentration, Autoclave H_2 -sensor (mass-ppm)
Ar	> 999,998	996,995 \pm 43	
O_2	< 0.4	120 \pm 1	20
N_2	< 0.35	698 \pm 2	
H_2O	< 0.23	b.d.l.	
H_2	< 0.005	2,030 \pm 42	3,208
CO	< 0.11	b.d.l.	
CO_2	< 0.11	27 \pm 1	

d. Termination of the experiment

The corrosion experiment was terminated after 823 days. A leachate (S46) was sampled from the autoclave after 818 days of leaching, a few days before the termination of the experiment.

The challenge was to prove that the UO_2 pellet surface had been un-oxidized during the whole experiment. A clear proof could only be given if the corroded pellet surface was analyzed using X-ray photoelectron spectroscopy (XPS). This is a surface sensitive analysis determining the binding energy of the outer electrons of an element and is sensitive to elemental composition and changes in oxidations state to a depth of ~ 10 atomic layers into the material.

The main problem is to avoid oxidation of the UO_2 pellet surface during the opening of the autoclave, the pellet drying step, the mounting of the pellet in a holder and finally, during the transport of the pellet to the XPS. In the case, that the pellet surface would be found oxidised there is no way to distinguish if the UO_2 oxidation occurred during the experiment or during the time between the autoclave opening and the XPS analysis.

The autoclave was opened in the N_2 purged glove box while the O_2 concentration (5 mbar, 22°C) in the glove box was monitored using an additional Orbisphere O_2 -sensor. The autoclave was purged with Ar during the dismantling and took 18 min. After the removal of the autoclave lid the UO_2 pellet was within 15 seconds transferred to a drying cell. The pellet drying cell was manufactured in the workshop at ITU, Figure 2-8.

The device (designation 26/04) consists of a quick connector (Swagelok), a valve (Swagelok, SS-6P4T-MM), a filter holder (Parker, VACUSEAL $\times 4\times 316$) with a filter (Swagelok, SS-4-VCR-2-0.5M) and an in-house manufactured pellet chamber. The chamber is shown in Figure 2-9.

In the other end of the chamber an identical set of filter and valve was connected and the device had in this end a vacuum house connector for connection to a vacuum pump. The device was tested for vacuum tightness with He-gas using a calibrated device and a certified procedure. The evacuation device was found to be leak tight (Certificate: Institute for Transuranium Elements, Workshop, He-leak test 26/04).

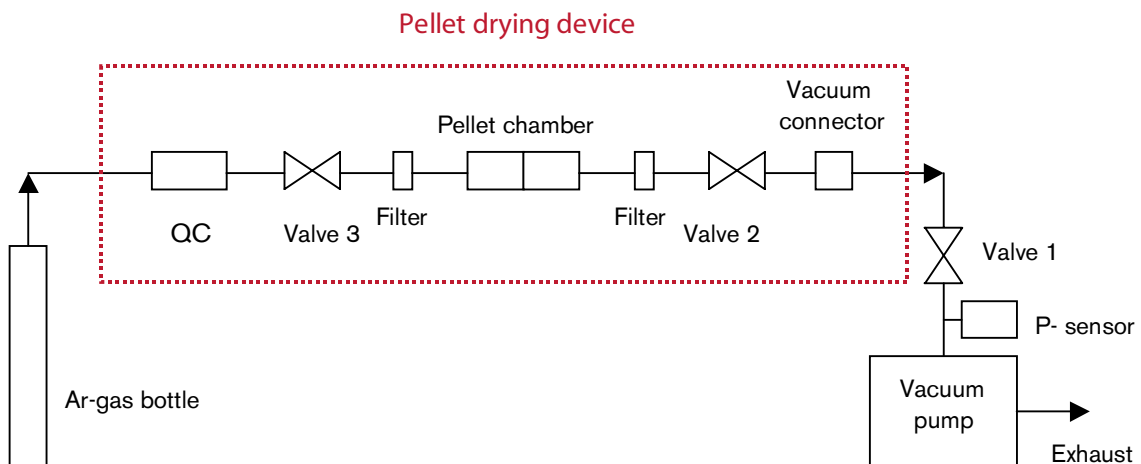


Figure 2-8. Schematic drawing of the pellet drying device.

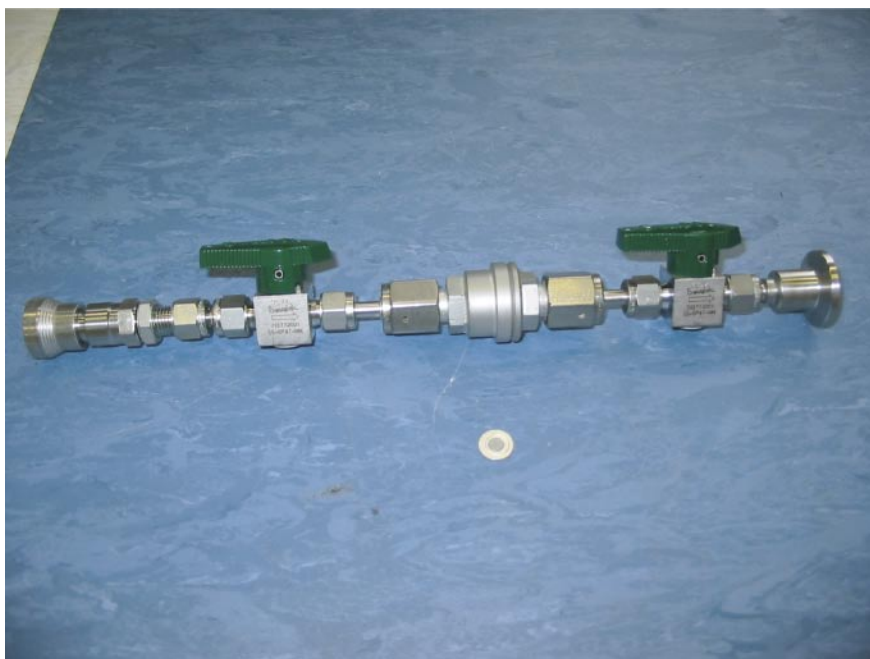


Figure 2-9. Device for drying of ^{233}U doped UO_2 pellet.

The pellet was dried under an alternating (3 minute cycles) atmosphere of Ar-gas (Argon 6.0 grade scientific) and vacuum down to 4×10^{-2} mbar using a vacuum pump (Leybold Trivac D8B, Germany). After approximately 20 min the vacuum decreased to 5×10^{-3} mbar indicating that all of the solution was removed. The relatively long drying time depended on the fact that the solution was retained in the $0.5 \mu\text{m}$ filter in the pellet drying device rather than removing it from the UO_2 pellet surface. After the drying process the pellet was mounted in a manufactured holder and directly transferred to the X-ray photoelectron spectroscopy (XPS) instrument.

After removal of the pellet from the autoclave the leachate was poured into a 500 ml PE-bottle and the bottle sealed. The autoclave was let dry. The spatial distribution of the ^{233}U in the autoclave was determined by α -autoradiography of two surface areas. The elemental composition of the deposits was determined by collecting the deposits and analyzing them with a scanning electron microscope coupled to an energy dispersive x-ray spectrometer (SEM-EDX) and a micro-sample x-ray diffractometer (μ -XRD). The isotopic composition and chemical composition was determined using a secondary ion mass spectrometer (SIMS). The amount of the deposits was estimated to be 50 mg.

Electrochemical test description

The experiments were carried out in an electrochemical cell under inert gas purging, Figure 2-10. The gas N_2 or N_2/H_2 was purified using an oxygen trap (Agilent Technologies). The set-up is located in a glove box, which is ventilated with N_2 . For short times (introducing of electrodes into solution, taking solution samples) it was ventilated with high purity N_2 (less than 0.5 vpm O_2).

The free corrosion potential of the UO_2 and the E_h of the 10 mM NaCl solution were followed using commercially available electrodes (Mettler-Toledo, InLab®302, InLab®501). The combination redox electrodes were checked before the experiments

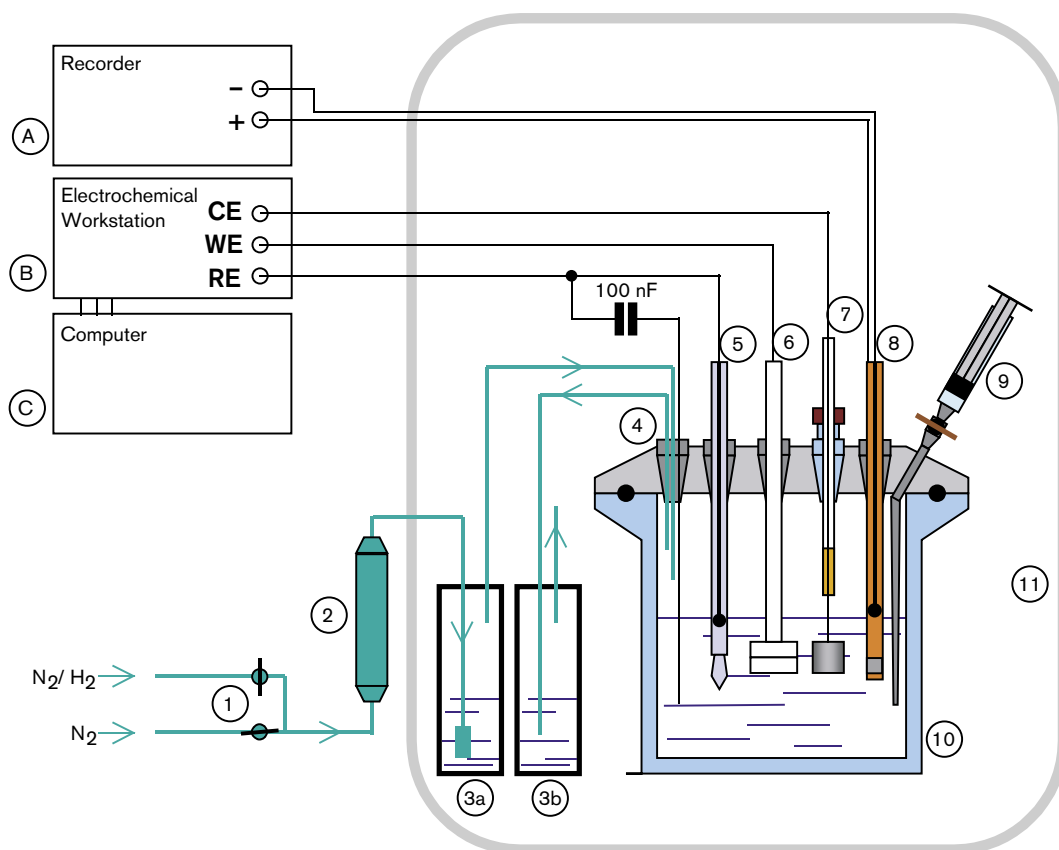


Figure 2-10. Schematic electrochemical setup for long-term experiments. A: Recording of redox potential; B: Corrosion potential measurement and impedance spectroscopy; C: Control of experiment. 1: Inert gas distribution system; 2: Oxygen trap; 3: Gas bubbler (3a with frit); 4: Gas in- and outlet for cell with Pt-wire auxiliary electrode for short circuiting the double junction reference electrode (5) via a 100 nF capacitor during impedance measurements. 6: Working electrode with UO_2 specimen facing downwards. 7: Pt-counter electrode ($\sim 3 \text{ cm}^2$); 8: Commercial redox combination electrode; 9: Syringe for solution sampling; 10: Cell with glass vessel (100 ml electrolyte volume) and PE cover; 11: Glove box.

with a standard redox buffer solution. The potential of the Ag/AgCl reference electrode was checked against the inner reference electrode of a redox combination electrode. The measured potentials were $205 \text{ mV}_{\text{SHE}}$ for the reference used with 10% doped UO_2 and $197 \text{ mV}_{\text{SHE}}$ for the reference used with 1% doped UO_2 .

Electrochemical measurements and impedance spectroscopy (EIS) was carried out with an electrochemical workstation IM6 (Zahner Elektrik). Potentials were recorded with the LSB 36 II (Linseis).

The solution (100 ml 10 mM NaCl) was bubbled for 24 h to reduce the oxygen contents to a minimum. Later only the gas phase above the electrolyte was purged to avoid potential fluctuations generated by gas bubbles.

After 165 hours (10% doped UO_2) the purging gas was switched to N_2 /(8% H_2). In case of 1% doped UO_2 this was done after 600 hours. The S/V ratio was in the range of $0.03\text{--}0.07 \text{ m}^{-1}$.

To reduce higher uranium oxides which may have formed at the sample surface during polishing the electrode was cathodically polarised for 10 min at -2.5 V at the beginning of the experiment. In case of 10%-doped UO_2 this treatment was done in the same solution as the experiment. In the second experiment the solution was exchanged after precathodisation to avoid contamination of the liquid during the polarisation. To follow the ongoing corrosion processes solution samples (3–5 ml each) were taken for analysis and impedance spectra were measured during the experiment.

Solution sampling and analysis

a. Static tests: sample preparation, instrumentation and calibration.

The solutions were analyzed for the concentration of different uranium isotopes using a high resolution inductively coupled plasma-mass spectroscopy (HR-ICP-MS) from ThermoQuest Finnigan MAT (ELEMENT 2) modified to handle radioactive samples.

The samples were first acidified to give a 0.5 M HNO_3 solution and contained 2 ppb of Th-232, Ho-165, In-115 and Co-59 as internal standards. The analysis was performed in the mass range 232–243 amu. The washing time was 3 min with 2% HNO_3 , and, every 4 samples, a blank solution was run to stabilize the 0 point. 1,000 ppm multielement standard solution was used. The standard solution contained 109 isotopes with a concentration of 10, 50, 200 ppt and 1, 5, 20 ppb. A Pu standard solution containing isotopes 239, 240, 241 and 242 with the same concentration as the multielement standard was also used.

α -spectrometry was performed by depositing a sample volume of 100 μl directly on a stainless steel disc while the disc was warmed up to 70°C on a heating plate. No blank was prepared since there was no contamination risk for ^{233}U .

The concentrations of ^{233}U were measured using an EG&G Octete α -spectrometer. The samples were measured in α -chambers LARS2 and LARS3 on level 1 (3 mm distance between the sample and the detector). The samples were counted for 1.0×10^6 seconds. A corresponding background was measured for the same time period.

The detector calibrations were performed using a certified mixed nuclide α -source (GU389, AEA Technology QSA GmbH, England) having almost the same geometry as the sample and placed at the same distance from the detector.

The identification of the peaks was made manually. Background stripping was applied for the evaluations. All peaks could be identified. The spectrum evaluation was performed as described in the ITU working instruction WI/NC/415, “ α -spectrometry for low level radioactivity determinations”.

b. Autoclave tests: sampling and analysis of leachate.

A constant pressure could be maintained in the autoclave during sampling by opening the valve between the gas supply and the main autoclave. The sampling of leachate was made in two steps: first a rinse sample was collected (5–8 ml) to remove the solution in the tubes and then the representative sample (approximately 10 ml) was collected. At least 5–6 samples were taken within each pressure range separated by a 1–2 month interval.

The leachate was sampled at different time intervals into 50 ml PE-vials. Sub-samples of the leachate were used for different analysis. The most reliable measurements of ^{233}U (and decay daughters) were performed by α -spectrometry after NdF_3 -precipitation and/or electro-deposition. An example of α -spectrum is shown in Figure 2-11. In some cases

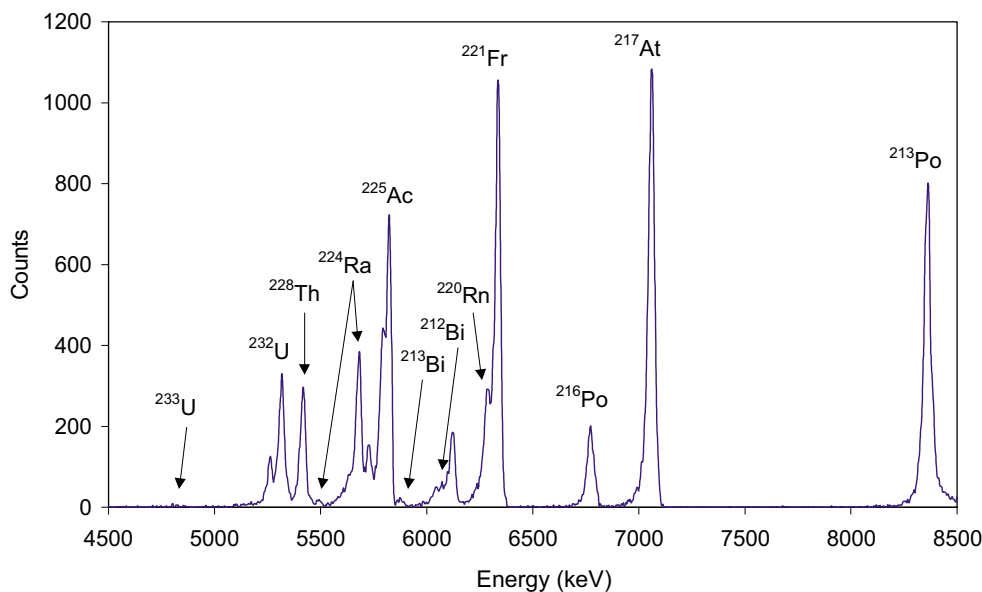


Figure 2-11. An α -spectrum obtained after NdF_3 co-precipitation of radionuclides in the leachate sample S46. The spectrum was counted for 1.2×10^6 s. All the decay daughters of ^{233}U and ^{232}U (tracer) can be seen in the spectrum.

the ^{233}U results were verified by ICP-MS measurement. The low concentration of ^{233}U and ^{238}U in the samples could also be confirmed with “less than” values analysing the samples by liquid scintillation counting. The concentration of stable elements including titanium in the leachate, originating from the autoclave, tubing and the stirrer, was determined by ICP-MS.

c. Solution analysis for ^{233}U during electrochemical measurements.

The ^{233}U content in solution was measured via α -spectrometry. The U concentration was calculated taking into account the isotopic composition and assuming congruent dissolution of the uranium isotopes.

2.2 Experimental results from leaching tests with α -doped $\text{UO}_2(\text{s})$

2.2.1 Static leaching of α -doped pellets under $\text{Ar} + 6\%\text{H}_2$ (ITU/CIEMAT/ENRESA)

Figure 2-12 shows the concentrations of uranium 238 and 233 in solution as a function of time for the experiments performed while bubbling $\text{Ar}/(6\%)\text{H}_2$. All data are summarized in Table 2-5. The pH did not show significant variations during the leaching time. In all cases during the contact time the pH was between ~ 7.1 – 7.5 . The redox potential measured in the solutions shows a general increasing trend with time, but remains negative throughout the duration of the experiment. The dissolved U concentrations show that both in the case of undoped UO_2 and of UO_2 containing 10% ^{233}U no uranium dissolution could be observed during almost 1 year of leaching. In the UO_2 with 10% ^{233}U the initial concentration of the ^{238}U in solution was higher than that for undoped UO_2 . However, no additional dissolution occurred after the initial release. The measured concentrations in solution actually tended

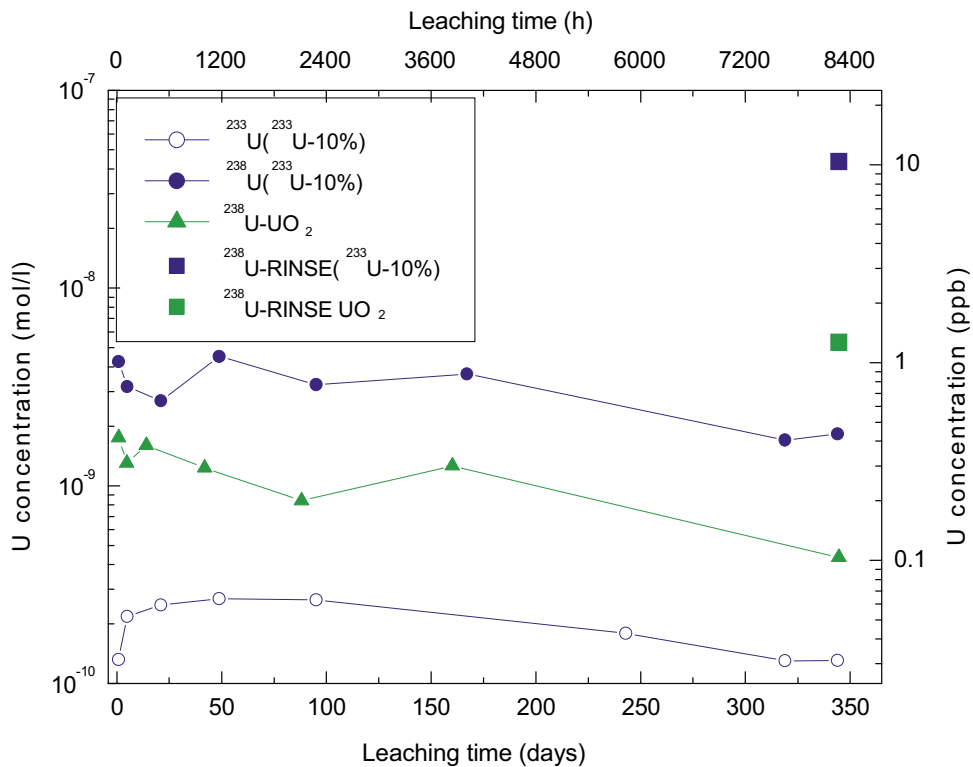


Figure 2-12. Concentration of U versus leaching time in experiments performed under 6% hydrogen in CW water (pH = 7.5).

to decrease for longer leaching times. The initial release can be attributed to the surface pre-oxidation conditions occurring before sample immersion. The $^{233}\text{U}/^{238}\text{U}$ ratio in solution was essentially the same as that in the solid pellets. This means that congruent dissolution of the material occurred. Also shown in the diagram are the results of the analysis of the rinse solutions of the leaching vessels. Relatively low concentrations are found also in the rinse, although if these values could be attributed unequivocally to uranium sorbed on the vessel walls they would indicate the occurrence of a somewhat higher degree of uranium mobilization from the fuel samples. It must be pointed out that the values plotted in Figure 2-12 for the rinse are concentrations in 50 ml of nitric acid, that is in a volume 8 times smaller than the nominal amount of leachant. Furthermore, the presence of fines in addition to the sorbed material cannot be ruled out.

Data for the leaching of UO_2 with 1% ^{233}U are not shown, due to problems with the leaching setup which caused the results of this experiment to be discarded.

2.2.2 Results from static leaching under anoxic conditions

Figure 2-13 shows the concentration of uranium in solution as a function of time under anoxic conditions. These tests are still ongoing. The pH did not show significant variations during the leaching time. All data are summarized in Table 2-6.

Table 2-5. Results from the experiments with UO₂ undoped and UO₂ doped with 10 w/o ²³³U under Ar/(6%)H₂. The concentrations found in the rinse solutions are also indicated.

	Weight (g)	Diameter (mm)	Height (mm)	Time (d)	Aliquot (ml)	Leachant Volume (ml)	Redox potential SHE corrected (mV)	²³⁸ U (mol/l)	²³³ U (mol/l)
UO ₂ (²³³ U-10%)	0.4142	6.5	1.19	0	400		-230.5	0	0
				0.7972	8	392	-463.5	4.25E-09	1.32E-10
				4.9222	5	387	-439.1	3.17E-09	2.19E-10
				21.03	8	379	-333.2	2.68E-09	2.50E-10
				48.835	9	370	-291.5	4.51E-09	2.68E-10
				95.085	8	362	-309.5	3.25E-09	2.64E-10
				242.9	12	350	-138.1	3.68E-09	1.80E-10
				318.9	10	340	-115.7	1.70E-09	1.30E-10
				343.9	340	340	-115.7	1.83E-09	1.31E-10
				343.9	rinse	50 (HNO ₃ -2M)	700	4.37E-08	
UO ₂	0.5033	6.5	1.45	0.000	400		-444.1	0	
				0.841	10	390	-385.5	1.75E-09	
				4.8076	6	384	-351.9	1.30E-09	
				14.046	8	376	-343	1.60E-09	
				41.851	9	367	-213	1.23E-09	
				88.101	8	359	-114.7	8.40E-10	
				160.1	8	351	-284.6	1.26E-09	
				344.58	351	351	-50.9	4.34E-10	
				344.63	rinse	50 (HNO ₃ -2M)	700	5.31E-09	

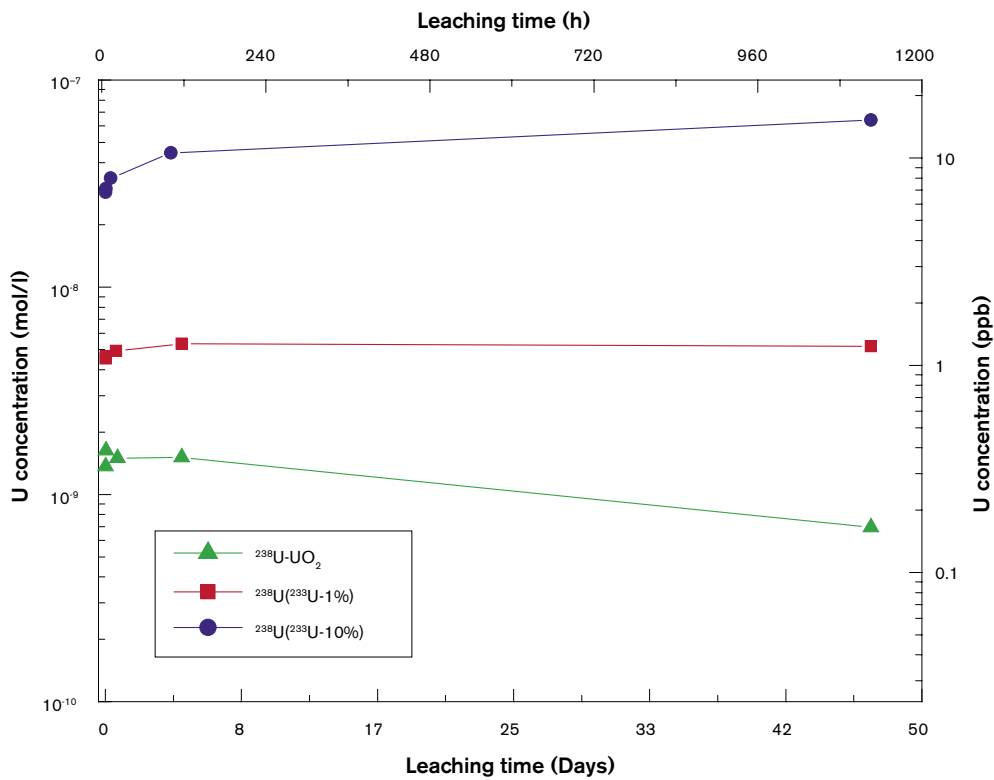


Figure 2-13. Concentration of U versus leaching time in experiments performed under anoxic conditions (Ar/(0.02%)CO₂) with CW water (pH = 7.5).

Table 2-6. Results from the experiments with UO₂ undoped and UO₂ doped with 10 w/o ²³³U under Ar/(0.02%)CO₂. The dissolution rate labeled “total duration” is the rate referred to the total time elapsed from the start of the experiment.

	Wt (g)	Diam (mm)	Height (mm)	S/V (m ⁻¹)	Time (days)	Aliquot (ml)	Leachant volume (ml)	Eh (mVSHE)	²³³ U (mol/l)	²³⁸ U (mol/l)	Diss Rate (mg/m ² d)	Diss rate total duration (mg/m ² d)
UO ₂ (²³³ U-1%)	0.3209	6.5	0.93	0.2	0.042	10	390	211.8		4.53E-09	269.5	269.5
					0.084	10	380	215.5		4.65E-09	6.5	131.7
					0.68	12	368	215		4.92E-09	0.5	8.6
					4.69	10	358	138.3		5.34E-09	0.12	1.36
					46.88	9	349	-59.5	8.30 E-11	5.18E-09	-	0.13
UO ₂ (²³³ U-10%)	0.4142	6.5	1.19	0.2	0.042	14	386	252.8		2.87E-08	1,707.6	1,707.6
					0.084	8	378	210.6		3.00E-08	70.3	850
					0.68	12	366	218.4		3.36E-08	6.7	58.8
					4.69	7	359	194.1		4.44E-08	3.2	11.3
					46.88	12	347	170.8	7.00 E-10	6.40E-08	0.55	1.6
UO ₂	0.5033	6.5	1.45	0.2	0.042	10	390	268.6		1.36E-09	80.9	80.9
					0.084	12	378	307.9		1.63E-09	14.6	46.2
					0.68	7	371	145.7		1.50E-09	-	2.6
					4.69	9	362	-0.3		1.51E-09	0.003	0.38
					46.88	9	353	-180.7		6.93E-10	-	0.02

The preliminary results show that in the UO₂ undoped samples no significant uranium dissolution could be observed under these conditions, similarly to what was seen in the leaching experiments performed under reducing conditions. However, in the case of UO₂ with 10% ²³³U the concentration of the ²³⁸U in solution was more than one order of magnitude higher than that for undoped UO₂. Moreover, the data seem to indicate a small amount of additional dissolution after the initial release. The concentration of ²³⁸U versus time increases only in the test performed with 10% of ²³³U. Concerning the UO₂-1%, the results indicate that no additional release occurred after the initial contact times. The different concentration at the beginning of the leaching experiments may be explained by a slightly higher oxidation of the doped samples. Due to the storage of the sample in the vessel above the water level until the Eh of the solution has reached anoxic conditions, there is the possibility of interaction with water vapour. These data would indicate that such oxidation process is faster for samples with higher α -activity.

Figure 2-14 shows the results obtained under similar “low” S/V conditions (but in MQ water) for the Pu-doped samples [RON/COB 2001,2003]. The corresponding values are summarized in Table 2-7.

Under these low S/V experimental conditions a dependence of the U dissolution on the α -activity is evident for the results shown in Figure 2-13 and, more clearly, in Figure 2-14. Based solely on the activity, though, the data for the UO₂-01 should correspond to higher dissolved concentration if compared to UO₂ containing 10% ²³³U. The higher initial values for the UO₂ doped with 10% ²³³U are probably due to the effect of the carbonate present in CW (and also supplied by the purging gas), and to possible preoxidation effects which cause the initial high release in the case of 10% ²³³U (see experimental section). In terms of dissolution rates, though, it is evident that also after the initial leaching stage the dissolution rate for UO₂-01 (i.e. the “slope” of the concentration vs time) is higher than for the α -doped with 10% ²³³U. It is remarkable to note that also for these two sets of tests the dissolution behaviour of the undoped UO₂ was very similar.

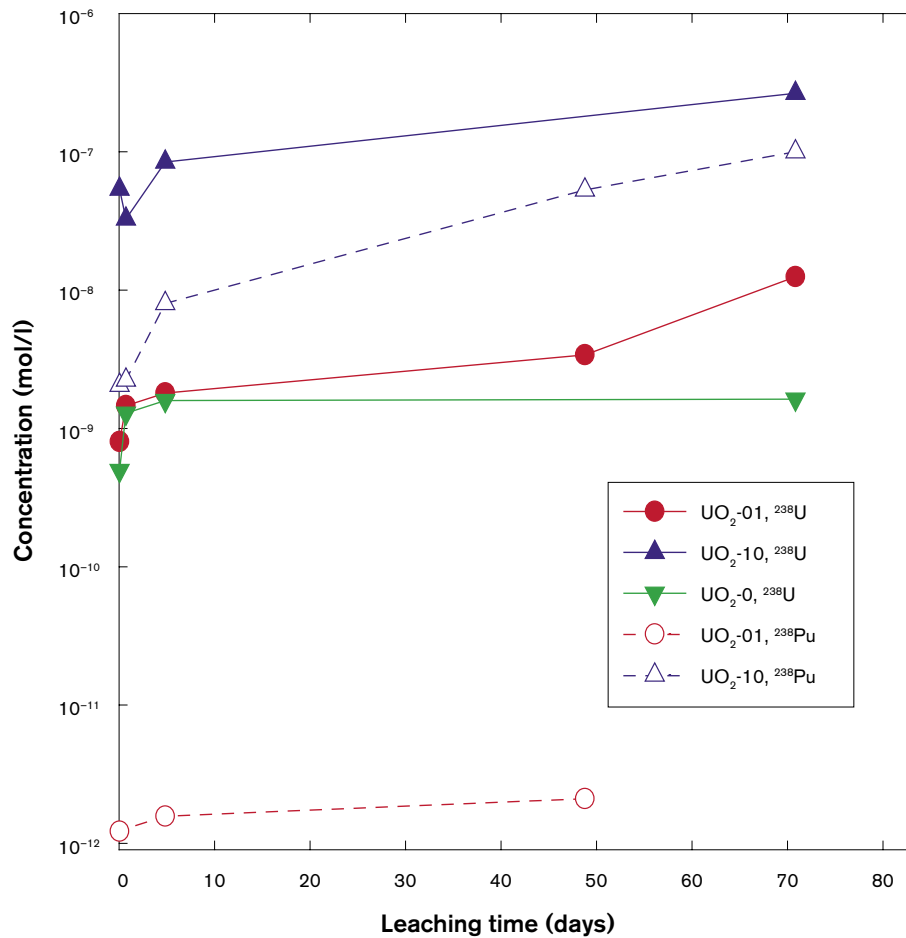


Figure 2-14. Concentration of U, Pu versus leaching time in experiments performed under anoxic conditions (N_2) in MQ water (pH 5.6 – 6.5) with ^{238}Pu doped UO_2 [RON/COB 2001,2003].

The redox potential measured in the solutions for the UO_2-0 and UO_2 with 1% ^{233}U after ~ 100 hours followed a general decreasing trend in all three reaction vessels. As previously observed [RON/COB 2001], a few days were necessary to reach low (i.e. negative) values of the potential. A partial exception to this behaviour was observed in the case of the experiments performed with higher ^{233}U concentration: in this case the E_h values remained positive. This may be associated with the radiolytic production of oxidizing species.

Table 2-7. Results from the experiments with UO₂ doped with ~ 0.1 w/o and ~ 10 w/o ²³⁸Pu under anoxic conditions (N₂) in MQ water [RON/COB 2001,2003]. The dissolution rate labeled “total duration” is the rate referred to the total time elapsed from the start of the experiment.

	Wt (g)	Diam (mm)	Height (mm)	S/V (m ⁻¹)	Time (d)	Leachant volume (ml)	²³⁸ U (mol/l)	²³⁸ Pu (mol/l)	²³⁹ Pu (mol/l)	Diss Rate total duration (mg/m ² d)	Diss Rate (mg/m ² d)
UO ₂ -0.1	0.4	5.86	1.46	0.5	0	160					
					0.056	150	8.03E-10	1.22E-12		6.88 E+00	6.88 E+00
					0.725	140	1.46E-09	(3.2E-12)		9.59 E-01	4.67 E-01
					4.823	130	1.80E-09	1.57E-12		1.78 E-01	3.95 E-02
					48.769	120	3.40E-09	2.10E-12		3.32 E-02	1.73 E-02
					70.829	110	1.25E-08			8.40 E-02	1.96 E-01
UO ₂ -10	0.631	5.85	2.72	0.6	0	160					
					0.055	150	5.38E-08	2.05E-09	7.70E-10	3.84 E+02	3.84 E+02
					0.725	140	3.27E-08	2.24E-09	5.98E-10	1.79 E+01	–
					4.824	130	8.45E-08	8.00E-09	2.68E-09	6.95 E+00	2.55 E+00
					48.769	120	–	5.30E-08	1.37E-08	0.0 E+00	
					70.829	110	2.65E-07	1.00E-07	2.61E-08	1.48 E+00	1.09 E+00
UO ₂ -0	0.588	4.98	3	0.5	0	160					
					0.056	150	4.96E-10			4.25 E+00	4.25 E+00
					0.725	140	1.29E-09			8.47 E-01	5.65 E-01
					4.824	130	1.59E-09			1.57 E-01	3.48 E-02
					48.769	120	–				–
					70.829	110	1.63E-09			1.09 E-02	2.89 E-04

2.2.3 Conclusions on static leaching of α -doped UO₂(s).

Several conclusions can be drawn on the basis of the experiments performed with α -doped UO₂ under anoxic and reducing conditions:

- A good reproducibility of data and trends was obtained for different experimental setups and procedures.
- A clear α -radiolysis enhancement of uranium dissolution was observed under anoxic conditions.
- Under anoxic conditions, no dissolution enhancing effects were observed for UO₂ containing 1% ²³³U: this would indicate that a possible threshold for observing radiolytic enhancement of dissolution lies between 1% and 10% ²³³U under these experimental conditions and for the timeframes considered so far.
- Under Ar/6%H₂ essentially no further dissolution was observed after the initial release up to an activity level corresponding to 10% ²³³U.
- No significant changes of pH were measured during or after the leaching experiments. Measured Eh trends generally correlated with the corresponding trends for U concentration as a function of leaching time.
- Preoxidation effects were observed especially when leaching at low S/V. The preoxidation occurred during the preliminary experimental stage when the sample is suspended above the equilibrating (purged with gas) leaching solution, and is exposed to water vapour: it correlates with the α -activity of the material. Although this process plays an important role, the long term behaviour observed in the experiments cannot be explained exclusively in terms of initial conditions.

Outlook

Among the numerous, still open questions, one aspect of the corrosion process for these types of materials must be highlighted: the role of Pu in determining (stabilizing?) the U-matrix corrosion.

Other experimental developments could be focused on singling out the effect of different available surface areas for water attack: this can be investigated by extending the experiments on crushed samples with controlled particle sizes [RON/MAT 2000] to low S/V configurations. Also, dynamic leaching tests may help in determining dissolution rates, at least at low α -activity levels.

2.2.4 Results from autoclave leaching of a 10% ²³³U doped pellet under various H₂ pressures (ITU/SKB).

The results are divided into three sections: the first considers the results obtained during the experiment itself, the second concerns the post-characterisation of the pellet and the third, the characterisation of the Ti-deposits.

Experimental results

The results of the measurements made during the experiment were divided into: (a) the background information such as the H₂ and O₂ concentrations, E_h, pH, temperature and total pressure (b) the concentration of stable elements in the leachate originating from the autoclave and finally, (c) the concentration of ²³³U in the leachate. The raw data of the parameters measured during the experiment are summarised in Table 2-8 and the elaborated data in Table 2-9.

The redox potential, E_h, was measured during leachate sampling and reflects the redox conditions in the autoclave at the sampling occasion. As can be observed in Figure 2-15 and Table 2-8 the redox potential decreased continuously during the first 200 days from -100 mV and reached a plateau of approximately -350 mV. After this point the E_h remains constant, even though the atmosphere changes from 16 bar pure H₂ to 0.15 bar H₂. The change of the conditions to 0.01 bar H₂/Ar had no influence on the redox conditions during the first 300 days after the change of the H₂ concentration but started thereafter to increase to a level of -100 mV. A possible conclusion is that the H₂ concentration in the range between 0.16 bar H₂ and 0.01 bar H₂ is just enough to inhibit the dissolution of the UO₂ at this specific α -dose rate. Only a repeated leaching experiment at such low H₂ concentrations could give a confirmatory answer.

The H₂ concentration in the gas phase in the autoclave was measured intermittently with two independent methods, while the experiment was run in pure H₂ the pressure could be measured both with the two pressure gauges (mechanical and digital) and the Orbisphere H₂ sensor. Independent of the pressure device used the H₂ concentration measured was identical. For convenience, the values obtained by the Orbisphere H₂ sensors are used in the calculation, as the Orbisphere sensors gives readings also in the part of the experiment when the H₂ concentration becomes a fraction of the total pressure. The results are given in Table 2-8. Using Henry's law the concentration of dissolved H₂ in the leachate could be calculated according to:

$$p = H \cdot x$$

where x is the mole fraction of the solute in the liquid phase, p the partial pressure of the solute in the gas phase in atmospheres and H the proportionality constant expressed in the units of atmospheres of solute pressure in the gas phase per unit concentration of the

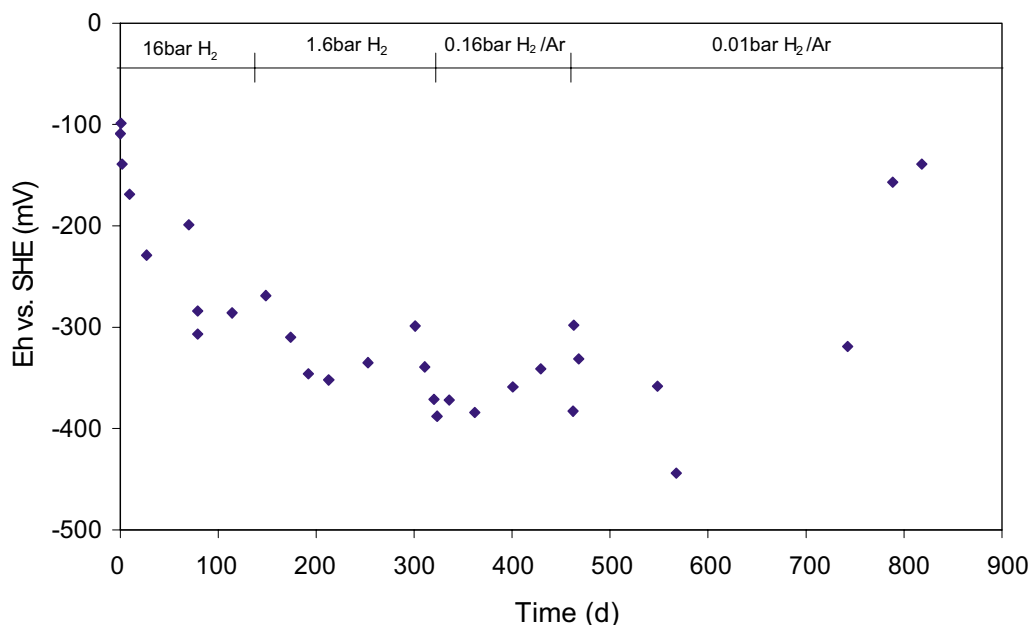


Figure 2-15. Redox potential, E_h , in the autoclave as a function of leaching time. The redox potential of the leachate was measured only during leachate sampling.

solute in the liquid phase [PER/GRE 1997]. The selected Henrys constant for H_2 under our conditions ($T = 25^\circ C$) was 125×10^6 Pa/M. In Figure 2-16 and Table 2-9 the concentration of dissolved H_2 in the autoclave against time is plotted. It can be concluded that during the initial part of the experiment the concentration of H_2 is the dominating species in the leachate (0.02 M). At a pressure of 0.16 bar H_2 the concentration of dissolved H_2 in the leachate is at the same level as the 0.012 M Na^+ , 0.01 M Cl^- and 0.002 M HCO_3^- . One of the more interesting results is that despite two purges (after 460 days and 550 days) with pure Ar gas the hydrogen concentration remained high and even recovered to a higher level than right after the Ar-purging. This phenomena can be either due to desorption of H_2 absorbed in the walls of the Ti-autoclave, and/or in the UO_2 pellet or most likely due to the reactions between Ti and water (see section Experimental, Autoclave set-up). Error due to false H_2 measurements could be excluded once a gas sample was collected from the autoclave, Table 2-8, after the second Ar-purge (670 days), and a gas mass spectrometry, Table 2-4 analysis made. A comparison of the two measurements, mass spectrometry versus the in situ H_2 sensor, showed a H_2 concentration that differed by $\sim 30\%$. This is fully acceptable since the stability/calibration of the H_2 sensor is not expected to be valid for more than one year. Also, the mass spectrometric analysis of the gas collected from the autoclave showed an $O_2/(O_2+N_2)$ ratio of 0.149. This indicates a contamination of the gas sample during sampling with glove box atmosphere or also with air during the measurement (as reference the $O_2/(O_2+N_2)$ ratio in air is 0.21). The contamination does not affect the results of the mass spectrometric measurement of H_2 .

The oxygen concentration in the solution was measured and the corrected values are given in Table 2-8. The O_2 concentrations in the solution were calculated using Henrys law and the selected Henrys constant of 78×10^6 Pa/M ($T = 25^\circ C$) and the result are shown in Figure 2-17 and summarised in Table 2-9.

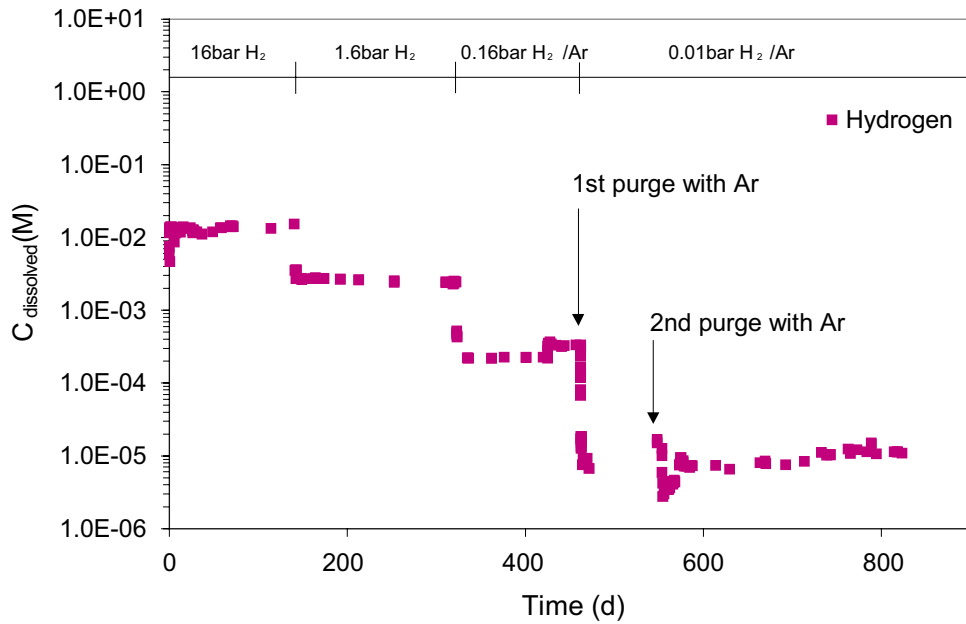


Figure 2-16. Concentration of H_2 in leachate as a function of leaching time. The H_2 concentration was measured inside the autoclave during the experiment.

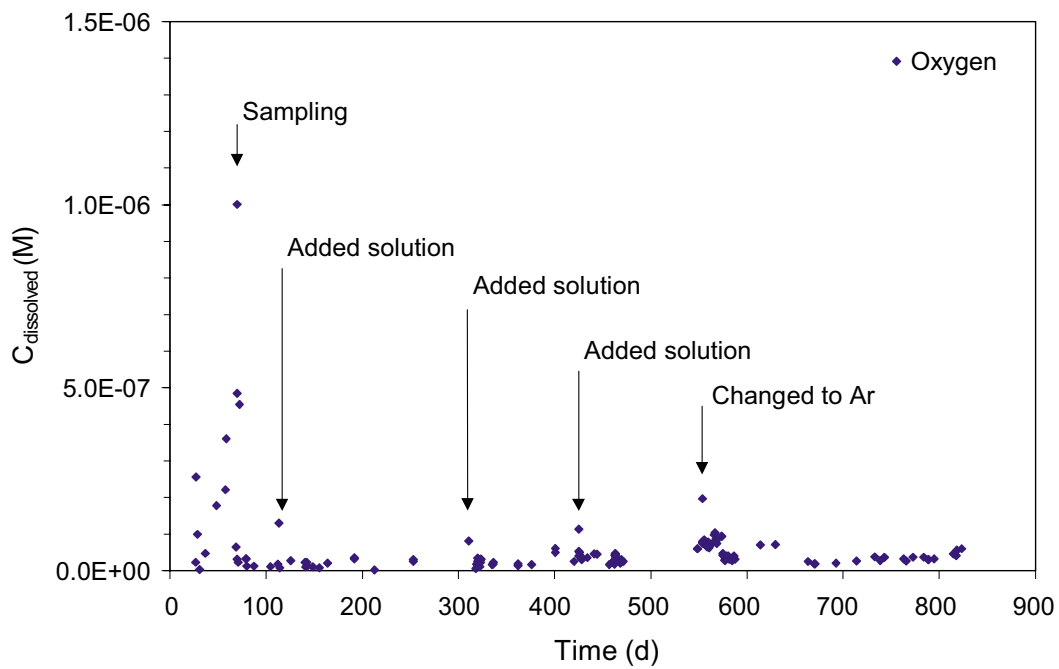


Figure 2-17. Concentration of O_2 measured intermittently inside the autoclave during the experiment. The practical detection limit is 1×10^{-9} M.

It can be seen that in general the oxygen concentration is low in the range of $2 \times 10^{-8} \text{ M}$. The practical detection limit is $\sim 1 \times 10^{-9} \text{ M}$. Additionally, it is interesting to observe in the graph the response from the O_2 -sensor at those moments when new solution ($10 \text{ mM NaCl} + 2 \text{ mM HCO}_3^-$) was added to the autoclave or when the gas bottle was changed and during the initial sampling occasions. The oxygen intrusion occurred, despite all precautions such as a sound experimental lay-out, tube flushing, solution bubbling, fast transfer of solution, presence of hydrogen and so on. On the other hand, one can also observe the fast removal (within few hours) of O_2 from the leachate. This indicates a relatively fast reaction between the externally added O_2 and an oxygen scavenger such as H_2 sorbed on the UO_2 surface which catalyses the reaction between H_2 and O_2 . This is probably the same O_2 scavenging mechanism as for the radiolytically produced O_2 .

One can conclude, from Table 2-9, that the concentration of stable elements (Mn, Fe, Co, Ni, Cu and Zn) in the 10 mM NaCl leachate solution was high during the first few days of the leaching experiment. Despite a thorough wash of all wetted Ti-surfaces in the autoclave before the start of the experiment leaching of the stable elements from the freshly prepared Ti-surfaces can not be avoided. In a few days the stable element concentrations were stabilised at different levels depending on the element, Figure 2-18.

The concentration of Ti in the leachate was measured over a longer period. During the initial 113 days, in 10 mM NaCl leachate, it behaved similarly to the other stable elements and reached a concentration of $5 \times 10^{-6} \text{ M}$. After addition of 2 mM HCO_3^- to the autoclave the concentration increased 10-fold to $3 \times 10^{-5} \text{ M}$, probably due to complexation of Ti(IV) with CO_3^{2-} . The concentration of Ti remained at this level throughout the rest of the experiment, implying that the Ti(IV) was relatively low.

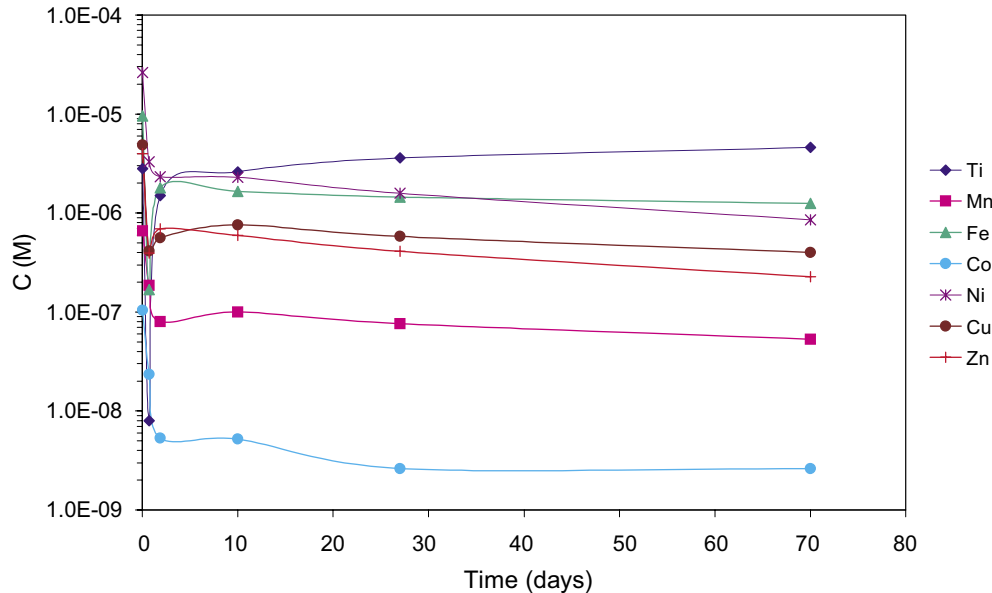


Figure 2-18. Concentration of stable elements leached from the Ti-surfaces in the autoclave as a function of time. The leachate consisted of 10 mM NaCl at pH 7 and $0.013 \text{ M H}_{2,\text{dissolved}}$ (16 bar H_2).

Table 2-8. Corrected raw data of the redox potential, E_H measured against standard hydrogen electrode, hydrogen concentration above the leachate (gas phase), oxygen concentration in leachate, the concentration in the leachate of stable elements originating from the autoclave, the ^{233}U and ^{225}Ac activity concentration (Bq/g leachate) in the leachate and the activity ratios between the ^{233}U decay daughters as function of leaching time. The errors for the ^{233}U and ^{225}Ac determination are given with 1σ total counting uncertainty. The short-lived radionuclide has been decay corrected to the sampling time.

Sample	Leaching time (days)	E_H (mV)	H_2 (mbar)	O_2 (mbar)	Ti (ppb)	Mn (ppb)	Fe (ppb)	Co (ppb)	Ni (ppb)	Cu (ppb)	Zn (ppb)	^{233}U (Bq/g)	Error ^{233}U (%)	^{225}Ac (Bq/g)	Error ^{225}Ac (%)	$^{225}\text{Ac}/^{233}\text{U}$	$^{221}\text{Fr}/^{225}\text{Ac}$	$^{217}\text{At}/^{221}\text{Fr}$	$^{213}\text{Po}/^{217}\text{At}$
10mM NaCl					< 0.2	2	2	< 0.2	10	2	13								
S1	0.02	-109	15,200	—	135	36	540	6	1548	310	261	6.4×10^{-4}	6	»	»	»	»	»	»
S2	0.7	-99	15,294	—	2	10	9	1	194	26	26	7.9×10^{-5}	19	»	»	»	»	»	»
S2	0.7	-99	15,294	—	2	10	9	1	194	26	26	1.2×10^{-4}	12	»	»	»	»	»	»
S3	1.9	-139	16,407	—	71	4	100	0.3	137	36	45	9.8×10^{-5}	27	»	»	»	»	»	»
S4	10	-169	16,292	—	108	5	92	0.3	135	48	39	8.3×10^{-5}	18	»	»	»	»	»	»
S5	27	-229	14,987	1.7×10^{-2}	172	n.m.	n.m.	n.m.	n.m.	n.m.	n.m.	7.2×10^{-5}	17	»	»	»	»	»	»
S6	70	-199	16,815	2.3×10^{-2}	240	3	70	< 0.2	50	26	15	2.0×10^{-5}	32	»	»	»	»	»	»
S7	79	-284	16,857	2.4×10^{-2}	214	n.m.	n.m.	n.m.	n.m.	n.m.	n.m.	2.2×10^{-4}	30	»	»	»	»	»	»
S7	79	-284	16,857	2.4×10^{-2}	214	n.m.	n.m.	n.m.	n.m.	n.m.	n.m.	8.5×10^{-5}	38	»	»	»	»	»	»
S8	113	n.m.	n.r.	9.6×10^{-2}	274	n.m.	n.m.	n.m.	n.m.	n.m.	n.m.	2.3×10^{-5}	31	»	»	»	»	»	»
	114	Changed from 0.01 M NaCl to 0.01 M NaCl + 2 mM HCO_3^-																	
10 mM NaCl + 2 mM HCO_3^-					3	n.m.	n.m.	n.m.	n.m.	n.m.	n.m.			»	»	»	»	»	»
S9	115	-286	15,907	6.4×10^{-2}	1,233	n.m.	n.m.	n.m.	n.m.	n.m.	n.m.	5.1×10^{-5}	20	»	»	»	»	»	»
	140	Lowered H_2 pressure from 16 bar to 1.6 bar																	
S11	149	Rinse		7.4×10^{-3}	n.m.	n.m.	n.m.	n.m.	n.m.	n.m.	n.m.	4.4×10^{-4}	6	»	»	»	»	»	»
S12	149	-269	3,200	7.4×10^{-3}	n.m.	n.m.	n.m.	n.m.	n.m.	n.m.	n.m.	2.7×10^{-4}	10	»	»	»	»	»	»
S13	174	Rinse			n.m.	n.m.	n.m.	n.m.	n.m.	n.m.	n.m.	n.m.		»	»	»	»	»	»
S14	174	-310	3,260	1.5×10^{-2}	n.m.	n.m.	n.m.	n.m.	n.m.	n.m.	n.m.	3.3×10^{-4}	8	»	»	»	»	»	»
S14	174	-310	3,260	1.5×10^{-2}	n.m.	n.m.	n.m.	n.m.	n.m.	n.m.	n.m.	3.0×10^{-4}	8	»	»	»	»	»	»
S15	192	Rinse		2.4×10^{-2}	n.m.	n.m.	n.m.	n.m.	n.m.	n.m.	n.m.	2.8×10^{-5}	34	»	»	»	»	»	»

Sample	Leaching time (days)	E _h (mV)	H ₂ (mbar)	O ₂ (mbar)	Ti (ppb)	Mn (ppb)	Fe (ppb)	Co (ppb)	Ni (ppb)	Cu (ppb)	Zn (ppb)	²³³ U (Bq/g)	Error ²³³ U (%)	²²⁵ Ac (Bq/g)	Error ²²⁵ Ac (%)	²²⁵ Ac/ ²³³ U	²²¹ Fr/ ²²⁵ Ac	²¹⁷ At/ ²²¹ Fr	²¹³ Po/ ²¹⁷ At
S16	192	-346	3,200	2.4×10 ⁻²	n.m.	n.m.	n.m.	n.m.	n.m.	n.m.	n.m.	2.5×10 ⁻⁴	9	»	»	»	»	»	»
S17	213	Rinse		1.4×10 ⁻³	n.m.	n.m.	n.m.	n.m.	n.m.	n.m.	n.m.	7.2×10 ⁻⁵	22	»	»	»	»	»	»
S18	213	-352	3,115	1.4×10 ⁻³	n.m.	n.m.	n.m.	n.m.	n.m.	n.m.	n.m.	4.7×10 ⁻⁵	20	»	»	»	»	»	»
S19	253	Rinse		2.2×10 ⁻²	n.m.	n.m.	n.m.	n.m.	n.m.	n.m.	n.m.	3.1×10 ⁻⁵	36	»	»	»	»	»	»
S20	253	-335	2,955	2.2×10 ⁻²	n.m.	n.m.	n.m.	n.m.	n.m.	n.m.	n.m.	8.4×10 ⁻⁵	15	2.7×10 ⁻²	9	4	0.66	1.74	0.88
S21	311	Rinse		1.8×10 ⁻²	n.m.	n.m.	n.m.	n.m.	n.m.	n.m.	n.m.	1.9×10 ⁻⁵	36	»	»	»	»	»	»
S22	311	-339	2,901	1.8×10 ⁻²	n.m.	n.m.	n.m.	n.m.	n.m.	n.m.	n.m.	4.3×10 ⁻⁴	13	»	»	»	»	»	»
S23	320	Rinse		1.8×10 ⁻³	n.m.	n.m.	n.m.	n.m.	n.m.	n.m.	n.m.	< d.l.		»	»	»	»	»	»
S24	320	-371	2,891	1.8×10 ⁻³	n.m.	n.m.	n.m.	n.m.	n.m.	n.m.	n.m.	2.1×10 ⁻⁴	10	1.5×10 ⁻²	2	56	0.92	1.21	0.88
	322	Lowered H ₂ pressure from 1.6 bar to 0.16 bar																	
S25	323	Rinse		2.3×10 ⁻²	n.m.	n.m.	n.m.	n.m.	n.m.	n.m.	n.m.	9.5×10 ⁻⁵	15	9.0×10 ⁻³	3	35	0.98	1.43	0.86
S26	323	-388	515	2.3×10 ⁻²	n.m.	n.m.	n.m.	n.m.	n.m.	n.m.	n.m.	1.3×10 ⁻⁴	12	2.1×10 ⁻²	2	72	1.02	1.12	0.89
S27	336	Rinse		1.3×10 ⁻²	n.m.	n.m.	n.m.	n.m.	n.m.	n.m.	n.m.	1.7×10 ⁻⁴	10	»	»	»	»	»	»
S28	336	-372	263	1.3×10 ⁻²	n.m.	n.m.	n.m.	n.m.	n.m.	n.m.	n.m.	9.6×10 ⁻⁵	15	1.8×10 ⁻²	2	124	0.96	1.21	0.86
S29	362	Rinse		1.0×10 ⁻²	n.m.	n.m.	n.m.	n.m.	n.m.	n.m.	n.m.	3.4×10 ⁻⁵	22	»	»	»	»	»	»
S30	362	-384	261	1.0×10 ⁻²	n.m.	n.m.	n.m.	n.m.	n.m.	n.m.	n.m.	9.6×10 ⁻⁵	12	1.9×10 ⁻²	2	140	0.90	1.23	0.84
S31	401	Rinse		3.6×10 ⁻²	750 ± 380	n.m.	n.m.	n.m.	n.m.	n.m.	n.m.	3.6×10 ⁻⁵	19	3.9×10 ⁻³	3	84	0.95	1.22	0.84
S32	401	-359	269	3.6×10 ⁻²	n.m.	n.m.	n.m.	n.m.	n.m.	n.m.	n.m.	7.5×10 ⁻⁵	13	1.7×10 ⁻²	2	176	0.74	1.40	1.02
S33	429	Rinse		2.2×10 ⁻²	n.m.	n.m.	n.m.	n.m.	n.m.	n.m.	n.m.	7.0×10 ⁻⁵	16	6.6×10 ⁻³	3	51	0.94	1.14	1.01
S33	429	Rinse		2.2×10 ⁻²	n.m.	n.m.	n.m.	n.m.	n.m.	n.m.	n.m.	2.3×10 ⁻⁵	25	1.4×10 ⁻²	2	331	0.88	1.13	0.83
S34	429	-341	423	2.5×10 ⁻²	n.m.	n.m.	n.m.	n.m.	n.m.	n.m.	n.m.	1.3×10 ⁻⁴	13	1.6×10 ⁻²	2	98	0.94	1.22	0.89
S34	429	-341	423	2.5×10 ⁻²	n.m.	n.m.	n.m.	n.m.	n.m.	n.m.	n.m.	9.8×10 ⁻⁵	16	1.8×10 ⁻²	3	66	0.93	1.25	0.89
S34	429	-341	423	2.5×10 ⁻²	n.m.	n.m.	n.m.	n.m.	n.m.	n.m.	n.m.	5.8×10 ⁻⁵	14	1.8×10 ⁻²	1	256	0.83	1.23	0.84
S34	429	-341	423	2.5×10 ⁻²	n.m.	n.m.	n.m.	n.m.	n.m.	n.m.	n.m.	5.9×10 ⁻⁵	13	3.1×10 ⁻²	2	180	0.88	1.15	0.83

Sample	Leaching time (days)	E _h (mV)	H ₂ (mbar)	O ₂ (mbar)	Ti (ppb)	Mn (ppb)	Fe (ppb)	Co (ppb)	Ni (ppb)	Cu (ppb)	Zn (ppb)	²³³ U (Bq/g)	Error ²³³ U (%)	²²⁵ Ac (Bq/g)	Error ²²⁵ Ac (%)	²²⁵ Ac/ ²³³ U	²²¹ Fr/ ²²⁵ Ac	²¹⁷ At/ ²²¹ Fr	²¹³ Po/ ²¹⁷ At
S35	462	-383	398	1.3×10 ⁻²	n.m.	n.m.	n.m.	n.m.	n.m.	n.m.	n.m.	1.6×10 ⁻⁴	12	7.7×10 ⁻³	3	35	1.05	1.00	1.02
	462	Changed atmosphere from 0.16 bar H ₂ to 3.1 bar Ar																	
S36	463	-298	21	3.5×10 ⁻²	n.m.	n.m.	n.m.	n.m.	n.m.	n.m.	n.m.	1.2×10 ⁻⁴	14	1.8×10 ⁻²	2	121	0.94	1.10	0.88
S37	468	-331	10	1.5×10 ⁻²	n.m.	n.m.	n.m.	n.m.	n.m.	n.m.	n.m.	1.4×10 ⁻⁴	9	1.3×10 ⁻²	2	70	1.08	1.13	0.77
S38	548	Rinse		4.4×10 ⁻²	100 ± 50	n.m.	n.m.	n.m.	n.m.	n.m.	n.m.	4.8×10 ⁻⁵	17	1.6×10 ⁻³	5	16	0.91		
S39	548	-352	19	4.4×10 ⁻²	n.m.	n.m.	n.m.	n.m.	n.m.	n.m.	n.m.	9.2×10 ⁻⁵	12	1.8×10 ⁻²	2	90	0.92	1.23	0.90
	554	Purged the autoclave with Ar at 3.1 bar pressure																	
S40	568	-444	5	6.1×10 ⁻²	n.m.	n.m.	n.m.	n.m.	n.m.	n.m.	n.m.	7.6×10 ⁻⁵	16	4.8×10 ⁻³	3	53	1.13	1.11	0.80
	670	Sampled a gas sample from the autoclave																	
S41	743	Rinse		2.6×10 ⁻²	n.m.	n.m.	n.m.	n.m.	n.m.	n.m.	n.m.	n.m.		n.m.		n.m.	n.m.	n.m.	n.m.
S42	743	-319	12	2.6×10 ⁻²	n.m.	n.m.	n.m.	n.m.	n.m.	n.m.	n.m.	n.m.		n.m.		n.m.	n.m.	n.m.	n.m.
S43	789	-157	17	2.2×10 ⁻²	n.m.	n.m.	n.m.	n.m.	n.m.	n.m.	n.m.	n.m.		n.m.		n.m.	n.m.	n.m.	n.m.
S44	789	Rinse		2.2×10 ⁻²	n.m.	n.m.	n.m.	n.m.	n.m.	n.m.	n.m.	n.m.		n.m.		n.m.	n.m.	n.m.	n.m.
S45	818	Rinse		4.1×10 ⁻²	n.m.	n.m.	n.m.	n.m.	n.m.	n.m.	n.m.	n.m.		n.m.		n.m.	n.m.	n.m.	n.m.
S46	818	-139	13	4.1×10 ⁻²	n.m.	n.m.	n.m.	n.m.	n.m.	n.m.	n.m.	5.2×10 ⁻⁵	13	2.1×10 ⁻²	2	205	0.93	0.84	0.95
	823	End of experiment																	

< d.l. means below detection limit.

n.m. means not measured.

— means negative values due to instability of the sensor due to fast change of initially applied pressure.

rinse means the first portion of solution that remained in the tubing since last sampling.

n.r. means no reading of the value.

» > 10×t_{1/2}, the radionuclide had decayed due to more than ten half-lives since between sampling and measurement.

Table 2-9. Summary of the leachate data as a function of leaching time. The ²²⁵Ra concentration was decay corrected to the sampling time. The error for the U and ²²⁵Ra determinations are given with 1σ total counting uncertainty. The error for the stable elements (Ti, Mn, Fe, Ni, Cu, Zn) is in the range of ± 30–50% (1σ). The error of the H₂ and O₂ measurements are estimated to be in the range of ± 30–40%.

Sample	Leaching time (days)	E _h (mV)	H ₂ (M)	O ₂ (M)	Ti (M)	Mn (M)	Fe (M)	Co (M)	Ni (M)	Cu (M)	Zn (M)	U _{tot} (M)	Error U _{tot} (%)	²²⁵ Ra (M)	Error ²²⁵ Ra (%)	Remarks:
10 mM NaCl					< 5×10 ⁻⁹	5×10 ⁻⁸	3×10 ⁻⁹	< 4×10 ⁻⁹	2×10 ⁻⁷	2×10 ⁻⁸	2×10 ⁻⁷					
S1	0.02	-109	1×10 ⁻²	—	3×10 ⁻⁶	7×10 ⁻⁷	1×10 ⁻⁵	1×10 ⁻⁷	3×10 ⁻⁵	5×10 ⁻⁶	4×10 ⁻⁶	7.6×10 ⁻¹¹	6	»	»	
S2	0.7	-99	1×10 ⁻²	—	8×10 ⁻⁹	2×10 ⁻⁷	2×10 ⁻⁷	2×10 ⁻⁸	3×10 ⁻⁶	4×10 ⁻⁷	4×10 ⁻⁷	9.4×10 ⁻¹²	19	»	»	
S2	0.7	-99	1×10 ⁻²	—	8×10 ⁻⁹	2×10 ⁻⁷	2×10 ⁻⁷	2×10 ⁻⁸	3×10 ⁻⁶	4×10 ⁻⁷	4×10 ⁻⁷	1.5×10 ⁻¹¹	12	»	»	
S3	1.9	-139	1×10 ⁻²	—	2×10 ⁻⁶	8×10 ⁻⁸	2×10 ⁻⁶	5×10 ⁻⁹	2×10 ⁻⁶	6×10 ⁻⁷	7×10 ⁻⁷	1.2×10 ⁻¹¹	27	»	»	
S4	10	-169	1×10 ⁻²	—	3×10 ⁻⁶	1×10 ⁻⁷	2×10 ⁻⁶	5×10 ⁻⁹	2×10 ⁻⁶	8×10 ⁻⁷	6×10 ⁻⁷	9.9×10 ⁻¹²	18	»	»	
S5	27	-229	1×10 ⁻²	2×10 ⁻⁸	7×10 ⁻⁶	1×10 ⁻⁷	8×10 ⁻⁶	2×10 ⁻⁸	1×10 ⁻⁵	1×10 ⁻⁶	5×10 ⁻⁶	8.6×10 ⁻¹²	17	»	»	Blk part. sampl. vial
S6	70	-199	1×10 ⁻²	3×10 ⁻⁸	5×10 ⁻⁶	5×10 ⁻⁸	1×10 ⁻⁶	< 4×10 ⁻⁹	9×10 ⁻⁷	4×10 ⁻⁷	2×10 ⁻⁷	2.4×10 ⁻¹²	32	»	»	
S7	79	-284	1×10 ⁻²	3×10 ⁻⁸	5×10 ⁻⁶	n.m.	n.m.	n.m.	n.m.	n.m.	n.m.	2.6×10 ⁻¹¹	30	»	»	
S7	79	-284	1×10 ⁻²	3×10 ⁻⁸	5×10 ⁻⁶	n.m.	n.m.	n.m.	n.m.	n.m.	n.m.	1.0×10 ⁻¹¹	38	»	»	
S8	113	n.m.	n.r.	1×10 ⁻⁷	6×10 ⁻⁶	n.m.	n.m.	n.m.	n.m.	n.m.	n.m.	2.7×10 ⁻¹²	31	»	»	
114	Changed from 0.01 M NaCl to 0.01 M NaCl + 2 mM HCO ₃ ⁻															
10 mM NaCl + 2 mM HCO ₃ ⁻					6×10 ⁻⁸	n.m.	n.m.	n.m.	n.m.	n.m.	n.m.			»	»	
S9	115	-286	1×10 ⁻²	9×10 ⁻⁹	3×10 ⁻⁵	n.m.	n.m.	n.m.	n.m.	n.m.	n.m.	6.0×10 ⁻¹²	20	»	»	
140	Lowered H ₂ pressure from 16 bar to 1.6 bar															
S11	149	Rinse			n.m.	n.m.	n.m.	n.m.	n.m.	n.m.	n.m.	5.2×10 ⁻¹¹	6	»	»	
S12	149	-269	2×10 ⁻³	1×10 ⁻⁸	n.m.	n.m.	n.m.	n.m.	n.m.	n.m.	n.m.	3.2×10 ⁻¹¹	10	»	»	
S13	174	Rinse			n.m.	n.m.	n.m.	n.m.	n.m.	n.m.	n.m.	n.m.		»	»	
S14	174	-310	2×10 ⁻³	2×10 ⁻⁸	n.m.	n.m.	n.m.	n.m.	n.m.	n.m.	n.m.	3.9×10 ⁻¹¹	8	»	»	
S14	174	-310	2×10 ⁻³	2×10 ⁻⁸	n.m.	n.m.	n.m.	n.m.	n.m.	n.m.	n.m.	3.5×10 ⁻¹¹	8	»	»	
S15	192	Rinse			n.m.	n.m.	n.m.	n.m.	n.m.	n.m.	n.m.	3.4×10 ⁻¹²	34	»	»	
S16	192	-346	2×10 ⁻³	3×10 ⁻⁸	n.m.	n.m.	n.m.	n.m.	n.m.	n.m.	n.m.	2.9×10 ⁻¹¹	9	»	»	
S17	213	Rinse			n.m.	n.m.	n.m.	n.m.	n.m.	n.m.	n.m.	8.5×10 ⁻¹²	22	»	»	

Sample	Leaching time (days)	E _h (mV)	H ₂ (M)	O ₂ (M)	Ti (M)	Mn (M)	Fe (M)	Co (M)	Ni (M)	Cu (M)	Zn (M)	U _{tot} (M)	Error U _{tot} (%)	²²⁵ Ra (M)	Error ²²⁵ Ra (%)	Remarks:
S18	213	-352	2×10 ⁻³	2×10 ⁻⁹	n.m.	n.m.	n.m.	n.m.	n.m.	n.m.	n.m.	5.6×10 ⁻¹²	20	»	»	
S19	253	Rinse			n.m.	n.m.	n.m.	n.m.	n.m.	n.m.	n.m.	3.7×10 ⁻¹²	36	»	»	
S20	253	-335	2×10 ⁻³	3×10 ⁻⁸	n.m.	n.m.	n.m.	n.m.	n.m.	n.m.	n.m.	1.0×10 ⁻¹¹	15	8.4×10 ⁻¹⁷	9	
S21	311	Rinse			n.m.	n.m.	n.m.	n.m.	n.m.	n.m.	n.m.	2.2×10 ⁻¹²	36	»	»	
S22	311	-339	2×10 ⁻³	8×10 ⁻⁸	n.m.	n.m.	n.m.	n.m.	n.m.	n.m.	n.m.	5.1×10 ⁻¹¹	13	»	»	
S23	320	Rinse			n.m.	n.m.	n.m.	n.m.	n.m.	n.m.	n.m.	< d.l.		»	»	
S24	320	-371	2×10 ⁻³	3×10 ⁻⁸	n.m.	n.m.	n.m.	n.m.	n.m.	n.m.	n.m.	2.6×10 ⁻¹¹	10	4.5×10 ⁻¹⁷	2	
	322	Lowered H ₂ pressure from 1.6 bar to 0.16 bar														
S25	323	Rinse			n.m.	n.m.	n.m.	n.m.	n.m.	n.m.	n.m.	1.1×10 ⁻¹¹	15	2.8×10 ⁻¹⁷	3	
S26	323	-388	3×10 ⁻⁴	3×10 ⁻⁸	n.m.	n.m.	n.m.	n.m.	n.m.	n.m.	n.m.	1.6×10 ⁻¹¹	12	6.4×10 ⁻¹⁷	2	
S27	336	Rinse			n.m.	n.m.	n.m.	n.m.	n.m.	n.m.	n.m.	2.0×10 ⁻¹¹	10	»	»	
S28	336	-372	2×10 ⁻⁴	2×10 ⁻⁸	n.m.	n.m.	n.m.	n.m.	n.m.	n.m.	n.m.	1.1×10 ⁻¹¹	15	5.4×10 ⁻¹⁷	2	
S29	362	Rinse			n.m.	n.m.	n.m.	n.m.	n.m.	n.m.	n.m.	4.0×10 ⁻¹²	22	»	»	
S30	362	-384	2×10 ⁻⁴	1×10 ⁻⁸	n.m.	n.m.	n.m.	n.m.	n.m.	n.m.	n.m.	1.1×10 ⁻¹¹	12	5.8×10 ⁻¹⁷	2	
S31	401	Rinse			2×10 ⁻⁵ ± 8×10 ⁻⁶	n.m.	n.m.	n.m.	n.m.	n.m.	n.m.	4.3×10 ⁻¹²	19	1.2×10 ⁻¹⁷	3	Ti analysed at CTH
S32	401	-359	2×10 ⁻⁴	5×10 ⁻⁸	n.m.	n.m.	n.m.	n.m.	n.m.	n.m.	n.m.	8.9×10 ⁻¹²	13	5.1×10 ⁻¹⁷	2	
S33	429	Rinse			n.m.	n.m.	n.m.	n.m.	n.m.	n.m.	n.m.	8.3×10 ⁻¹²	16	2.0×10 ⁻¹⁷	3	
S33	429	Rinse			n.m.	n.m.	n.m.	n.m.	n.m.	n.m.	n.m.	2.7×10 ⁻¹²	25	4.4×10 ⁻¹⁷	2	
S34	429	-341	3×10 ⁻⁴	3×10 ⁻⁸	n.m.	n.m.	n.m.	n.m.	n.m.	n.m.	n.m.	1.6×10 ⁻¹¹	13	5.0×10 ⁻¹⁷	2	
S34	429	-341	3×10 ⁻⁴	3×10 ⁻⁸	n.m.	n.m.	n.m.	n.m.	n.m.	n.m.	n.m.	1.2×10 ⁻¹¹	16	5.7×10 ⁻¹⁷	3	
S34	429	-341	3×10 ⁻⁴	3×10 ⁻⁸	n.m.	n.m.	n.m.	n.m.	n.m.	n.m.	n.m.	6.9×10 ⁻¹²	14	5.6×10 ⁻¹⁷	1	
S34	429	-341	3×10 ⁻⁴	3×10 ⁻⁸	n.m.	n.m.	n.m.	n.m.	n.m.	n.m.	n.m.	7.1×10 ⁻¹²	13	9.3×10 ⁻¹⁷	2	
S35	462	-383	3×10 ⁻⁴	2×10 ⁻⁸	n.m.	n.m.	n.m.	n.m.	n.m.	n.m.	n.m.	1.9×10 ⁻¹¹	12	2.4×10 ⁻¹⁷	3	

Sample	Leaching time (days)	E _h (mV)	H ₂ (M)	O ₂ (M)	Ti (M)	Mn (M)	Fe (M)	Co (M)	Ni (M)	Cu (M)	Zn (M)	U _{tot} (M)	Error U _{tot} (%)	²²⁵ Ra (M)	Error ²²⁵ Ra (%)	Remarks:
	462	Changed atmosphere from 0.16 bar H ₂ to 3.1 bar Ar														
S36	463	-298	1×10 ⁻⁵	5×10 ⁻⁸	n.m.	n.m.	n.m.	n.m.	n.m.	n.m.	n.m.	1.4×10 ⁻¹¹	14	5.5×10 ⁻¹⁷	2	
S37	468	-331	6×10 ⁻⁶	2×10 ⁻⁸	n.m.	n.m.	n.m.	n.m.	n.m.	n.m.	n.m.	1.7×10 ⁻¹¹	9	3.9×10 ⁻¹⁷	2	
S38	548	Rinse			2×10 ⁻⁶ ± 1×10 ⁻⁶	n.m.	n.m.	n.m.	n.m.	n.m.	n.m.	5.7×10 ⁻¹²	17	4.9×10 ⁻¹⁸	5	Ti analysed at CTH
S39	548	-352	1×10 ⁻⁵	6×10 ⁻⁸	n.m.	n.m.	n.m.	n.m.	n.m.	n.m.	n.m.	1.1×10 ⁻¹¹	12	5.5×10 ⁻¹⁷	2	
	554	Purged the autoclave with Ar at 3.1 bar pressure														
S40	568	-444	4×10 ⁻⁶	8×10 ⁻⁸	n.m.	n.m.	n.m.	n.m.	n.m.	n.m.	n.m.	9.1×10 ⁻¹²	16	1.5×10 ⁻¹⁷	3	
	670	Sampled a gas sample from the autoclave														
S41	743	Rinse			n.m.	n.m.	n.m.	n.m.	n.m.	n.m.	n.m.	n.m.		n.m.		
S42	743	-319	8×10 ⁻⁶	4×10 ⁻⁸	n.m.	n.m.	n.m.	n.m.	n.m.	n.m.	n.m.	n.m.		n.m.		
S43	789	-157	1×10 ⁻⁵	3×10 ⁻⁸	n.m.	n.m.	n.m.	n.m.	n.m.	n.m.	n.m.	n.m.		n.m.		
S44	789	Rinse			n.m.	n.m.	n.m.	n.m.	n.m.	n.m.	n.m.	n.m.		n.m.		
S45	818	Rinse			n.m.	n.m.	n.m.	n.m.	n.m.	n.m.	n.m.	n.m.		n.m.		
S46	818	-139	1×10 ⁻⁵	6×10 ⁻⁸	n.m.	n.m.	n.m.	n.m.	n.m.	n.m.	n.m.	6.2×10 ⁻¹²	13	6.3×10 ⁻¹⁷	2	
	823	End of experiment														

< d.l. means below detection limit.

n.m. means not measured.

— means negative values due to instability of the sensor due to fast change of initially applied pressure.

rinse means the first portion of solution that remained in the tubing since last sampling.

n.r. means no reading of the value.

» > 10×t_{1/2}, the radionuclide had decayed due to more than ten half-lives since between sampling and measurement.

The most interesting element to follow is uranium and the concentrations of uranium in the leachate sampled at different leaching times are given in Table 2-9 and Figure 2-19.

It can be concluded that the concentration of uranium did not change when 2 mM HCO_3^- was added to the autoclave after 114 days of leaching, as would have been expected if UO_2 had been oxidised/dissolved and sorbed on the autoclave walls as UO_2^{2+} . Additionally, it could be concluded that the radiolytically produced O_2 during the whole experimental period of 823 days had no impact on the UO_2 dissolution despite the low $[\text{H}_2]_{\text{dissolved}}$ concentration of $1 \times 10^{-5} \text{ M}$ for a period of 361 days. As a matter of fact, a $[\text{H}_2]$ of $1 \times 10^{-5} \text{ M}$ can be considered, as the highest $[\text{H}_2]$ needed to inhibit oxidation of UO_2 giving a surface dose rate of 680 Gy/h and an average dose rate of 82.8 Gy/h in the range of 0–35.2 μm from the UO_2 surface.

Assuming that all radiolytically produced H_2O_2 was converted to O_2 the calculation shows that a $[\text{O}_2]_{\text{dissolved}}$ of $1 \times 10^{-2} \text{ M}$ should be reached within 450 days of irradiation (the time until the autoclave was purged with Ar). The total amount of radiolytically produced O_2 during the whole experiment was $6.3 \times 10^{-4} \text{ mol}$. It is clear that if all of this oxygen could oxidise UO_2 one would get a $[\text{UO}_2]$ of $1.3 \times 10^{-3} \text{ M}$, above the solubility limit of schoepite. On the other hand, the measured $[\text{O}_2]_{\text{dissolved}}$ was in the range of 10^{-9} – 10^{-8} M , Table 2-9.

The reason that the ^{233}U decay daughters were studied intensively is that one of the daughters is ^{225}Ra . It could be concluded from the ^{233}U doped UO_2 pellet characterisation that ^{225}Ra would be present in the pellet and since the chemical behaviour of Ra and Sr is similar the study of the corrosion rate of Ra could give hints on the behaviour of Sr in an old fuel. The concentration of ^{225}Ra in the leachate was obtained by calculation of the concentration of ^{225}Ac obtained from the α -spectrometry, Figure 2-11. The decay scheme of the ^{233}U -chain is shown below:

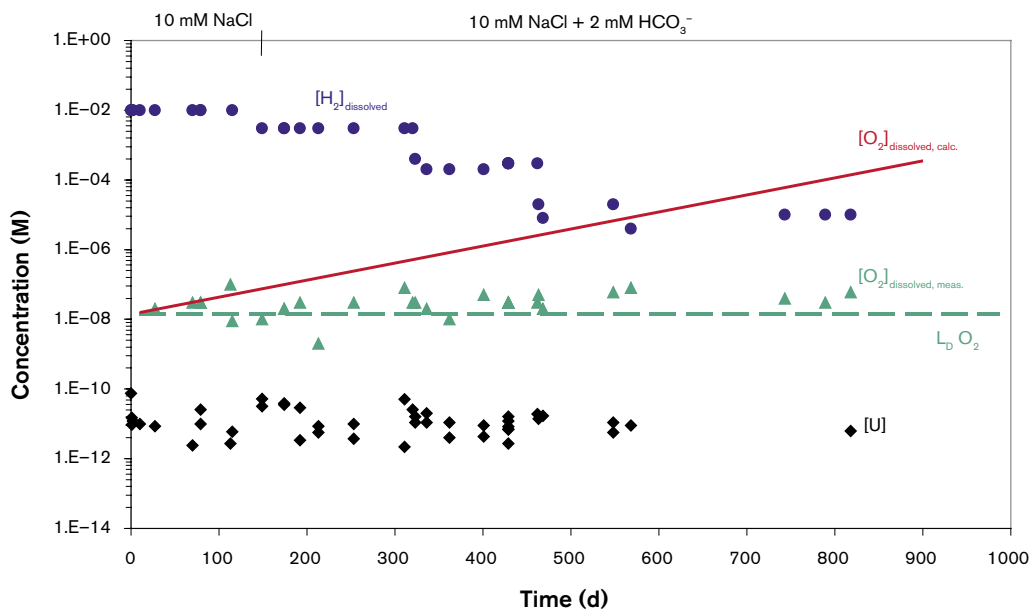
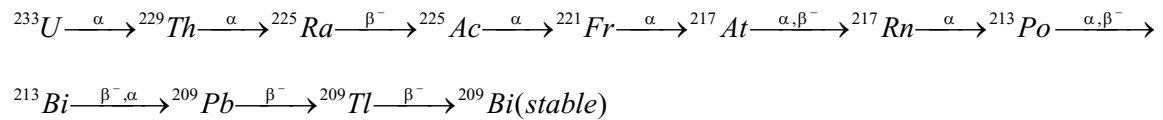


Figure 2-19. Measured H_2 , O_2 and total U concentrations in the leachate as a function of time. The red line represents the calculated radiolytic oxygen concentrations.

^{233}U ($t_{1/2}$ 1.594×10^5 years) and ^{229}Th are not in secular equilibrium, since the ^{233}U powder used to fabricate the UO_2 pellet was separated from the ^{233}U decay daughters only 38 years ago. On the other hand, the decay daughters following the ^{229}Th ($t_{1/2}$ 7.345×10^3 years) exists in a steady state. The proof for this is that the activity ratio of the decay daughters is close to 1, Table 2-8. Using α -spectrometry it is not possible to measure β^- -decaying radionuclide and therefore we must make the qualified guess that it is Ra^{2+} that is leached from the UO_2 -pellet rather than Ac^{3+} . On the other hand, one could argue that ^{229}Th (the parent of ^{225}Ra) is leached from the pellet, but this is highly unlikely since Th forms strong bonds with O-atoms in the UO_2 lattice. Additionally, Th is not redox sensitive like U and no ^{229}Th could be found in the NdF_3 precipitated leachate prepared and counted directly after sampling. Finally, the absence of ^{229}Th and its decay daughters in leachates that have been standing for a month or longer give a strong indication that no ^{229}Th is leached from the pellet. On the basis of the arguments given above, Ra is leached from the UO_2 pellet and the values for ^{225}Ac were used to calculate the concentration of ^{225}Ra in the leachate (Table 2-9). The $[\text{Ra}]_{\text{leachate}}$ was used to calculate the molar ratio of $^{233}\text{U}/^{225}\text{Ra}$ in the leachate and was found to be $\sim 3.3 \times 10^4 \pm 6 \times 10^3$ (Table 2-9) while the same ratio in the pellet is $\sim 1.1 \times 10^9 \pm 3.7 \times 10^7$ (data from the characterisation section on ^{233}U doped UO_2 pellets). It can be concluded that the concentration of radium is $3.3 \times 10^4 \pm 6 \times 10^3$ times higher than expected from a congruent corrosion of the UO_2 pellet. The preferential leaching is probably due to the fact that Ra is released by other processes as the recoil of Ra out of the grain because of the decay of Th. Despite the low solubility product of RaCO_3 (in the range of 10^{-10}M) and a relatively high $[\text{CO}_3^-]$ no RaCO_3 will precipitate due to the low $[\text{Ra}]$ of $\sim 5 \times 10^{-17}\text{M}$.

The pH of the sampled solutions was measured with a combined pH electrode with saturated KCl as reference (WTW Sentix Mic, Germany) and a pH-meter (WTW pH340/ION, Germany). The pH-electrodes were calibrated with two standard buffer, pH 4.01 and 9.21, at the ambient temperature of 19°C . A minimum volume of 0.75 ml of the sample was necessary to cover the tip of the electrode. The results of the measurements are given in Table 2-10. A comparison of the pH between the 10 mM NaCl solution added to the autoclave and the leachate sampled within the first 112 days of experiment showed no changes (pH 7). After 112 days of leaching the leachate composition was changed to 10mM NaCl + 2mM HCO_3^- and also in this case no significant changes of pH could be observed when comparing the pH of the loading solution (pH 8.5) and the leachate sampled after different leaching time. It can therefore be concluded that the $[\text{H}^+]$ concentration in the leachate did not change due to radiolysis or UO_2 corrosion (calculated stoichiometric contribution is not measurable).

Table 2-10. The pH of the solutions added to the autoclave and the leachates sampled from the autoclave.

Sample	pH
10 mM NaCl	6.5 ± 0.1
S1	7.0 ± 0.1
S5*	8.3 ± 0.1
Changed leachate composition	
10 mM NaCl + 2 mM HCO_3^-	8.5 ± 0.1
S14	8.4 ± 0.1
S24	8.4 ± 0.1
S35	8.2 ± 0.1
S42	8.1 ± 0.1

*Problem with stability of electrode due to small amount of solution.

The temperature inside the autoclave varied with the seasons being warmer, up to 27°C, during the winter and considerably lower during the summer (20°C) when the air-condition was on. The average temperature during the whole experiment was $22.5 \pm 3^\circ\text{C}$.

The changes of the total pressure in the autoclave are shown in Figure 2-20. It can be seen that the total pressure was never lower than 1.5 bar (above the ambient pressure) to avoid O₂ intrusion into the autoclave.

Post-characterisation of the pellet

A post-characterisation of the UO₂ pellet was made to determine its state after the leaching. The UO₂ pellet was investigated by XPS (X-ray photoelectron spectroscopy) to determine the U(IV)/U(VI) ratio of the UO₂ pellet surface, scanning electron microscope (SEM) to determine the structural changes of the surface UO₂ surface and SEM-EDX (energy dispersive x-ray spectrometer) to investigate the influence of the deposits of TiO₂.

XPS-analysis of the pellet

The container with the UO₂ pellet was introduced into a bag connected to the entrance chamber of the XPS. The pellet, now fixed in the XPS-holder, was removed from its container. In order to remove the oxygen from the bag and thereby avoid oxidation of the UO₂, the bag was five times alternating flushed with Ar and vacuum pumped. Finally, the UO₂ specimen was transferred to the OMICRON spectrometer under inert atmosphere. The spectrometer was evacuated under high vacuum (6×10^{-8} Torr). The UO₂ pellet was in the spectrometer within 2 hours after the opening of the autoclave. It remained in the vacuum chamber for 2 hours to get rid of the last amount of water inside the pores of the pellet. A spot of $1 \times 1 \text{ mm}^2$ was analysed by X-ray photoelectron spectroscopy, using Mg K_α radiation [COB/HAV 2002]. We analysed the upper and bottom side of the specimen. The upper side, as located in the autoclave, gave a spectrum that nicely corresponded to TiO₂. The overview spectra, Figure 2-21, showed mainly O, Ti, C, Na and U. The U-4f signal is surprisingly small, showing the UO₂ sample to be covered by an over-layer. The main metallic element in the over-layer is Ti. The Ti-2p detail spectra, Figure 2-22, show two types of Ti. The doublet at low binding energy ($2p_{3/2}$ at 459.3 eV) is typical for TiO₂.

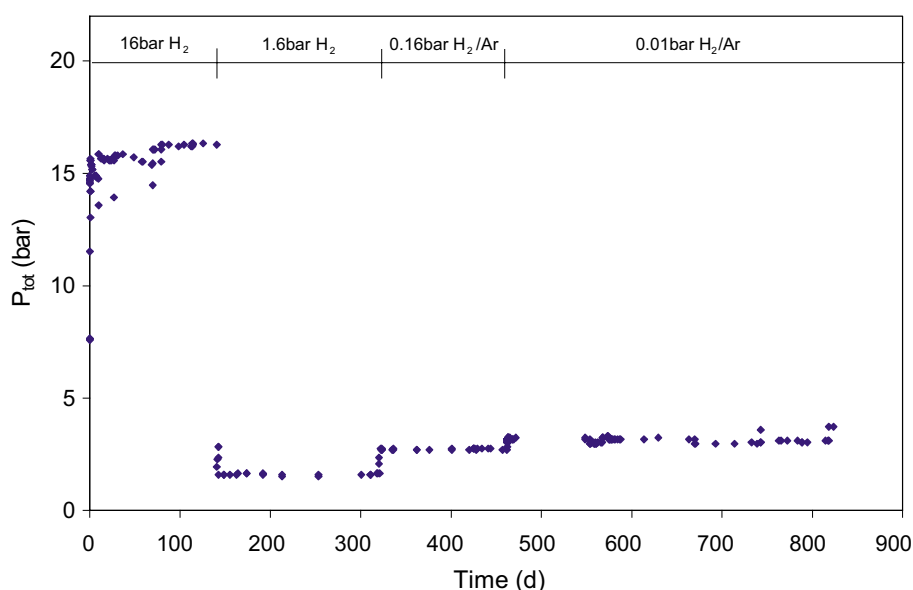


Figure 2-20. Absolute pressure measured in the autoclave with a digital manometer (PARR Instruments, USA) during the experiment.

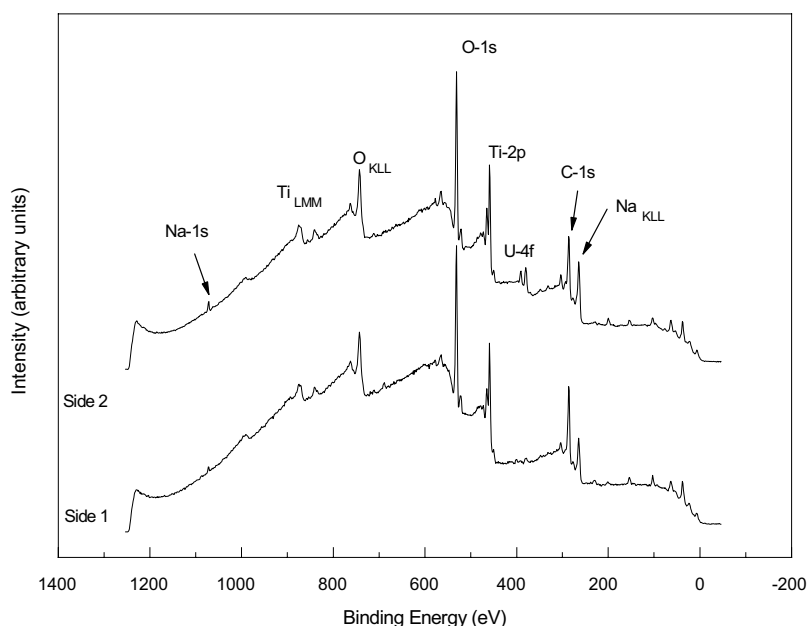


Figure 2-21. The overview XPS spectra of the upper UO_2 pellet surface (spectra denominated “side 1”, that faced upwards in the autoclave during the experiment and the XPS spectra for “side 2” that faced the bottom of the autoclave).

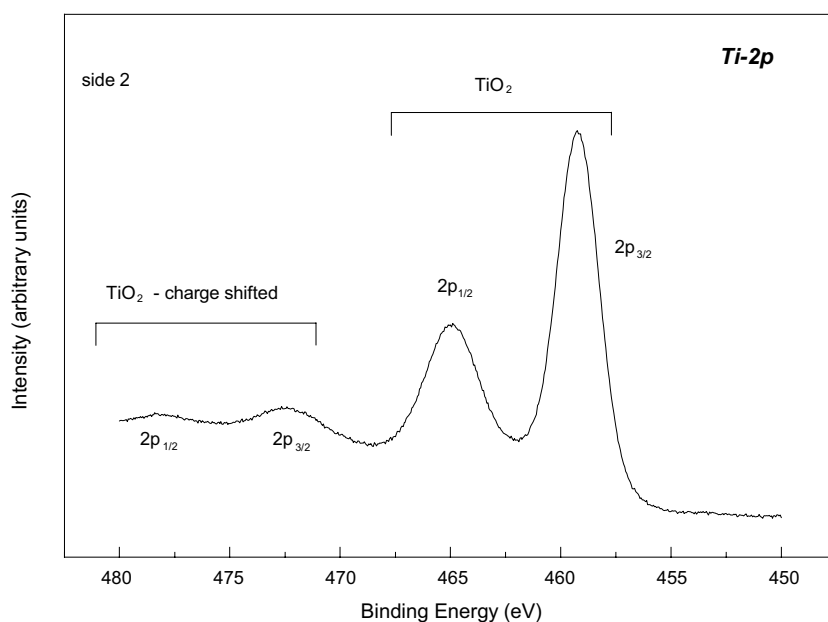


Figure 2-22. The Ti-2p spectra of the UO_2 pellet surface that faced the bottom of the autoclave during the experiment.

The doublet at high binding energy ($2p_{3/2}$ at 472.5 eV) is charge shifted – its binding energy does not correspond to any chemical species. For the shifted signal we can in fact not be sure, if it is really TiO_2 . But it is reasonable to assume this, because its strong charging shift (13.25 eV) shows that this type of Ti is an insulator. Quite interestingly, we did not observe such charge shifted component for the other surface elements (C, U) except for O. Thus there seem to be insulating regions of pure TiO_2 on the surface, presumably grains of TiO_2 . These grains are supported on a continuous thin over-layer of TiO_2 , thin enough to not give any charging effects.

After turning around the pellet and analysing the pellet surface that had faced the bottom of the autoclave (“side 2”), a weak signal of UO_2 was detected, while on the other side (“side 1”) it was missing. A continuous TiO_2 grain layer covered the “side 1”. The UO_2 line, detected on “side 2”, is typical for stoichiometric UO_2 , with a $4f_{5/2}$ at 390.8 eV binding energy, accompanied by a satellite at 387.4 eV, Figure 2-23. The C-1s signal at 285.6 eV comes mainly from free carbon, Figure 2-24. There is only a weak contribution from carbonates, which should appear around 289–291 eV (they are responsible for the slight shoulder in that region). All the other lines in that region are attributed to Na Auger emissions and a K-1s line.

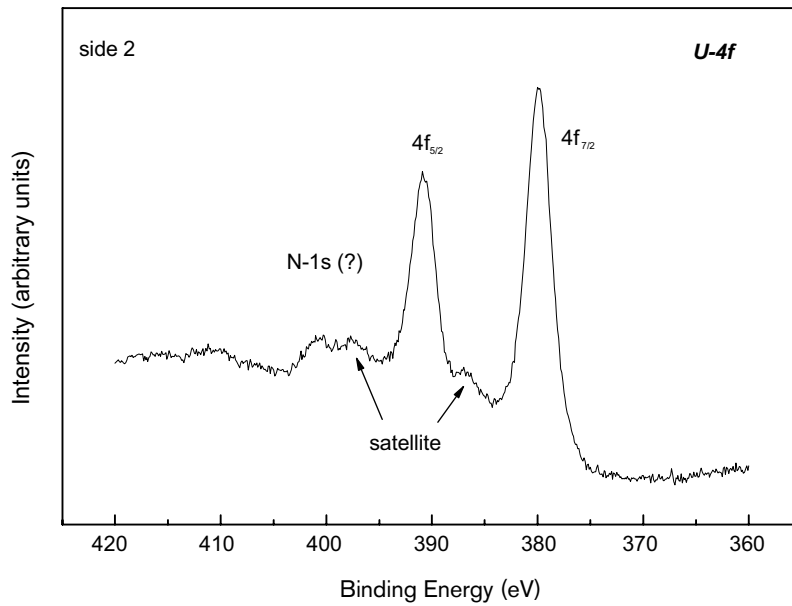


Figure 2-23. $U-4f$ part of the XPS spectra acquired from the UO_2 pellet surface that had faced the bottom of the autoclave. Both the $4f_{5/2}$ and the $4f_{7/2}$ peaks could be used for de-convolution of the peak to determine the $U(\text{IV})/U(\text{VI})$ ratio.

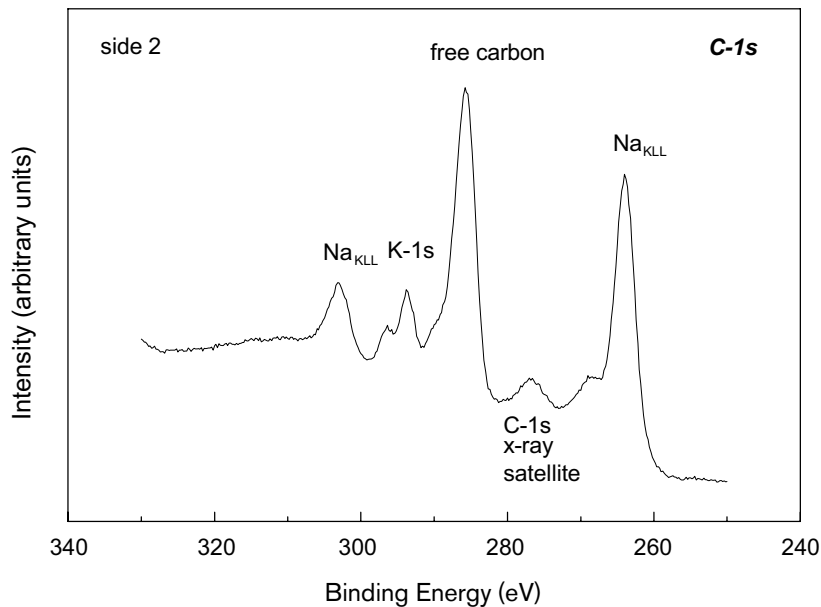


Figure 2-24. XPS spectra of the UO_2 pellet surface facing the bottom of the autoclave during the experiment.

It could be concluded that the UO_2 pellet surface was stoichiometric $\text{UO}_{2.00}$. This means that the careful dislodging from the autoclave, the drying process and the transport did not contribute to any oxidation of the pellet surface. It can therefore be concluded that the UO_2 surface was not oxidized during the whole experimental period including the period when the pellet was in contact with a very low H_2 concentration (10–13 mbar H_2).

The XPS spectrum exhibited a clear presence of TiO_2 on the both pellet sides but mostly on the side facing upwards due to the fact that when the stirring stopped the TiO_2 particles started to deposit. The amount of TiO_2 deposits was clearly less on the surface facing downwards in the autoclave and made it possible to determine the U(IV)/U(VI) ratio.

SEM-EDX analysis of the pellet

Directly after the XPS analysis the pellet was transferred to a Scanning Electron Microscope (SEM) to look for macroscopic changes of the UO_2 pellet and changes of the surface structure. The SEM used in this study was a Philips 515 with an Energy Dispersive X-Ray (EDX) device from TRACOR Northern. It was operated at a voltage of 25 kV and a spatial resolution of about 3 nm could be achieved. The acquisition time for the EDX spectra was 100 seconds. The EDX quantitative analysis was performed using the PAP correction (standard) method. The specimen thickness contributing to the EDX signal is typically of the order of 2–3 μm . An electron back-scattered (BSE) detector was used to visualise element (Z number) contrast of the different phases present. Using the EDX detector it was possible to estimate the coverage of the TiO_2 deposits on the pellet surfaces.

Under the SE microscope two different structural damages of the pellet could be observed, Figure 2-25. Firstly, the pellet surface that had pointed downwards in the autoclave showed

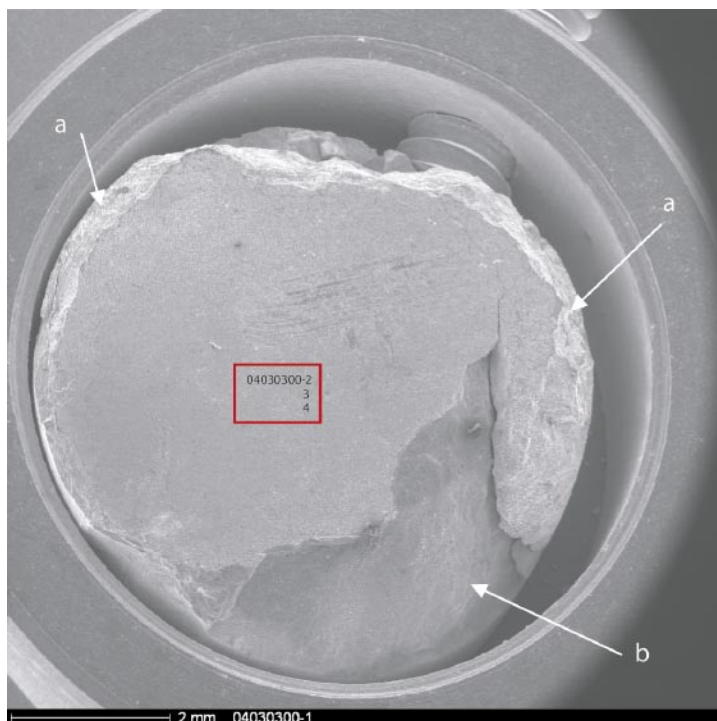


Figure 2-25. SEM picture of the pellet that had faced downwards in the autoclave. It can be noticed that some parts are broken off. The small edges broken off on the right and left side of the pellet (marked “a”) are due to handling when the pellet was mounted in the pellet holder at the start of the experiment. The large pieces missing (marked “b”) were broken off during handling just before the XPS analysis because the screw, seen at the top right hand, was tightened too hard the causing the breaking of the UO_2 pellet.

broken off edges at the circumference of the UO_2 pellet. The edges were broken off during the mounting of the pellet into the autoclave pellet holder at the start of the leaching experiment. The holder was simply too tight for the pellet and a light force needed to be applied to fix the pellet in the holder.

Secondly, a significant piece of the pellet was broken off after the leaching experiment. This happened when turning around the pellet and remounting it during the XPS analysis. Since this operation was made inside a bag, the force applied to tighten the screw was too large and a piece of the UO_2 pellet was lost. This had the consequences that no mass balance of the UO_2 pellet before and after the leaching could be made. Finally, no significant changes could be observed comparing the SEM pictures of the centre of the pellet before and after the leaching experiment, Figure 2-26 and the SEM picture of the pellet in the UO_2 pellet characterization part.

The SEM-EDX spectra of the general pellet surface that had faced the bottom of the autoclave (the pellet area showed in Figure 2-26, localised in the square in Figure 2-25) demonstrate that it was covered with TiO_2 deposits to ~ 30 at-%, Figure 2-27.

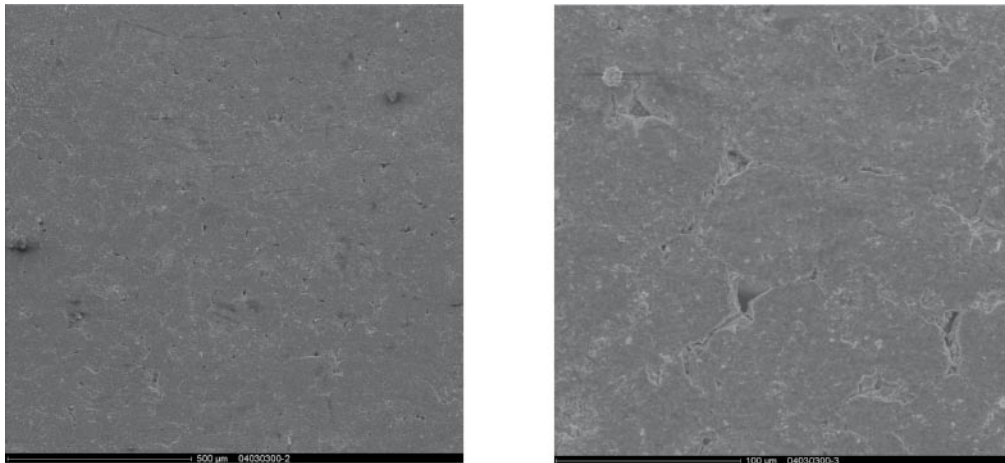


Figure 2-26. SEM picture of the part of pellet, marked in the Figure 2-25 as 04030300-2 and -3, that had faced downwards in the autoclave in two different magnifications. The left picture is taken in magnification 1,000 x and the right with a magnification of 4,000 x.

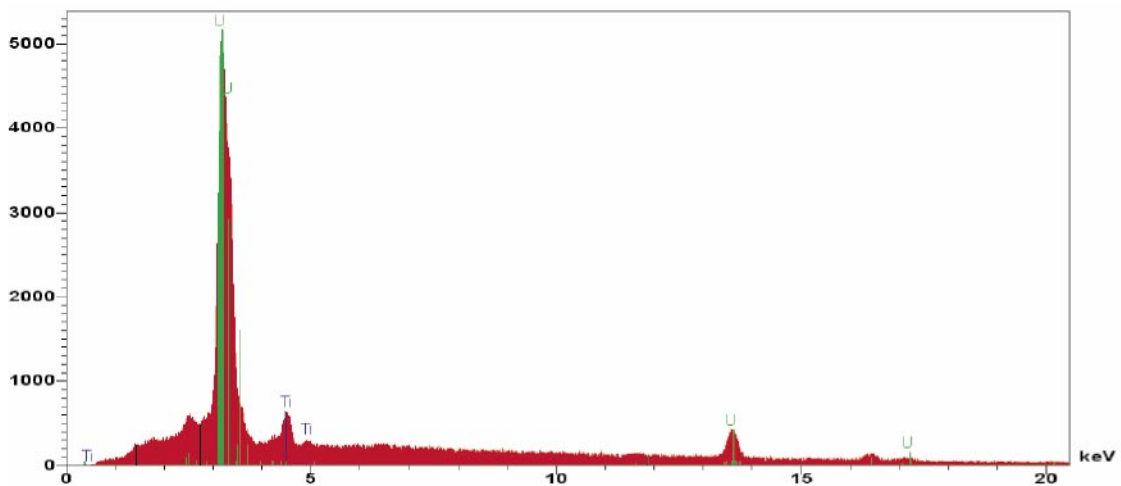


Figure 2-27. SEM-EDX spectra taken of the general surface of the pellet that had faced downwards in the autoclave. It can clearly be seen that U dominates the overall composition.

The surface was investigated at higher magnification and revealed small particles loosely attached to the UO_2 surface. These particles had different sizes and shapes, Figure 2-28. A SEM-EDX analysis of the four particles investigated showed that the UO_2 particles on the surface were generally much larger (4–12 μm) and significantly more dense than the Ti deposits (1–2 μm). It also confirmed that the particles either consisted of U or Ti and not of a mixture. During the SEM analysis it could be observed that the Ti particles produced a charging effect, a clear evidence of poor electrical conductivity indicating that the Ti particles partly consisted of an insulating outer layer, most probably TiO_2 .

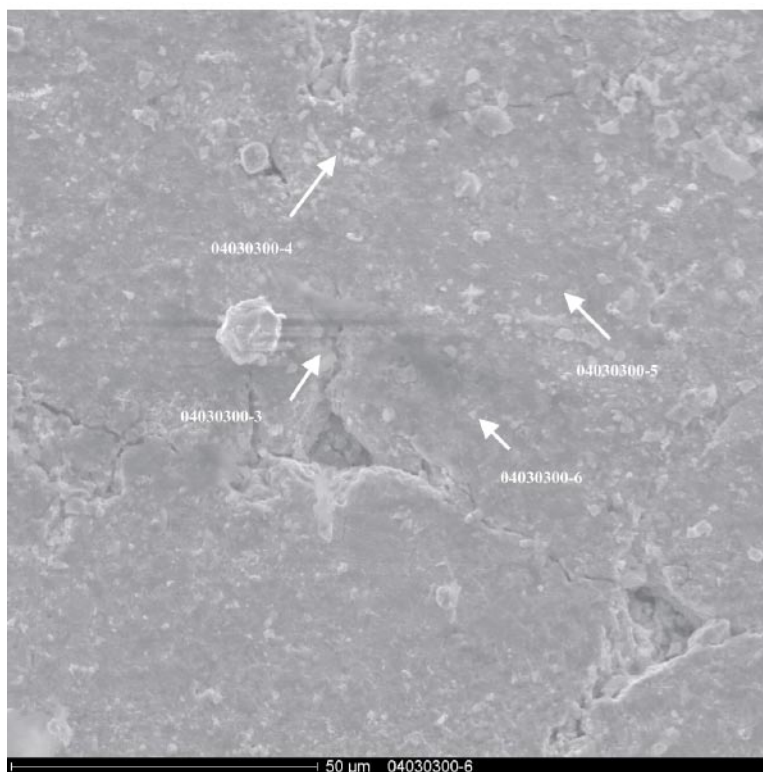


Figure 2-28. Magnifications of the centre of the UO_2 pellet area seen in Figure 2-26. The four types of particles on the surface were magnified and a SEM-EDX spectrum was made of each particle, shown in Figures 2-29–2-32.

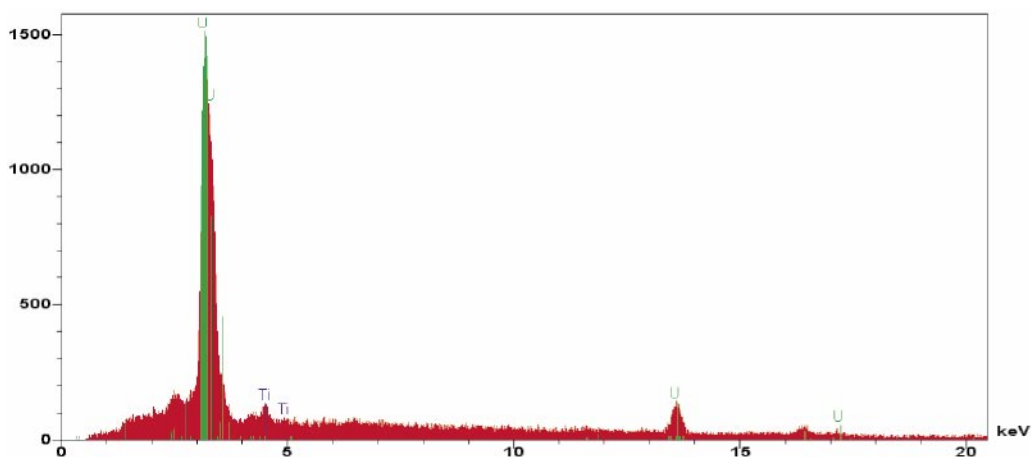


Figure 2-29. SEM-EDX spectra taken of particle 04030300-3 located on the surface of the pellet that had faced downwards in the autoclave, see Figure 2-28. It can clearly be seen that the particle consists of U (85 at-%) while the Ti peak (18 at-%) is at background level.

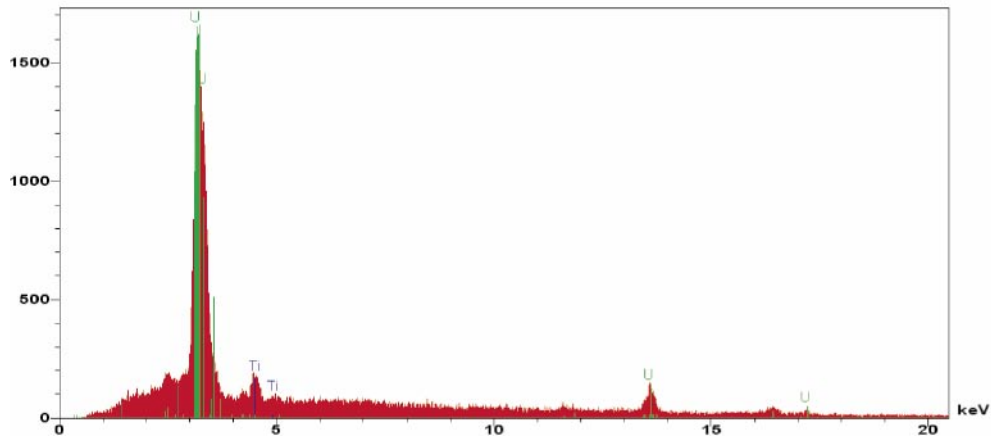


Figure 2-30. SEM-EDX spectra taken of particle 04030300-4 located on the surface of the pellet that had faced downwards in the autoclave, see Figure 2-28. The particle consists of U (73 at-%) and the Ti peak (27 at-%) corresponds to background level.

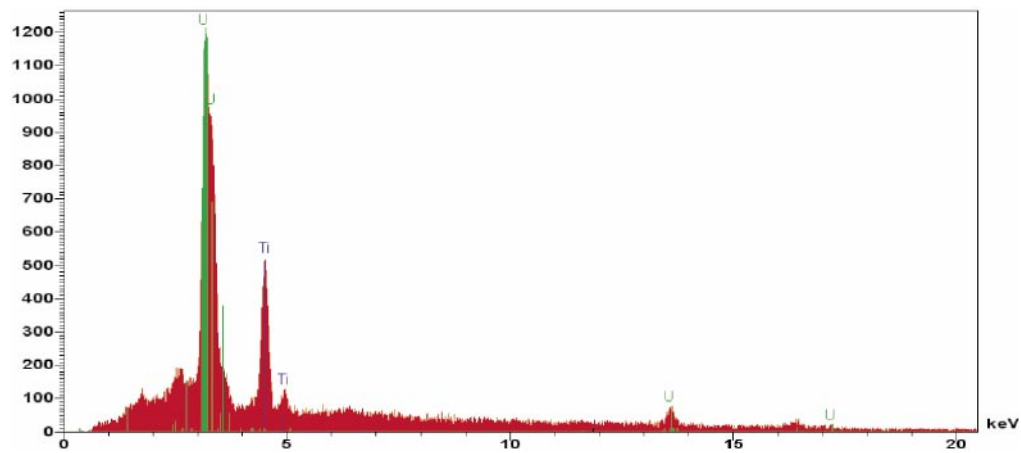


Figure 2-31. SEM-EDX spectra taken of particle 04030300-5 located on the surface of the pellet that had faced downwards in the autoclave, see Figure 2-28. The particle consists mainly of Ti (61 at-%) and the scatter from the UO_2 surface contributes to the background in the UO_2 peak (39 at-%).

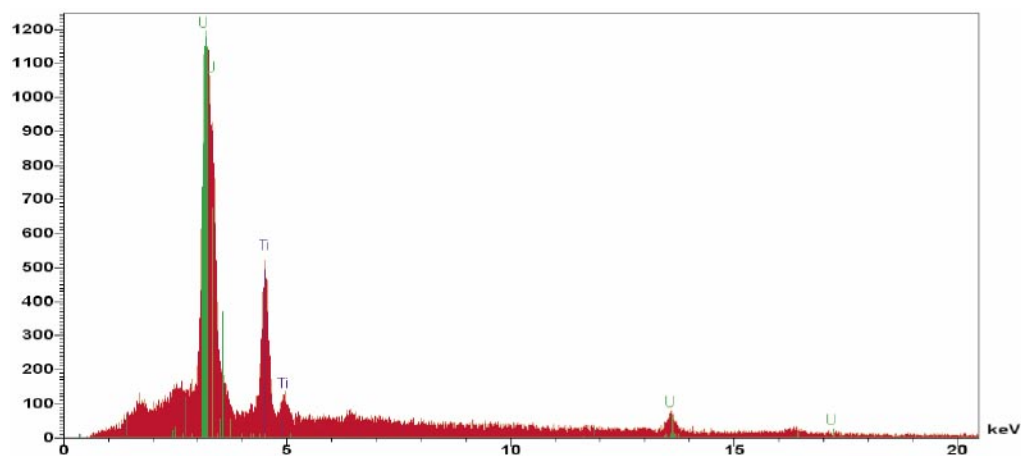


Figure 2-32. SEM-EDX spectra taken of particle 04030300-6 located on the surface of the pellet that had faced downwards in the autoclave, see Figure 2-28. Also this particle consists mainly of Ti (61 at-%) while the scatter from the UO_2 surface contributes to the background in the UO_2 peak (39 at-%).

Analysis of the deposits in the leaching vessel

The deposits encountered in the vessel after a leaching experiment are produced/introduced through different processes; (a) abrasion of the vessel by the stirrer during stirring, (b) UO_2 particles attached onto the UO_2 pellet before loading, (c) by handling of the UO_2 material in the vessel during loading, (c) precipitation of U(VI) phases under oxidizing conditions or of small amounts of U(IV) hydroxides under reducing conditions. It is important to investigate the distribution of the U and any potential influence of abraded material on the UO_2 corrosion process. The deposits obtained from the bottom of the autoclave were therefore analysed by different techniques (α -autoradiography, SEM-EDX, XRD and SIMS) to determine the chemical composition and physical state of the U and the Ti deposits.

α -autoradiography

The spatial distribution of the U-activity at the bottom of the autoclave was investigated by pressing a α -sensitive cellulose nitrate film (CN85, KODAK, France) against the bottom of the autoclave. Two different surface areas of the bottom were searched. The first film, denominated “UP”, covered an area of 21.6 cm^2 ($27 \times 80 \text{ mm}$) and was irradiated for 118.2 h. The second film “UP2” faced an autoclave surface area of 22.4 cm^2 ($28 \times 80 \text{ mm}$) and was irradiated for 99.3 h. After the exposure the film was etched in 6.5 M NaOH at 60°C for 16 min. Subsequently, the etched film was rinsed for 15 min in milliQ-water. In order to identify the intensive α -radiation spots the etched film was investigated with an optical microscope (Leica 12×5) equipped with a camera. It could be concluded that the ^{233}U activity was heterogeneously distributed on the autoclave surface, Figure 2-33. A large number of spots could be identified $> 28 \text{ spots/cm}^2$.

In order to be able to count individual α -tracks the films were searched with a Zeiss AxioPlan 2 microscope, typically with a magnification of 5 x and 10 x. The number of α -tracks in each spot varied between 125 (1 mBq) and $> 100,000$ (1 Bq). The distribution of spots on an area of 7.04 cm^2 gave 23 large spots, 32 medium size spots and 142 small spots. Between the spots the areas contained only a few α -tracks in the range of $0.02\text{--}0.05 \text{ Bq/cm}^2$.



Figure 2-33. α -autoradiography of the first irradiated CN85-film “UP”. The picture shows that most of the α -activity is in form of U-particles. The U-particles have different grain sizes, proportional to the ^{233}U activity. U-particles located at some distance from the film give blunt spots.

SEM-EDX analysis of the deposits

A very informative and quick method to determine the composition of the deposits from the bottom of the autoclave is to retrieve some of the deposits on a small planchette and analyse it using a SEM coupled to an EDX detector. The same SEM-EDX equipment was used as described above.

The area searched on the planchette contained only a few UO_2 particles (approximately 1 particle per 5 mm^2) among the large amount of Ti particles. In Figure 2-34 one of the found UO_2 particles is shown in SE-mode and BS-mode (back-scatter mode optimised for detection of U). The SE-picture shows the sharp edges of the $10 \mu\text{m}$ -size UO_2 particle indicating no corrosion. The general size of the detected UO_2 particles varied in the range of 1– $10 \mu\text{m}$ and confirmed the results from the α -autoradiography.

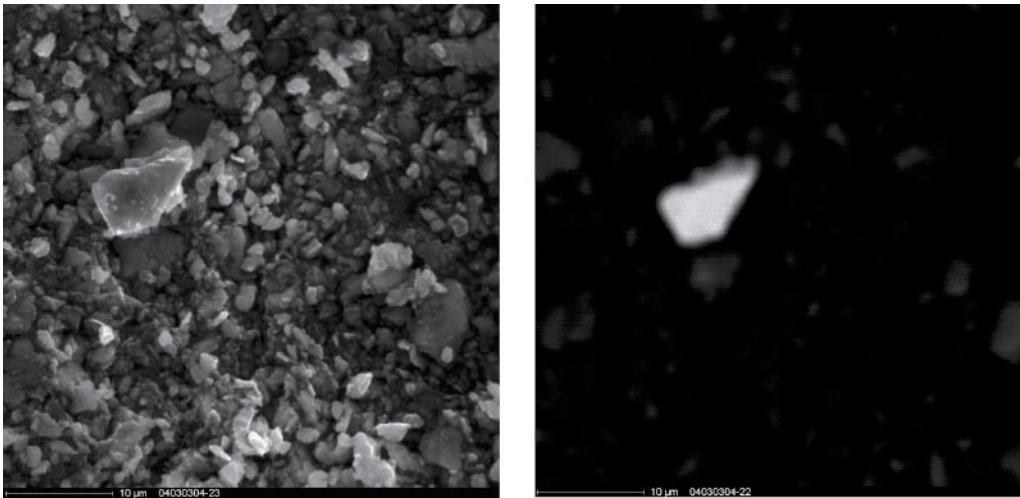


Figure 2-34. SE-picture of a UO_2 particle detected among the Ti-particles in the deposit (left) and the same particle in the BS-mode (right).

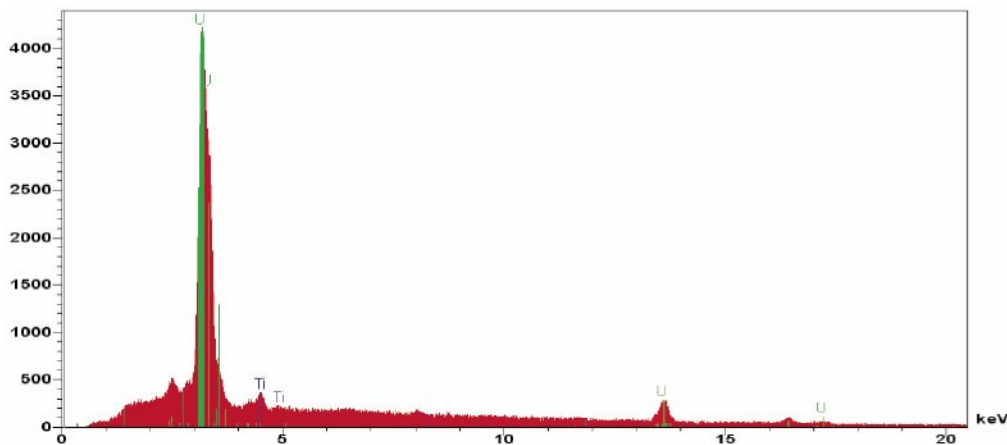


Figure 2-35. SEM-EDX spectrum corresponding to the UO_2 particle shown above in Figure 2-34. The acquisition time was 100 second.

The corresponding SEM-EDX spectrum for the UO_2 particle is shown in Figure 2-35 shows and exclusively verify the uranium content. The minor contribution of Ti in the spectra is due to the fact that it is difficult to prevent scattered photons from the large amount of Ti particles on the planchette from reaching the EDX-detector. The picture also shows the large number of Ti particles with a size of around $1\ \mu\text{m}$. The corresponding EDX-spectra of the Ti-particles is shown in Figure 2-36.

XRD of the deposits

The deposits from the bottom of the autoclave were analysed with a standard X-ray diffraction apparatus equipped with the strongest possible x-ray source and a collimator, which makes it possible to analyse small samples, Figure 2-37. The X-ray are produced from electron irradiation of a Mo-target giving X-rays of Mo $\text{K}_{\alpha 1}$ with a wavelength of $0.70926\ \text{\AA}$, a beam diameter of $100\ \mu\text{m}$ and an intensity of 10^7 photons/s. The calibration of the XRD was made using a LaB_3 prepared in the same geometry as the sample. Deposit

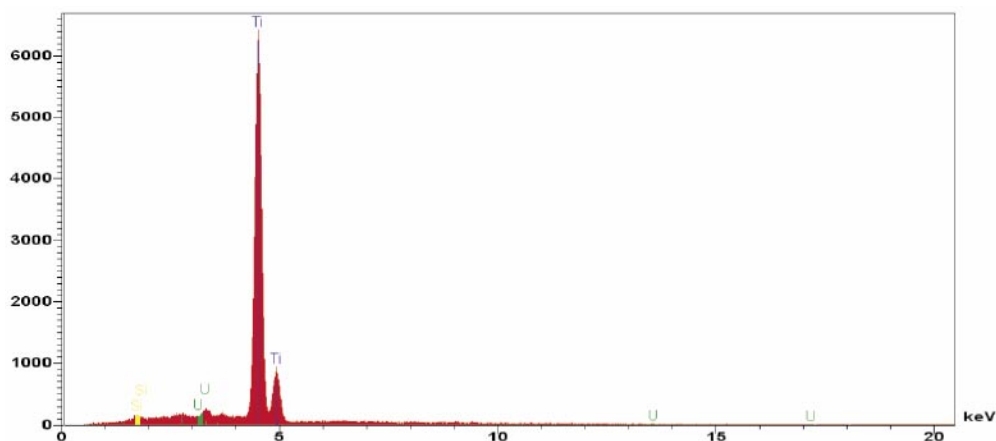


Figure 2-36. SEM-EDX spectrum of the Ti-particles on the planchette. The acquisition time was 100 second.



Figure 2-37. Set-up for micro-XRD used to determine the composition of the deposits from the bottom of the autoclave.

from the bottom of the autoclave was carefully collected and transferred to a container. A small amount (50 μg) of the powder was mixed with a two-component glue and transferred to a micro tube (diameter 100 μm). The glue-powder mixture was sucked up into the micro-capillary to a length of 200 μm , dried and fixed in the XRD, Figure 2-38. The sample was measured for 30 min. Using the obtained spectrum, Figure 2-39, and the library database the following conclusions could be made. Firstly, no UO_2 crystal phase could be found. Secondly, a clear Ti-metal hexagonal phase could be identified ($a = 2.950 \text{ \AA}$, $c = 4.686 \text{ \AA}$). A coarse estimation is that the Ti-metal content is about 10–15% of the total amount. This estimation is based on the fact that a pure Ti-metal would give approximately 1,000 counts in the highest abundant peak during a 30 min measurement. In our case we have got ~ 150 counts in 30 min. Thirdly, the Ti mixture spectrum contains clear evidence of an amorphous structure.

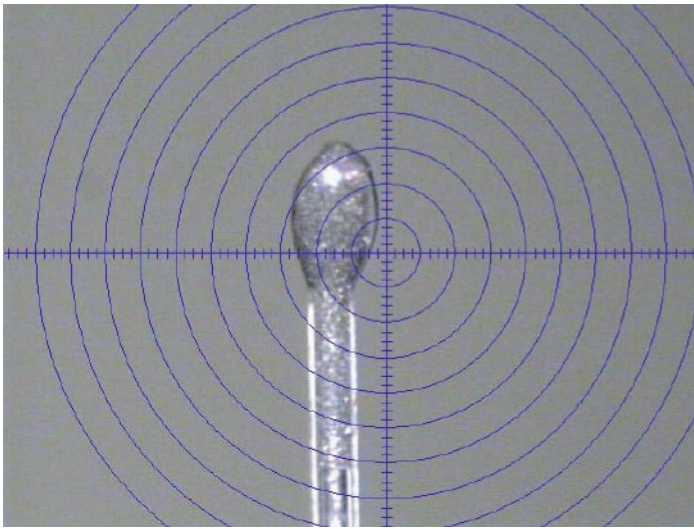


Figure 2-38. XRD2 Sample prepared for micro-XRD containing approximately 50 μg ($\sim 100 \mu\text{m}$ sphere) of the deposits collected from the bottom of the autoclave.

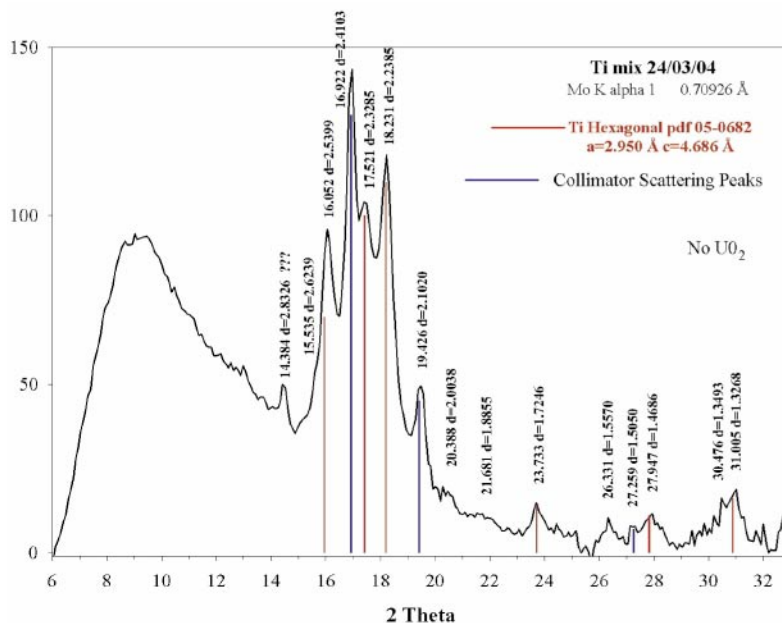


Figure 2-39. Micro X-ray diffraction spectrum of the autoclave deposits.

SIMS of the deposits

The deposits from the autoclave bottom were sampled and analysed by SIMS (Cameca IMS 6 F). The investigated surfaces were sputtered with O_2^+ ions. The sputtering time to obtain the different U ratios in the detected UO_2 particle was 600 s. A more detailed description of the SIMS and the analytical conditions is given in references [TAM/BET 1998, 2000, TAM/WAL 2001].

A graphite tape, attached to a SIMS holder, was pushed against the bottom surface of the autoclave forcing parts of the deposits to stick onto the tape. The sample was transferred to the SIMS and analysed with respect to U and Ti.

The surface was searched for ^{48}Ti , selected due to its high abundance and no mass interference from ^{48}Ca as there was no Ca present in the leachate. The signal from the oxides $^{48}Ti^{16}O$ and $^{48}Ti^{16}O_2$ was also analyzed. The relative intensities of the ^{48}Ti , $^{48}Ti^{16}O$ and $^{48}Ti^{16}O_2$ could not be determined, since no standard material was available for calibration.

Nevertheless, a qualitative estimation of the composition of the Ti deposits could be made. The results shown in Figure 2-40 indicate a strong signal from ^{48}Ti , a weaker signal from $^{48}Ti^{16}O$ and a weak signal from $^{48}Ti^{16}O_2$. Considering that the signals are not intensity calibrated, the results indicate that the Ti particles consist of metallic Ti in the middle, covered with a partly oxidized TiO layer and with a thin TiO_2 outer layer.

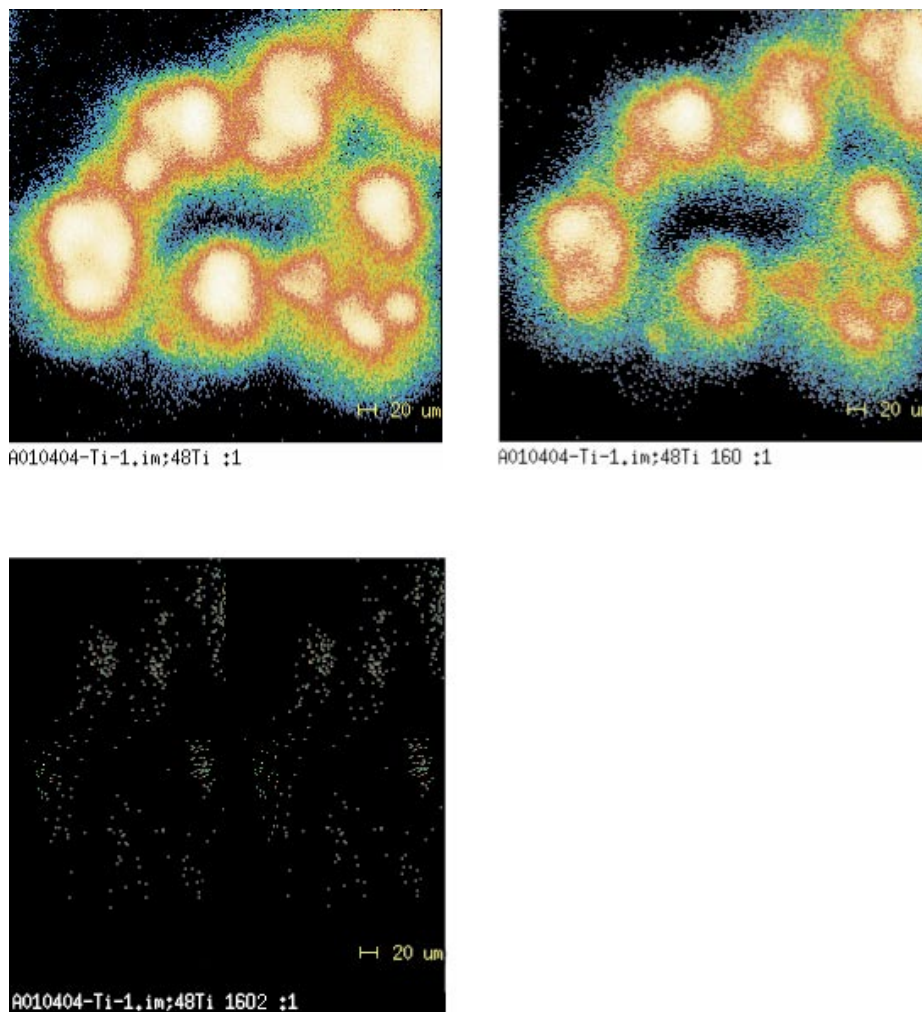


Figure 2-40. Images of a Ti deposit recovered from the bottom of the autoclave. The top left picture shows the image of the Ti concentration, the top right the TiO concentration and the lower left the TiO_2 concentration.

The mass settings were changed so that mass 238 was included and another surface area on the planchette was scanned, Figure 2-41. The area shows once again the dominating signals from Ti and TiO compared to TiO₂, but also the signal from mass 238 (²³⁸U) that is at the background level, clearly showing that no U was deposited on the TiO₂ particles.

It can be concluded that the U found in the deposits originates only from UO₂ particles which is also confirmed by α -autoradiography and α -track analysis.

The second aim of the SIMS analysis was to locate a UO₂ fragment and confirm its isotopic composition. This confirmation was necessary since the sampled leachate analysed by different ICPMS showed a ²³³U/²³⁸U ratio deviating from 0.1. The sampled surface on the planchette was searched and only one UO₂ fragment was found on a searched area of ~ 10 mm². The graphic images at mass 233 and 238 are shown in Figure 2-42. It is difficult to judge from the image if it is a single particle covered with Ti-particles or a U particle that was broken into several pieces during sampling (pressing the planchette against the autoclave bottom). The isotopic ratios: ²³³U/²³⁸U, ²³⁴U/²³⁸U, ²³⁵U/²³⁸U of the UO₂ particle are given in Table 2-11.

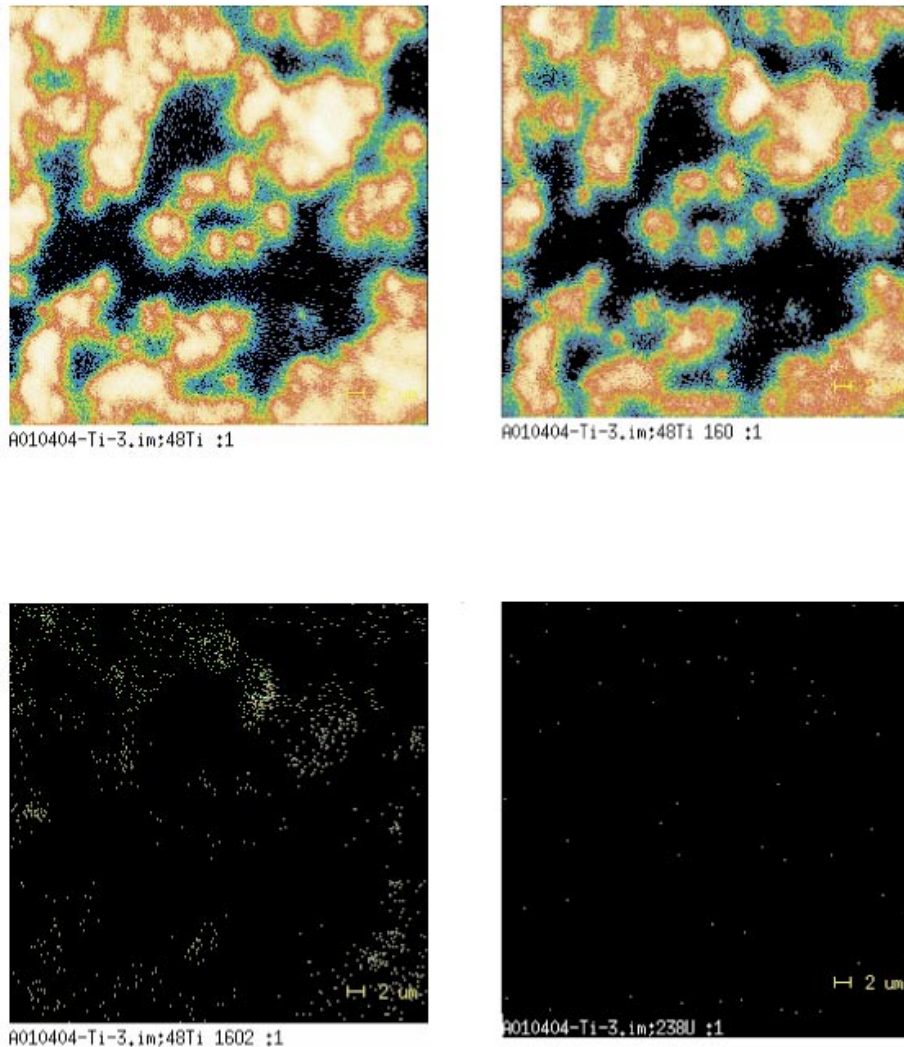


Figure 2-41. Images of a Ti particle found in the deposits recovered from the bottom of the autoclave. The top left picture shows the image of the Ti concentration, the top right the TiO concentration, the lower left the TiO₂ concentration and the lower right the ²³⁸U concentration. It can be seen that the signal at mass 238 is of the same level as the background.

Table 2-11. Overall isotopic ratios: $^{233}\text{U}/^{238}\text{U}$, $^{234}\text{U}/^{238}\text{U}$ and $^{235}\text{U}/^{238}\text{U}$ of an UO_2 particle found in the deposit obtained from the bottom of the autoclave. Each ratio was measured for 50 cycles.

Ratio	Mean value	S.D.	Mean error (%)
$^{233}\text{U}/^{238}\text{U}$	1.123×10^{-1}	2.4×10^{-3}	1.1
$^{234}\text{U}/^{238}\text{U}$	1.7×10^{-3}	2×10^{-4}	7.8
$^{235}\text{U}/^{238}\text{U}$	4.0×10^{-3}	3×10^{-4}	5.4

The isotopic composition of the UO_2 particle confirms the composition of the UO_2 pellet as described in the chapter on UO_2 pellet characterisation, which means a $^{233}\text{U}/^{238}\text{U}$ ratio of 0.11. The composition of the UO_2 particle also shows that the particles found on the bottom of the autoclave are pieces broken off from the pellet and not precipitated U which is also confirmed from Figure 2-42. The Ti particle sizes that can be determined from the SIMS pictures are very approximative since the particles were deformed during sampling.

Conclusions on the autoclave leaching under different H_2 pressures

The predetermined conditions for this corrosion experiment was to leach a 10 wt-% ^{233}U doped UO_2 pellet in 10 mM $\text{NaCl} + 2 \text{ mM } \text{HCO}_3^-$ solution at different hydrogen pressures, starting with 16 bar pure H_2 and continuing in decreasing order: 1.6 bar pure H_2 , 0.16 bar H_2/Ar and 0.01 bar H_2/Ar mixture. The experiment was performed in a glove box under N_2 atmosphere at $22 \pm 3^\circ\text{C}$ in a stirred titanium autoclave for a period of more than 2.2 years. The pellet was characterised and annealed before start of the experiment. A post-characterisation was made of the leached pellet.

It could be concluded that:

- No oxidation of UO_2 occurred (XPS results) despite the low final $[\text{H}_2]$ of $1 \times 10^{-5} \text{ M}$ and a leaching time of 2.2 year.
- The uranium concentrations correspond to UO_2 in equilibrium with U(IV) (seen from the $[\text{U}]_{\text{leachate}}$) at all $[\text{H}_2]$ ranging from $1 \times 10^{-2} - 1 \times 10^{-6} \text{ M}$.

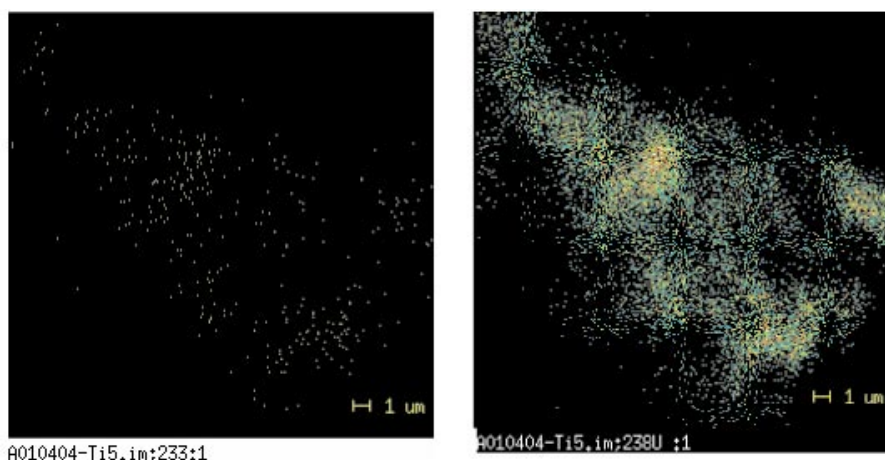


Figure 2-42. Images of a UO_2 particle found in the deposits recovered from the bottom of the autoclave. The left picture shows the image of the mass 233 (^{233}U) and the right mass 238 (^{238}U). This UO_2 particle was used to determine the $^{233}\text{U}/^{238}\text{U}$ ratio.

- E_h measured during the experiment was in the range of -100 to -350 mV.
- pH of the leachate corresponded to the added solutions indicating absence of $[H^+]$ consumption/production reactions in the autoclave.
- Calculated produced $[O_2]_{\text{radiolytically}} \gg [O_2]_{\text{measured}}$ indicating a consumption of O_2 through a UO_2 surface catalysed reaction between O_2 and H_2 .
- Rinse of the autoclave could not be used to determine dissolved UO_2 due to presence of UO_2 fragments (α -radiography, SEM-EDX).
- Fragments of titanium produced due to friction between the Ti-covered magnetic stirrer and the bottom of the Ti-autoclave did exist in the leachate.
- The Ti-fragments were characterised and were composed of a Ti-centre covered with an intermediate layer of TiO and an outer layer of TiO_2 (SIMS, micro-XRD).
- The reaction between metallic Ti and water produced H_2 and/or desorption from the Ti walls of the autoclave make it difficult to obtain a pure Ar atmosphere in the autoclave at the end of the experiment.

2.2.5 Results from electrochemical testing of α -doped UO_2 (ITU)

Corrosion potential

The results of the potential measurements are shown in Figure 2-43 and Figure 2-44. In case of 10% doped UO_2 , Figure 2-43 the measured E_h decreased during N_2 purging from initially $+360$ mV_{SHE} to $+210$ mV_{SHE} after 165 hours. When purging with $N_2/(8\%)H_2$ was started the E_h rapidly decreased to -300 mV_{SHE}. After 300 hours a sudden increase upto $+20$ mV_{SHE} was observed. The free corrosion potential reached after ~ 15 hours

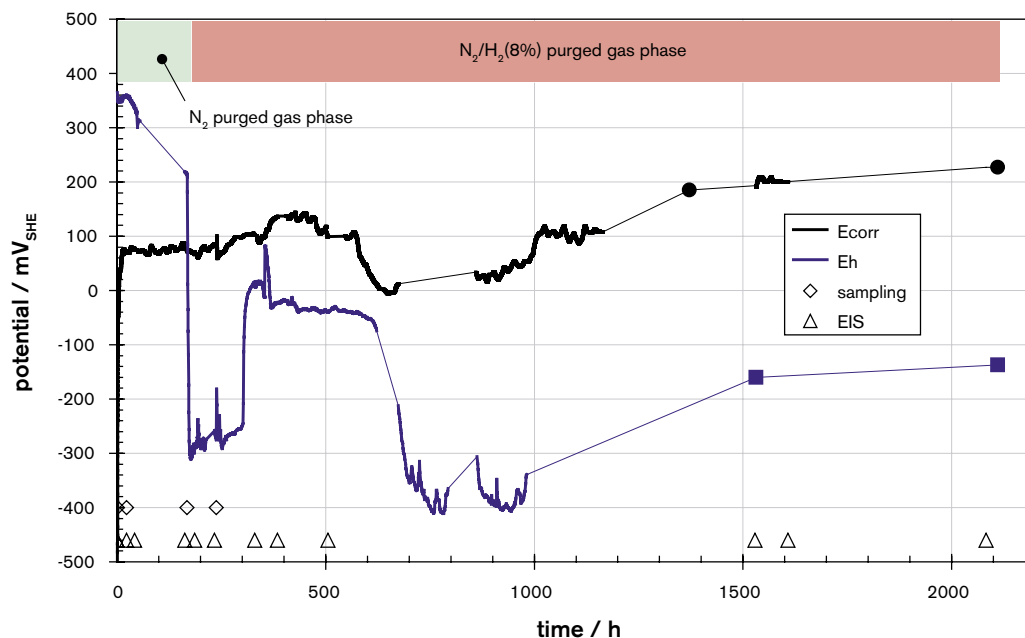


Figure 2-43. Long-term corrosion test of 10% ^{233}U doped UO_2 in 0.01 Mol NaCl-solution. The gas phase in the vessel was purged with N_2 for the first 167 h, then the purging gas was changed to $N_2/8\%H_2$.

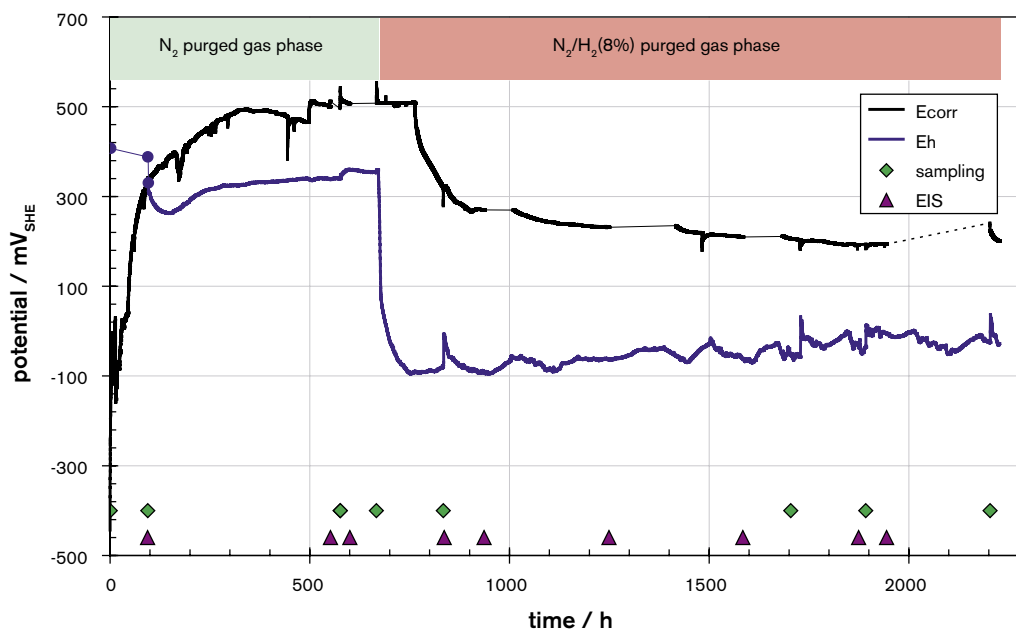


Figure 2-44. Free corrosion potential and redox potential as function of time. Long-term corrosion test of 1% ^{233}U doped UO_2 in 0.01 Mol NaCl-solution. The gas phase in the vessel was purged with N_2 for the first 672 h, then the purging gas was changed to $\text{N}_2/8\%\text{H}_2$.

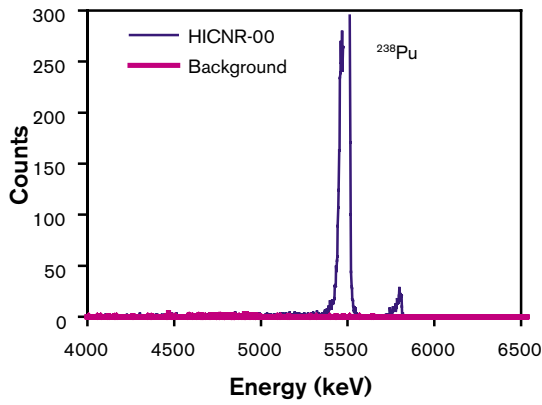
+80 mV_{SHE} . At this level it stayed constant in a range of ± 20 mV for 500 hours. Then the corrosion potential dropped 100 mV down to 0 mV_{SHE} . Also the measured Eh decreased to -400 mV_{SHE} . From then on both potentials are slowly increasing. In 1,000 hours the corrosion potential rises about 230 mV and the E_h rises about 260 mV indicating more oxidative behaviour of the solution.

The behaviour of the 1% doped UO_2 is similar but the measured potentials are higher (Figure 2-44). During purging with N_2 the corrosion potential reaches +500 mV_{SHE} while the Eh is around +300 mV_{SHE} . Purging with $\text{N}_2/\text{H}_2(8\%)$ leads to a potential drop of 200 mV in case of the corrosion potential. The Eh stabilises at -100 mV_{SHE} and increases then in 1,000 hours by about 100 mV while the corrosion potential is very slowly decreasing.

Results from ^{233}U solution analysis

The results from α -spectrometry measurements of the ^{233}U content in solution, calculated taking into account the isotopic composition and assuming congruent dissolution of the uranium isotopes are shown as obtained spectra in Figure 2-45. It can be seen that the blank solution, which was taken before introducing the α -doped UO_2 electrode, was not contaminated with ^{233}U . A slight contamination with ^{238}Pu and $^{243},^{244}\text{Cm}$ from the glove box environment was detected.

Figure 2-46 shows the U concentration with time for the experiment with 10% doped UO_2 . The U concentration in solution is in the range of some ppb and is decreasing with time. It seems that during the precathodisation the solution was contaminated with small amounts of U and that adsorption and/or precipitation of U-species occurs with time.



α-background and solution before introduction of ^{233}U -doped UO_2 electrode shows no contamination of the electrolyte with ^{233}U (left hand side).

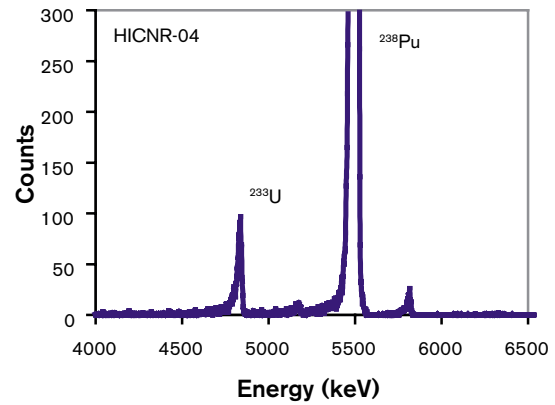
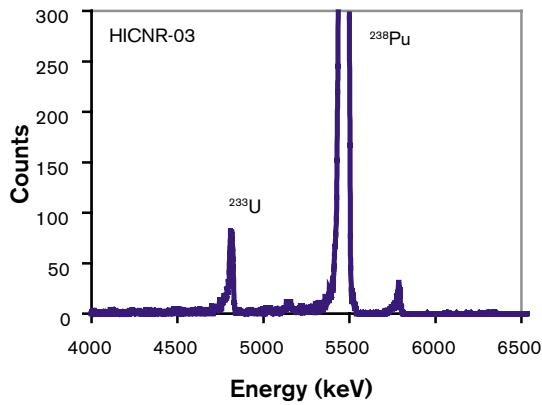
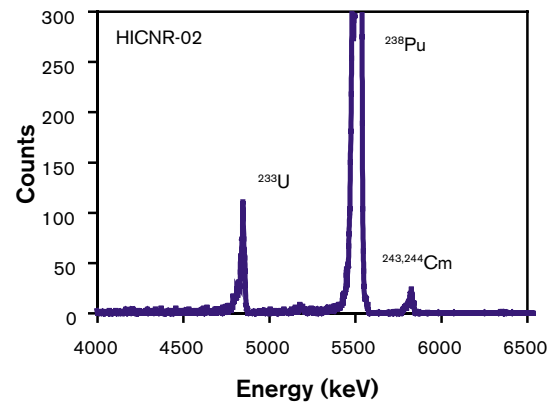
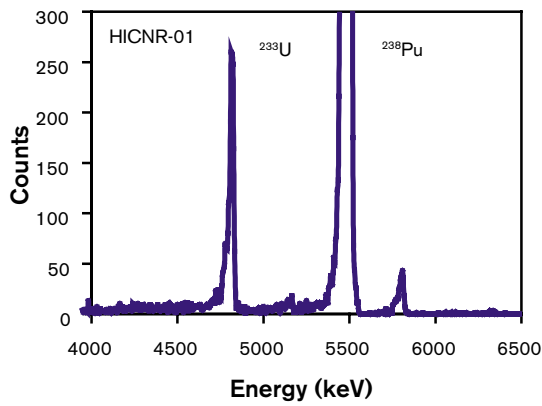


Figure 2-45. *α-spectrometric ^{233}U determination in solution samples taken during corrosion potential measurement of 10% ^{233}U doped UO_2 .*

To avoid contamination, the solution was exchanged after precathodisation in the case of the 1% doped UO_2 . Unfortunately, samples taken during the latter experiment have not been analyzed yet because of laboratory remodelling.

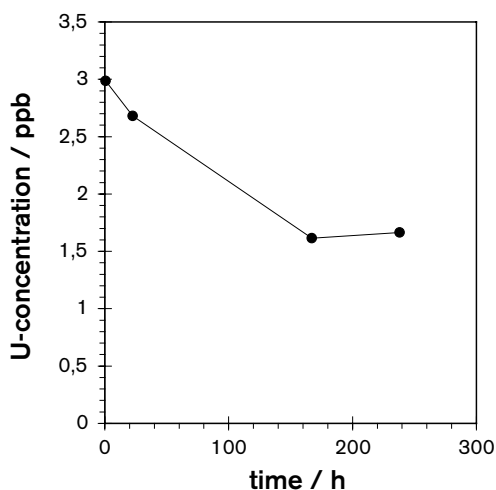


Figure 2-46. *U concentration in solution during corrosion potential measurement of 10% ^{233}U doped UO_2 determined by α -spectrometry of ^{233}U .*

Corrosion rates

Potentiostatic polarisation

Corrosion rates can be determined by extrapolation of the current potential distribution from the anodic potential range in which the dissolution is the main process determining the free corrosion potential. This Tafel extrapolation gives the corrosion current from which the corrosion rate is calculated by Faraday's law. Under oxidic conditions the potential corrosion rate dependency was experimentally measured by Marx et al. [ENG/MAR 1999]. They found a slope of 82 mV [MAR 2000]. Sunder and Shoesmith claim values of 40–60 mV for carbonate-free solutions and values of 90 mV for carbonate containing electrolytes [SHO/SUN 1988].

Directly after the corrosion potential measurement on the 1% doped UO_2 , potentiostatic polarisation experiments were carried out on the same electrode in the same electrolyte (i.e. under the same conditions). The potential was held for 10 hours at the same value while the current vs time was measured. This was followed by impedance spectroscopy (EIS) in the frequency range from 10 kHz down to 300 μHz with a duration of 12 hours. The AC amplitude was 20 mV. The applied potential was stepwise increased by +100 mV, starting at 296 mV_{SHE}.

In Figure 2-47 the current densities and the charge vs time are shown. The given polarisation potential E_{pol} is the applied potential corrected by the IR-drop across the bulk resistance R_{bulk} of the electrode, which is determined by EIS. At 300 mV_{SHE} – near the measured free corrosion potential – the current density is very low (4 nA/cm²), stable and not noisy. 100 mV more anodic the mean current density has not changed much but it is very noisy.

This might indicate the onset of local processes. At 500 mV_{SHE} it seems that the noise-generating processes die away with time and the mean current density is also low (7 nA/cm²). At 600 mV the current becomes noisier with time and also the mean value has increased to 14 nA/cm². At 700 mV and above the current density is significantly higher (0.2 $\mu\text{A}/\text{cm}^2$ and 2 $\mu\text{A}/\text{cm}^2$) and increasing with time. The electrode corrodes actively.

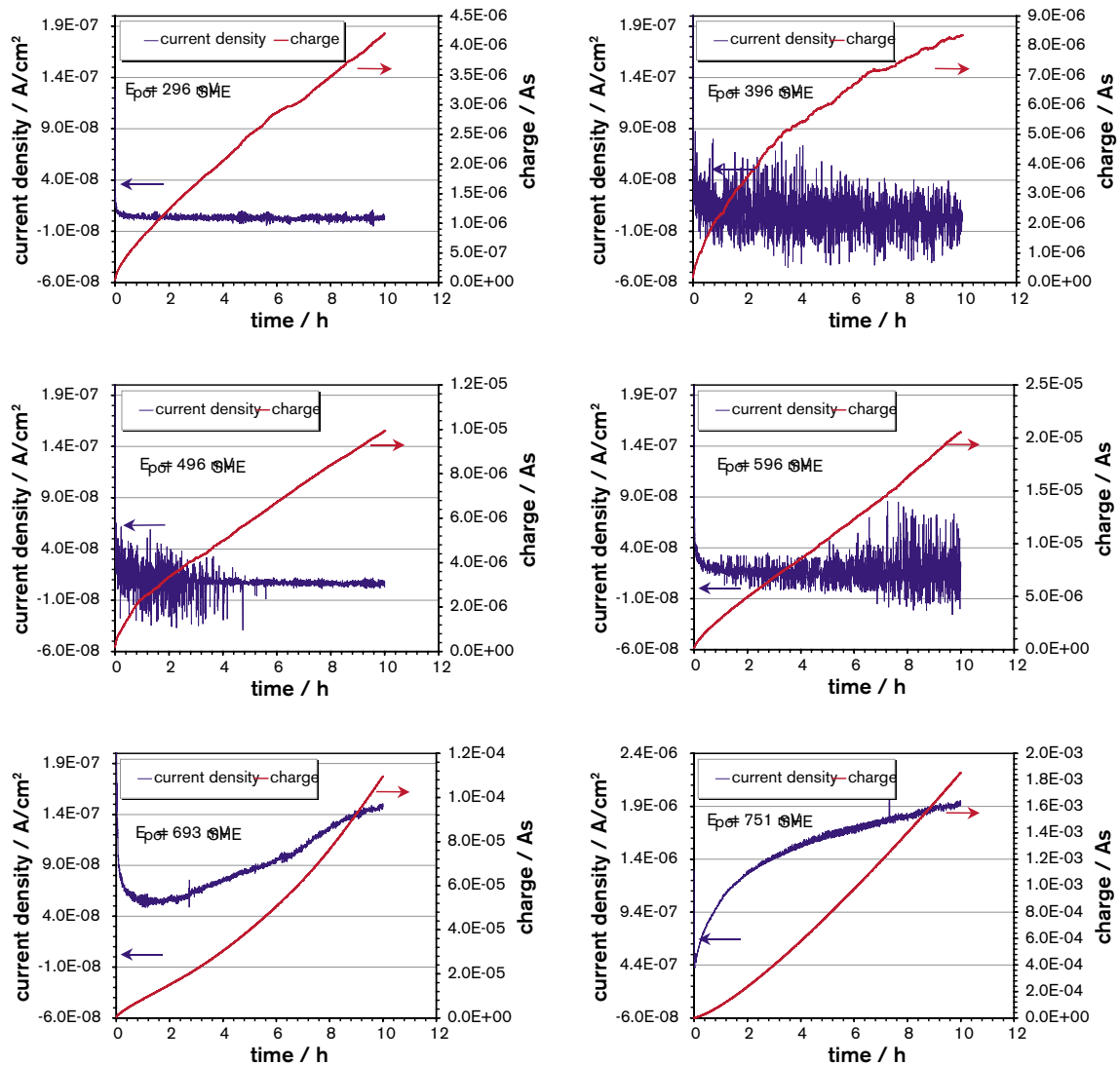


Figure 2-47. Current densities and charge during potentiostatic polarisation experiments performed on 1% ²³³U doped UO₂. Each 10 h polarisation was followed by impedance spectroscopy at the same potential (12 h).

The evaluation of the of the data in this range gives a straight line (the anodic Tafel line):

$$E_{\text{pol}} = b_a * \log(i) + n$$

with $b_a = (72 \pm 12)$ mV and $n = (1,166 \pm 12)$ mV (E_{pol} in mV, i in A/cm²), Figure 2-48.

A comparison with the data measured by Marx et al. under oxidic conditions shows much lower corrosion rates under influence of hydrogen for the same potentials, Figure 2-49.

It is also seen that an extrapolation of the Tafel line to the corrosion potential is an extrapolation over several orders of magnitude in the corrosion rate. This can easily lead to an uncertainty in the determination of the corrosion rate and also of the corrosion current of an order of magnitude.

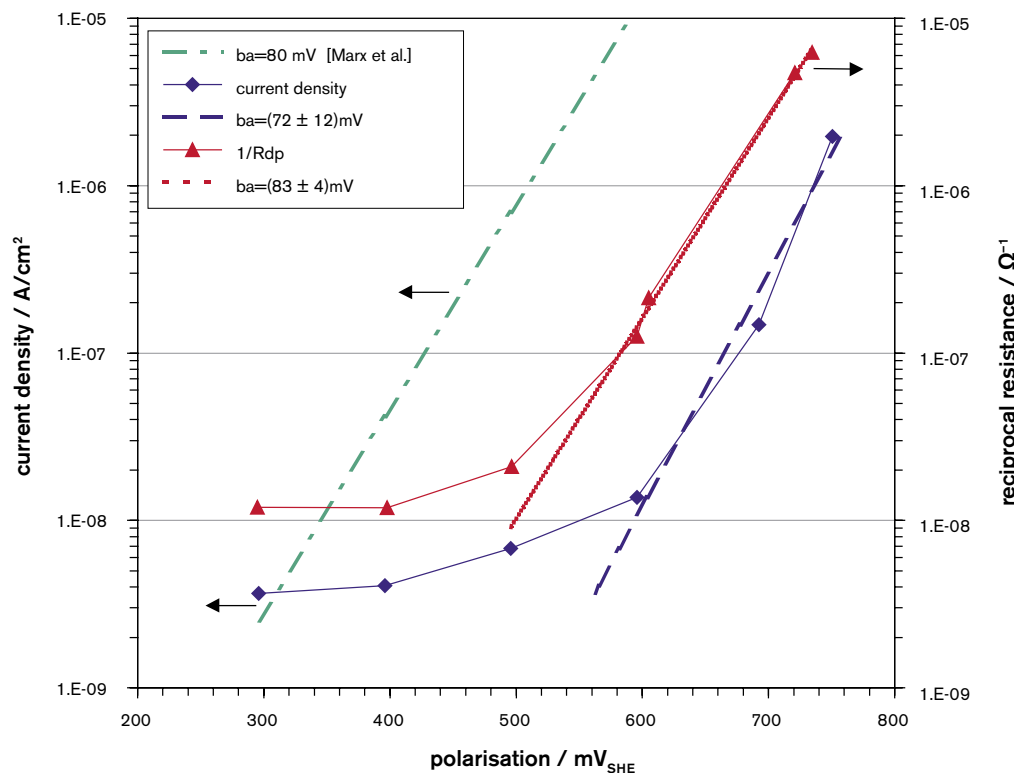


Figure 2-48. Comparison of anodic Tafel slopes derived from polarisation experiments under oxic conditions [ENG/MAR 1999, MAR 2000] and under $N_2/H_2(8\%)$ purging.

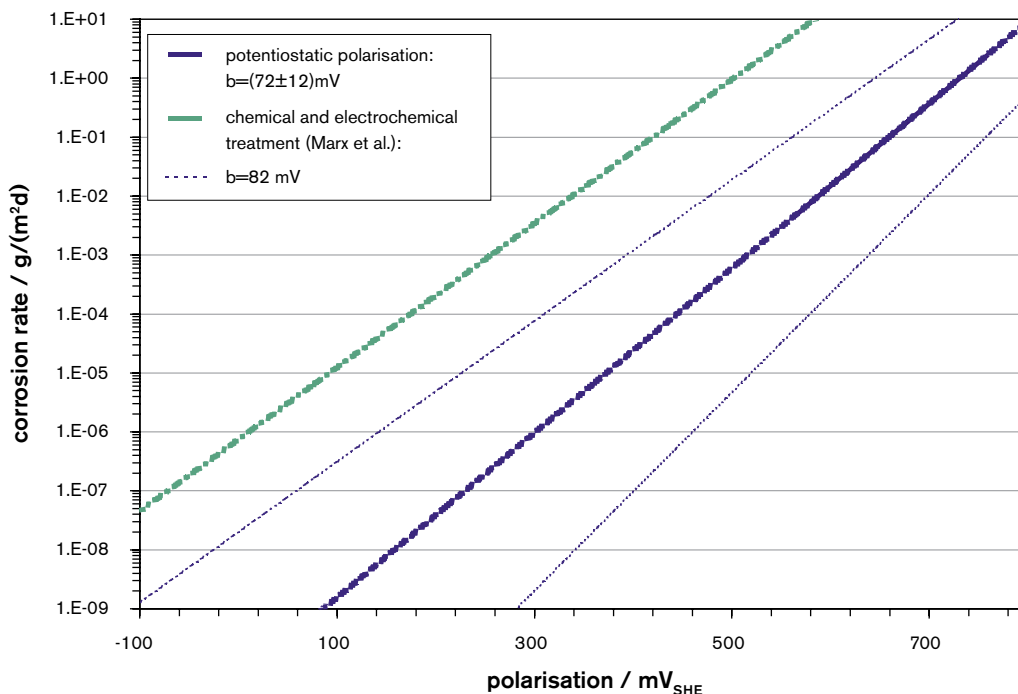


Figure 2-49. Comparison of anodic Tafel slopes derived from polarisation experiments under oxic conditions [MAR 2000] and under $N_2/H_2(8\%)$ purging. The dotted thin blue lines give the uncertainty range.

Impedance spectroscopy (EIS)

AC impedance spectroscopy offers another method of determining corrosion rates. The problem here is that due to the very low corrosion rate of UO_2 especially under anoxic and reducing conditions a very high corrosion or polarisation resistance has to be measured, e.g. measurements in the range of 1–10 μHz are necessary to determine a 1 $\text{G}\Omega$ resistance in parallel to a capacitance of 10 μF . Given the duration of the measurements the practical frequency limit is at least two orders of magnitude higher (100 μHz – 1 mHz). The only way in this case is to fit the measured data assuming a model circuit. Neglecting diffusion processes a fit was obtained using a simple equivalent circuit consisting of a resistance (polarisation resistance) and a non-ideal capacitance (double layer capacitance) in parallel and a second resistance in series (the sum of UO_2 bulk resistance and solution resistance). This procedure leads to large errors in the resistance determination which easily can exceed 100%. Furthermore diffusion processes are likely in a non-stirred electrolyte containing only traces of oxygen. Taking this into account by using a Nernstian diffusion impedance in series, much better fits were obtained. Figure 2-50 and Figure 2-51 show the potential dependency of the bulk resistance R_{bulk} and the related bulk capacitance C_{bulk} , the polarisation resistance R_{pol} and the double layer capacitance C_{dl} . R_{bulk} and C_{bulk} are constant. R_{pol} is decreasing dramatically with potentials more anodic than 500 mV_{SHE} . That corrosion starts at about 600 mV_{SHE} is also reflected in the change of the double layer capacitance C_{dl} at this potential.

At potentials 100 mV more anodic than the free corrosion potential the reciprocal polarisation resistance is proportional to the current $R_{\text{pol}}^{-1} = \ln(10) \cdot b_a^{-1} \cdot I$. From this relation an anodic Tafel slope $b_a = (83 \pm 4) \text{mV}$ was obtained, Figure 2-48. On the other hand also the current can be calculated from R_{pol} . Comparing these calculated values (black triangle in Figure 2-52 with the directly-measured potentiostatic currents (green circle in Figure 2-52), one sees that they are a factor 3–10 times higher, which means that this resistance (R_{pol}) may be an underestimate.

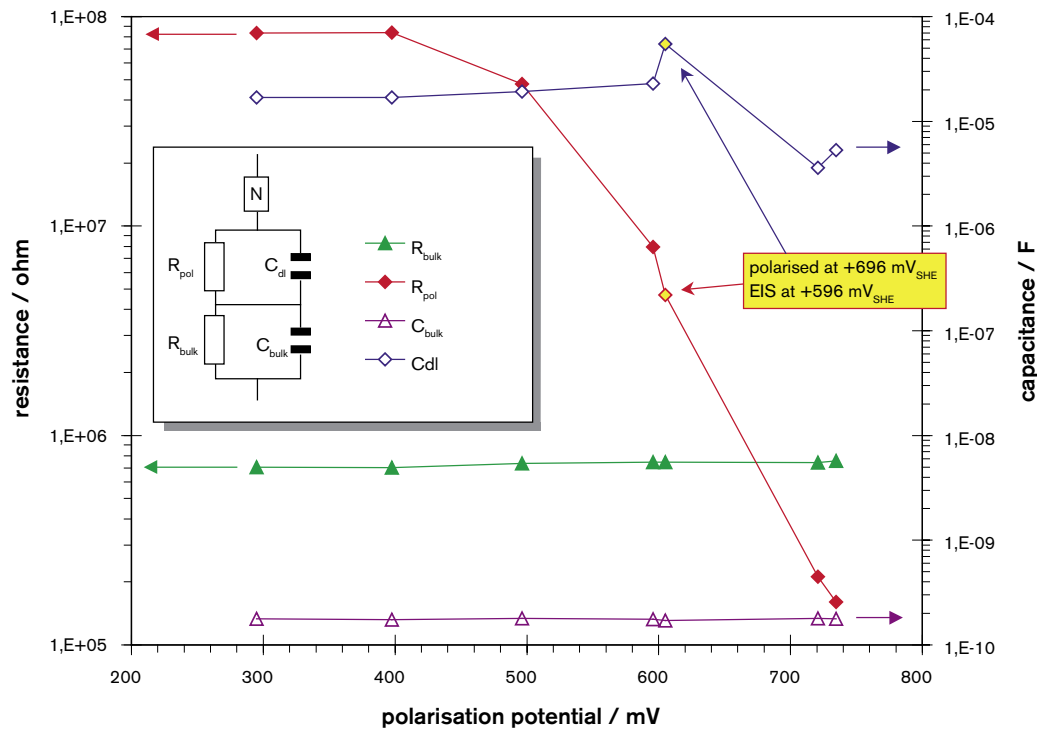


Figure 2-50. Dependency of resistive and capacitive impedance elements on polarisation potential.

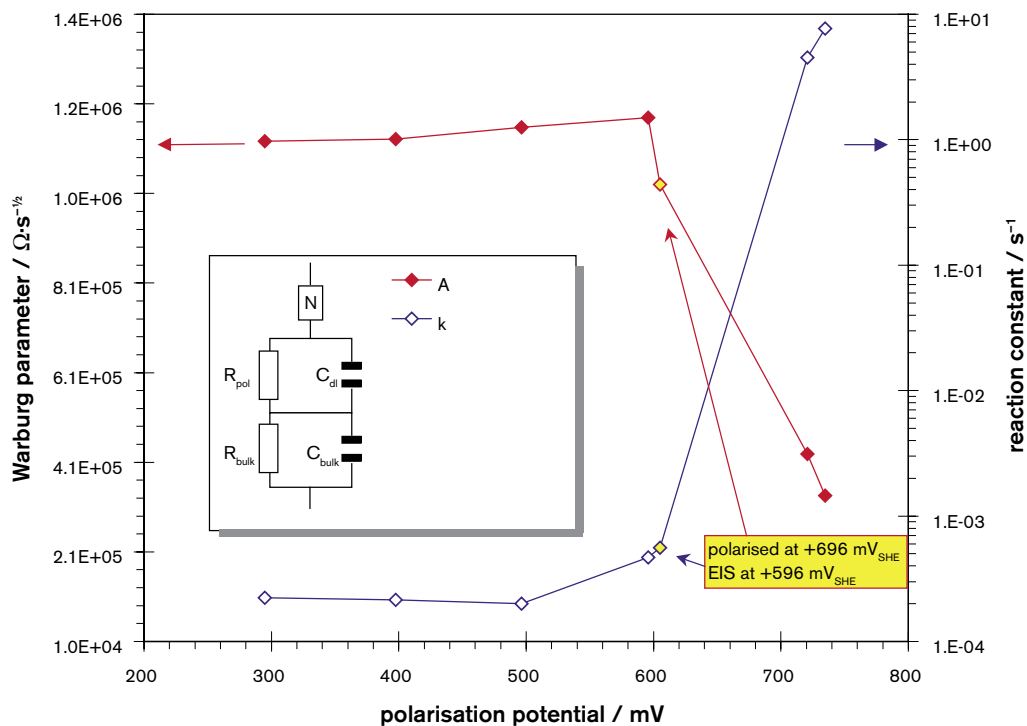


Figure 2-51. Dependency of diffusion related impedance elements on polarisation potential.

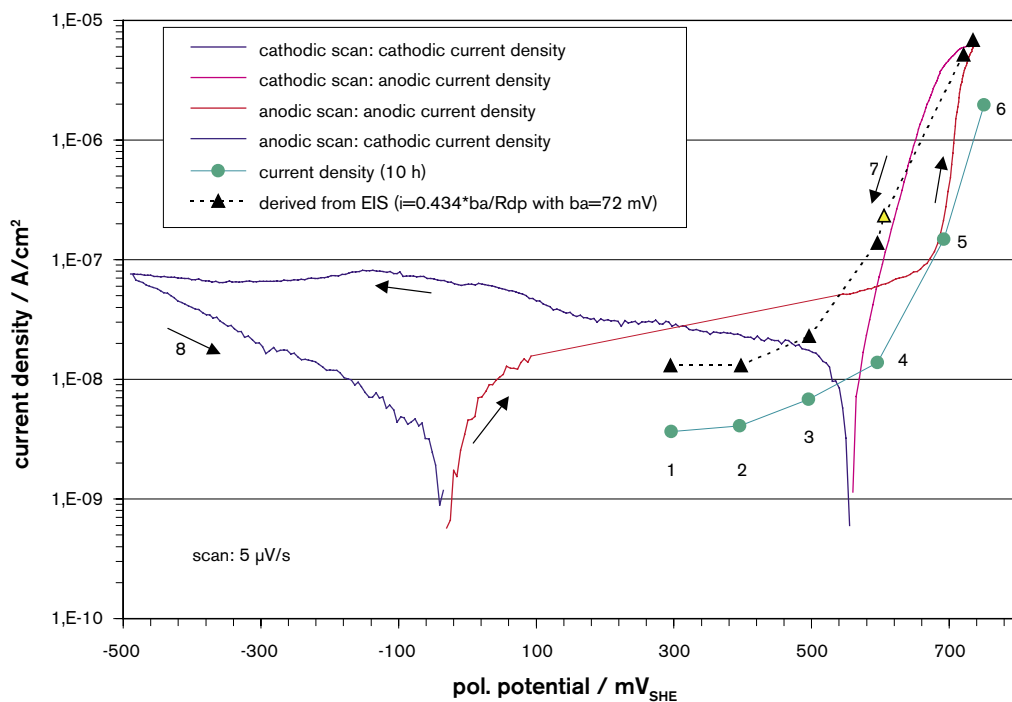


Figure 2-52. Polarisation experiments performed on $1\% \text{ }^{233}\text{U}$ doped UO_2 . Numbers indicate sequence of measurements. Green dots indicate potentiostatic polarisations over 10 h followed by impedance spectroscopy at the same potential (12 h).

The Nernstian impedance element is described by two parameters the Warburg parameter A and a reaction constant k .

$$A = \frac{|v_k| \cdot p_k \cdot R \cdot T \cdot a}{z^2 \cdot F^2 \cdot C_k \cdot \sqrt{D_k} \cdot A_{el}} \quad k = \frac{D_k}{d_N^2}$$

with p_k the reaction order, v_k the stoichiometric number, C_k the concentration ($x = 0$), D_k the diffusion coefficient of substance k , A_{el} the surface area of the electrode and d_N the Nernst layer thickness. The reciprocal of the rate constant k corresponds to the time needed for the diffusion through the Nernst layer.

In Figure 2-51 is seen that the diffusion related parameters are also changing at +600 mV_{SHE}. The rate constant increases by more than 3 orders of magnitude. At the free corrosion potential the corrosion current can be estimated using the Stern-Geary relation $I_{corr} = B/R_{pol}$, with $B = 0.434 (b_a|b_c|)/(b_a+|b_c|)$, where b_a and b_c are the anodic and cathodic Tafel slopes.

For UO_2 in aqueous systems B is in the range of 20 to 30 mV. The corrosion rates for 10% and 1% doped UO_2 were calculated assuming $B = 25$ mV [WEG/BOT 2001] (see Table 2-12 and Table 2-13).

Table 2-12. Corrosion rates of 10% ²³³U doped UO_2 in 10 mM NaCl solution derived from impedance measurements.

Inert gas purging	t h	$E_h^{(1)}$ mV _{SHE}	E_{corr} mV _{SHE}	R_{pol} MΩ	$i_{corr}^{(3,4)}$ A/cm ²	$v^{(2)}$ g·m ⁻² ·d ⁻¹
N ₂	23	357	71	3	1.4E-07	1.8E-01
N ₂	42	340	76	5	9.5E-08	1.2E-01
N ₂	162	218	77	16	2.9E-08	3.5E-02
N ₂ /H ₂ (8%)	186	-298	66	16	3.0E-08	3.6E-02
N ₂ /H ₂ (8%)	234	-258	85	17	2.7E-08	3.3E-02
N ₂ /H ₂ (8%)	330	16	101	22	2.2E-08	2.6E-02
N ₂ /H ₂ (8%)	385	-23	137	18	2.6E-08	3.2E-02
N ₂ /H ₂ (8%)	506	-39	99	61	7.8E-09	9.4E-03
N ₂ /H ₂ (8%)	1,529	-160	193	108	4.4E-09	5.3E-03
N ₂ /H ₂ (8%)	1,607		201	126	3.8E-09	4.5E-03
N ₂ /H ₂ (8%)	2,082	-137	227	166	2.8E-09	3.4E-03

(1): measured with Mettler-Toledo InLab®501 Redox combination electrode (Pt).

(2): calculated taking into account $n = 2 e^-$.

(3): calculated from $I_{corr} = B/R_{pol}$ with $B \sim 25$ mV.

(4): geometric surface area $A_{el} = 0.053$ cm².

Table 2-13. Corrosion rates of 1% ²³³U doped UO₂ in 10 mM NaCl solution derived from impedance measurements.

Inert gas purging	t h	E _h ⁽¹⁾ mV _{SHE}	E _{corr} mV _{SHE}	R _p MΩ	i _{corr} ^(3,4) A/cm ²	v ⁽²⁾ g·m ⁻² ·d ⁻¹
N ₂	94	391	340	9	8.0E-08	9.7E-02
N ₂	552	338	496	108	7.0E-09	8.5E-03
N ₂	600	360	508	113	6.7E-09	8.1E-03
N ₂ /H ₂ (8%)	837	-14	318	111	6.8E-09	8.3E-03
N ₂ /H ₂ (8%)	936	-94	271	1,157	6.5E-10	7.9E-04
N ₂ /H ₂ (8%)	1,249	-63	271	2,295	3.3E-10	4.0E-04
N ₂ /H ₂ (8%)	1,584	-63	212	2,497	3.0E-10	3.7E-04
N ₂ /H ₂ (8%)	1,874	-34	195	1,691	4.5E-10	5.4E-04
N ₂ /H ₂ (8%)	1,944	-7	191	5,117	1.5E-10	1.8E-04

(1): measured with Mettler-Toledo InLab®501 Redox combination electrode (Pt)

(2): calculated taking into account n = 2 e⁻

(3): calculated from I_{corr} = B/R_{pol} with B ~ 25mV

(4): geometric surface area A_{el}=0.033 cm²

Conclusions on electrochemical tests with α-doped UO₂

Various electrochemical methods have been applied to the aqueous corrosion of UO₂ under anoxic conditions typical for a final repository. These have given a reasonably consistent results down to 10⁻¹⁰ A/cm². Unfortunately not all chemical and analytical results have been available in order to confirm the electrochemical data. Nevertheless the following observations can be made.

Firstly, using the Tafel slopes measured under N₂/H₂(8%) purging we see corrosion rates 3 orders of magnitude lower than those measured by Marx under oxidic conditions in the previous program.

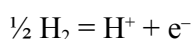
Secondly, the 10% doped material has corrosion rates is about 10 times higher than the 1% doped material. This is evidently due to the higher radiolysis in the interfacial water layers of the 10% doped material.

Thirdly, the influence of purging N₂/H₂(8%) instead of N₂ is obvious and reduces the corrosion rate by an order of magnitude possibly even more in the 1% doped material. Nevertheless in the instability of the redox and corrosion potentials at the longer time frames of the 10% doped material test shows the difficulties of maintaining such highly anoxic conditions.

Finally, we see the breakdown of the low current range at potentials above 500–600 mV_{SHE}; although there is a large number of possible models we have used a relatively simple model that gives good fits for all impedance tests carried out in this program. Using this model it is found the increase in the current is accompanied by a rapid increase of the oxygen diffusivity (or other oxidising agents) due to the high potential field. Nevertheless this represents a very extreme situation that is unlikely to occur in a repository. This demonstrates how strongly diffusion processes can dominate corrosion processes in an underground repository.

2.2.6 Dissolved hydrogen and redox conditions

The presence of dissolved hydrogen in various aqueous solutions is often reported as creating reducing conditions. In fact hydrogen is thermodynamically able to reduce most of the oxidized forms of the various radionuclides as well as molecular radiolytic oxidants such as H₂O₂ and O₂. However, at the relatively low temperatures used in most of the experiments discussed here, hydrogen is kinetically hindered and is not expected to react e.g. with molecular oxidants. Experimental studies using different amounts of dissolved hydrogen in the presence of oxidized forms of U(VI) [SPA/DEV 2004], Np(V) [CUI/ERI 1996] or Tc(VII) [GUP/ATK 1989] indicate that hydrogen does not reduce these forms to the less soluble lower redox states at room temperature. The values of the very low redox potentials measured at room temperature in the pH range of most groundwaters in hydrogen containing solutions are often interpreted as indicating reducing conditions. As it will be shown in the following section, the use of the term reducing conditions is justified in our systems, but not because of the presence of dissolved hydrogen in the bulk solution only. In most cases the concentration of dissolved hydrogen is several orders of magnitude higher (~ 0.8 mM under 1 bar H₂, i.e. H₂ bubbling) than this of the other redox species in the system. The potential of Pt-electrode, used normally as a sensor for the redox potential, will be determined mainly by the concentration of protons and the partial pressure of hydrogen according to the equilibrium:



$$E_{\text{red}} \text{ (mV)} = E_{\text{Pt}} - E_{\text{ref}} = E_0 + \frac{RT}{nF} \log \frac{a_{\text{H}^+}}{P_{\text{H}_2}} - E_{\text{ref}} = 0 - 59.2 \text{ pH} - E_{\text{ref}} \approx -490 - E_{\text{ref}}$$

where:

E_{red} – is the redox potential,
 R – the general gas constant,
 T – the absolute temperature,
 F – Faraday's constant.

Hence redox potentials of the order of ~ -500 mV are to be expected in solutions of pH ~ 8.2 and saturated with hydrogen at 1 bar. In this case the redox conditions are strongly reducing at the surface of the redox sensor, which is a known hydrogen catalyst, but not in the bulk of the solution. In the bulk undissociated molecular hydrogen is not expected to cause any reduction of the redox species at low temperatures. If all molecular hydrogen in the bulk solution were active, no oxidized form of any radionuclide would exist in solution due to the large surplus of hydrogen. In fact, if small amounts of e.g. dissolved oxygen, hydrogen peroxide or dissolved forms of oxidized radionuclides such as U(VI) are present in the solution at the same time as hydrogen, the redox potential will depend on both redox couples -a mixed potential is measured, more positive than in the presence of only dissolved hydrogen. The potential may increase depending on the rate of production of oxidants, at the same time as they are partially consumed at the electrode due to the usually higher amounts of hydrogen.

In the case of redox potential measurements under anoxic conditions in redox un-buffered solutions such as the carbonate groundwaters used in our tests, very low concentrations of dissolved oxygen (of the order of 10⁻⁹–10⁻¹⁰ M) are the only redox species expected to influence the redox potentials measured [SPA/WER 2001]. While the measured values of the redox potentials are difficult to relate to such low oxygen concentrations without a special treatment of the sensor and proper calibration, the evolution of the redox potentials towards lower values indicates correctly a decrease of the levels of dissolved oxydants in the solution. In the same way an increase of the redox potential, e.g. in the presence of α -radiolysis products, indicates correctly an increase of the levels of dissolved oxidants.

2.2.7 Discussion of the results obtained with ^{233}U doped UO_2 pellets in the presence of dissolved hydrogen and comparison with literature data

The results of the static batch experiments under Ar flushing (Figure 2-13 and 2-14) indicate a clear effect of α -radiolysis in the enhancement of uranium dissolution. A summary of the conclusions regarding the influence of the decreasing α -field on the dissolution rates of $\text{UO}_2(\text{s})$ is given in [GRA/CAC 2005]. In any case, due to the low range of α -particles, oxidizing conditions are created near the $\text{UO}_2(\text{s})$ surface, contributing in the observed increase of the uranium concentrations and of the molecular oxidant concentrations in the solution. The α -radiolysis of a few tens of microns thick water layer is expected to produce mainly molecular radiolytic products such as hydrogen peroxide [SHO 2000]. In the presence of metal oxide surfaces such as $\text{UO}_2(\text{s})$, hydrogen peroxide is known to be decomposed to oxygen and water [CHR/FOR 1990, SHO/SUN 1991, GIM/BAR 1996]. The oxygen and hydrogen peroxide produced in the layer near the pellet surface leached in the autoclave should only partially be consumed through reactions with the UO_2 surface to oxidize it and produce uranyl carbonate species. A part of the molecular oxidants should diffuse away and accumulate in the solution and the head space of the autoclave. For example, in measurements with ^{238}Pu -doped pellets in concentrated chloride brines [KEL/BOH 2002], increases of oxygen concentrations in the system are measured together with the increase of uranium concentrations in solution.

In our autoclave test, the observed oxygen sensor readings at the detection limit and the absence of increases of radiolytic oxygen concentrations in bicarbonate containing solutions contacting ^{233}U doped UO_2 during long time periods can not be explained by oxygen consumption through reactions with hydrogen activated by α -radiolysis in homogeneous solution. Recently reported measurements [PAS/LAV 2001] of the production of H_2O_2 in hydrogen saturated solutions during α -radiation (5 MeV He ions) indicate that the presence of hydrogen concentrations of 0.008 to 0.8 mM (0.01–1 bar H_2) did not influence the production of radiolytic oxidants. Practically equal amounts of hydrogen peroxide were measured under hydrogen and argon atmospheres. Very low accelerator current intensities and dose rates were used in this study, so that α -track crossing is not likely to have occurred. The discrepancies between experimental data and radiolytic modeling may be due to inhomogeneity effects in the case of α -radiation [PAS/LAV 2001], or to the need to correct the radiolytic scheme [JON 2004]. However this discrepancy does not affect the obtained experimental results, but rather indicates that further modeling efforts are needed. New experiments are planned in the frame of the EU project NF-PRO to study the influence of an initial large excess of dissolved hydrogen on the oxidant production by α -radiolysis in homogeneous solutions. Preliminary results [JEN/ALB 2004] with ^{238}Pu solutions saturated with H_2 under 10 bar pressure indicate the same behaviour as in those described in [PAS/LAV 2001], i.e. almost no effect of dissolved hydrogen as compared to Ar is observed in the production of radiolytic oxygen in homogeneous solutions in the absence of UO_2 surfaces. As discussed below, no oxidation of the $\text{UO}_2(\text{s})$ surface could be detected by XPS and no measurable increases of U in the solution indicating the consumption of oxygen through production of uranyl carbonate species was observed. The only plausible explanation of the low and constant oxygen levels measured simultaneously with very low and constant uranium levels in the presence of α -radiolysis seems to be oxidant consumption by hydrogen activated somewhere in the system. Then if oxidants can not be consumed by hydrogen activated through α -radiolysis in homogeneous solution, the explanation for the low oxidant and uranium concentrations observed in our tests seems to be oxidant consumption by hydrogen activated at the surface of α -doped $\text{UO}_2(\text{s})$.

In the following a few experimental studies where similar effects have been observed on irradiated actinide oxide surfaces are presented.

Baker et al. [BAK/LES 1966] noted that the corrosion of metallic uranium by water vapor, producing a layer of $^{235}\text{UO}_2(\text{s})$ and $\text{H}_2(\text{g})$, was inhibited by the presence of oxygen. By using tracer $^{18}\text{O}_2$ and normal water, it was shown that the oxygen was converted to H_2^{18}O on the surface of $\text{UO}_2(\text{s})$.

Haschke et al. [HAS/ALL 1996] observed a pressure decrease in a 2:1 (H_2+O_2) gas mixture over $^{239}\text{PuO}_2(\text{s})$ at 25°C , which was interpreted as caused by the catalytic formation of water on the surface of $\text{PuO}_2(\text{s})$. Even though the role of α -radiation in the activation of hydrogen in both these studies has not been discussed in the original publications, its influence can not be excluded.

The results of an α -radiolysis study of $\text{NpO}_2(\text{s})$ doped with 0.7% ^{244}Cm in the presence of moistures up to 8 wt% water [ICE/TOT 2004], show that radiolytic gas generation quickly reaches a steady state plateau at relatively low total pressures. The presence of the plateau is interpreted by the authors as a clear evidence of a significant back reaction (i.e. the recombination of the radiolytic products O_2 and H_2 to water) where the forward reaction (radiolytic decomposition of water) is equal to the back reaction, behaviour noticed also in other similar systems studied by these authors.

The mechanism of this reaction in the case of depleted $\text{UO}_2(\text{s})$ surfaces would imply an activation of any of the reactants (H_2O_2 , O_2 or H_2) on the surface of $\text{UO}_2(\text{s})$. There are indications in the literature that the surfaces of $\text{UO}_2(\text{s})$ or of the other light actinide oxides can act as a hydrogen catalysts. In a literature review of the catalytic properties of actinides [COL 1984] it is pointed out that the unique electronic structure of the light actinides with overlapping 5f, 6d and 7s bands, makes it possible to describe them as “complex transition metals”, and thus good candidates for catalysts. The large size of actinide ions allows for coordination numbers and polyhedra unknown or unusual for d-element ions. Consequently many reactive species can be coordinated and maintained in unusual spatial orientations. There are reports [IMI/TAN 1979] that $\text{ThO}_2(\text{s})$ acts as a non-metallic hydrogenation catalyst for butadiene and methyl butene. A detailed study of the mechanism indicated that it involves H_2 dissociation on $\text{ThO}_2(\text{s})$ surfaces. In a hydro-metallurgical study [BUN/ZOG 1958], it was reported that inactive $\text{UO}_2(\text{s})$ can act as a hydrogen catalyst and cause the precipitation of U(VI) from concentrated carbonate solutions as $\text{UO}_2(\text{s})$ at temperatures of $110\text{--}145^\circ\text{C}$ and hydrogen pressures of 1–3 MPa. The property of inactive $\text{UO}_2(\text{s})$ surfaces to activate hydrogen and reduce U(VI) carbonate species [SPA/DEV 2004] or potentially dissolved oxygen [EKE/JON 2004] has been reported recently. However, the effect of UO_2 surfaces in activating hydrogen in the absence of radiation seems to be much smaller than in its presence. Thus no water formation could be detected with depleted $\text{UO}_2(\text{s})$ [DEV/HAS 2003] using the same PVT method as used in [HAS/ALL 1996] for $^{239}\text{PuO}_2(\text{s})$. The lowest U concentrations measured in the inactive $\text{UO}_2(\text{s})$ systems in the presence of high concentrations of H_2 and higher temperature were a few ppb [SPA/DEV 2004] or even ppm [EKE/JON 2004], while the effect of air contamination influenced very much and almost irreversibly the concentrations of uranium. The mechanism of hydrogen activation in the case of irradiated UO_2 surfaces is discussed further in section 3.2.4.

Another trend observed in all the experiments with α -doped samples even under relatively low concentrations of dissolved hydrogen are the very low (and in general decreasing with time) concentrations of all uranium isotopes. Extremely low concentrations of uranium are reported in similar studies [OLL/ALB 2003] in the presence of an actively corroding iron strip. If α -radiolysis of hydrogen-containing solutions does not influence the production of radiolytic oxidants by activating molecular hydrogen, then even the small amounts of U(IV) required to equilibrate the solution with $\text{UO}_2(\text{s})$ should be oxidized to U(VI) in the layer adjacent to the surface. Additional amounts of U(IV) would then dissolve to saturate the solution and this U(IV) would also be oxidized. By this mechanism an increase of the U concentration in solution should occur. The concentrations of uranium are expected

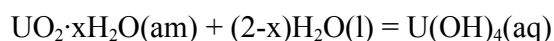
to increase continuously, even in the case of the presence of small amounts of dissolved hydrogen in the solution based on the available experimental data on α -radiolysis of hydrogen saturated solutions [PAS/LAV 2001]. However, under the leaching in the presence of 6% hydrogen (corresponding to ~ 0.05 mM dissolved hydrogen), the concentrations of the uranium seem to decrease in the long term instead of increasing (Figure 2-12). The same holds for the concentrations of uranium measured during electrochemical tests under $N_2 + 8\% H_2$ flushing (Figure 2-46), where through electrochemical measurements it is possible to determine a dissolution rate remarkably lower than under oxidizing conditions.

Even more convincing is the example of the very low and practically constant concentrations of uranium measured in the case of the pellet leached in the autoclave under different H_2 pressures (Figure 2-19). No measurable increase in the concentrations is noted even when the autoclave atmosphere was changed to Ar and only small amounts of hydrogen resulting from desorption from the autoclave walls are present. The SIMS analysis shows at the same time that no measurable amounts of uranium can be detected on the TiO_2 surfaces of the autoclave.

It is remarkable that the concentrations of uranium do not increase even when air contamination is clearly detected in the autoclave by the oxygen sensor (Figure 2-17) during solution sampling or refilling. Such levels of oxygen would be sufficient to oxidize all U(IV) present in the solution to U(VI). The concentrations of uranium in the bulk solution of the autoclave, where the sample is taken, indicate that they correspond to the lowest values measured in solutions contacting depleted $UO_2(s)$ surfaces during measurements of crystalline uranium dioxide solubility. Due to the high sensitivity of U(IV) to traces of atmospheric oxygen, such measurements are usually carried out in the presence of strong reductants in the bulk solution such as Eu(II), $Na_2S_2O_4$, Fe(s) or dissolved hydrogen activated chemically at high temperatures, which are shown through separate tests [PAR/POH 1988, RAI/FEL 1990, RAI/YUI 2003] to reduce rapidly any traces of U(VI) in solution. Thermodynamic considerations indicate that U(IV) is stable in solution only for extremely low partial pressures of oxygen (considered as the only oxidant in the system) of the order of 10^{-65} atm [RAI/FEL 1990]. It seems impossible to achieve such concentrations and eliminate completely traces of diffusing atmospheric oxygen, especially through flushing with gas mixtures containing relatively low amounts of hydrogen, as in the case of static and electrochemical tests. The oxygen sensor indicates that such contamination occurs even in the case of the autoclave test. Further, we study dynamic systems, where the radiolysis continues to produce oxidants all the time and not systems at equilibrium. For this reason only comparisons of the measured U concentrations with the ones measured in equilibrium studies as solubility measurements are possible. While inside the test vessel and in contact with $UO_2(s)$, any potential sorption sites are saturated relatively fast in comparison with the long duration of the leaching tests and sorption in vessel walls should not influence too much the sample concentration taken in the bulk solution. However, with such low uranium levels analytical errors as well as sampling problems due to sorption-desorption from previous samples in the vials, during centrifugation or filtration should be considered when discussing the analyzed uranium concentrations.

The solubility of crystalline uranium dioxide is discussed extensively in several publications [FUG 1993, NEC/KIM 2001, RAI/YUI 2003], mainly because of the discrepancies between the values obtained by determinations of the free energy of formation of $UO_2(cr)$ (by measurements of the enthalpy of formation of $UO_2(cr)$ through calorimetric measurements and its entropy of formation through low temperature heat capacity measurements) and the orders of magnitude larger values obtained by solubility measurements at near neutral pH ranges. A discussion of the most recent data is given in the NEA-TDB Update [GUI/FAN 2003]. In the case of $UO_2(s)$ even brief contact with air results in the oxidation of the

surface layer, making it difficult to perform solubility determination from undersaturation. Uranium dioxide has a tendency to over-saturation and especially at room temperature the formation of UO_2 crystals is very slow. For this reason high temperature studies are recommended [RAI/YUI 2003]. The use of reductants in the solution reduces traces of U(VI) in the solid sample or created by traces of oxygen in the test vessel to U(IV), which at room temperature and near neutral pH precipitates to give only amorphous/microcrystalline $\text{UO}_2(\text{s})$. According to [NEC/KIM 2001] the solubility data determined with $\text{UO}_2(\text{cr})$ in neutral and alkaline aqueous solutions, must be ascribed to the dissolution of an amorphous surface layer according to:



For microcrystalline or X-ray amorphous $\text{UO}_2(\text{s})$, expected to precipitate in near neutral solutions e.g. in cases of U(VI) reduction, or for crystalline UO_2 at room temperature the lowest concentrations reported are 2×10^{-9} M [YAJ/KAW 1995] by using $\text{Na}_2\text{S}_2\text{O}_4$ as holding reductant. The value recommended in the in the NEA-TDB Update for $\text{Ks}_{(1,4)}^0$ is $10^{-8.5}$.

All studies cited in [GUI/FAN 2003] and [NEC/KIM 2001], as those of [YAJ/KAW 1995, RAI/FEL 1990, RAI/YUI 2003] indicate that the U(IV) concentrations in equilibrium with $\text{UO}_2(\text{cr})$ and $\text{UO}_2(\text{am})$ are almost the same at pH above 6. The lowest concentrations measured for crystalline UO_2 above pH ~ 4 appear to be those of Parks and Pohl [PAR/POH 1988] in the presence of high pressures of hydrogen and 100–300°C. They obtained uranium concentrations of the order of $\sim 10^{-9.5}$ M for all data at pH > 4 .

The low concentrations of uranium indicate at the same time that they originate from a reduced UO_2 surface, since this is the source of uranium in our system and any oxidation there would cause an increase of the levels of uranium in the bulk solution. The investigation of the surface by surface sensitive techniques as XPS indicates the absence of any oxidation of the surface, even after a long leaching period under Ar and only traces of desorbed hydrogen. Similar results are reported in a study [SUN/BOY 1990] of the effects of α -radiolysis on the oxidation/dissolution of $\text{UO}_2(\text{s})$ in solutions saturated with 0.1–1 bar H_2 and 100°C. The vacuum transporting vessel used to transfer the pellet to XPS apparatus was similar to the one used in our study (Figure 2-9). No differences in the oxidation state of the surface in Ar and H_2 atmosphere were observed in the absence of radiation. In the presence of α -radiation from an ^{241}Am source, the results indicate a clear oxidation of the surface in Ar atmosphere, while under H_2 atmosphere the results indicate no oxidation, but rather a reduction of the surface with increased α -dose.

In conclusion, the low concentrations of oxygen, uranium and the other observations indicate the presence of an active reducing agent in our systems, which besides consuming radiolytic oxidants and air contamination oxygen, causes also the reduction of traces of any U(VI) present. Again the only reasonable explanation for the role of dissolved hydrogen in our systems seems to be its activation at the irradiated $\text{UO}_2(\text{s})$ surface. A potential mechanism of hydrogen activation on irradiated UO_2 surfaces based on recent studies of the radiolysis of water sorbed on the surfaces of various oxides is discussed further in section 3.2.4.

The confirmation of the effect of relatively low concentrations of dissolved hydrogen in successfully hindering the oxidative dissolution of α -doped $\text{UO}_2(\text{s})$, where the expectations based on the data from homogeneous radiolysis of hydrogen-saturated solutions were relatively low, is one of the major outcomes of the SFS project.

3 Corrosion of spent fuel in the presence of dissolved H₂

In the frame of this project, the leaching of a high burn-up fuel in 5 M NaCl solutions saturated with 3.2 bar H₂ (FZK-INE) as well as the leaching of MOX fuel fragments in dilute bicarbonate containing solutions under 50 bar H₂ (ITU/SKB) were studied.

The study on spent fuel corrosion in brine is relevant to disposal in rock salt. Assuming that saline solutions in the vicinity of the waste package would find access to these packages, they will corrode, and after breaching of the container and the cladding the brine will interact with the spent fuel matrix. To assess the ability of this waste form to retain radionuclides in the case of water access, and to understand the corrosion controlling processes, it is required to perform experiments, which simulate the overall system consisting of real spent fuel, canister material (Fe based), salt solution and gas phase. Both, the dissolution rate of the spent fuel itself, and the release/retention of radionuclides are expected to be governed more by geochemical constraints encountered in the near field of the waste package, rather than by inherent material properties of the fuel. Since the container corrosion rate may be high (~ 100 μm/yr), large amounts of hydrogen will be produced. The loss rate of the container material may be high initially but will decrease within approximately 1,000 years as convergence occurs in a repository situated in a salt host rock. Thus, hydrogen pressures will increase to some tens of MPa. The built up of hydrogen overpressure in a repository is considered to produce problems with respect to the overall safety [BON/COL 2000]. As a consequence of the H₂ overpressure overall reducing conditions are assured in near field. However, close to the spent fuel surface (some μm) the persistence of oxidizing radiolytic species cannot be ruled out. In the frame of our experimental work special attention is directed towards the evolution of hydrogen and its effect on the overall corrosion behavior of high burn-up spent fuel.

The study of the influence of molecular hydrogen on the leaching rate of irradiated fuel was performed using MOX-fuel to investigate a fuel with higher α-activity as compared to irradiated UO₂ fuel. The MOX fuel used in this experiment had an average burn-up of 48 MWd/kg U and was leached in a 10 mM NaCl + 2 mM HCO₃⁻ solution (in future called leachate). The H₂-pressure in the autoclave was 53 bar corresponding to a H₂ concentration of 43 mM in the leachate. The experiment was run in a Ti-autoclave with all wetted surfaces made of titanium. The main purpose is to demonstrate that high concentrations of molecular hydrogen inhibit the oxidation of UO₂, despite a high α-dose and correspondingly high production of oxidative radiolytic species. The setup is designed for leaching studies, without measurement of stable molecular radiolysis products (H₂, O₂ and H₂O₂), to determine the threshold when the H₂ concentration is too low to compensate for the oxidative radiolytic products oxidizing the UO₂.

The experimental details and the results obtained are presented below, followed by a comparison with literature data and a general discussion of the hydrogen effect on spent fuel leaching.

3.1 Experimental

3.1.1 Spent fuel characterization

High burn-up spent fuel (FZK-INE)

The spent fuel sample originates from a fuel element irradiated for 1,226 days (1986–1989). It is known that the average burn-up of this fuel did not exceed 50 MWd/kg U and the temperature remained below 1,700°C, despite the fact that maximum burn-ups of 55 MWd/kgU during 4 cycles were reached.

The average power ratings of the first two cycles were 30–32 kW/m and of the 4th cycle only 18 kW/m. The fuel is not considered as a “ramped” fuel [GOL/WEG 2003].

For this experiment spent fuel pellet denoted as K8 (6.6 g fuel) was cut from segment N203 from fuel rod No. 1108, which was received from SIEMENS/KWU. The pellet cutting procedure was performed in the year 1992 under N₂ atmosphere. Other samples from the same segment were used immediately for corrosion tests [GRA/LOI 1996], whereas the remaining pellets, including K8 were sealed in “gas tight” stainless steel capsules, and 2 capsules were packed together into an aluminum capsule. All capsules were placed into a 5 l tinplate drum. All of these work steps were carried out under inert (N₂) atmosphere. But later on, these sealed packages were stored in air atmosphere. Pellet K8 was stored under these conditions for 7 years until its use in the present corrosion test. As shown in the optical micrographs of Figure 3-1 the cutting surface of the pellet was in part covered by a white layer, probably formed due to the contact with small quantities of air that penetrated inside the capsule during 7 years of storage. Figure 3-2 shows sections of the spent fuel pellet surface after the end of the 3 years static corrosion test under 40 bar Ar/8% H₂ overpressure.

Nuclide inventories of the fuel samples were calculated by means of the KORIGEN code [FIS/WIE 1983] using a neutron cross section library applicable to high burn-up values.

Calculated specific nuclide radioactivity inventories and specific elemental mass inventories for reference date Feb 1st, 1992, are given in Table 3-1.

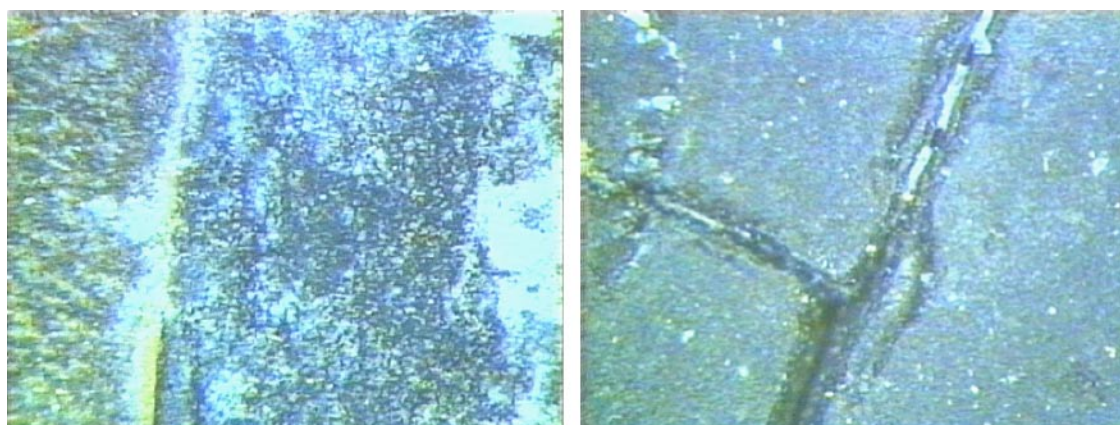


Figure 3-1. Surface section of high burn-up spent fuel pellet K 8, after seven years of storage and before its use in the corrosion test.

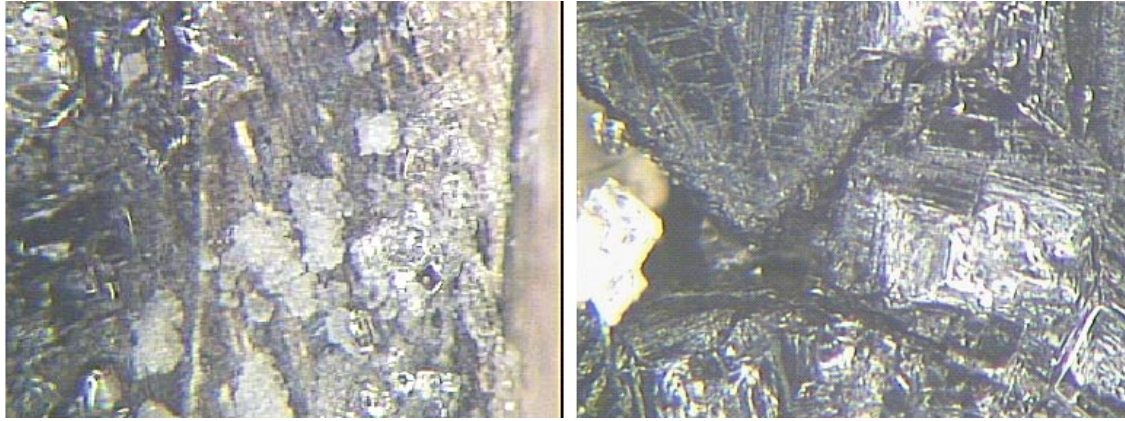


Figure 3-2. Surface section of high burn-up spent fuel pellet K 8, after 3 years corrosion in 5 M NaCl brine under 3.2 bar H_2 overpressure. The reaction layer consists of NaCl crystals.

Table 3-1. Specific nuclide radioactivity inventories and specific elemental mass inventories of high burn-up (50 MWd/kg U) spent fuel for reference date Feb 1st, 1992 according to calculations using the KORIGEN code [FIS/WIE 1983].

	Inv Nucl Bq/g U	Inv Elem g/g U
Ru-106	4.587E+09	0.003612
Cs-134	4.978E+09	0.003908
Cs-137	6.204E+09	0.003908
Eu-154	4.036E+08	0.000210
Eu-155	2.179E+08	0.000210
Sb-125	1.777E+08	0.000022
Sr-90	4.238E+09	0.001204
Ce-144	4.718E+09	0.003604
Tc-99	6.855E+05	0.001138
Am-241	4.678E+07	0.000493
Am-243	2.525E+06	0.000493
Np-237	1.816E+04	0.000718
Np-239	2.525E+06	0.000718
Cm-242	9.253E+07	0.000108
Cm-244	4.569E+08	0.000108
Pu-238	3.340E+08	0.011290
Pu-239/40	5.196E+07	0.011290
Pu-241	8.242E+09	0.011290
U-238	3.316E+02	0.935400

MOX fuel characterisation and preparation (ITU/SKB)

The MOX-fuel used in the leaching experiment has a burn-up of 48 MWd/kg U. The fuel was irradiated under normal conditions in a pressurised water reactor. The composition of the main fission products and actinides in the fuel is given in Table 3-2. Oxygen potential measurement of the MOX fuel showed that it is very close to stoichiometry, $UO_{2.00}$.

The mixed oxide fuel consists of Pu-grains, composed of ~ 25 wt-% Pu in natural UO₂, embedded in an UO₂ matrix. α -autoradiography showed a radial homogenous distribution of the plutonium spots. Both fine and coarse porosity could be observed in the fuel matrix. The pore diameter ranged from < 1 μm to 8 μm with a peak at ~ 1 μm . The matrix grain size distribution was smaller at $r/r_0 = 1$ and peaked at 4–5 μm compared to the grains at $r/r_0 = 0.25$ that peaked at 5–7 μm .

The MOX-fuel was cut from a fresh fuel rod in a hot cell under nitrogen atmosphere (< 2% O₂). An optical inspection of the fuel slice was performed, Figure 3-3. The fuel slice (slice B) was measured with a micrometer and was found to be 1.089 mm thick. The zircalloy cladding was removed and the individual fuel fragments were isolated, Figure 3-4. The geometrical surface area of the individual fuel fragments was calculated using pictures of both sides of each fuel fragment.

Table 3-2. Composition of analyzed radionuclides in the MOX-fuel. The reference date is 18th December 2002.

Radionuclide	Activity in fuel (Bq/g fuel)
Fission products	
⁹⁰ Sr	1.5×10 ⁹
¹²⁵ Sb	1.3×10 ⁷
¹³³ Cs	Stable
¹³⁴ Cs	1.3×10 ⁸
¹³⁵ Cs	4.6×10 ⁴
¹³⁷ Cs	3.5×10 ⁹
¹⁴⁴ Ce	4.9×10 ⁵
¹⁵⁴ Eu	2.0×10 ⁸
Actinides	
²³⁴ U	2.1×10 ⁴
²³⁵ U	1.8×10 ²
²³⁶ U	1.8×10 ³
²³⁸ U	9.5×10 ³
²³⁷ Np	1.0×10 ⁴
²³⁸ Pu	5.7×10 ⁸
²³⁹ Pu	2.4×10 ⁷
²⁴⁰ Pu	8.0×10 ⁷
²⁴¹ Pu	1.1×10 ¹⁰
²⁴² Pu	5.3×10 ¹
²⁴¹ Am	3.7×10 ⁸
^{242m} Am	4.0×10 ⁶
²⁴³ Am	7.9×10 ⁶
²⁴² Cm	8.4×10 ³
²⁴⁴ Cm	1.4×10 ⁹

The MOX-fuel pieces B4+B5 were selected so that an initial fuel surface to leachant volume (S/V) ratio of 0.282 m⁻¹ was obtained, similar to the ratio used in the ²³³U doped UO₂(s) experiment (section 2.1.3). The surface area of the fuel (pieces B4+B5) is 50.8 mm² and their total weight is 0.399 g. No annealing of the MOX-fuel was made prior to the experiment.

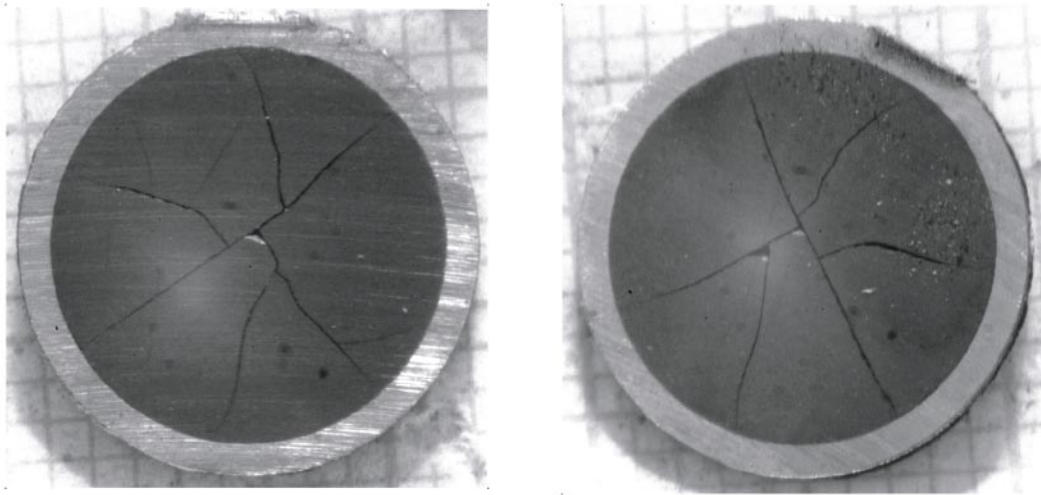


Figure 3-3. Pictures of MOX-fuel with cladding photographed from both sides. The purpose of the photographs was to find fuel pieces that had straight fuel rod longitudinal fractures making it possible to measure the geometrical surface area with enough accuracy.

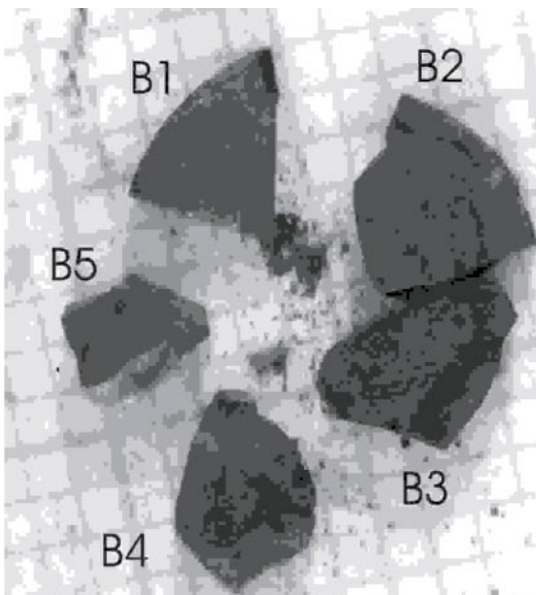


Figure 3-4. Picture of the MOX fuel obtained after cutting and removal of zircalloy cladding. It can be seen that part of the rim structure is intact despite the high fuel burn-up. The pieces B4+B5 were selected for the leaching experiment.

3.1.2 Leach test description

Spent fuel corrosion experiment in 5 M NaCl brine under 3.2 bar external H_2 overpressure (FZK-INE)

The experimental work was divided in two parts, i.e. the pretreatment of the fuel pellet, denoted K8 by (1) several wash cycles under anoxic conditions followed by (2) the static test under the external applied H_2 overpressure of 3.2 bar. The wash cycles with complete renewal of the solution were carried out to ensure that the main part of the instant release fraction was removed, and to dissolve oxidized layers possibly formed on the cut pellet surface during storage.

Wash procedure

Quartz glass vessels of approximately 280 ml volume were used, Figure 3-5. They were equipped with fittings on the top to allow the introduction of an Ar gas atmosphere, the connection with the gas sampling device and solution sampling under reverse streaming Ar gas. Prior to the start of each test run the system (leachate and vessel) was flushed with Ar and then remained undisturbed.

The leachate was replaced entirely by fresh Ar flushed 200 ml NaCl-solution (5 M) after 1, 3, 21, 42, 80 days; afterwards a static phase of 212 days followed. Sampling of gases and solution was performed 1, 3, 21, 42, 80, 157 and 292 days after start of the wash procedure. Figure 3-5 shows the glass reaction vessel used for the wash procedure, during sampling of solution.

Autoclave static test

The effect of H₂ overpressure on the overall corrosion behavior of high burn-up spent fuel in 5 m NaCl brine was studied over a total duration of 3 years as a static test. To apply the desired H₂ overpressure a Ti/Pd-lined stainless steel autoclave (Berghof Company, Germany) with a total volume of 500 ml, equipped with an external pressure gauge and two ball valves, gas samples and solution samples to be taken under reverse streaming Ar. The Ti/Pd liner material is known to be very corrosion resistant and to maintain inert conditions during the experiment. Figure 3-6 shows schematically the design of the autoclave used. The starting salt solution volume for this test was 200 ml. By inserting 40 bar of a gas mixture of Ar / 8% H₂, a hydrogen partial pressure of approximately 3.2 bar was achieved. Then, after closing the valve and disconnecting from the Ar/H₂ pressure supply, the autoclave was stored at room temperature in the hot cell under air atmosphere.

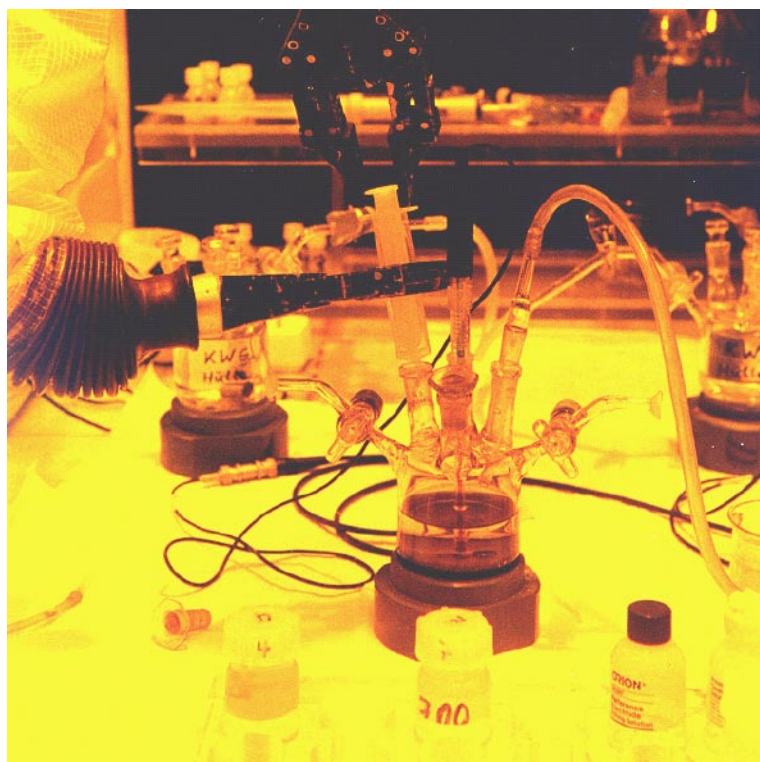


Figure 3-5. Glass reaction vessel used to perform the wash procedure of pellet K8.

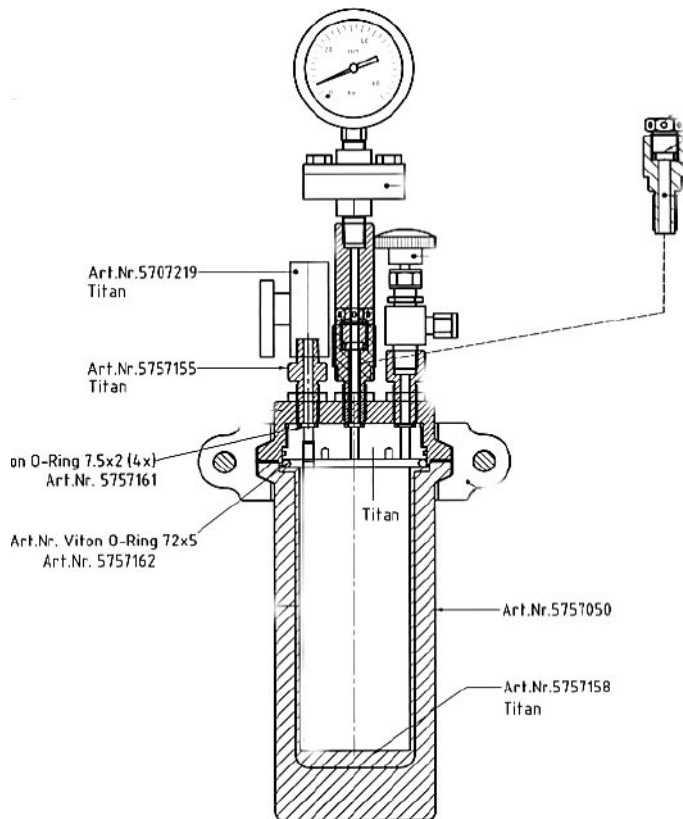


Figure 3-6. Design of the autoclave used for spent fuel corrosion tests under 40 bar external Ar/8% H_2 overpressure. Autoclave material: stainless steel, interior material (liner, lid): Ti/5%Pd, volume: 500 ml.

The system pressure remained constant at 40 bars during each leaching interval, until sampling of gases and solutions were performed. Sampling was carried out at 53, 117, 213, 461, 697, 915, 1,095 days after start of the static test. After each sampling 40 bar Ar/ 8% H_2 was applied again and kept constant until the next sampling.

This experiment was terminated unintentionally after a total duration of 1,097 days under H_2 overpressure due to a failure of the burst disk of the autoclave, resulting in an eruption of ca 14 ml NaCl-brine out of the autoclave. Consequently, the autoclave was not air tight anymore. To reduce the potential intrusion of air, the autoclave was connected to the Ar-supply and was flushed with Ar gas again. The autoclave was opened 11 days after the burst disc failure. The solution was analyzed again and the fuel pellet, which was found to be covered by a layer of NaCl crystals, was recovered.

Autoclave leaching of MOX fuel under 50 bar H_2 (ITU/SKB)

MOX-autoclave set-up

The leaching experiment was performed in an autoclave with a total volume of 200 ml (Parr Instruments Co, USA). The autoclave is constructed so that the autoclave solution could be purged with gas during fuel loading and leachate samples could be withdrawn without letting oxygen enter the autoclave.

A considerable effort was invested to adapt the MOX-autoclave for hot cell handling and hot cell servicing. This necessitated use of computer aided drawings to optimize the autoclave size and the position of valves for manipulator handling, Figure 3-7.

The autoclave was manufactured of Ti, quality grade II-weldable, with a composition of 99.3 wt-% Ti, 0.3 wt-% Fe and the trace elements: C, N, O and H. Additionally, all wetted surfaces of the autoclave set-up e.g. pellet holder, magnetic stirrer, valves, security valves and tubing were made of titanium. Graphite seals were used to avoid metallic or organic seals that exhibit either a high sorption of actinides or poor radiation resistance. The autoclave set-up was certified for an H₂-pressure of 68 bar.

The leachate in the autoclave was initially stirred using a magnetic stirrer. The leachate was collected using the pressure inside the autoclave to push the solution from the bottom of the autoclave into a 20 ml PE-sampling vial. The complete autoclave set-up is shown in Figure 3-8.

Leachate

Only ultra pure milliQ-water (>18 MΩ/m, UHQ, Elgastar) and pro analysis grade chemicals (Merck, suprapur) were used. The initial solution consisted of 10 mM NaCl and 2 mM HCO₃⁻. The pH of the initial solution was measured with a combined KCl pH-electrode (WTW SenTic Mic, and WTW pH340/ION analysator, Germany).

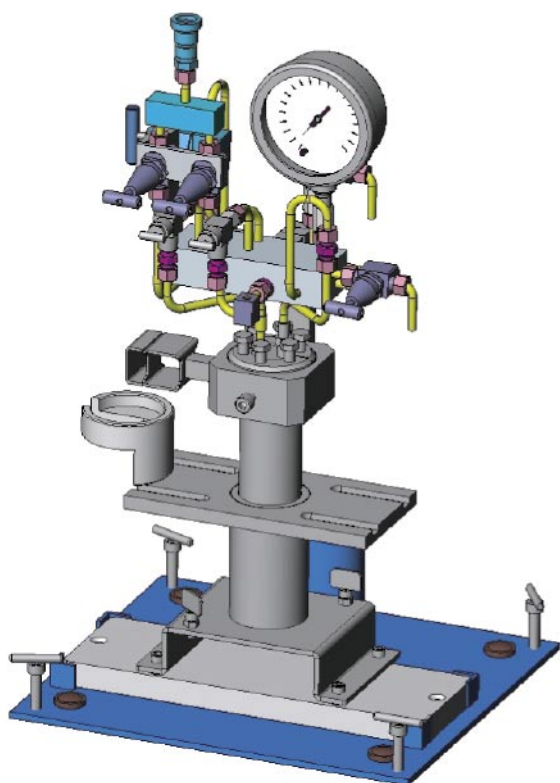


Figure 3-7. Drawing made in 3-D CAD of the MOX autoclave (with a total volume of 200 ml) together with the six valves and grips for manipulator handling, autoclave support and holder for stirrer. The lower part of the drawing (blue) is the moveable table to be able to move the whole set-up weighting 25 kg in the hot cell.

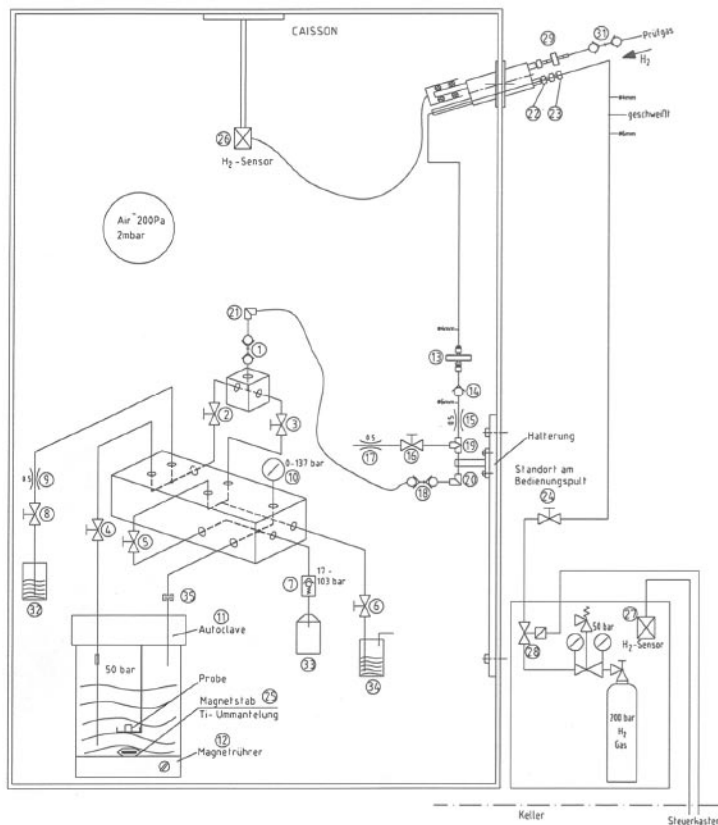


Figure 3-8. Principal scheme of the MOX autoclave installation in hot cell Z112 at ITU. New equipment for H₂ detection in the hot cell had to be developed together with safety routines for the surveillance office as well as automatic shutdown of H₂-gas supply.

Loading of the MOX autoclave

The time that passed between the fuel cutting, de-cladding, sample transfer and the actual start of the leaching experiment was 2 weeks. Before the start of the experiment the autoclave was washed several times with milliQ-water. The two MOX-fuel pieces B4+B5, Figure 3-4, were loaded into the fuel holder. The holder with the fuel was dipped into 103.5 ml of a H₂ purged leachate for a period of 20 min. This fuel wash was performed to remove the oxidized U(VI)-layer present on fuel surface due to exposure to the air atmosphere in the hot cell. After the wash, the fuel was directly lowered into the autoclave that was filled with 180.0 ml of H₂ pre-purged leachate. The leachate was purged with H₂ during the whole loading sequence. This was made to assure reducing leaching conditions around the fuel as soon as possible after the fuel wash. The mounting of the autoclave lid took about 20 min. Directly after the mounting of the lid the autoclave was pressurized with pure H₂ to 53 bar. The S/V-ratio at the start of the experiment was 0.282 m⁻¹.

Autoclave test description

The static corrosion experiment of the MOX fuel started on 18 December 2002 and was run for a period of 494 days at 53.1 ± 1.7 bar (2σ confidence level) H₂-pressure without opening the autoclave. Hydrogen gas of highest purity grade (Linde/AGA, Scientific 6.0) was used to pressurize the autoclave and for purging the tubing. The leachate was stirred with a magnetic stirrer at a speed of 100 rpm during the first 6 months and after this first period no more stirring was applied. The experiment was run at a room temperature of $22 \pm 4^\circ\text{C}$.

The H₂-pressure in the autoclave was kept constant during sampling by opening the autoclave connection to the gas supply adjusted to 53 bar. The pressure was measured continuously. A fully acceptable pressure leak rate of < 15 Pa/h, at 53 bar H₂ pressure, was measured during the experiment.

The number of sampling occasions was limited due to the small amount of solution in the autoclave (180 ml) and to the impossibility to refill the autoclave during the experiment. The sampling intensity was optimized taking into consideration: a/ the number of samplings, b/ the sample volume that is necessary for analysis, c/ the amount of leachate wasted for rinsing the tubes (the leachate that is not in contact with the fuel), d/ the number of samplings at each H₂ concentration (to determine the threshold for suppression of UO₂ corrosion), e/ sufficient time between two samplings to obtain a steady state leaching concentration with at least three samples at each level and, f/ the total time of the experiment. The sampling of leachate was made in two steps: first a rinse sample was collected (5 ml) to remove the solution in the tubes and then the representative sample (approximately 3 ml) was collected. Samples were withdrawn from the autoclave after 3 hours, 26 days, 203 days and 494 day.

3.1.3 Analytical procedures

Gas and solution analysis (FZK-INE)

During the wash cycles and the static phase, samples from the gas atmosphere in the autoclave were taken each time before solution was sampled. The glass reaction vessel and the high pressure autoclave were connected over a three port valve with an evacuated (10⁻⁶ bar) 50 cm³ gas collection cylinder, a vacuum pump, and the Ar gas supply. The Ar/H₂ overpressure was then slowly reduced from 40 to roughly 1.5 bar over a tube of ca 1.5 m length. Then, the connecting tube system was evacuated and flushed with Ar and evacuated again several times to remove the remaining amount of air as best as possible. The gas composition was analyzed quantitatively by a quadrupole mass spectrometer (GAM 445, Balzers, Liechtenstein).

The calibration was performed using a gas mixture with known amounts of H₂, N₂, O₂, Kr and Xe in Ne. Figure 3-9 shows the autoclave, when connected to the vacuum pump, to the Ar supply and to the fitting of the gas collection cylinder. The gas collection cylinder was located outside the hot cell, and connected via a feed through with the related components in the hot area. A filter disc was inserted at the interface to retain active particles from the cylinder. Figure 3-10 shows the gas collection cylinder outside the hot cell, when connected with the tube system.

Solution samples (10 ml) were taken immediately after the gas sampling, under reverse Ar gas streaming to avoid air intrusion. All solution samples were filtered through a 0.45 µm filter to retain unintentionally sucked fuel particles. Aliquots were additionally filtered by 1.8 nm ultrafilters (Amicon Centricon 10). By comparison of the solution concentrations of the ultrafiltrated aliquot to that of the 0.45 µm filtrate upper limits for colloid formation shall be identified. Solutions were analyzed by α-spectrometry (²³⁸Pu, ^{239/40}Pu), γ-spectrometry (¹²⁵Sb, ^{134/137}Cs, ¹⁴⁴Ce, ²⁴¹Am, ^{154/155}Eu), LSC (⁹⁰Sr, ²⁴¹Pu) and ICP- MS (⁹⁹Tc, ²³⁷Np, ²³⁸U).

Radiochemical and gas analyses procedures are described in detail in [GRA/LOI 1996]. Measured pH – data were corrected for liquid junction potential. Liquid junction potentials were obtained by measuring the pH value (pH_{exp}) of the leachants with known activity a_{H+} [GRA/MUL 1990]. Reported pH_{EQ3/6} values are consistent with Pitzer's pH convention (e.g. implemented in the EQ3/6 software package [WOL 1992]). A detailed discussion on the conversion of measured pH_{exp} values into -lg(m_{H+}) and pH_{EQ3/6} values are given in [ALT/MET 2003].

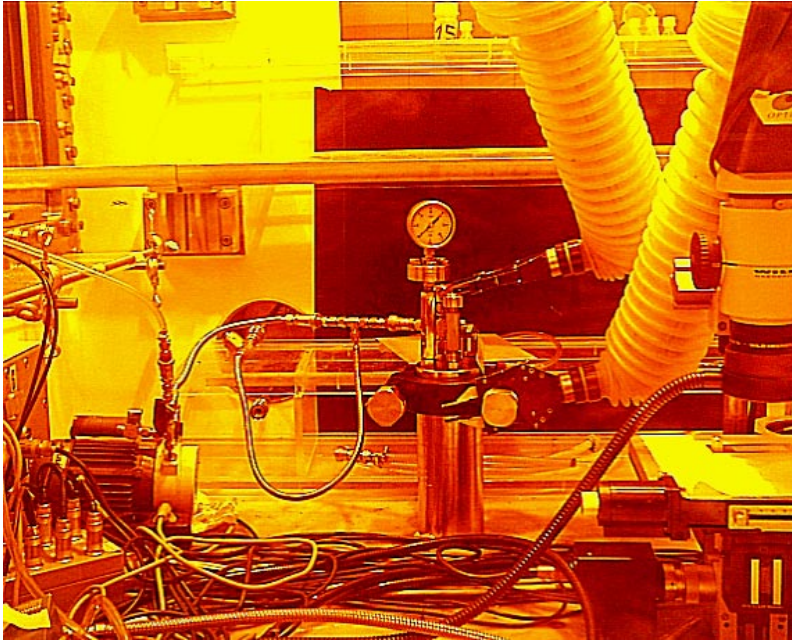


Figure 3-9. High pressure autoclave (Berghof Company, Germany) used for corrosion test of spent fuel pellet K8 under 40 bar Ar/ 8% H_2 overpressure (total volume 500 ml), connected to the vacuum pump and the Ar supply and a gas collection cylinder outside the hot cell prior to take gas samples.



Figure 3-10. Gas collection cylinder outside the hot cell (volume 50 cm^3).

Analysis of the MOX leachate (ITU)

The MOX-leachate was sampled into 20 ml PE-vials. Sub-samples of the leachate were used for different analysis without pre-filtration. The samples were analyzed to determine the concentration of the leached fission products and actinides using high-resolution inductively coupled plasma mass spectrometry (HR-ICP-MS); radiometric methods were also applied.

The leachate was analyzed using HR-ICP-MS (Element 2, Thermo Electron, Germany) located in a glove box and adapted for handling of radioactive samples. Before the analysis all samples were acidified to give a 1 M HNO₃ sample solution. Two batches of samples were prepared, one batch was non-spiked and the second was spiked with a standard consisting of 1 ppb of each element: Sc, Co, In, Ho and ²³⁶U. An external calibration of the HR-ICP-MS was made using two multi-element standards (Agilent Life Sciences/ Chemical Analysis, Germany) denominated internally at ITU as (1+3) and (2A+4). The first mixed standard (1+3) contained: Ce, Dy, Er, Eu, Gd, Ho, La, Lu, Nd, Pr, Sc, Sm, Tb, Th, Tm, Y, Yb and Au, Hf, Ir, Pd, Pt, Rh, Ru, Sb, Sn, Te and was diluted to give concentrations of 50 ppt, 200 ppt, 1 ppb, 5 ppb and 20 ppb. The second mixed standard (2A+4) contained: Ag, Al, As, Ba, Be, Ca, Cd, Co, Cr, Cs, Cu, Fe, Ga, K, Li, Mg, Mn, Na, Ni, Pb, Rb, Se, Sr, Tl, U, V, Zn, Bi, In and B, Ge, Mo, Nb, P, Re, S, Si, Ta, Ti, W, Zr. This second standard was diluted to the same concentrations as for standard 1+3. Additionally, two quality assurance (QA) solutions were prepared and run at different times between the samples to check the HR-ICP-MS performance. These QA-samples contained the internal standards (Sc, Co, In, Ho and ²³⁶U) and the calibration standards (1+3), alternatively (2A+4). The evaluation of the measurement data was made manually. The raw data were corrected for instrumental drift and the blank intensities were subtracted. Calibration of all U and Pu isotopes was performed versus the ²³⁶U intensities of the standard series. Correction for mass bias was performed. The fission product concentrations were corrected for the influence of naturally abundant elements.

3.2 Results and discussion on spent fuel leaching

3.2.1 Leaching of high burn-up spent fuel in 5 M NaCl solution under 40 bar Ar / 8% H₂ overpressure (FZK-INE)

Effect of internal final H₂ overpressure on release rates in salt solutions

In previous experiments, the relation between the release rates of radionuclides and of an internal generated H₂ overpressure in the range between 0.0001 and 2.8 bar was studied by analyzing results from various spent fuel corrosion tests under initially Ar-atmosphere. These studies comprised corrosion tests of high burn-up spent fuel pellets in 5 M NaCl solution, in the absence of carbonate, in the presence/absence of iron and its corrosion products, where the evolution of hydrogen was monitored continuously. The results obtained from these tests indicate that the release rates of important radioelements decrease, if the final H₂ system overpressure increases. The maximum internal H₂ overpressure within these tests was found to be 2.8 bar. It was built up due to the corrosion of the Fe powder during the last sampling interval of 1,049 days of a long-term co-dissolution test using spent fuel pellet and initially metallic Fe powder in 5 M NaCl-solution. Simultaneously, the progress of matrix dissolution appeared to stop, as indicated from the rate of release of the Sr inventory of the fuel into solution (dissolution rate < 1×10⁻⁸/d). The concentrations of important radioelements such as Am, Pu, Tc, U in solution were significantly lower than anticipated from the total amount of dissolved fuel [GRA/LOI 1996].

The decrease of release rates of Cs, Sr, Pu and U in terms of fraction of the inventory in the aqueous phase (FIAP) per day as a function of the final H₂ overpressure built up during the related sampling interval is shown in Figure 3-11.

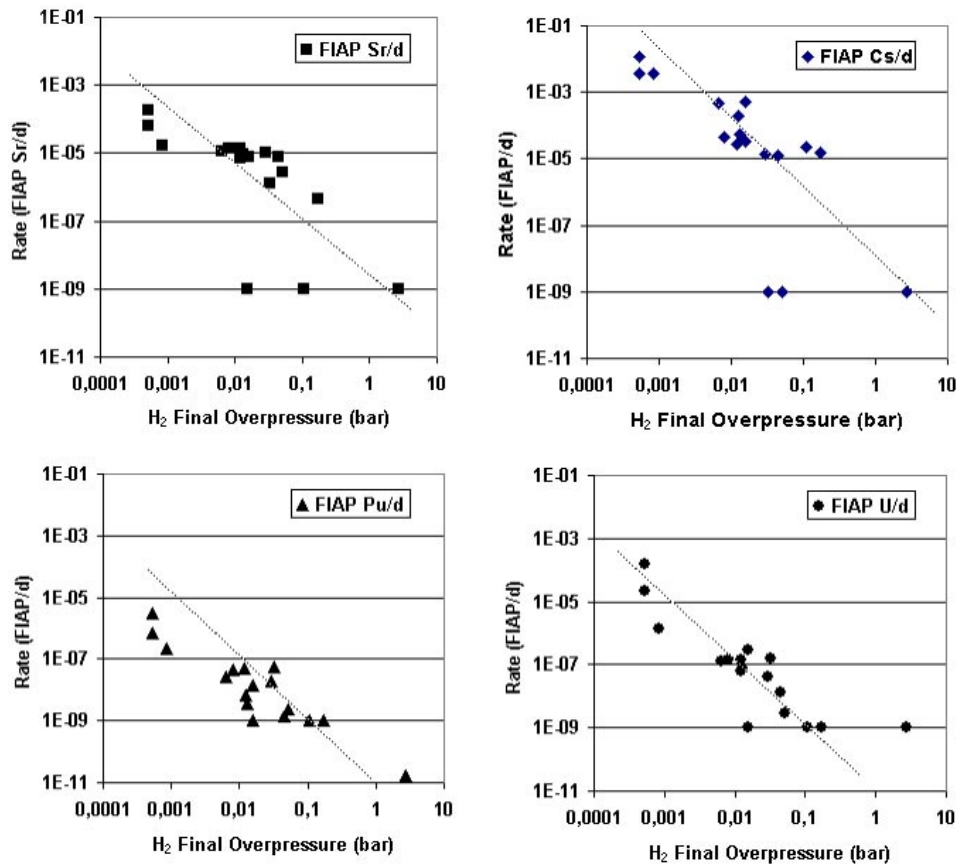


Figure 3-11. Released fractions of the fuel inventory in the aqueous phase (FIAP) of Sr, Cs, U, Pu per day as a function of hydrogen final overpressure from various spent fuel corrosion tests in 5 M NaCl solution.

The results of these previous tests are used for comparison with these obtained from the present spent fuel corrosion test under external H₂ overpressure. In the present test spent fuel was corroded in the absence of Fe powder, and under 3.2 bar H₂ overpressure, applied from an external source as described in section 3.1.2.

All spent fuel samples studied in the present and the previous tests were taken from the same fuel, from the same fuel rod and fuel segment, and were used as pellet sized segments (section 3.1.1.).

Effect of external applied H₂ overpressure on the corrosion behaviour of spent fuel

The results of the static corrosion test obtained under 3.2 bar H₂ overpressure during 1,095 days are presented together with the data of the preceding wash cycles. In the related diagrams, Figures 3-12 and 3-13, the release of important radioelements into solution is shown in units of fraction of the inventory in the aqueous phase (FIAP) as a function of time and the associated released fractions of fission gas (FG: Kr, Xe) are plotted as well. The concentrations (mol/l) of the released elements as a function of time are shown in Figures 3-16 and 3-17 and in Table 3-5. All FIAP values of important radionuclides obtained in the course of the wash cycles and of the static test under H₂ overpressure are summarized in Table 3-3, while the results of the gas phase analysis are summarized in Table 3-4.

a. Radionuclide release during wash cycles

More than 84% of the instant release fraction (IRF, labile radionuclide fraction, encountered upon the fuel sheath gap, fracture surfaces, grain boundaries to be released instantaneously upon water contact to the fuel) was released into solution, as indicated by the Cs release within the first 80 days, when the solution was replaced 5 times. During this time the released fraction of Cs (FIAP_{Cs}) decreased from initially ca 10⁻² to 10⁻³, Figure 3-12.

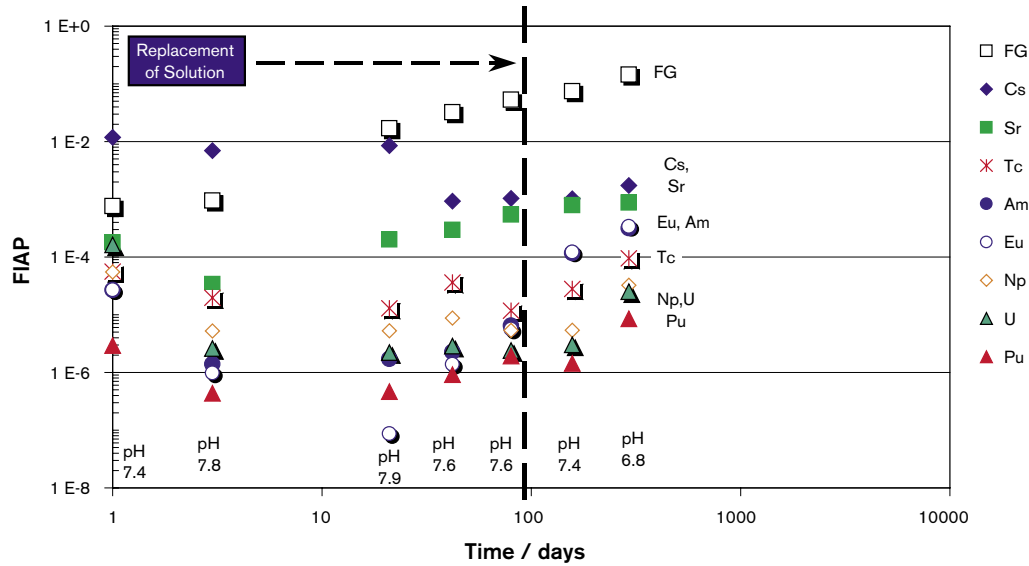


Figure 3-12. Fractions of radionuclide inventories in the aqueous phase (FIAP) during 292 days pre-treatment (wash cycles) of spent fuel pellet K8 in 5 M NaCl solution under initial Ar-atmosphere. Measured Eh values were between 300 and 500 mV.

Table 3-3. Fractions of the inventory in the aqueous phase obtained during wash cycles and corrosion of spent fuel pellet K8 under 3.2 bar H₂ overpressure.

Corrosion of high burn-up spent fuel pellet K8 in 5 M NaCl solution in the absence of carbonate.												
Fraction of the radionuclide inventory in the aqueous phase (FIAP).												
	Identification	pH korr	cum time/d	FG	Cs	Sr	Eu	Am	Tc	Np	Pu	U
SF Washcycl *	K8 W1	7.34	1	7.61E-04	1.18E-02	1.79E-04	2.71E-05	2.69E-05	5.60E-05	5.52E-05	2.92E-06	1.62E-04
SF Washcycl *	K8 W2	7.79	3	9.51E-04	6.98E-03	3.40E-05	9.77E-07	1.40E-06	1.97E-05	5.23E-06	4.36E-07	2.59E-06
SF Washcycl *	K8 W3	7.98	21	1.69E-02	8.52E-03	2.02E-04	8.70E-08	1.71E-06	1.30E-05	5.28E-06	4.66E-07	2.22E-06
SF Washcycl *	K8 W4	7.67	42	3.22E-02	9.32E-04	2.94E-04	1.39E-06	2.26E-06	3.63E-05	8.79E-06	9.19E-07	2.86E-06
SF Washcycl *	K8 W5	7.6	80	5.30E-02	1.04E-03	5.43E-04	5.64E-06	6.48E-06	1.18E-05	5.36E-06	1.92E-06	2.39E-06
SF Washcycl *	K8 W6	7.36	157	7.42E-02	1.02E-03	7.91E-04	1.22E-04	1.16E-04	2.81E-05	5.41E-06	1.44E-06	3.02E-06
SF Washcycl	K8 W6a	6.83	292	1.45E-01	1.73E-03	8.74E-04	3.38E-04	3.15E-04	9.49E-05	3.25E-05	8.51E-06	2.51E-05
Static test												
SF H2 Overpr*	K8 S1	4.9	53	7.61E-04	4.02E-04	3.49E-05	7.02E-05	5.72E-05	2.73E-05	3.40E-05	5.60E-06	4.49E-07
SF H2 Overpr	K8 S2	6.5	117	9.09E-04	4.62E-04	5.12E-05	3.95E-06	2.08E-06	1.36E-05	2.63E-06	2.63E-06	9.02E-08
SF H2 Overpr	K8 S3	7.7	213	1.02E-03	5.74E-04	6.13E-05	6.03E-06	2.92E-06	1.63E-05	8.77E-07	1.91E-06	6.99E-08
SF H2 Overpr	K8 S4	6.3	461	1.41E-03	5.27E-04	1.14E-04	2.63E-06	1.58E-06		1.43E-06	5.45E-07	6.65E-08
SF H2 Overpr	K8 S5	6.27	697	1.50E-03	6.04E-04	1.68E-04	1.28E-06	5.76E-07		1.77E-06	5.44E-07	1.29E-08
SF H2 Overpr	K8 S6	7.8	915	1.58E-03	7.54E-04	1.66E-04	2.20E-05	8.56E-06	1.08E-05	7.61E-07	3.64E-07	2.04E-07
SF H2 Overpr	K8 S7	7.7	1,095	1.70E-03	8.38E-04	2.26E-04	1.41E-05	2.05E-05	3.29E-06	4.08E-07	1.22E-06	1.05E-07
Burst disk fail.	K8 S8	7.8	1,110		7.03E-04	2.08E-04	1.78E-05	2.12E-05	2.93E-05	2.81E-06	9.76E-06	1.89E-06
* = fresh NaCl-brine												
Reference test		9.75	ca 4.5y	4.52E-02	1.55E-02	3.12E-05	< 2.86E-07	< 2.48E-07	1.11E-05	< 7.29E-06	< 2.04E-08	1.6985E-07
SF pellet K4+Fe												

Table 3-4. Compositions of the gas phases in the free gas volume during corrosion of spent fuel pellet K8 in 5 M NaCl solution during the static test under 40 bar Ar/ 8% H₂ external overpressure. including blank measurements of the connection between autoclave and gas vessel (blank 1, blank 2) measured by mass spectrometry. Reference samples are from the last interval of long-term corrosion of pellets K9 and K4+Fe under initial Ar-atmosphere.

Static test under 40 bar Ar/8% H₂ Overpressure (hot cell atmosphere: air)									
	1. Sampling	2. Sampling	3. Sampling	4. Sampling	5. Sampling	6. Sampling	7. Sampling	Blank 1	Blank 2
	K 8 S1	K 8 S2	K 8 S3	K 8 S4	K 8 S5	K 8 S6	K 8 S7		
Interval	53 d	64 d	96 d	248 d	236 d	218 d	180 d		
	%	%	%	%	%	%	%	%	%
Ar	94.1523	94.1615	92.5750	95.63620	93.0954	90.6229	93.0588	98.6480	99.3410
CO ₂	0.0036	0.0033	0.0037	0.00710	0.0024	0.0056	0.0022	0.0079	0.0025
H ₂	5.9084	5.8073	7.3787	4.30000	6.8631	6.8793	6.9208	0.0182	0.0068
Kr	0.0005	0.0002	0.0001	0.00054	0.0001	0.0001	0.0001	0.0003	0.0001
N ₂	0.0130	0.0133	0.0220	0.02336	0.0254	1.9598	0.0074	1.0600	0.5087
Ne	0.0130	0.0116	0.0130	0.02008	0.0088	0.0131	0.0092	0.0436	0.0104
O ₂	0.0022	0.0023	0.0070	0.00437	0.0046	0.5190	0.0014	0.2220	0.1300
Xe	0.0008	0.0006	0.0005	0.00084	0.0003	0.0002	0.0001	0.0000	0.0001

Static test under initial Ar atmosphere (hot cell atmosphere: N₂ or air, respectively)		
	K 9 S5	K4+Fe S5
Interval	1,183 d	1,182 d
	%	%
Ar	81.760	26.7100
CO ₂	0.010	0.0029
H ₂	13.860	73.0950
Kr	0.047	0.0044
N ₂	0.378	0.1230
Ne	0.022	0.0090
O ₂	3.440	0.0022
Xe	0.482	0.0489

Table 3-5. Concentrations of radioelements obtained during wash cycles and corrosion of spent fuel pellet K8 in 5 M NaCl solution under 3.2 bar H₂ overpressure.

Corrosion of high burn-up spent fuel pellet K8 in 5 M NaCl brine in the absence of carbonate											
Concentrations (Mol/l)											
	Identification	pH korr	Cum time/d	Cs	Sr	Eu	Am	Tc	Np	Pu	U
SF Washcycl *	K8 W1	7.34	1	1.01E-05	7.04E-08	1.08E-09	1.61E-09	1.90E-08	4.92E-09	4.07E-09	1.87E-05
SF Washcycl *	K8 W2	7.79	3	6.07E-06	1.37E-08	1.13E-11	8.54E-11	6.79E-09	4.76E-10	6.18E-10	3.06E-07
SF Washcycl *	K8 W3	7.98	21	7.41E-06	8.11E-08	3.55E-12	1.04E-10	4.48E-09	4.81E-10	6.62E-10	2.62E-07
SF Washcycl *	K8 W4	7.67	42	8.04E-07	1.17E-07	5.59E-11	1.37E-10	1.24E-08	7.93E-10	1.29E-09	3.35E-07
SF Washcycl *	K8 W5	7.6	80	8.97E-07	2.17E-07	2.29E-10	3.95E-10	4.04E-09	4.86E-10	2.71E-09	2.82E-07
SF Washcycl *	K8 W6	7.36	157	8.77E-07	3.14E-07	4.90E-09	7.02E-09	9.56E-09	4.86E-10	2.01E-09	3.52E-07
SF Washcycl	K8 W6a	6.83	292	1.68E-06	3.92E-07	1.54E-08	2.15E-08	3.66E-08	3.31E-09	1.35E-08	3.31E-06
Static test											
SF H2 Overpr*	K8 S1	4.9	53	3.44E-07	1.38E-08	2.81E-09	3.44E-09	9.27E-09	3.04E-09	7.81E-09	5.21E-08
SF H2 Overpr	K8 S2	6.5	117	4.12E-07	2.11E-08	1.65E-10	1.31E-10	4.83E-09	2.45E-10	3.82E-09	1.09E-08
SF H2 Overpr	K8 S3	7.7	213	5.43E-07	2.68E-08	2.68E-10	1.95E-10	6.12E-09	< 8.70E-11	2.96E-09	8.99E-09
SF H2 Overpr	K8 S4	6.3	461	5.63E-07	5.32E-08	1.24E-10	1.12E-10	1.17E-08	1.51E-10	8.98E-10	9.12E-09
SF H2 Overpr	K8 S5	6.27	697	6.34E-07	8.54E-08	6.56E-11	4.45E-11		2.04E-10	9.74E-10	1.92E-09
SF H2 Overpr	K8 S6	7.8	915	9.19E-07	9.24E-08	1.24E-09	7.23E-10		< 9.57E-11	7.13E-10	3.32E-08
SF H2 Overpr	K8 S7	7.7	1,095	1.06E-06	1.39E-07	8.80E-10	1.92E-09	< 1.74E-09	< 5.71E-11	2.66E-09	1.91E-08
Burst disk fail.	K8 S8	7.8	1,110	1.13E-06	1.54E-07	7.74E-10	2.38E-09	1.86E-08	4.71E-10	2.55E-08	4.10E-07
Reference test		9.75	ca 4.5y	1.91E-05	1.78E-08	< 6.40E-12	< 2.15E-11	5.42E-09	< 9.40E-10	< 4.09E-11	2.84E-08
SF pellet K4+Fe											

Using the data of Sr release into solution as indicators for the progress of matrix degradation, the dissolution of the UO₂-matrix, was calculated to be between ca 10⁻⁵/d (initial stage) and ca 10⁻⁶/d (after 292 days). This is ca 1–2 orders of magnitude higher than found in an earlier test carried out under anoxic conditions, when corroding pellets K 9 and K 10 [GRA/LOI 1996]. The reason for the relative high Sr release might be the formation of an oxidized surface layer on the pellet due to potential air intrusion into the supposed air-tight storage capsule, where it was kept over 7 years after cutting. The released fractions of the fission gas inventories (Kr, Xe) increased at first strongly up to ca 10⁻¹ and could not be correlated with the release behavior of Cs. U and radioelements considered to be bound to the matrix, such as Tc, Np, Pu, Eu and Am released slowly during the first 80 days. Their FIAP values are found to be ca two orders of magnitude below the FIAP of Sr. Between 80 and 292 days of the wash cycle (still in the absence of external H₂ overpressures, when only a small quantity of solution was sampled, and no solution was replaced) a significant increase of Eu and Am fractions (ca 2 orders of magnitude) and a less pronounced increase in the Np, Pu, U and Tc fractions (max. 1 order of magnitude) was found as compared to the initial wash cycles under replenishment conditions. During this stage there was almost no increase in the FIAP of either Sr or Cs.

The pH varied between 7.4 and 7.8 during the initial stage of the test up to 80 days followed by a decrease to 6.8.

b. Radionuclide release under H₂ overpressure

The effect of H₂ overpressure is illustrated in Figure 3-13, where the released fractions of important radioelements are plotted as a function of time. The results are contained from all seven samplings during 1,095 days of corrosion under 3.2 bar external H₂ overpressure. It is found that fractions of Sr and Cs were released significantly slower under H₂ overpressure than in the preceding wash cycle under Ar-atmosphere. Although under these

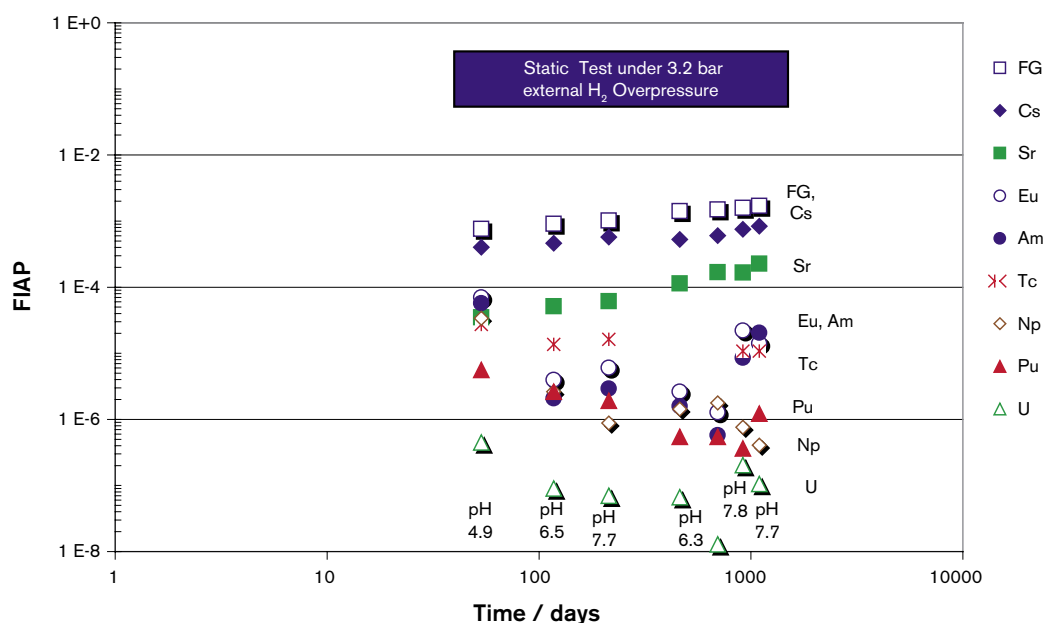


Figure 3-13. Fractions of radionuclide inventories in the aqueous phase (FIAP) during 1,095 days corrosion of spent fuel pellet K8 in 5 M NaCl solution under external H₂ overpressure. Measured Eh values were between –300 and –500 mV.

conditions a slow down of the matrix dissolution rate was indicated by the lower Sr release, matrix dissolution continues at a rate of ca $10^{-7}/d$. Grain boundary release of Cs was found to continue under hydrogen overpressure. However, the amount of released fission gases was now very close or below the detection limit.

FIAP values for U, Pu, Am and Eu were found to be strongly decreasing with time during the first 697 days. However, 915 days after the start of the static tests (6th sampling interval) a simultaneous increase of the U, Am and Eu fractions was observed, while the related fractions of Cs, Sr, Tc, Np, Pu remained in the same range or continued to decrease. Because of the constant Sr release rate and the very low release of fission gases, one can exclude that enhanced fuel dissolution is responsible for this increase of U, Am and Eu concentrations.

Additional evidence for the effect of H₂ overpressure can be obtained, when comparing the amount of radionuclides released in solution during 213 days of the static phase of the wash cycle and after the first 213 days under 3.2 bar H₂ overpressure, as shown in Figure 3-14. All analyzed radionuclides were found to be released at a significantly lower extent under H₂ overpressure, with differences ranging from a factor of more than 100 (⁸⁵Kr, ¹⁴⁴Xe, ²³⁸U) to a factor of about 3 (¹³⁷Cs). The amount of Sr in solution was found to be at factor 14 lower, indicating clearly a slow down of the matrix dissolution rates, if the Sr release is considered to be a real indicator of the progress of matrix dissolution.

The measured values of the compositions of the gas phase, which was present during the static test under H₂ overpressure, are summarized in Table 3-4 together with reference data from spent fuel corrosion under Ar-atmosphere.

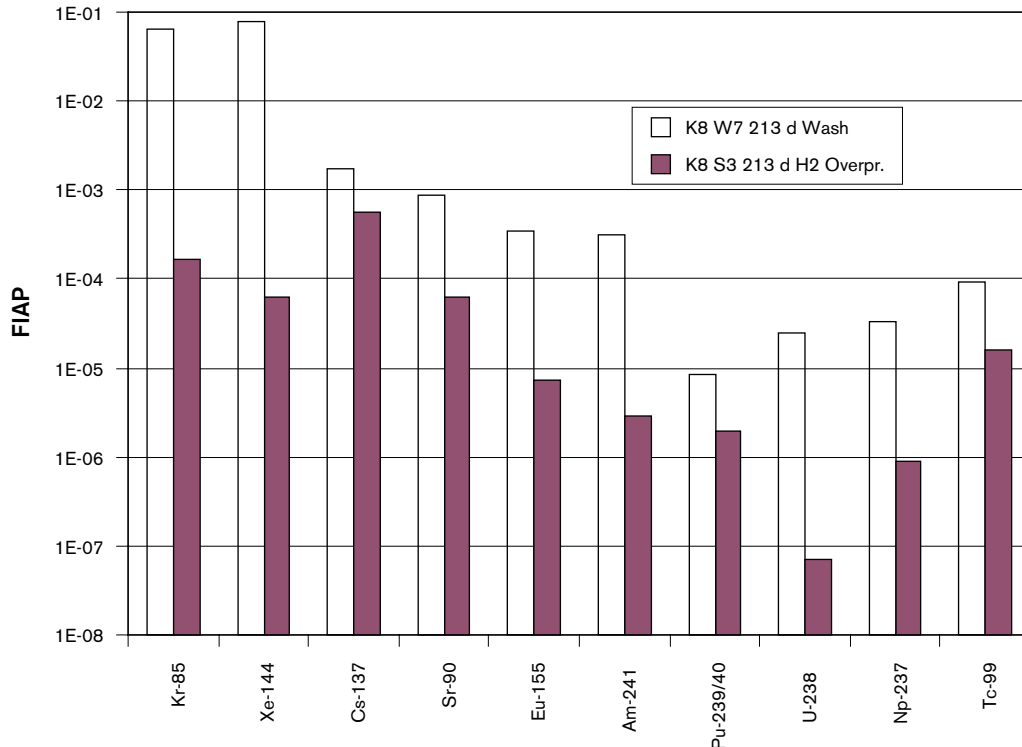


Figure 3-14. Fractions of radionuclide inventories in the aqueous phase (FIAP) after 213 days corrosion of spent fuel pellet K8 in 5 M NaCl solution during (i) the wash cycle in the time interval of 80–293 days, when no solution was replaced and in (ii) the static test under external H₂ overpressure.

Effect of internal and external applied H₂ overpressure on the overall matrix dissolution during the entire test duration

The impact of internal H₂ overpressures in the range between 0.001 bar and 3.2 bar on the UO₂ matrix dissolution can be demonstrated very distinctly, when comparing the total UO₂ matrix dissolution during the entire test time at various conditions, when H₂ overpressures of this size were effective. H₂ overpressures of 2.8 bar and above in these experiments were achieved either by corrosion of the initially added Fe powder (tests “K3+Fe”, “K4+Fe”), or by externally applied H₂ overpressure (test “K8”). In the frame of this study, we assume that the Sr inventory is distributed homogeneously in the UO₂ matrix, and that the release of Sr is a suitable indicator of the matrix dissolution progress [GRA/LOI 1996]. However, because this fuel was irradiated at a relatively high burn-up in association with partly high linear power rates one cannot exclude completely segregation processes transferring parts of the Sr outside of the matrix. This aspect will be discussed more detail in the last paragraphs of section 3.2.1. The amount of matrix dissolution during each test is calculated from the total amount of the released Sr inventory, which consists of its fractions in solution, on the vessel wall and on the Fe corrosion products, if present.

Figure 3-15 summarizes the effect of H₂ overpressure on the matrix dissolution in terms of the overall Sr release during the entire test duration. The impact of H₂ overpressure on the UO₂ matrix dissolution (Sr release) is evident from these results, when corroding pellet K8, before (K8 Wash) and after the application of external H₂ overpressure (K8 H₂ overpr.). During all wash cycles a total fraction of 2×10^{-3} of the matrix was dissolved during 292 days, whereas after the application of the H₂ overpressure a total fraction of only 4×10^{-4} was dissolved during 1,095 days. The amount of total matrix dissolution was found to be only slightly higher than found, when corroding pellets K3 and K4 in the presence of Fe powder. The significant difference of dissolution rates obtained during the wash cycles of pellet K8 compared to results of tests with pellets K9 and K10 can be explained by the fact that pellet K8 was pre-oxidized due to air penetration into the storage capsules (see section 3.1.1). In contrast, pellets K9 and K10 were used in the respective experiments immediately after cutting in N₂ atmosphere.

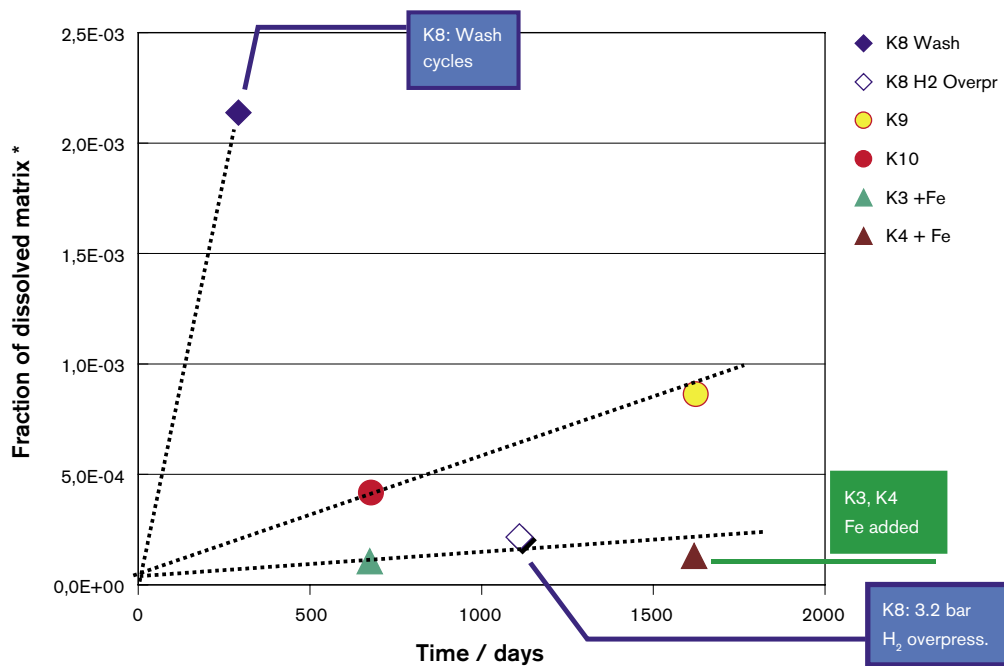


Figure 3-15. Fraction of dissolved matrix during high burn-up spent fuel corrosion tests in 5 M NaCl brine under various conditions (*based on the total Sr release and under the assumption that no Sr is sorbed on the fuel surface).

Evolution of solution concentrations

The evolution of solution concentrations is shown in Figure 3-16 and in Figure 3-17, where Cs, Sr, Tc, Pu, Np, U, Am and Eu concentrations during both the wash procedure and during the static test are plotted as a function of time. Additionally, for comparison Figure 3-17 contains the final solution concentrations found at the end of the 4.5 year test when corroding spent fuel pellet K4 in the presence of metallic Fe powder, where a 2.8 bar H₂ overpressure was built up [GRA/LOI 2000].

From both diagrams it obvious that the concentrations of redox sensitive radionuclides i.e. U, Tc, Np and Pu decreased due to the impact of H₂ overpressure. The strongest decrease was observed for U, whose concentrations decreased from about 10⁻⁶ M after 52 days to about 2×10⁻⁹ M after 697 days. Uranium is the major component of the fuel matrix (about 95%) and the evolution of its concentrations during this period indicates a precipitation process occurring in the autoclave. The number of potential solid uranium phases expected to form under such conditions is relatively small: UO₂(s) is the only U(IV) phase and metaschoepite or Na-diuranates as U(VI) phases. During the whole period up to 697 days the concentrations of uranium in the autoclave are below the solubilities of the potential U(VI) phases as seen from Figure 3-24. This decrease of the concentrations of uranium and other redox sensitive radionuclides is very probably due to a reduction of their oxidized forms present in the pre-oxidized layer formed on the fuel surface during the leaching under Ar, when radiolysis of water creates oxidizing conditions. At the end of the last wash cycle under Ar before the start of the leaching under external H₂ pressure, the concentrations of U in solution after 292 days were about 3×10⁻⁶ M. From the observed trend of the U concentrations during the first 697 days, it is possible that at the first day of the leaching under 3.2 bar external H₂ pressure the concentrations of uranium and other redox sensitive elements were even higher than those measured after 52 days (see section 3.2.3). Their decrease together with the below detection limit concentrations of molecular oxidants as O₂ and H₂O₂ indicate a potential reduction of U(VI) and other oxidized forms of the redox sensitive elements.

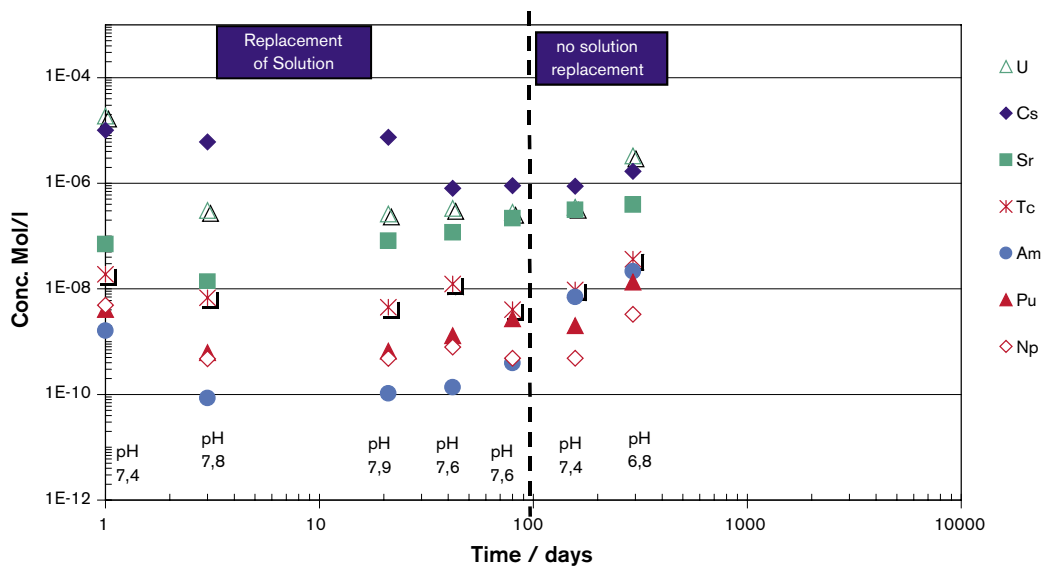


Figure 3-16. Radionuclide concentrations during 292 days pre-treatment (wash cycles) of spent fuel pellet K8 in 5 M NaCl solution under initial Ar-atmosphere. Measured Eh values were between 300 and 500 mV.

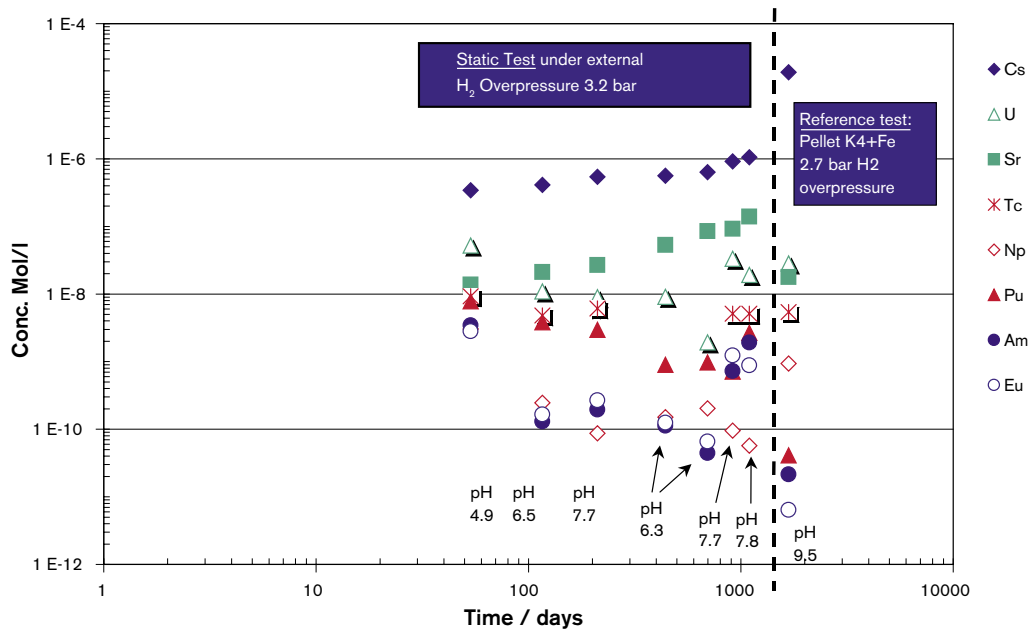


Figure 3-17. Radionuclide concentrations during 1,095 days corrosion of spent fuel pellet K8 in 5 M NaCl solution under external H₂ overpressure. Measured Eh values were between –300 and –500 mV.

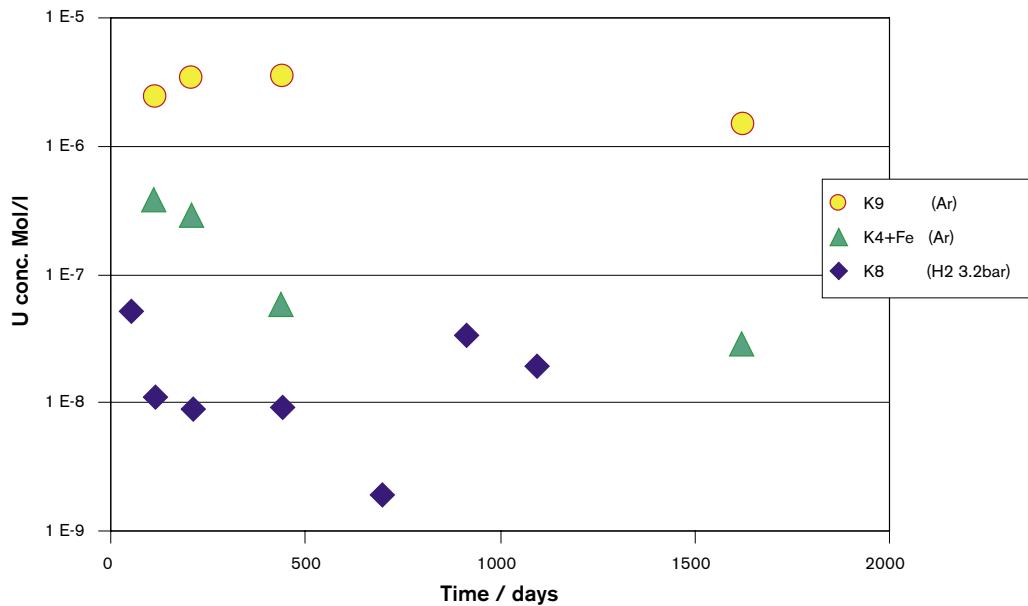


Figure 3-18. Concentrations of U during 1,095 days corrosion of spent fuel pellet K8 in 5 M NaCl solution under external H₂ overpressure in comparison to reference samples K9 and K4+Fe in absence/presence of Fe-powder under initial Ar-atmosphere.

During the next sampling after 915 days apparently air contamination of the solution occurred, as indicated by the gas analysis, Table 3-4 which shows the presence of both oxygen and nitrogen. It is probable that this air contamination happened during the sampling, since the ratios of N₂ and O₂ are quite close to that in air. The solution analysis data indicate that this apparently very small and short time air contamination was accompanied only with a significant increase of the uranium concentrations from 2×10^{-9} M to 3×10^{-8} M and a simultaneous increase of the Am and Eu concentrations, whereas all

other radionuclide concentrations remained unaffected, Figure 3-17. Thus, there was no indication of an enhanced fuel dissolution, which could be responsible for this increase, because potential matrix dissolution indicators such as Sr, Cs, Kr, Xe did not show any exceptional increase at the same time, Figure 3-13. It is interesting to notice that the concentrations of the U, Am and Eu are almost the same as the ones measured at the start of the experiment, indicating a possible dissolution of an easier soluble amorphous $UO_2 \cdot xH_2O(am)$ precipitate formed in the previous period under external H_2 pressure. In the following period (697–1,095 days) the concentrations of the U decrease again to reach the same final U concentration as observed in the reference test (K4+Fe) in the presence of corroding Fe (and 2.7 bar H_2).

The concentrations of Tc during the leaching of pellet K8 decreased by about a factor of 21, to 1.7×10^{-9} M, which is the same as in the reference test using pellet K4+Fe. Am and Eu- concentrations decreased by about a factor of 12 to final 10^{-9} M, but these concentrations are still more than two orders of magnitude higher than found in reference test K4+Fe. In the presence of Fe powder considerable amounts of initially mobilized radionuclides of the fuel inventory were retained upon the Fe corrosion products, in particular Am and Eu, but also Tc, Pu and U.

Under H_2 overpressure of 3.2 bar final Pu concentrations were determined to be 2.7×10^{-9} M, when corroding pellet K8 (a decrease by a factor of roughly 5), which is about 2 orders of magnitude higher than in the presence of Fe corrosion products (K4+Fe), as shown in Figure 3-19.

Np concentrations decreased under H_2 overpressure by about a factor of 57 and were close to or below the detection limit (ca 10^{-10} M). In contrast to Pu, Am and Eu, this final Np concentration is one order of magnitude lower than in the presence of Fe (K4+Fe).

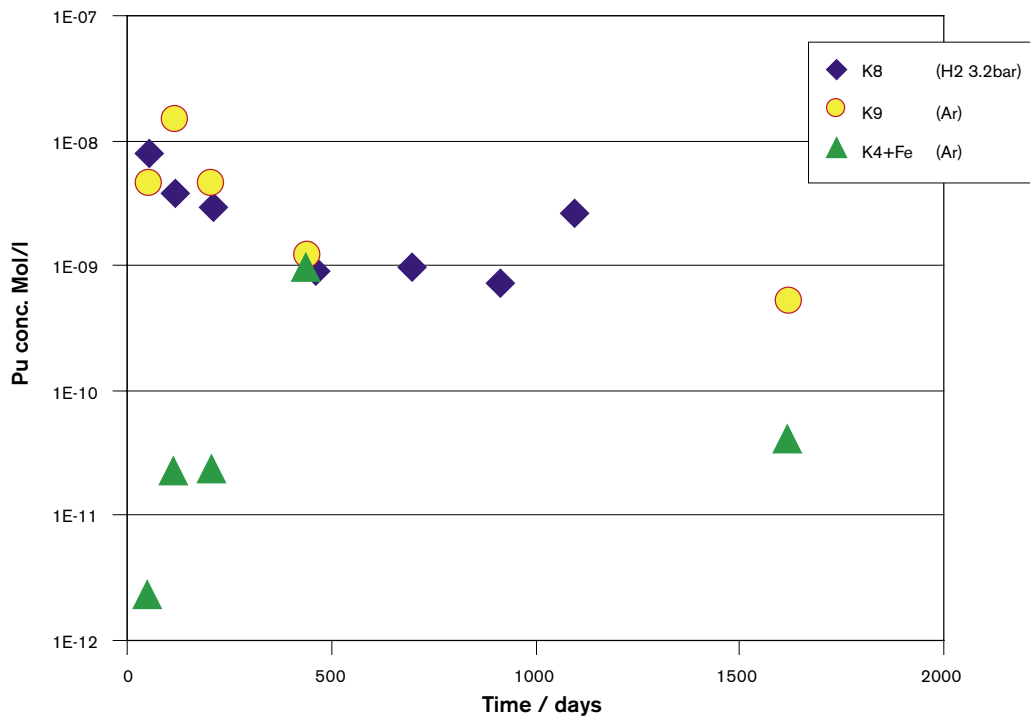


Figure 3-19. Concentrations of Pu during 1,095 days corrosion of spent fuel pellet K8 in 5 M NaCl solution under external H_2 overpressure in comparison to reference samples K9 and K4+Fe in absence/presence of Fe-powder under initial Ar-atmosphere.

The concentrations of Sr reached 2.7×10^{-8} M during the first period of 213 days of the static test under H_2 overpressure. In contrast, during the last phase of the wash cycles under Ar-atmosphere Sr concentrations of 3.9×10^{-7} M were reached for the same contact time between fuel sample and solution. During the 3 years K8 test, an increase of Sr concentrations from 1.4×10^{-8} M to 1.4×10^{-7} M was found. The evolution of Sr concentrations during this test is compared to that during corrosion under Ar-atmosphere in the absence (K9) and presence of Fe powder (K4+Fe), Figure 3-20.

It is observed that Sr concentrations are highest (8×10^{-7} M) during the test of pellet K9, and lowest during corrosion of pellet K4 in the presence of Fe (2×10^{-8} M).

In Figure 3-21, the variation of Cs concentrations as a function of time in the present experiment is compared to the variations of the Cs concentrations in the tests with pellet K9 (no Fe-addition) and K4 (presence of Fe). Cs concentrations increased from 8×10^{-7} M to 1×10^{-6} M when leaching pellet K8 under H_2 overpressure. The Cs concentrations from the test with pellet K8 are lowest.

The relative low Cs concentration in the present experiment is likely due to the preceding extensive wash cycles, where the greatest part of the Cs inventory from the instant release fraction (IRF) was washed out. The significant higher Cs concentrations obtained in the reference tests K9 and K4+Fe can be related to the fact that only two wash cycles each of 30 days were performed before start of the static test, whereas in the case of testing pellet K8 six wash cycles over 292 days reduced the Cs inventory significantly before the start of the static tests. The course of the evolution of the Cs concentration indicates that the Cs release is probably “still” dominated by contributions from the grain boundaries because of the change of the Cs concentration with time is faster than the change of Sr concentrations with time, Figure 3-20.

The effect of air oxygen penetration after the burst disk failure on the concentrations of radionuclides is shown in Figure 3-22. The graph shows the concentrations of radionuclides at the last sampling before failure (after 1,095 days), and 11 days later, when air contact

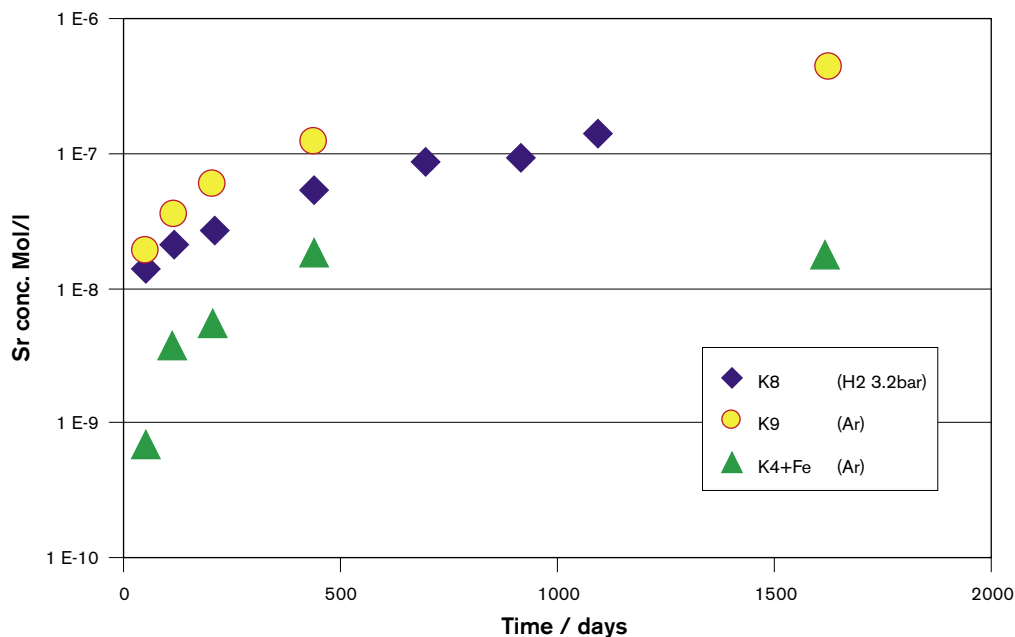


Figure 3-20. Concentrations of Sr during 1,095 days corrosion of spent fuel pellet K8 in 5 M NaCl solution under external H_2 overpressure in comparison to reference samples K9 and K4+Fe in absence/presence of Fe-powder under initial Ar-atmosphere.

even at small amounts took place. The graph reveals that the concentrations of redox sensitive radioelements Tc, U, Pu and Np are affected very distinctly. They increased by roughly one order of magnitude. Less affected are the concentrations of Cs, Sr, Eu and Am, where only a very small increase can be detected.

All solution concentrations of radioelements obtained in the course of the wash cycles and of the static test under H₂ overpressure are summarized in Table 3-5.

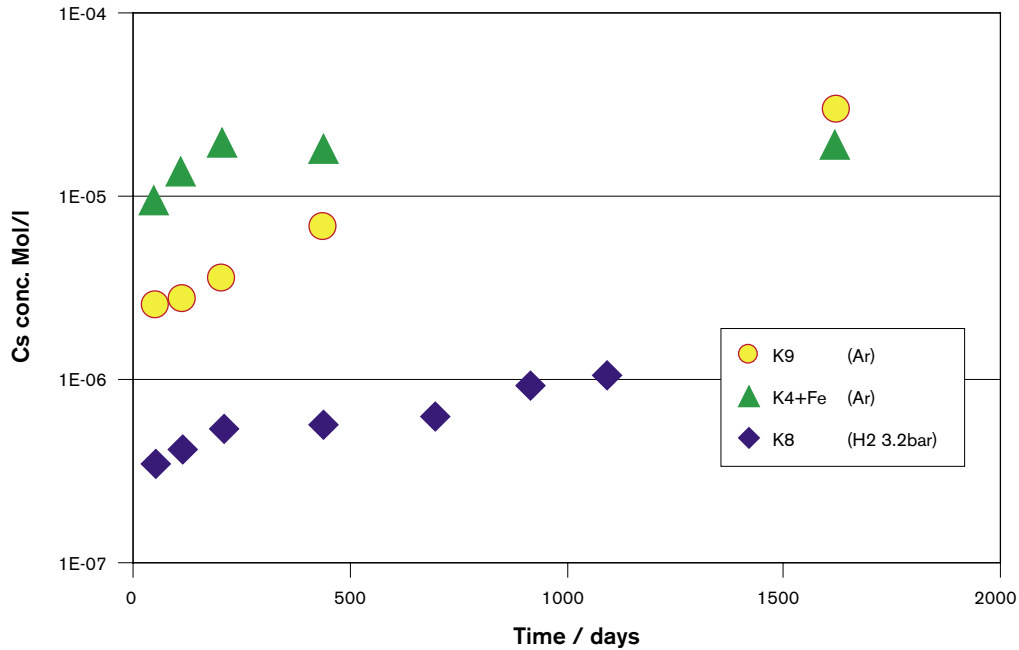


Figure 3-21. Concentrations of Cs during 1,095 days corrosion of spent fuel pellet K8 in 5 M NaCl solution under external H₂ overpressure in comparison to reference samples K9 and K4+Fe in absence/presence of Fe-powder under initial Ar-atmosphere.

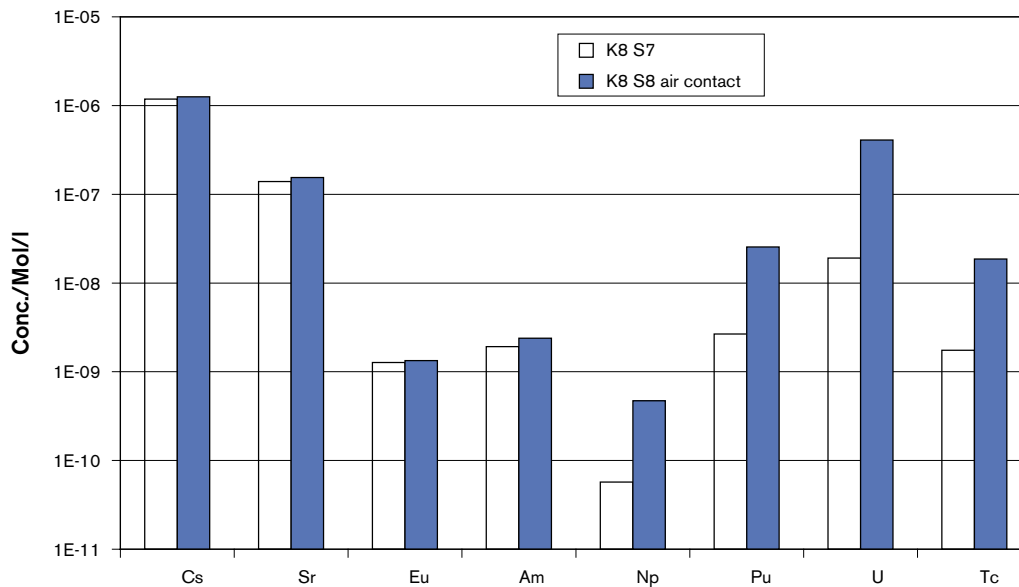


Figure 3-22. Radionuclide concentrations after 1,095 days corrosion of spent fuel pellet K8 in 5 M NaCl solution under external H₂ overpressure and after short term air contact due to failure of the burst disk. The pH values were 7.7 and 7.8, while measured Eh values were -50 and 100 mV, respectively.

Comparison of measured U concentration and solubilities of U(IV) and U(VI) solids

Concentrations of U measured in the present experiment under 3.2 bar H₂ overpressure ($2 \times 10^{-9} \leq U < 5 \times 10^{-8}$ M), are compared to calculated solubilities of the most common anticipated U(IV) and U(VI) solids in 5.0 M NaCl solution (i.e. 5.6 m NaCl). Calculations are based on the thermodynamic data-set for U(IV) and U(VI) aqueous species and solids of [NEC/KIM 2001] and [FAN/NEC 2002, NEC/ALT 2003], respectively. Since U concentrations were analyzed in the present corrosion experiment after 2 nm ultrafiltration, any potential contribution of colloids can be neglected for comparison of measured and theoretical U concentrations. Variations in Eh are not included in the solubility calculations.

The pH measured 53 days after the end of the washing cycles, pH = 4.9 (i.e. $-\log(m_{H^+}) \leq 5.5$), is quite acidic compared to the pH of the following samplings. The measured U concentration ($10^{-7.3}$ M) is relatively close to the U(IV) calculated for the measured solution composition. Under the experimental conditions after the first sampling, characterized mainly by $6.3 \leq \text{pH} \leq 7.8$ ($6.9 \leq -\log(m_{H^+}) \leq 8.4$, respectively), the solubility of the U(IV) solid $\text{UO}_2 \cdot x\text{H}_2\text{O}(\text{am})/\text{U}(\text{OH})_4(\text{am})$ is predicted to be $10^{-8.5 \pm 1.0}$ M. In the studied pH range, the U(IV) concentration is dominated by $\text{U}(\text{OH})_4(\text{aq})$ and is not significantly affected by the pH. For the same pH range and NaCl concentration, calculated solubilities of metaschoepite ($\text{UO}_3 \cdot 2\text{H}_2\text{O}(\text{cr})$) and Na-diuranate ($\text{NaUO}_2\text{O}(\text{OH})(\text{cr})$) are in the range of $10^{-7.5}$ to 10^{-5} M (Figure 3-23). Taking into account the uncertainties in the respective solubility products of metaschoepite and Na-diuranate ($\log K_{\text{sp}}^\circ(\text{UO}_3 \cdot 2\text{H}_2\text{O}(\text{cr})) = -22.8 \pm 0.4$ and $\log K_{\text{sp}}^\circ(\text{NaUO}_2\text{O}(\text{OH})(\text{cr})) = -29.5 \pm 1.0$), the concentration range of U(VI) enlarges to $10^{-8.5}$ to $10^{-4.8}$ M for the considered pH range and NaCl concentration. There is a strong dependence of U(VI) solubility on pH between $6.9 \leq -\log(m_{H^+}) \leq 8.0$. For $-\log(m_{H^+}) \leq 7.2$, the theoretical U(VI) concentrations is controlled by the solubility of metaschoepite, whereas it is controlled by the solubility of Na-diuranate at $-\log(m_{H^+}) \geq 7.2$.

The change in the U concentration with time during the static test, Figure 3-18 cannot be explained (solely) with a solubility control of the U(VI) solids mentioned above. During the experiment, the pH fluctuated between 6.3 and 7.8, which affects strongly the U(VI) solubility. However, the pH variation is not reflected in the measured U concentration, Figure 3-24. In contrast, the measured U concentration up to the fourth sampling (697 days) decreases and approaches (within the uncertainty of the thermodynamic data) the calculated solubility of the tetravalent $\text{UO}_2 \cdot x\text{H}_2\text{O}(\text{am})/\text{U}(\text{OH})_4(\text{am})$, Figure 3-24. After 697 days, an increase in the measured U concentration by one order of magnitude (from $10^{-8.7}$ to $10^{-7.7}$ M) is accompanied by a pH increase from 6.3 to 7.8. The increase in the U concentration cannot be explained with the calculated solubility of the tetravalent U solid. Measured U concentrations of the last two samplings prior to the burst disk failure agree well with the solubility of Na-diuranate, calculated for the respective conditions. For the experiment under 3.2 bar H₂ overpressure (K8), the comparison of measured and calculated U concentrations indicates that the U concentrations are lower than the solubilities of the U(VI) solids (except for the last two samplings before the burst disk failure). Taking into account the uncertainty of the thermodynamic data, the experimental U concentrations prior to the burst disk failure are essentially the same as the calculated U(IV) solubilities.

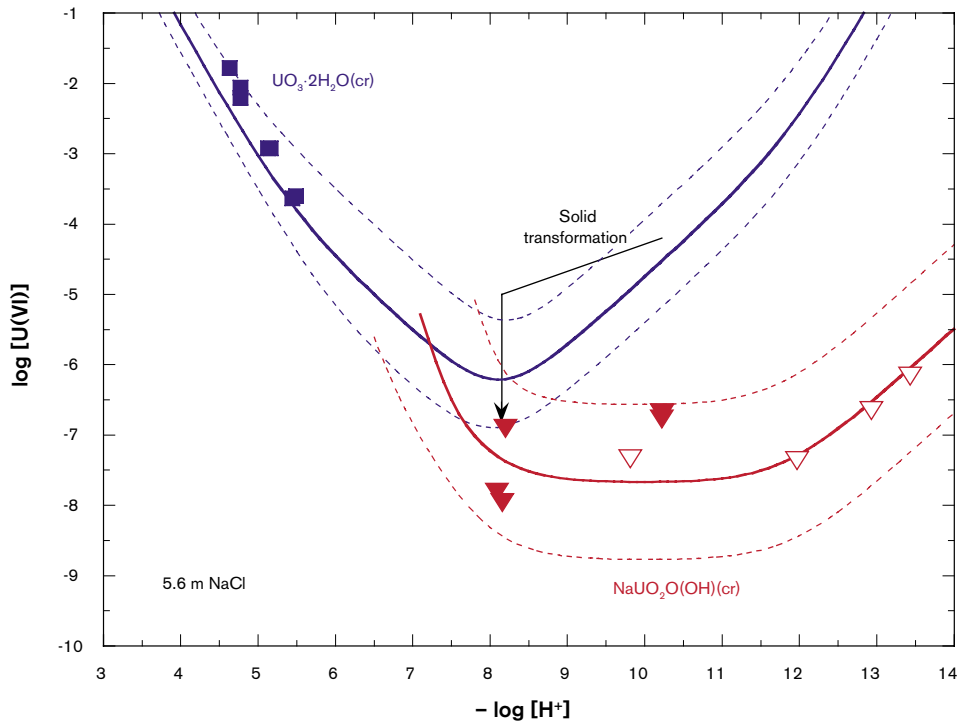


Figure 3-23. Solubility of metaschoepite ($UO_3 \cdot 2H_2O(cr)$) and Na-diuranate ($NaUO_2O(OH)(cr)$) in 5.6 m NaCl solution as a function of $-\log(m_{H^+})$ (after [NEC/ALT 2003]). Squares denote measured metaschoepite solubility, triangles denote measured Na-diuranate solubility, respectively.

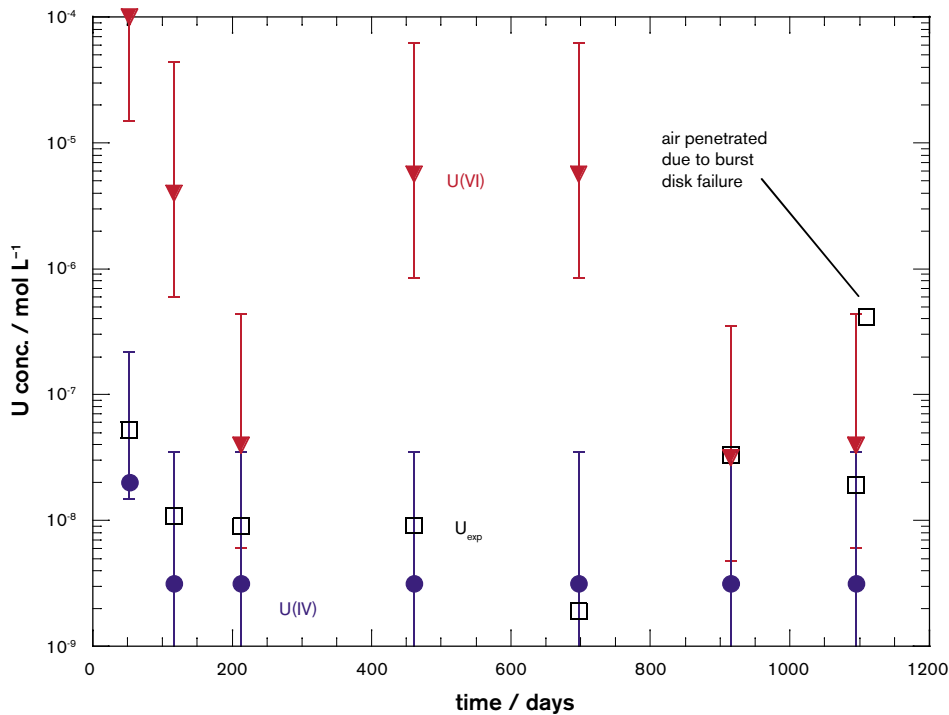


Figure 3-24. Measured U concentrations compared to calculated solubilities of tetravalent and hexavalent U solids. Measured concentrations are denoted by open squares (U_{exp}), calculated solubility of $UO_2 \cdot xH_2O(am)/U(OH)_4(am)$ are denoted by filled circles, calculated solubility of metaschoepite ($UO_3 \cdot 2H_2O(cr)$) and Na-diuranate ($NaUO_2O(OH)(cr)$) are denoted by filled triangles.

Comparison of measured Np and Pu concentrations with solubilities of Np and Pu solids

Under the conditions of the present experiment (K8), measured Np concentrations ($Np < 10^{-8.5}$ M), are far below the solubility of pentavalent solids, such as $NpO_2OH(\text{altered})$. Within the analytical uncertainty (Np concentrations are close to detection limit), the measured concentrations agree well to the calculated solubility of the tetravalent $NpO_2 \cdot xH_2O(\text{am})/Np(OH)_4(\text{am})$, i.e. $10^{-9.0 \pm 1.0}$ M, Figure 3-25. For the experiments under Ar atmosphere, the same conclusion regarding the measured Np concentrations and Np(IV) solubility may be drawn, Figure 3-25.

Both in the present experiment (K8) and in experiment (K9), a considerable decrease in Pu concentration with time, i.e. by more than one order of magnitude is observed. After 300 days, the measured Pu concentration is close to the calculated solubility of the tetravalent $PuO_2 \cdot xH_2O(\text{am})/Pu(OH)_4(\text{am})$, i.e. $10^{-10.4 \pm 0.5}$ M, Figure 3-26. Under the relevant conditions (5.6 m NaCl and $6.9 \leq -\log(m_{H^+}) \leq 8.4$), solubilities of penta- and hexavalent Pu solids are by orders of magnitude higher than the Pu(IV) solubility. The continuous decrease in Pu during the first 220 days of both experiments may be interpreted as a reduction of Pu(V) or Pu(VI) species into Pu(IV). In experiment K4, the measured Pu concentrations were close to the calculated solubility of $PuO_2 \cdot xH_2O(\text{am})/Pu(OH)_4(\text{am})$, Figure 3-26.

The thermodynamic data-set of Neck and Kim [NEC/KIM 2001] was used to calculate solubilities of tetravalent actinides, An(IV). As for the calculation of the U(IV) solubility, the solubilities of the other $AnO_2 \cdot xH_2O(\text{am})/An(OH)_4(\text{am})$ solids are independent of pH at 5.6 m NaCl and $6.9 \leq -\log(m_{H^+}) \leq 8.4$.

Conclusions on the effect of hydrogen on spent fuel corrosion in 5 M NaCl

The results from the present experiment have shown that a slow down of the Sr release, which may reflect the progress of matrix dissolution, was affected by the H_2 overpressure. This observation was found to be associated with a very low release of fission gases ($<$ detection limit) and strong retention effects of important radionuclides.

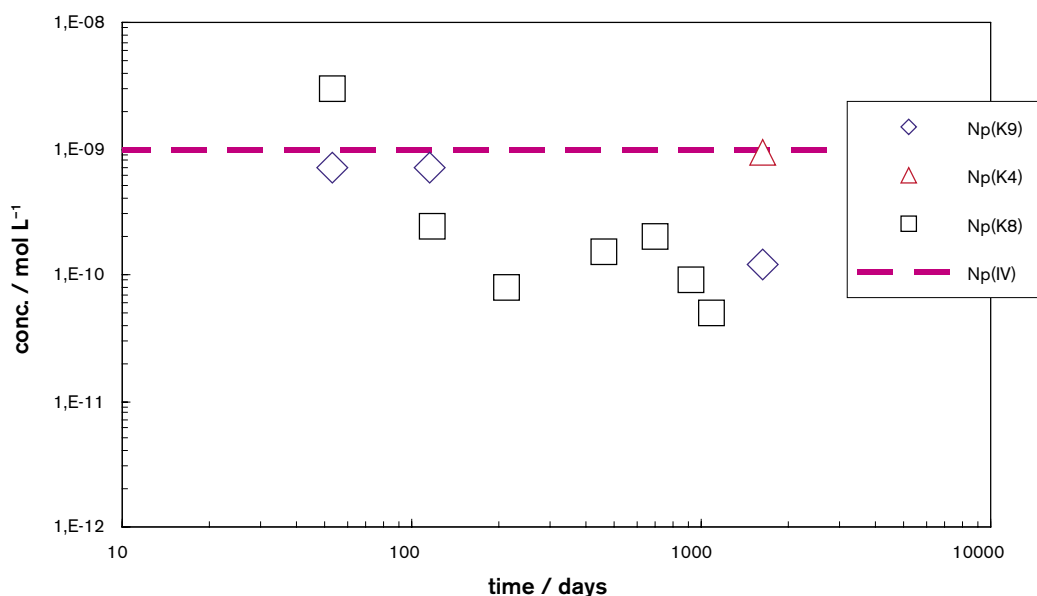


Figure 3-25. Measured Np concentrations compared to calculated solubilities of a tetravalent Np solid, i.e. $NpO_2 \cdot xH_2O(\text{am})/Np(OH)_4(\text{am})$. Symbols denote measured concentrations in experiments K4, K8 and K9; the line denotes the calculated solubility limit.

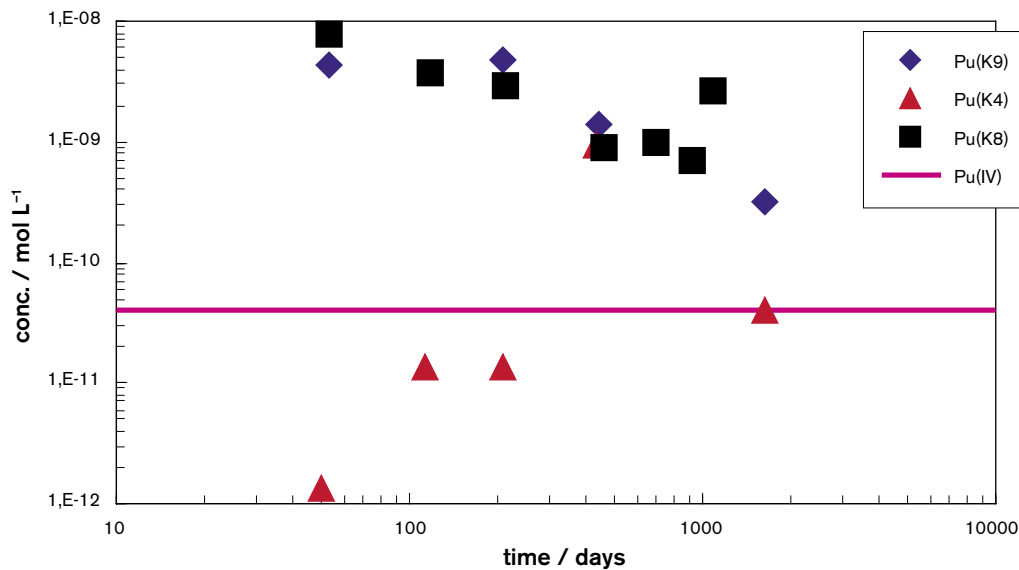


Figure 3-26. Measured Pu concentrations compared to calculated solubilities of a tetravalent Pu solid, i.e. $\text{PuO}_2 \cdot x\text{H}_2\text{O}(\text{am})/\text{Pu}(\text{OH})_4(\text{am})$. Symbols denote measured concentrations in experiments K4, K8 and K9; the line denotes the calculated solubility limit.

The concentrations of U and Tc were found to be similar, and the concentrations of Np were lower than encountered in the presence of Fe. Hence, one can assume that the oxidative effect of radiolysis products and its consequences on the overall spent fuel corrosion behavior was suppressed to a large extent.

However, the Sr concentrations increased by roughly 10 times, and despite retention effects, the level of solution concentrations of Eu, Am, Pu was higher than in the test with Fe powder present. In this context it should be considered that the applied overpressure of 3.2 bar H_2 is relatively low in comparison to some tens of MPa, which can be expected in a flooded repository, or applied in similar experimental spent fuel corrosion studies related to the hydrogen effect in diluted aqueous solutions [SPA/WER 2000].

Indicators of matrix dissolution progress

Behavior of strontium

The slow down of the Sr release in solution under H_2 overpressure was less pronounced than in the reference test K4+Fe, when Fe powder was present, Figure 3-20. However, in this context it has to be considered that the fuel sample K8 suffered (in part) pre-oxidation during 7 years of storage; moreover, we cannot yet completely exclude that due to the irradiation history a part of the Sr can be encountered outside of the matrix (e.g. grain boundaries), because of segregation processes.

Sr remains within the UO_2 matrix at moderate burn-up and linear power. This is completely consistent with nearly all observations from spent fuel leaching, which illustrate congruency of U with Sr, showing that Sr is a good indicator of matrix dissolution. At high burn-up and linear power, a perovskite phase forms. This perovskite phase is characterized by a highly variable composition, $[(\text{Ba}, \text{Sr}, \text{Cs})(\text{U}, \text{Pu}, \text{Zr}, \text{REE})\text{O}_3]$ and may contain small fractions of Sr [JEF 1967, KLE 1985, KLE/PAS 1985, FOR/MAT 1988].

Nonetheless, for an ‘experimental’ fuel like the fuel of pellet K8, with high burn-up and moderate to high linear power, some segregation can not be excluded. Studies of the effect of power ratings (11.2 and 23.5 kW/m) have shown that the Sr instant release fraction was

five times higher for fuels exposed to high linear powers than for fuels run at moderate burn-ups and power ratings [IMO 1986].

Hence, for the studied fuel (pellet K8), given the high linear power ratings it is likely that Sr segregation occurred. However, the average burn-up and the temperature were below the threshold (50 MWd/kgU, 1,700°C) [GOL/WEG 2003], where Sr segregation can be clearly observed.

Behavior of Kr/Xe

The release of the fission gases was influenced without any doubt by the H₂ overpressure, because the released fractions of ⁸⁵Kr and ¹⁴⁴Xe decreased by two orders of magnitude, very close or below the detection limit, when the H₂ overpressure was applied for the first time. These low releases of ⁸⁵Kr and of ¹⁴⁴Xe remained at these low levels during the entire three years of the test. However, it is not clear, to what extent the FG release could be related to the dissolution of the matrix, or to the release from the grain boundaries.

Indicators on the exclusion of oxidative dissolution of the matrix

Several measurable indicators can be used to rule out oxidative dissolution of the matrix or at least strongly suppress its oxidation, e.g. the O₂ content in the gas phase, the measured Eh values, or the concentration levels of redox sensitive radioelements.

O₂ content in the gas phase

There are indications that most of the oxidative radiolytic species were not available for matrix oxidation/dissolution, but consumed by H₂ in association with a catalytic process. In the reference test K4+Fe, when initially metallic Fe powder corroded simultaneously with fuel, the O₂ level was below the detection limit. In the presence of 3.2 bar H₂ overpressure (and in the absence of Fe), the O₂ in the free gas volume was always below the detection limit of 0.04% (displayed value < 0,007%), except in one case, when a value of 0,519% was measured, but in association with a N₂ content of 1.95%. However, there is no evidence of air intrusion into the autoclave at this interval, because the release of all radionuclides, which may indicate the matrix dissolution progress remained in the same order of magnitude and did not show any extraordinary increase, Figures 3-13, 3-17. Moreover, the measured Eh value was in the negative range (-500 mV). Thus, the most plausible explanation is an air intrusion directly into the tube system via one of the fittings or tube connections during the sampling procedure and not in the free gas volume of the autoclave.

In contrast, during corrosion tests of the reference samples *under initial Ar atmosphere* the O₂ content in the gas phase was always found to be over the detection limit, even if the amounts of N₂ were distinctly below 1%. In this context, the highest O₂ content was encountered in the gas volume as 3.44% during the 1,183 days interval of the reference test with pellet K9 when the N₂ content was 0,378%.

Measured E_h values

It is general accepted, that E_h values measured in spent fuel corrosion tests are very difficult to interpret, because oxidizing and reducing species are formed simultaneously. But they can be used as an indicator of (air) oxygen contact with the solution, if they are found to be in the positive range. During the entire test under H₂ overpressure the measured E_h values (combined Metrohm Pt wire electrode, with reference to Ag/AgCl) were found to be

always in the negative range. In particular, at the sixth sampling, where the sudden increase of U, Am and Eu concentration was found, the associated E_h value was -500 mV. Measured E_h values during the wash cycles of pellet K8 were scattering around 400 mV and during reference test with pellet K9 at about 200 mV.

3.2.2 Results of MOX fuel leaching under 50 bar H_2 (ITU/SKB)

The results are divided to consider the background information such as the E_h , pH, T, total P, concentrations of H_2 , H_2O_2 , O_2 , concentrations of stable element and radionuclide in the leachate.

Leaching conditions

The autoclave can be considered as a closed system and therefore some assumptions can be made without actual measurements. The conditions inside the autoclave are clearly reducing with a $E_h < 0$ mV due to the concentration of 43 mM dissolved H_2 .

The initial solution had a pH of 8.52 and since solution was only withdrawn and no solution added the pH is assumed to be constant i.e. the container is inert. The change of the pH over the leaching period will be negligible when one considers the low concentration of U in the leachate from the global electrochemical dissolution reaction of the UO_2 :



and the buffering effect of bicarbonate. The experiment was run at $22 \pm 4^\circ C$.

The H_2 pressure in the autoclave is fairly constant and fluctuates only with the hot cell temperature and once due to a leak at a gas bottle manometer that occurred following a leachate sampling, after approximately 200 days, Figure 3-27. The manometer was exchanged within a few days.

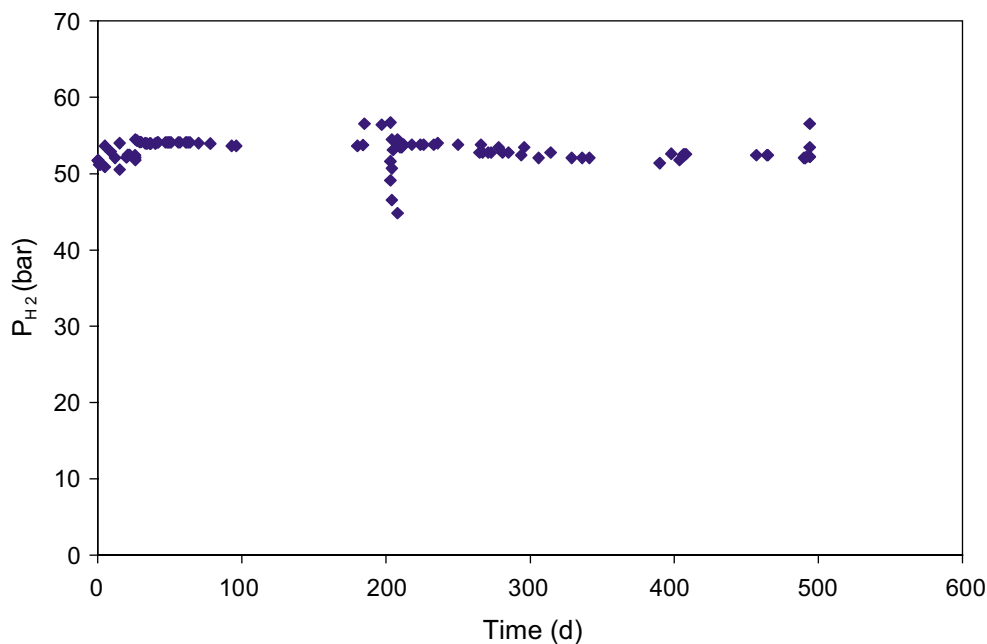
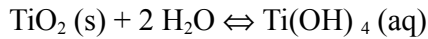


Figure 3-27. H_2 pressure in the MOX autoclave as a function of leaching time.

The O₂ and H₂O₂ concentrations are expected to be very low under the reducing conditions prevailing in the autoclave. This is also confirmed by the low UO₂ leaching rates. The hydrogen carbonate in the leachate will come into equilibrium with the 53 bar H₂ gas giving a mixed atmosphere consisting of H₂+0.02% CO₂.

The concentration of stable elements in the leachate as function of leaching time is shown in Figure 3-28. The elemental composition of the leachate reveals a Ti concentration that corresponds to the equilibrium between TiO₂(s) and the leachate. The hydrolysis of Ti is strong and the dominating species at pH above 4 is Ti(OH)₄. The solubility product of TiO₂(s) is 10^{-5.5} M [BAE/MES 1976] according to the reaction:



Iron comes from the titanium autoclave but since the ratio of Fe/Ti in the leachate is much higher than the ratio in the autoclave material most of the iron must come from an additional source. This source is most probably a part made of stainless steel as can be seen on the levels of Cr, Ni, Mn and Mo (not shown in Figure 3-28). The only part made of stainless steel that is continuously connected to the autoclave but is not in direct contact with the leachate is the manometer. A mixture of Cu and Zn is used in brass. Brass is used in the seat of the needle valves.

Radionuclide concentrations in leachate

The results of the analysis of the leachate are given in Table 3-6 and summarized in Figure 3-29. The interpretation of the leaching results is complicated by the fact that MOX fuel contains grains of UO₂-PuO₂ embedded in a pure uranium oxide matrix. This fact implies that most of the fissions, during the reactor irradiation, occur in the U-Pu grains resulting in an uneven distribution of fission products in the fuel matrix. Additionally, high local α-radiation fields exist in the U-Pu grains, since ^{243,244}Cm, ²³⁸Pu and ²⁴¹Am dominate the number of α-emissions, Table 3-2. On the other hand, the sintering process tends to promote a solid solution mixing of the U-Pu grains with the UO₂ matrix at a sintering temperature of 1,200°C and the irradiation in the reactor makes Pu-atoms diffuse from the U-Pu grains into the UO₂ matrix due to the high temperature and the long irradiation

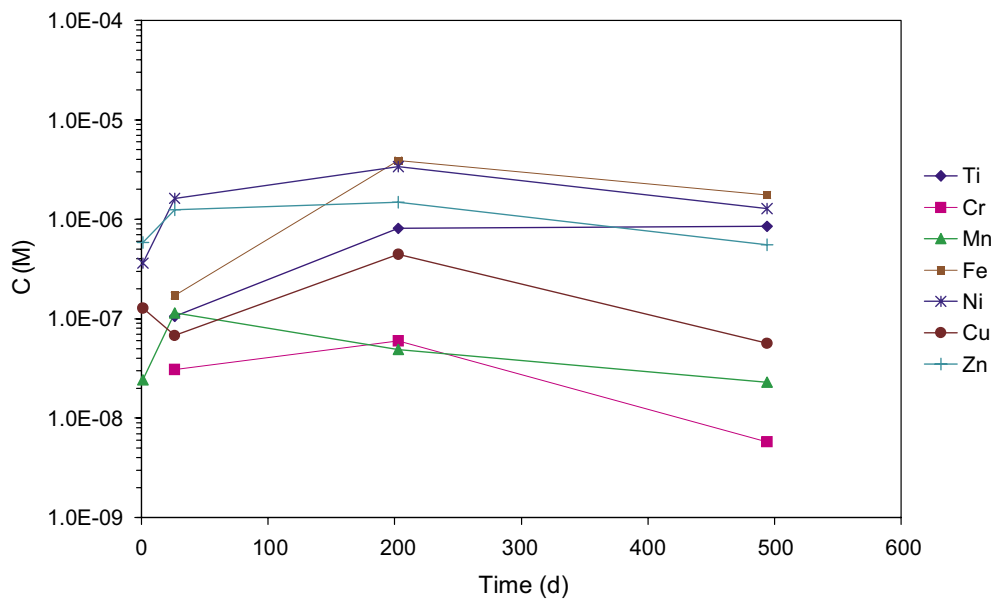


Figure 3-28. Concentration of stable elements in the MOX leachate as a function of leaching time. The errors are in the range of 10–20% (1s).

time (high burn-up). Nevertheless, a considerable amount of actinides will be present in the U-Pu grains giving a high dose to the water above these U-Pu grains some distance from the UO₂ matrix. Even so, the stable radiolytic products, assumed to be accumulated in a 10–20 µm thick solution layer above the fuel surface, can easily diffuse the distance of 4–7 µm corresponding to the U-Pu grain diameter and react with the UO₂ matrix. The steadily increasing S/V ratio with time favours the α-radiolytic process by increasing the H₂O₂(O₂) concentration in the solution and thereby increasing the probability for oxidation/dissolution of the UO₂ matrix.

Additionally, it must be pointed out that analysis were done for all elements present in fuel but only the most redox-sensitive and Cs could be detected. Even though radiometric methods were used to find short-lived radionuclides (¹²⁵Sb, ¹⁴⁴Ce, ¹⁵⁴Eu, ²⁴¹Am), no additional elements than those found by HR-ICPMS could be detected. Strangely, we could not find any lanthanide in the leachate. No chemical separations were made to determine ⁹⁰Sr.

Table 3-6. Concentration of fission products and actinides in the MOX-leachate expressed as mole per litre leachate. The uranium concentrations have been corrected for presence of U in the blank (10 mM NaCl + 2 mM HCO₃⁻ solution) and in case of UTEVA separation for U originating from the UTEVA extraction chromatography resin. The analytical errors were estimated to be 20% (1σ). The reference date is 18th December 2002.

Radionuclide	Concentration (M)				
	Wash1	S1	S2	S4	S6
Fission products					
¹³³ Cs	contam	contam	contam	contam	contam
¹³⁴ Cs	1.5×10 ⁻¹¹	3.9×10 ⁻¹²	4.6×10 ⁻¹²	5.5×10 ⁻¹¹	4.0×10 ⁻¹¹
¹³⁵ Cs	5.4×10 ⁻⁹	9.1×10 ⁻¹⁰	1.3×10 ⁻⁹	1.9×10 ⁻⁸	1.4×10 ⁻⁸
¹³⁷ Cs	7.8×10 ⁻⁹	1.4×10 ⁻⁹	2.6×10 ⁻⁹	3.0×10 ⁻⁸	2.1×10 ⁻⁸
Cs_{tot} (incl ¹³³Cs)	2.3×10⁻⁸	4.1×10⁻⁹	6.8×10⁻⁹	8.8×10⁻⁸	6.2×10⁻⁸
⁹⁹ Tc	5.0×10 ⁻¹⁰	3.8×10 ⁻¹⁰	< 4×10 ⁻¹²	< 4×10 ⁻¹²	1.4×10 ⁻¹¹
Mo_{tot} (all isotopes)	6.5×10⁻⁹	3.4×10⁻⁸	2.2×10⁻⁸	3.8×10⁻⁹	4.0×10⁻¹⁰
Actinides					
²³⁷ Np	2.2×10 ⁻¹¹	2.0×10 ⁻¹⁰	2.9×10 ⁻¹¹	<6×10 ⁻¹²	<6×10 ⁻¹²
²³⁴ U (sep)	1.6×10 ⁻¹¹	1.1×10 ⁻¹⁰	1.5×10 ⁻¹²	3.4×10 ⁻¹³	n.m.
²³⁵ U (sep)	2.9×10 ⁻¹⁰	2.3×10 ⁻⁹	2.7×10 ⁻¹¹	7.6×10 ⁻¹²	n.m.
²³⁸ U (sep)	8.3×10 ⁻⁸	5.5×10 ⁻⁷	7.0×10 ⁻⁹	1.6×10 ⁻⁹	n.m.
U _{tot} (sep)	8.3×10 ⁻⁸	5.5×10 ⁻⁷	7.0×10 ⁻⁹	1.6×10 ⁻⁹	n.m.
U_{tot} (non-sep)	8.9×10⁻⁸	4.7×10⁻⁷	5.7×10⁻⁹	2.0×10⁻⁹	3.2×10⁻¹⁰
U-ratios					
²³⁴ U/ ²³⁸ U	2.0×10 ⁻⁴	2.0×10 ⁻⁴	2.1×10 ⁻⁴	2.1×10 ⁻⁴	n.m.
²³⁵ U/ ²³⁸ U	3.6×10 ⁻³	4.2×10 ⁻³	3.9×10 ⁻³	4.8×10 ⁻³	n.m.
²³⁹ Pu	7.8×10 ⁻¹¹	9.6×10 ⁻¹⁰	2.9×10 ⁻¹⁰	4.3×10 ⁻¹¹	1.2×10 ⁻¹¹
²⁴⁰ Pu	6.1×10 ⁻¹¹	6.7×10 ⁻¹⁰	2.3×10 ⁻¹⁰	3.4×10 ⁻¹¹	1.1×10 ⁻¹¹
²⁴¹ Pu	2.3×10 ⁻¹¹	2.1×10 ⁻¹⁰	8.0×10 ⁻¹¹	1.1×10 ⁻¹¹	3.1×10 ⁻¹²
²⁴² Pu	1.3×10 ⁻¹¹	1.6×10 ⁻¹⁰	5.0×10 ⁻¹¹	7.6×10 ⁻¹²	2.4×10 ⁻¹²
Putot (incl. ²³⁸Pu)	1.8×10⁻¹⁰	2.0×10⁻⁹	6.5×10⁻¹⁰	9.5×10⁻¹¹	2.8×10⁻¹¹
Additional data					
Sampling (d)	0	0.1	26	206	494
Sampled amount leachate (g)	103.5	1.174	1.741	3.597	18.119
S/V (m ⁻¹)	0.491	0.282	0.287	0.302	0.351

contam means that the samples were contaminated in hot cell
n.m. means not measured

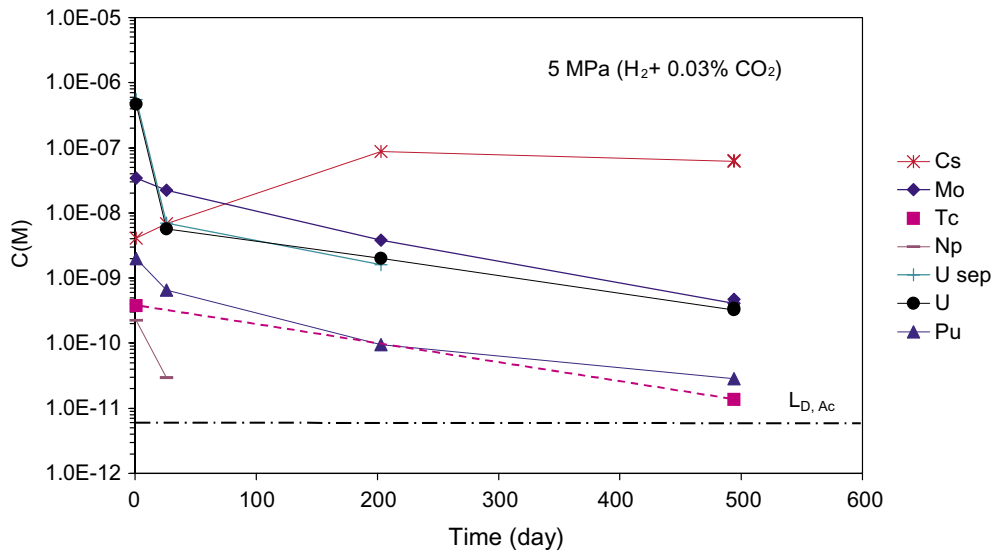


Figure 3-29. Concentration of fission products and actinides in the MOX leachate as a function of leaching time. The errors are in the range of 10–20% (1 s). The crosses represent an independent U determination using UTEVA separation.

Cs

The concentration of ^{134}Cs and ^{137}Cs in the leachate was determined by γ -spectrometry and the results were confirmed by measurements using HR-ICP-MS. Additionally, the concentration of ^{135}Cs was determined by HR-ICP-MS. ^{133}Cs was detected in the leachate but was not used in the evaluation since the sample was contaminated with stable Cs. The ratios $^{134}\text{Cs}/^{137}\text{Cs}$ and $^{135}\text{Cs}/^{137}\text{Cs}$ were constant in the leachate. As the different Cs ratios in the fuel were known the total Cs concentration in the leachate could be calculated. It can be concluded that the [Cs] increased initially, but reach a concentration plateau of 10^{-7} M after 200 days of leaching (Figure 3-29). There are no solid phases of Cs that could form a Cs-precipitate; moreover sorption of Cs is negligible in 10 mM NaCl + 2 mM HCO_3^- solution and therefore can not explain the halt in the Cs dissolution.

Leachate S1 collected 3 hours after start of the leaching gave a rather high Cs concentration, which most probably arises from dissolution of oxidized U left on the MOX fuel surface after the wash since the fuel surface was not dried off before insertion into the autoclave.

The initial increase of the Cs concentration likely corresponds to Cs dissolved from inter-granular positions in the fuel since the Cs concentration has increased by a factor of ~ 9 (between 26 days leaching and 494 days leaching) while the concentration of U during this time period had decreased. The fraction of leached Cs of the total inventory in the fuel was 1.4×10^{-3} . The small cumulative fraction of inventory and the fact that no more Cs is leached after 200 days indicate that all Cs available in the inter-granular positions has been leached out and that this will mostly come from the Pu-rich grains.

^{99}Tc

Technetium exists under reducing conditions in the UO_2 matrix either as metallic Tc forming metallic inclusions together with Mo, Ru, Rh, Pd or as partly oxidized TcO_2 dispersed in the UO_2 matrix. Technetium metal is relatively stable towards oxidation since it first must be oxidized in the UO_2 matrix to TcO_2 , then dissolved and finally oxidized to TcO_4^- , a very soluble species. Tc(IV) precipitates in neutral oxygen-free solutions as $\text{Tc}(\text{OH})_4$ and re-crystallizes after some time to TcO_2 .

The decrease of the concentration of Tc in the leachate with time is similar to the concentration decrease observed for U and Pu, and to some extent Mo. The reduction by a factor of almost 10 indicates that initially dissolved Tc precipitates as $\text{Tc}(\text{OH})_4$. The most interesting result is that despite the intensive α -radiolysis and production of $\text{H}_2\text{O}_2/(\text{O}_2)$ no further oxidation of $\text{Tc} \rightarrow \text{TcO}_2 \rightarrow \text{TcO}_4^-$ has occurred. This indicates that the UO_2 matrix has not been oxidized.

Mo

Molybdenum in the fuel is associated with metallic inclusions and is considered to be an indicator of UO_2 dissolution since it is one of the most redox sensitive elements. Mo oxidizes in the sequence: elemental Mo \rightarrow $\text{MoO}_2 \rightarrow \text{MoO}_4^{2-}$. Once Mo(VI) is formed it is difficult to reduce it to lower oxidation state. The decreased concentration of Mo follows the general trend of U, Pu and Tc.

Np

Neptunium is, like Mo and Tc, a redox sensitive element and under aerated conditions is oxidized in water to Np(V). It should be noted that the concentration of ^{237}Np was below the detection limit of 6×10^{-12} M in the two last samples. It is therefore difficult to make any conclusions.

U

The most important findings is that the concentration of U in the leachate decreased from an initial pre-oxidized [U] of 5×10^{-7} M by three orders of magnitude ([U] after 494 day leaching was 3×10^{-10} M) despite a high α -radiation field yielding high surface concentrations of oxidising species $\text{H}_2\text{O}_2/(\text{O}_2)$, Figure 3-29. The uranium concentration did not reach a steady state. The decrease in concentration follows the same trend as Pu, Tc, and partially as Mo.

The average mole-ratios of $^{234}\text{U}/^{238}\text{U}$ and $^{235}\text{U}/^{238}\text{U}$ in the leachate were found to be 2×10^{-4} and 4×10^{-3} with a standard deviation of 6×10^{-6} and 5×10^{-4} , respectively. The ratio $^{235}\text{U}/^{238}\text{U}$ in the leachate is similar to the ratio in the MOX fuel (3×10^{-3}). These constant uranium ratios indicate congruent corrosion of the UO_2 matrix.

A rough calculation of the production of oxidizing species due to the decay of ^{244}Cm , ^{238}Pu and ^{241}Am (which dominate the α -activity, see Table 3-2) in the MOX fuel over a period of 494 days indicates an O_2 production of 1.2×10^{-5} mol. If one assumes that UO_2 is the foremost scavenger for O_2 , the concentration of UO_2^{2+} in the leachate should reach $\sim 7 \times 10^{-5}$ M.

Pu

All of the Pu-isotopes (^{238}Pu , ^{239}Pu , ^{240}Pu , ^{241}Pu and ^{242}Pu) behaved identically in the leachate, Table 3-6. The ratio of the different Pu-isotopes against ^{240}Pu measured in the leachate and in the analyzed fuel showed identical ratios demonstrating an initial congruent dissolution of Pu from the U-Pu oxide grains. The general decrease of the Pu concentration with time is similar to the behaviour of U, Mo and Tc, Figure 3-29.

Ratio of elements in fuel and leachate

The dissolution process of elements from the UO_2 matrix was studied by comparing the ratios of $\text{FP}/\text{U}_{\text{tot}}$ and $\text{An}/\text{U}_{\text{tot}}$ in the fuel and in the leachate, Table 3-7. ORIGEN code calculation matched the analyzed concentrations of fission products and actinides in the fuel.

Table 3-7. Molar ratio of FP/ U_{tot} and An/ U_{tot} in the MOX fuel and leachate. The uncertainties are estimated to be 50% (1s). The reference date is 18th December 2002.

	ORIGEN	Fuel	Wash1	S1	S2	S4	S6
Cs_{tot}/U_{tot}	0.0074	0.0081	0.26	0.0087	1	44	190
$^{99}Tc/U_{tot}$	3×10^{-3}	n.a.	6×10^{-3}	8×10^{-4}	$< 7 \times 10^{-4}$	$< 2 \times 10^{-3}$	0.04
Mo_{tot}/U_{tot}	0.012	n.a.	0.07	0.07	4	2	1
$^{237}Np/U_{tot}$	4×10^{-4}	5×10^{-4}	2×10^{-4}	5×10^{-4}	5×10^{-3}	< 0.003	< 0.002
Pu_{tot}/U_{tot}	0.033	0.034	2×10^{-3}	4×10^{-3}	0.1	0.05	0.09

n.a. means not analyzed

Except for a hot cell contamination of Wash1 with Cs, as this element has high abundance in all types of fuels, the ratios of FP/U and An/U in Wash1 and leachate S1, sampled 3 hours after start of leaching, are similar. Since the fuel wash (sample Wash1) was performed under oxidizing conditions and S1 was sampled under reducing conditions this suggests that leachate S1 corresponds to release of FP and An contained in a pre-oxidized UO_{2+x} or $UO_3 \cdot 2H_2O$ layer.

Assuming that most of the ^{99}Tc and Pu reside in the Pu-rich grains, the much lower ratios of $^{99}Tc/U$ and Pu/U in leachate S1 compared to the fuel indicate that Pu-enriched grains are less oxidized than the UO_2 matrix. The ratio $^{237}Np/U_{tot}$ in the fuel, Wash1 and S1 are similar indicating that Np is either more susceptible to oxidation than Tc and Pu or that Np has moved out of the Pu-islands into the grain boundaries and is congruently dissolved with superficial oxidized UO_2 .

Discussion of MOX leaching data

It is clear that in this experiment the leaching of MOX-fuel goes through several stages. The following processes could be identified:

- initial dissolution of the pre-oxidized UO_{2+x} or $UO_3 \cdot 2H_2O$ layer,
- inhibition of oxidation of the underlying UO_2 by dissolved H_2 ,
- reduction and precipitation of redox-sensitive elements.

Firstly, as the UO_2 surface is pre-oxidized, the $UO_3 \cdot 2H_2O$ layers will immediately be dissolved together with the incorporated fission products (Cs, Mo, Tc) and actinides (Np, Pu, Am, Cm). The thickness of the pre-oxidized layer was calculated to be ~ 100 atomic layers. In this case the U will be present in the leachate as $UO_2(CO_3)_3^{4-}$ and $UO_2(CO_3)_2^{2-}$ [CAR/ENG 1997, SKI 1996].

In the second stage the absence of atmospheric oxygen makes it impossible to further oxidize the UO_2 matrix. Therefore, only oxygen produced from radiolysis can promote further oxidation of UO_2 . The two orders of magnitude decrease of the [U] within 23 days shows that no more U was dissolved. A strong indication of an inhibited oxidation of the UO_2 matrix is the fact that the Cs reached a steady state concentration of 10^{-7} M after 206 days of leaching. This was unexpected since Cs is not a redox sensitive element and the fraction of inventory in aqueous phase (FIAP) was only 10^{-3} . On the other hand, the ratio $(Cs_{tot}/U_{tot})_{leachate}/(Cs_{tot}/U_{tot})_{fuel}$ was found to be 2×10^4 after 494 days of leaching which shows that the Cs dissolves preferentially and probably originates from the grain boundaries.

In the third stage, Tc, Np and Pu released from the pre-oxidized layer and present in solution in their higher oxidation states are reduced, probably to the tetravalent state, and precipitate due to their low solubility.

The influence of dissolved hydrogen on the oxidation of UO_2 depends on several processes that are coupled. This will be discussed in a separate section.

Summary on MOX leaching

The oxidation and dissolution of an irradiated mixed oxide fuel has been studied under 53 bar H_2 pressure in a Ti-autoclave. It can be concluded that 43 mM $[\text{H}_2]_{\text{dissolved}}$ in 180 ml of a 10 mM $\text{NaCl} + 2 \text{ mM } \text{HCO}_3^-$ solution inhibited oxidation and dissolution of 0.4 g irradiated MOX fuel despite an α -dose rate of 13 Gy/s and a β -dose rate of 2 Gy/s. The $[\text{U}]$ in the leachate after a leaching time of 494 days reached $3 \times 10^{-10} \text{ M}$.

After a leaching time of ~ 200 days the Cs concentration reached a plateau. It is presumed that this represents Cs that was preferentially dissolved from superficial grain boundaries. This plateau in Cs concentration strongly implies the absence of U oxidation.

The higher Pu/U ratio in the fuel, compared to that in the leachate S1, could be explained if most of the pre-oxidized UO_2 originated from the depleted UO_2 surrounding the Pu-enriched grains. The Pu-rich grains are the site of most of the fissioning and contain most of the fission products, including the lanthanides that are known to stabilize the UO_2 matrix against oxidation. These facts explain the absence of lanthanides in the leachate.

The similar behaviour of the Tc, Mo, U, Np, and Pu in the leachate indicates that these elements were congruently dissolved during the initial fuel loading of the autoclave and thereafter precipitated or co-precipitated. The most probable explanation is that U, Pu, Tc and Mo were reduced to the tetravalent state and were precipitated as hydroxides.

No fuel dissolution rate could be calculated since no U is oxidized after the initial dissolution of the pre-oxidized $\text{UO}_3 \times 2\text{H}_2\text{O}$ layer.

3.2.3 Discussion of the results on spent fuel leaching in the presence of dissolved H_2 and comparison with literature data

Some experimental observations during the studies of high burn-up spent fuel leaching in 5 M NaCl solutions and of MOX fuel leaching in the presence 5 MPa hydrogen, common to other studies reported in the literature, will be discussed first. A discussion of the dissolution rates obtained with spent fuel and MOX fuel as well as with α -doped materials follows. Finally the possible mechanisms of hydrogen activation in the case of spent fuel are discussed, together with suggestions for improved radiolytic modeling of the whole system.

During the leaching of spent fuel in 5 M NaCl , the concentration of radiolytic oxygen was below the detection limit during the whole period, Table 3-4, indicating a practically oxidant free atmosphere in the autoclave. The same observation was made in the case of the leaching of spent fuel in the presence of metallic iron [GRA/LOI 2000] and in a study of spent fuel powder leaching at higher dissolved H_2 concentration [SPA/CUI 2004]. As discussed in section 2.2.7, experimental studies of water radiolysis [PAS/LAV 2001] with similar concentrations of dissolved hydrogen as in our case with spent fuel in 5 M NaCl indicate almost no effect of hydrogen on the production of radiolytic hydrogen peroxide. However, in the case of spent fuel the system is dominated by γ -radiolysis, which influences a much larger volume of solution and the concentrations of molecular radiolytic products such as oxygen and hydrogen peroxide are expected to decrease due to the activation of molecular H_2 by reactions with radicals as $\text{OH}\cdot$ in water or with $\text{Cl}_2\cdot^-$ in chloride rich systems, as proposed in [KEL/BOH 2004]. The gas analysis methods do not allow the determination of oxygen concentrations below those corresponding to $[\text{O}_2]_{\text{diss}} \sim 10^{-8} \text{ M}$.

However, if one considers the conditions inside the 5 M NaCl loaded autoclave after 697 days, an estimation of the oxygen concentrations can be obtained also from the uranium concentrations ($\sim 2 \times 10^{-9}$ M) in solution, due to the rapid reaction of U(IV) with oxygen [NEW 1975] in the near neutral pH range. U(VI) phases can be excluded, since their solubility under the given conditions is $\sim 3,000$ times higher than the measured U concentrations, Figure 3-24. Since those levels of uranium are even slightly lower than those calculated from the reported solubility of $\text{UO}_2(\text{s})$ in the given solutions, they would indicate that almost all uranium in solution is in its tetravalent state. Thermodynamic calculations show that uranium in this oxidation state is stable in solution for oxygen fugacities below 10^{-65} atm [RAI/FEL 1990]. All these observations indicate the presence of a large sink of oxidants in the spent fuel- H_2 containing solutions. It is possible that in the systems with metallic iron present this sink is iron. However, the analysis of the iron corrosion products after 478 and 674 days leaching of pellet K3 by EDX and X-ray diffraction, is described in [GRA/LOI 1996], p. 58. The EDX analysis showed that the iron particles were coated by an iron (hydr-)oxide layer with Fe, Cl and O as the main components. Additionally, a newly formed phase of hexagonal crystal plates was found. X-ray diffraction identified α -Fe and magnetite as crystalline phases and “two remaining reflections... may be related to the main reflections of the hexagonal Fe-O-Cl phase, tentatively identified as indication for the presence of green rust I. A relative good agreement was found between chemical composition, the shape of the crystals and X-ray reflections of this phase”. The products of iron corrosion when consuming oxidants are not of this type and especially green rust is reported to be very sensitive to traces of oxygen [HAN 2002, CUI/SPA 2002]. These corrosion products were formed very probably in a phase of the spent fuel leaching when the concentrations of the oxidants in solution were extremely low. It follows that if iron has not consumed the oxidants then the hydrogen produced by the anoxic corrosion of iron consumed most of the radiolytic oxidants. Under oxygen free conditions green rust on iron surfaces is shown to reduce U(VI) and precipitate $\text{UO}_2(\text{s})$ [CUI/SPA 2002], while no uranium precipitates or extensive sorption were observed on iron corrosion products during simultaneous corrosion with fuel. Very probably U(VI) and part of the oxidants were scavenged by hydrogen on the fuel surface.

However, when no iron is present, the only system to consider as possible oxidant sink is the irradiated fuel surface contacting H_2 saturated solutions. Radiolytic calculations of the whole system should be able to indicate if the decrease of oxidant concentrations at such levels is possible by only homogeneous radiolysis of hydrogen saturated solutions.

The decrease of the concentrations of all redox sensitive radionuclides and especially of the uranium observed after the start of the leaching under H_2 atmosphere both for MOX fuel and pellet K8, is observed consistently in all other published studies [GRA/LOI 2000, JEN/ALB 2002, SPA/EKL 2002, OLL/ALB 2003, SPA/CUI 2004], whereas an increase caused by their oxidative radiolytic dissolution would have been expected. This decrease is very probably due to the reduction of the small amounts of U(VI) species initially released in solution due to the dissolution of a pre-oxidized layer at the start of the experiments. Experimental studies indicate that pre-washing of UO_2 materials lowers this amount, but it seems very difficult to avoid it completely. The dissolution of this layer is clearly indicated in Figure 3-30 from the rapid increase of the FIAP of Cs and Sr during the first couple of samplings. In all cases the uranium concentrations in these irradiated systems in the presence of hydrogen decrease to very low values, sometimes below the ones calculated from the reported solubilities of pure $\text{UO}_2(\text{s})$ systems under similar pH and temperature ranges [NEC/KIM 2001, RAI/YUI 2003, GUI/FAN 2003]. This is the case for the MOX fuel leaching, Figure 3-29, where the uranium concentrations have decreased to the same levels as the ones obtained with inactive crystalline UO_2 in the presence of chemically activated hydrogen at high temperatures [PAR/POH 1988]. There are no known U(VI) phases expected to form in the relatively simple composition solutions studied, which have

solubilities below 10^{-7} – 10^{-8} M. The solubility of the U(VI) mineral schoepite, expected to form under these conditions, is several orders of magnitude higher. As discussed in section 2.2.7, the $\text{UO}_2(\text{s})$ precipitated from near neutral solutions at room temperature in inactive systems is usually amorphous or microcrystalline, giving rise to U concentrations at equilibrium almost an order of magnitude higher than the crystalline phase at pH above 4 [GUI/FAN 2003]. From this follows that the surface of the precipitated $\text{UO}_2(\text{am})$ in the case of MOX leaching should be quite near to the stoichiometric composition. It is possible that the lowest U concentrations measured in the $\text{UO}_2(\text{cr})$ solubility study of Parks and Pohl [PAR/POH 1988] as compared to other studies are due also to the fact that they used a holding reductant which protected and potentially reduced the $\text{UO}_2(\text{s})$ surface, while the hydrated ions or solid reductant buffers used in other studies just consume traces of oxygen or of U(VI) in the bulk solution.

Experimental studies show that the reduction of the U(VI) originating from the pre-oxidized layer occurs on the surface of the spent fuel itself [ALB/JEN 2003], since very low levels of uranium are found in the vessel rinse. More than 99% of the uranium was precipitated on the surface of the spent fuel itself [OLL/ALB 2003]. The ability of the spent fuel in causing this reduction in the presence of hydrogen seems to be quite high, at least higher than that of Fe surfaces. From the data reported in [OLL/ALB 2003], the transfer of relatively low uranium concentrations (40–200 ppb) present in solutions contacting metallic Fe under 10 bar H_2 pressure to a similar vessel containing spent fuel equilibrated during long time under the same conditions caused a quick lowering of the uranium concentrations to much lower levels (a few ppb). The rapid decrease of the concentrations of molybdate in the case of MOX leaching, Figure 3-29, indicating its potential reduction, was not observed for UOX fuel under similar conditions [SPA/WER 2000, SPA/CUI 2004], but it was observed in the case of the leaching of ϵ -metallic particles extracted from spent fuel [CUI/LOW 2004] under much lower H_2 concentrations (Ar+10% H_2). During the leaching of synthetic ϵ -particles, in which the high β field present in the ones extracted from spent fuel and in the MOX fuel is absent, no decrease of Mo levels was observed, but instead an increase.

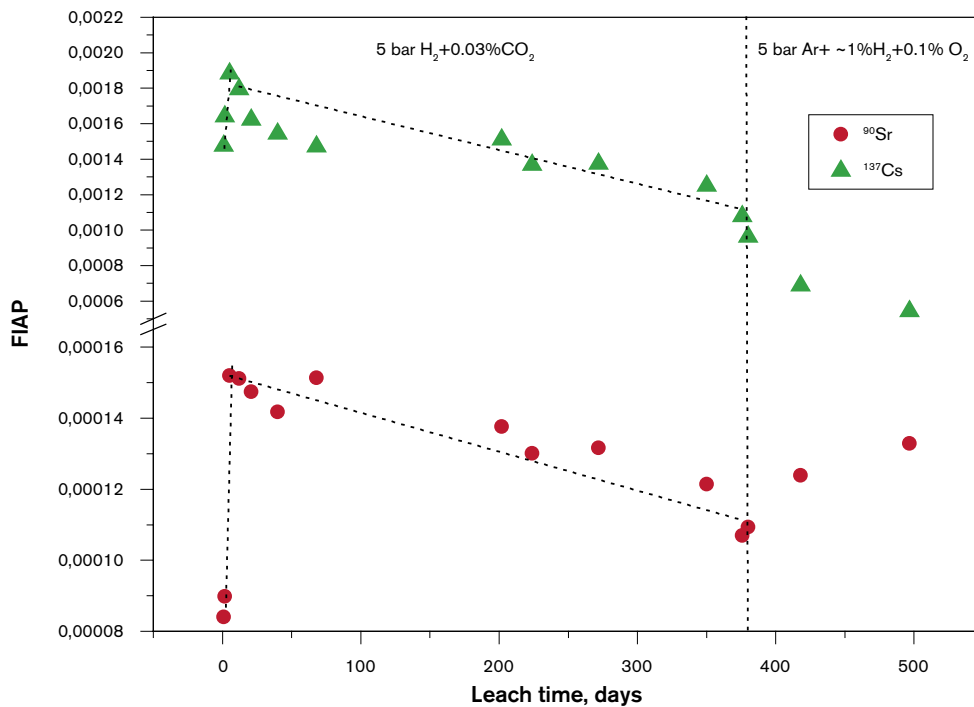
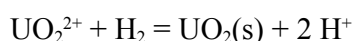


Figure 3-30. Evolution of Fraction of Inventory in the Aqueous Phase (FIAP) for ^{90}Sr and ^{137}Cs with time during the leaching of 1.7 g fuel powder under 0.5 MPa H_2 or 0.5 MPa Ar [SPA/CUI 2004].

The releases of Cs during the leaching of UOX fuel powder under relatively high H₂ concentrations [SPA/WER 2000, SPA/CUI 2004] were similar to the MOX case, i. e. it is not possible to calculate a dissolution rate for spent fuel based on Cs releases. However in all three cases the experimental data justify fuel dissolution rates based on Cs releases well below 10⁻⁷/year (see also below).

The acidification of the solution in the case of the high burn-up (HBU) spent fuel leaching in un-buffered 5 M NaCl solutions during the first 53 days to pH 4.9 corresponds to the production of a small amount of protons (~ 25 μM). The pre-leaching data indicate that under the oxidizing conditions of this phase, some amount of U(VI) may have precipitated as sodium diuranate, especially when the pH increases. The hydrolysis of U(VI) followed by polycondensation-colloid formation and precipitation of polyuranates is accompanied by acidification. Even though this hypothesis seems plausible, it does not explain why this process should start after renewing the solution to pure 5 M NaCl and changing atmosphere to 3.2 bar hydrogen. Another possibility is that this acidification is the result of the reduction of U(VI) hydrolytic species by the H₂/2H⁺ couple according to the general equation:



which requires an activation of molecular hydrogen somewhere in the system. The preceding step of the reduction of polynuclear uranyl hydrolytic species expected to exist in solution at this pH interval to U(OH)₄(aq) is also accompanied by proton release due to the very strong hydrolysis of U(IV):



This acidification has not been reported in other studies and the factors which may have caused it this case are the absence of carbonate buffering and the relatively large amounts of U(VI) present at the start of the leaching due to both the pre-oxidation of the pellet during storage and the radiolytic oxidation of additional amounts during the pre-washing. A comparison with the data of the MOX fuel leaching, Figure 3-29 shows that the presence of 2 mM bicarbonate would buffer completely the protons released by a potential reduction of about 1 μM uranium measured at the start of the leaching. The same holds for the other samplings in 5 M NaCl leaching, when the amounts of uranium potentially reduced are small and/or dissolution of polyuranates counteracts the acidification. This observation is consistent with the relatively long period (~ 700 days) to reach very low uranium concentrations (~ 10^{-9.1} M) in the test at 5 M NaCl as compared to others [SPA/WER 2000, SPA/CUI 2004]. In this case both the relatively high amount of U(VI) present (possibly also as solid U(VI) phases) and the lower concentration of dissolved hydrogen (~ 0.85 mM due to the ~ 3 times lower solubility of hydrogen in 5 M NaCl as compared to dilute solutions) may be a potential explanation.

The increase in uranium concentrations approximately to the level measured at the start of the experiment observed in the case of HBU leaching in 5 M NaCl which is not accompanied by a similar increase of matrix bound nuclides has been observed systematically in other studies in the presence of hydrogen [SPA/EKL 2002, SPA/CUI 2004] when air contamination occurred. This indicates very probably the dissolution of a solid UO₂(s) phase that precipitated at the start of the leaching under hydrogen, apparently easier to dissolve than the fuel matrix itself, and which contains various amounts of co-precipitated nuclides.

The relatively high Sr releases observed in the K8 test may be interpreted as indicating that this concentration of dissolved hydrogen (~ 0.85 mM) is not sufficient to hinder efficiently the oxidative dissolution of the fuel matrix, alternatively that there is an additional source

of segregated Sr besides the dissolution of the matrix, due to the high burn-up and linear power of the fuel. Against both these hypothesis are the much lower Sr releases observed in the case of the pellet K4 leached in the presence of metallic iron, especially during the final stage when the pressure of hydrogen reached about 2.7 bar. Even though this hydrogen pressure is still lower than in the case of the leaching of pellet K8, a substantial decrease of the Sr releases was observed. In this case the presence of Fe(II) ions may have influenced the results by causing a more efficient scavenging of radiolytic oxidants in combination with hydrogen. Literature data [ALB/JEN 2003, OLL/ALB 2003] indicate also a more efficient reducing environment if both Fe(II) ions and hydrogen are present. The leaching of pellet K14 in the presence of magnetite [LOI/KIE 2002], where both radiolytic oxygen measurements and matrix oxidation indicators are high, indicates that only Fe(II) ions or magnetite surfaces are not equally efficient.

In the case of pellet K8, there was both a long term (7 years) oxidation by air during storage and long washing cycles under Ar. They dissolved easily extractable radionuclides such as Cs from the fuel grain boundaries, but also caused further oxidation of the matrix, as indicated by the oxygen concentrations measured during the wash cycles. It is possible that these oxidized parts of the matrix and/or Sr-containing U(VI) phases precipitated during the wash cycles continue to contribute to the increase of the concentrations of the various radionuclides during the leaching under hydrogen overpressure, in spite of the fact that the apparent absence of molecular radiolytic oxidants in the leach solution and the low uranium concentrations would indicate that no large amounts of the matrix seem to be oxidized under such conditions. In the case of pellet K4, even though there seems to take place an oxidative dissolution of spent fuel during the first period, the initial concentrations of Sr in solution are very low and increase relatively quickly during the first 487 days, Figure 3-20. In the case of pellet K8, the Sr releases start from a higher level and the release rates decrease until reaching levels of 10^{-7} FIAP/day, to remain afterwards constant. The only apparent lowering of the Sr release in the presence of external hydrogen pressure occurs during the period 697–931 days, when air contamination possibly occurred. Even using the lowest Sr fractional release rate, a fuel dissolution rate of the order of 2×10^{-5} /yr is obtained based on the Sr releases for pellet K8. However, both iron and hydrogen will be present in the repository and in such solutions the long term fuel dissolution rates obtained in the final period of the leaching of pellet K4 based on Sr release rates are 3.7×10^{-7} /yr.

On the other hand relatively high incremental fractional release rates of Sr (IFR(t), see below) were observed also in the autoclave leaching of spent fuel powder [SPA/CUI 2004] in the presence of almost 5 times higher dissolved hydrogen concentrations (~ 4 mM). In this case the FIAP (Fraction of Inventory in the Aqueous Phase, [GRA/LOI 1996]) of ^{90}Sr decreases with time, indicating that the amount of Sr released from the matrix decreases with time. An Incremental Fractional Release rate (“IFR”) between the sampling steps at times t and t–1 can be derived in the following way:

$$IFR(t) = \frac{FIAP(t) - FIAP(t-1) \cdot \left(1 - \frac{V_{\text{sampled}}(t-1)}{V_{\text{solution}}(t-1)}\right)}{\Delta t}$$

where V_{sampled} is the volume of the solution removed from the system by sampling and V_{solution} is the solution volume prior to sampling. IFR(t) gives a more detailed description of the release rates (FIAP/day) for the non redox sensitive fission products such as ^{137}Cs and ^{90}Sr . When estimating rates based on such low Sr levels (less than 0.3 ppb ^{90}Sr) and variation with time (a 0.08 ppb Sr increase in concentration in one year), the analytical errors may be large, while in the case of Cs they are probably less due to the relatively higher concentrations.

The incremental fractional release rates calculated for ^{90}Sr from spent fuel powder leaching under 5 bar H_2 [SPA/CUI 2004] are relatively high (the lowest positive one is about $9 \times 10^{-6}/\text{yr}$), but a negative Sr-IFR(t) value is obtained when the time interval between samplings is the longest, plotted on the x-axis of Figure 3-31. Considering that these rates are for a fuel powder, for a 5–50 times lower surface area, this gives a long term dissolution rate for real fuel of $\sim 3 \times 10^{-7}/\text{year}$.

However, the lines tentatively drawn through the IFR(t) rates for both ^{137}Cs and ^{90}Sr , show that they decrease systematically with time. Another interesting observation from the IFR(t) data shown in Figure 3-31 towards the end of the leaching period under 5 bar H_2 , the IFR(t) values for Cs are consistently negative, even under Ar atmosphere and in presence of air contamination, as indicated by the gas analysis data. While the evolution of FIAP indicates that both the Sr and Cs releases decrease with time, the more detailed time analysis with IFR(t) for each interval shows exactly when no more Cs is released from the fuel. Apparently all the amount of Cs contained in the grain boundaries and/or in the surface monolayer is leached out after about 375 days. This process seems to take more time for Sr. In any case, more than 99% of ^{137}Cs inventory in the fuel sample leached under 5 bar H_2 is still contained in the fuel matrix.

The use of ^{90}Sr as an indicator of the matrix dissolution under the conditions valid for the autoclave leachings of spent fuel powder [SPA/WER 2000, SPA/CUI 2004] may be affected by the fact that the total amount of ^{90}Sr released in these cases is less than the amount of ^{90}Sr contained in a monolayer of fuel sample and also less than the reported 0.1% of the Sr inventory in the grain boundaries [GRA/STR 1992]. Hence it seems not very reliable to

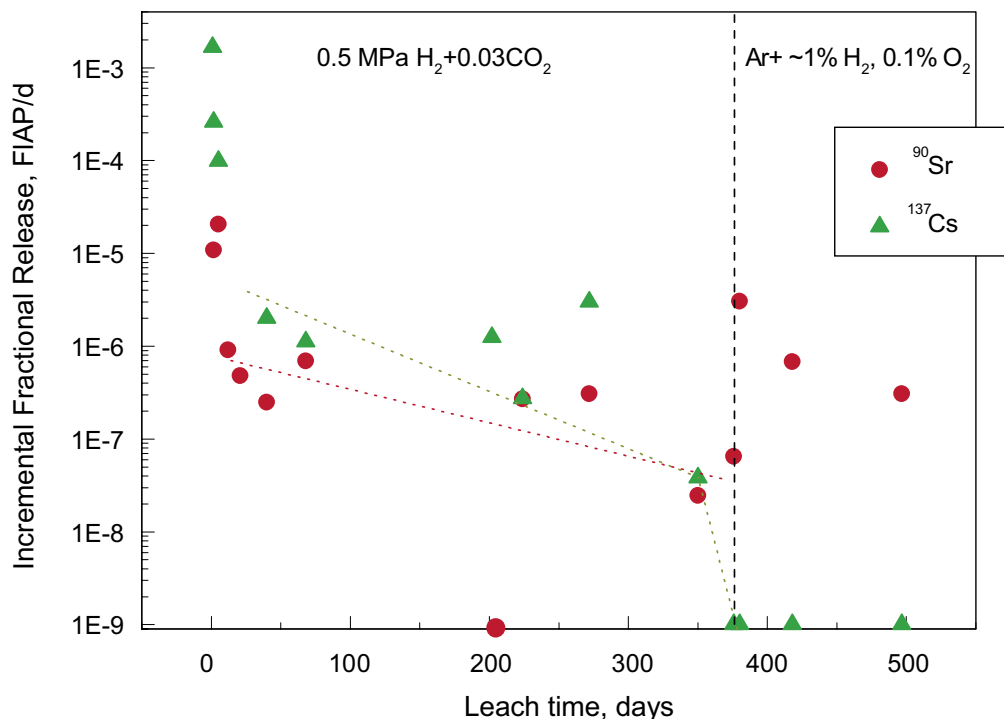


Figure 3-31. Release rates for Sr and Cs during each interval for spent fuel powder leaching under 5 bar H_2 or Ar, data from [SPA/CUI 2004]. In the x-axis are plotted data resulting in negative releases.

discuss matrix dissolution based on data derived from dissolution of less than a monolayer of fuel. The analysis of Sr-releases is a well established method for estimating the rate of the oxidative dissolution of spent fuel, when several layers of the $\text{UO}_2(\text{s})$ matrix are altered during the period in which release rates are analyzed [GRA/FOR 1990, LOI/GRA1 2001]. The effect of the hydrogen pressure and temperature on Sr releases may have different explanations, but it seems that under these conditions the IFR(t) release rates of Sr are relatively high, especially at the first samplings. They decrease rapidly and are much lower towards the end of the leachings, becoming practically zero at 50 bar [SPA/WER 2000] and when lowering the temperature to 25°C. Therefore it seems not probable that they are coupled to an oxidation-dissolution of the $\text{UO}_2(\text{s})$ matrix.

In favor of the hypothesis that these Sr releases are due to processes like e.g. the reduction of the $\text{UO}_2(\text{s})$ matrix surface layer, which decreases the Sr stability in the surface layer [CRO 2002] and is followed by releases which decrease with time and/or grain boundary contribution of Sr segregated phases, or dissolution of imperfect crystals is that these phenomena are expected to contribute a Sr release which is limited in time.

This is supported by the data on the continuation of the leaching at 50 bar H_2 , after adding new solution (~ 580 ml after 382 days, to substitute solution removed by sampling) to the autoclave and leaching the same fuel sample [SPA/EKL 2002] under H_2 and then Ar.

In this case the FIAP of both Cs and Sr decrease with time, Figure 3-32, and towards the end of the test period it seems that the fuel is not releasing any more Sr, since many negative IFR(t) values are calculated, even in the last period under Ar atmosphere, Table 3-8.

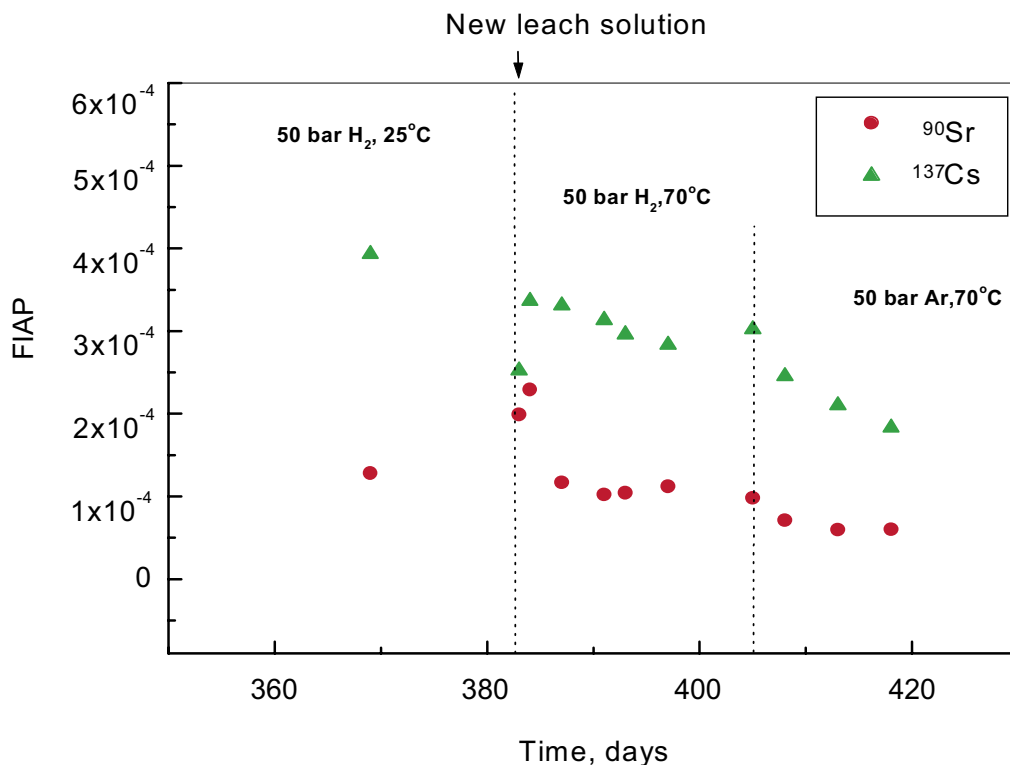


Figure 3-32. Calculated FIAP for the leaching of 2 g fuel powder after addition of new leach solution under 50 bar H_2 or Ar.

Table 3-8. Calculated IFR(t) for Sr and Cs after addition of new leach solution for spent fuel leaching data from [SPA/EKL 2002].

Day	⁹⁰ Sr IFR(t)	¹³⁷ Cs IFR(t)
383	5.8×10^{-6}	-2.4×10^{-5}
384	3.8×10^{-5}	3.0×10^{-4}
387	-3.3×10^{-5}	1.3×10^{-5}
391	-2.1×10^{-6}	8.1×10^{-20}
393	3.9×10^{-6}	4.3×10^{-6}
397	3.9×10^{-6}	4.0×10^{-6}
405 (Ar)	-8.6×10^{-7}	1.5×10^{-5}
408 (Ar)	-6.6×10^{-7}	-3.7×10^{-5}
413 (Ar)	-1.2×10^{-6}	-9.8×10^{-6}
418 (Ar)	1.1×10^{-6}	-5.3×10^{-6}

In a flow-through study of spent fuel powder under various redox conditions [RÖL/SPA 2001], a decrease of the dissolution rates of the spent fuel by 3–4 orders of magnitude was measured in solutions containing ~ 0.8 mM dissolved H_2 (1 atm. H_2) as compared to the dissolution rates obtained under oxidizing conditions. The dissolution rates were proportional to the solubilities of uranium dioxide at a given pH, indicating that the driving force for the dissolution is the degree of undersaturation with uranium, a behavior noted also in the autoclaves. In this case due to the low pH (for values of $pH < 5$) and the presence of bicarbonate at the higher pH values, the surface should be free from U(VI) phases and cause the catalytic decomposition of hydrogen peroxide to oxygen and water on UO_2 surfaces [SHO 2000]. The rate-determining step for the oxidation of the spent fuel matrix by oxygen is a one electron transfer step. Under these conditions the rates should be dependent on both oxygen and proton concentrations [SHO 2000, TOR/BAR 1997, DEP/CAS 1996], since the cathodic reduction of oxygen for pH below 7 involves the participation of protons. Thus in the event of oxidation of $UO_2(s)$ by oxygen, the rate-determining step and as a consequence the measured overall rates, would depend on pH following a curve of slope non zero for $pH < 7$. This is not the case with the experimental data, the rate dependence on pH under H_2 parallels a curve passing through $UO_2(cr)$ solubility data of Parks and Pohl [PAR/POH 1988].

There exists a large database on dissolution rates under oxidizing conditions [FOR/WER 1992, GRA/FOR 1990] and by assuming a decrease of 3–4 orders of magnitude occurring in solutions containing 0.8 mM dissolved H_2 , long term dissolution rates for spent fuel of the order of $10^{-7}/yr$ – $10^{-8}/yr$ are obtained. A parallel reasoning may be used for the rates determined by electrochemical measurements with α -doped electrodes, where similar decreases in the dissolution rates as compared to oxidizing conditions were observed, and further experimental support for low dissolution rates is obtained by the uranium solution concentration evolution with time, Figure 2-46.

In the case of spent fuel, besides the α -radiation discussed in section 2.2.7, β - and γ -radiation are also present and influence a large volume of solution; furthermore ϵ -metallic particles are present in $UO_2(s)$ matrix. The effect of hydrogen on the suppression of the degree of oxidation and dissolution of UO_2 electrodes under γ -radiation and 50 bar H_2 or SIMFUEL electrodes containing ϵ -metallic particles under lower P_{H_2} (0.002–0.014 MPa) has been discussed in a recent study [KIN/SHO 2004]. It is argued that the observed phenomena can be explained not only with a decrease of the radiolytic oxidant levels by homogeneous γ -radiolysis of hydrogen saturated solutions, but also through a mechanism

that involves a surface activation of hydrogen. Electrochemical measurements indicate a reduction of the surface by the $H_2/2H^+$ couple activated on UO_2 active sites, probably by $H\cdot$ radicals generated by interfacial γ -radiolysis, or on ϵ -metallic particles in the case of SIMFUEL. The catalysis of $H_2/2H^+$ on metallic particles suppresses the potential of the entire UO_2 surface through galvanic coupling between metallic particles and the rest of the surface, depending on the size and distribution of the ϵ -metallic particles within the $UO_2(s)$ matrix.

The ϵ -metallic particles have been extracted recently from spent fuel by non-oxidative dissolution of UO_2 matrix and their leaching behavior in Ar and Ar+10% H_2 has been investigated. The results show a strong activation of hydrogen in their presence – the concentrations of all oxidized forms of radionuclides, including molybdate, decrease in the solutions saturated with only 10% H_2 , indicating a potential reduction [CUI/LOW 2004]. The strong β -radiation of ϵ -metallic particles extracted from fuel plays an important role in hydrogen activation, since an increase of Mo concentrations with time is observed during the leaching of synthetic inactive metallic particles. The characterization of the ϵ -particles extracted from spent fuel indicates that they have a disperse nanoparticle distribution, related to the mechanism of their formation from separate atoms created by fission. In view of the results of [BRO/NOE 2004, KIN/SHO 2004], this type of structure indicates a much better protective capacity through galvanic coupling with the $UO_2(s)$ surface than in the case of the relatively large ϵ -particles in SIMFUEL, created by melting of the components.

In conclusion, during the leaching of spent fuel in hydrogen-saturated solutions several factors contribute to the activation of hydrogen. A quantification of the various contributions is necessary and desirable, but also related to difficulties. The effect of hydrogen on the dissolution of depleted $UO_2(s)$ or the reduction of U(VI) carbonate species may be due principally to catalytic properties of the oxide surfaces. Besides the well known processes of homogeneous solution activation of hydrogen by radical-rich radiations such as β - and γ -radiation, the experimental data also indicate some effects of dissolved hydrogen that are difficult to explain with only a decrease of the levels of radiolytic oxidants in the bulk solution. Such are the very low levels of molecular radiolytic products after long leaching periods, the decrease of concentrations of uranium and other redox sensitive elements to very low levels corresponding to the solubilities of their reduced forms and indicating their reduction. Finally, above a certain level of dissolved hydrogen, very low (and systematically decreasing with time) releases of non-redox sensitive fission products are observed in most cases. Even if one assumes that both a reduction and radiolytic oxidation occur simultaneously, for $[H_2] > 1$ mM the predicted increase of the levels of redox sensitive components by radiolytic oxidation of the fuel does not seem to start even at very low levels, corresponding to the calculated solubilities of their reduced states.

In the case of spent fuel the presence of ϵ -metallic particles, with properties to catalyze hydrogen demonstrated both in the case of non-radioactive [KIN/SHO 2004] and radioactive ϵ -particles [CUI/NIL 2004], certainly plays an important role and could explain all the above mentioned observations. However, the effect is also observed in tests with α -doped $UO_2(s)$ and with no metallic particles present. In this case, as well as in the tests with external γ -radiation [KIN/QUI 1999] or α -radiation [SUN/BOY 1990] interfacial radiolytic processes may play an important role (see section 3.2.4).

Substantial efforts have been carried out in the frame of this project by the radiolysis and the modeling groups to improve the radiolytic model by including new reactions in the radiolytic schemes in the case of high chloride containing solutions. This has improved the modeling of experimental data obtained under hydrogen atmosphere in accordance with the strategy chosen at the start of the project for homogeneous radiolytic modeling of the whole system. As a consequence, much lower oxidant concentrations are obtained

in high chloride H_2 containing solutions and the increases in U concentrations calculated are much lower. However, it would probably be over-ambitious to try to explain all the experimental observation with the traditional radiolytic scheme in the case of the granitic and clay groundwaters. Attempts to include potential surface activation of hydrogen as those reported in [LUN/CHR 2002] may improve further the modeling of the experimental data.

In view of all the experimental results obtained in this project, including α -doped materials, high burn-up spent fuel and MOX fuel, it is considered that for concentrations of hydrogen of about 1 mM (slightly higher than in the leaching of HBU pellet in 5 M NaCl and much higher than the one used in most α -doped tests), a fractional dissolution rate of the order of $4 \times 10^{-7}/\text{yr}$ can be supported. This concentration of hydrogen is in any case much lower than that expected for the various European repository concepts [JOH/POI 2005].

3.2.4 Mechanism of the hydrogen effect

In connection with the studies on the dissolution of radioactive materials in the presence of dissolved hydrogen, its aqueous concentration rather than its partial pressure should be reported. Due to the different hydrogen solubilities in various solutions, a hydrogen partial pressure of e.g. 3 bar in salt brine systems corresponds roughly to the same levels of dissolved hydrogen in dilute groundwaters at 1 bar. Furthermore, the concentrations of dissolved hydrogen in the case of e.g. spent fuel leaching are usually several orders of magnitude higher than the concentrations of radiolytic oxidants or of the oxidized forms of the radionuclides; thus cases when a large excess of dissolved hydrogen is present, as in our experiments, are discussed below.

The results of the present studies on the dissolution of ^{233}U doped UO_2 as well as high burn-up spent fuel and MOX fuel in the presence of various concentrations of dissolved hydrogen (~ 0.05 – 13 mM for α -doped $\text{UO}_2(\text{s})$, 0.85 mM for spent fuel in brines and ~ 43 mM for MOX fuel) indicate that dissolved hydrogen has a large impact on the dissolution rates of these materials. As shown in this study, the release rates of several spent fuel components in concentrated NaCl solutions decreases almost linearly with the partial pressure of hydrogen in the system, up to release rates of the order of $10^{-9}/\text{day}$ at relatively low partial pressures of hydrogen between 0.1 and 1 bar. If one considers the low solubility of hydrogen in such concentrated solutions, the impact of hydrogen concentrations in the range 2.7×10^{-5} – 2.7×10^{-4} M is very large. These data indicate that molecular hydrogen is activated and participates in reactions with radiolytic oxidants.

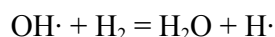
There are two possible ways to activate dissolved molecular hydrogen under our experimental conditions: by the ionizing radiations produced by the irradiated materials and by their surfaces ($\text{UO}_2(\text{s})$) and, in the case of the spent fuel, also the ϵ -metallic particles contained in the fuel matrix). Below is presented a preliminary discussion of these pathways and especially of the potential influence of surfaces, based on experimental observations made in the course of this project and on literature data.

In several spent fuel radiolytic modeling studies [ERI 1996, CHR 1998, LUN 2002, JON/NIE 2003, GRA/MEN 2004] it has been demonstrated that dissolved hydrogen substantially decreases the dissolution rates of spent fuel. The kinetic modeling of the whole system of radiolytic reactions, including those with the fuel surface, shows that it is possible to calculate an oxidant consumption in hydrogen containing solutions caused by the mixed radiation of the fuel, i.e. γ - and β -radiation contribute in the consumption of the molecular oxidants produced mainly by α -radiation. Although oxidizing and reducing species are produced in equivalent amounts, the low reactivity of molecular hydrogen towards stable species leads to locally oxidizing conditions near the fuel surface. The same holds true

even in the case of solutions containing various amounts of excess dissolved hydrogen, i.e. there is an excess of oxidants at each point of the solution, even though the presence of hydrogen lowers considerably the amount of molecular oxidants, especially in the case of low LET radiations such as γ - and β -radiation. By kinetic modeling of the various radiolytic reactions, even in the presence of high pressures of hydrogen, the conditions in solution and especially near the surface are locally oxidizing, mainly due to the continuous generation of molecular radiolytic oxidants by α -radiolysis. Thus in all these cases, even when dissolved U(VI) is partially reduced/precipitated [JON/NIE 2003, LIU/NER 2002], the concentrations of uranium in solution are predicted to increase with time (even though at much lower rates).

Our experimental data as well as related published studies [SUN/BOY 1990, KIN/QUI 1999, GRA/LOI 2000, SPA/WER 2000, LOI/GRA 2001, RÖL/SPA 2001, SPA/EKL 2002, OLL/ALB 2003, SPA/CUI 2004, KIN/SHO 2004] indicate that above a certain concentration of dissolved hydrogen, which depends on various factors, (e.g. the type and the intensity of the radiation field), the concentrations of the molecular products of water radiolysis in the bulk solution apparently reach extremely low values, since the concentrations of U decrease to very low values. Contrary to the expectations from the influence of dissolved hydrogen in the homogeneous radiolysis of water [PAS/LAV 2001], it seems that this limit is much lower for pure α -radiolysis than for the mixed α , β , γ radiation of the spent fuel.

The activation of hydrogen by low LET (Linear Energy Transfer) radical rich radiations as γ - and β -radiation is a well known process. In pure water it occurs through reactions of the type:



in which molecular hydrogen converts an oxidizing radical ($\text{OH}\cdot$) to water and a reducing radical ($\text{H}\cdot$). Recent experimental data [PAS/ISA 1999] indicate that even low levels of dissolved hydrogen are sufficient to decrease the amounts of molecular radiolytic oxidants produced by γ -radiation below detection limit, as well as to quickly consume small amounts of added H_2O_2 [PAS/LAV 2001]. In the frame of this project [KEL/BOH 2004] has introduced the following reaction in the chloride-containing systems:



which has a similar effect on the hydrogen activation in high chloride concentration solutions as the reaction with $\text{OH}\cdot$.

The effect of α -radiation through this mechanism is expected to be smaller, since in this case mainly molecular oxidants are produced. The results of the radiolytic modelling within this project will provide a quantitative estimation of its effect in the activation of molecular hydrogen in chloride rich solutions. However, in the case of spent fuel the β - and γ -fields influence a much larger volume of solution. Then an important question to discuss is: Can homogeneous γ - or β -radiolysis of hydrogen-saturated solutions reduce stable species like U(VI) to stable U(IV) species in solutions (and eventually to $\text{UO}_2(\text{s})$), or the small amounts of Fe(III) in iron-containing systems to Fe(II)? If this is possible, then the low concentrations of uranium and all other observations can be explained by this mechanism. The most probable case may be that of γ -radiolysis. This means that the observations of King et al. [KIN/QUI 1999] of the reduction of the $\text{UO}_2(\text{s})$ surface under γ -radiation are correct and the result could be expected from knowledge on homogeneous γ -radiolysis of hydrogen saturated solutions- i.e. if the bulk solution is reducing, the same conditions should also hold at the $\text{UO}_2(\text{s})$ surface. In any case, experimentally observed effects as the consumption of a large part of hydrogen peroxide added in the study of

[PAS/LAV 2001] by γ -radiolysis does not necessarily mean that γ -radiolysis creates reducing conditions – the addition was made to increase the levels of H_2O_2 above detection limit, i.e. not all added H_2O_2 was consumed. Further, hydrogen peroxide is a molecular product of the radiolysis, it is included in all radiolytic schemes and there is no reduced form of it which is not accounted for in the calculations. The problem of introducing U(VI) or Fe(III) may be tested by introducing in the radiolytic scheme also their reduced counterparts, respectively U(IV) and Fe(II). Radiolytic calculations of the concentrations of molecular oxidants produced in semi-closed systems such as autoclaves by α -radiolysis of spent fuel in homogeneous hydrogen saturated solutions (not including the uranium data files, containing reactions of uranium species with radiolytic radical and molecular species, but including the H_2O_2 decomposition at the surface) may show better the evolution of the oxidant concentrations in these systems.

Recently Quinones et al. [QUI/COB 2004] have published results of the effect of gamma radiolysis in simulated granitic groundwater solutions saturated with 1 atm H_2 , where apparently large amounts of oxidants were produced, as indicated by the amounts of oxidized uranium in solution. This shows that even in the case of γ -radiolysis the radiolytic yields have to be known more accurately in order to make reliable predictions. If the same holds for spent fuel dissolution tests in similar solutions, the absence of oxidants and the low uranium concentrations should then be due mainly to the neutralization of these oxidants by the interactions caused by the other types of radiation.

In another experimental work carried out under this same project [KEL/BOH 2004], the production of oxidants by γ -radiolysis in 5 M NaCl in the presence of ~ 0.85 mM dissolved H_2 was very small, but increased substantially in the presence of 10^{-4} M Br^- . In the study of CIEMAT [QUI/COB 2004] the presence of bromide in the granitic bentonitic groundwater (GBW) does not seem to enhance the production of oxidants; their production seems higher in the more dilute and bromide free granitic groundwater.

In all European repository concepts, at the time of water contact with spent fuel, γ -radiation is expected to have decayed to levels that would have negligible consequences for fuel dissolution. The effect of solution composition on homogeneous α -radiolysis of hydrogen saturated solutions is expected to be minor, because experimental data show no measurable decrease of radiolytic oxidant levels in water. However, in order to better understand the role of the different radiations in the activation of hydrogen in the case of fresh spent fuel, and the role of different minor solution components on γ -radiolysis, further experimental work is necessary.

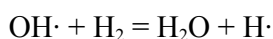
The radiolysis of water produces oxidizing and reducing species in equivalent amounts, but since the oxidizing molecular products such as H_2O_2 and O_2 are reactive towards stable species like U(IV) in solution, while the main molecular reducing species, H_2 , is inert at the temperatures of most of the studies, a net oxidation of the uranium dioxide matrix is expected followed by oxidation of $\text{UO}_2(\text{s})$ surfaces and the release of U(VI) species and other radionuclides. The presence of dissolved H_2 lowers very much the steady state concentrations of molecular and radical oxidizing species, but the total sum of steady state concentrations of H_2O_2 , O_2 and oxidizing radicals is always higher than that of the reducing radicals. This is due to the fact that molecular hydrogen does not count in the oxidizing or reducing balance towards stable species such as U(IV)–U(VI): hydrogen itself can not reduce stable species as U(VI) or Fe(III), while the same does not hold for O_2 and H_2O_2 which react readily with U(IV) and Fe(II).

In the case of spent fuel homogeneous radiolysis of hydrogen-saturated solutions by β - and γ -radiation (where the sample is taken) may be discussed first. By considering that radiolysis creates oxidizing conditions in the bulk solution, all the uranium sampled in the

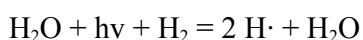
bulk solution should be U(VI) just by the effect of γ -radiolysis, even though the amounts of oxidants are very small and e.g. oxygen can not be detected in the gas phase. It is then difficult to explain why no more uranium is released from the UO_2 matrix. Even the small amounts of U(IV) required by the thermodynamic driving force to equilibrate with $\text{UO}_2(\text{s})$ (“non-oxidative dissolution”) would be oxidized in the bulk solution by α - β -, γ -radiolysis of hydrogen-containing solutions and thus cause an increase of the U concentrations in the bulk. All these observations indicate the presence of a large sink of oxidants in H_2 containing solutions in contact with spent fuel. The same holds for spent fuel leaching in the presence of iron, when oxidant-sensitive corrosion products such as green rust [GRA/LOI 1996] and magnetite were found on the surface of the corroding iron. Similar conclusions as in the case of the discussion of α -doped $\text{UO}_2(\text{s})$ (section 2.2.7) seem to hold even regarding the activation of hydrogen on spent fuel surfaces.

All experimental data indicate that the effect of UO_2 surfaces in activating hydrogen in the absence of radiation is much lower than in its presence. Much lower uranium concentrations are obtained in the irradiated cases; air contamination influences very much the concentrations of U in the depleted UO_2 - H_2 saturated solutions, while in the case of spent fuel it appears that the system neutralized completely small amounts of oxygen from air contamination and very little effect was noticed in the releases of, e.g. ^{137}Cs [SPA/CUI 2004]. No differences in the oxidation state of the $\text{UO}_2(\text{s})$ surface under Ar or H_2 in the absence of radiation were observed in the studies of [SUN/BOY 1990, KIN/QUI 1999], but a reduction was reported in the presence of radiation and H_2 in both cases.

Our experimental data and published studies, especially those involving α -radiation, indicate that processes occurring at the irradiated $\text{UO}_2(\text{s})$ surfaces play an important role in the observed effects. While experimental and modeling studies on homogeneous radiolysis have been carried out for decades and the field is thoroughly investigated, mechanistic studies of the effect of the ionizing radiations on water adsorbed on surfaces of different oxides including uranium dioxide, i.e. interfacial radiolysis, are relatively recent. In this case in addition to standard radiolytic processes, energy, charge or matter can be transferred through the interface, while catalytic or steric effects can alter the decomposition or reactivity of adsorbed molecules [LAV/TAN 2003]. Several studies have shown radiation-induced generation of hydrogen from adsorbed water, particularly on oxide surfaces. The effect of the presence of oxide surfaces on the radiolytic yield of hydrogen was investigated in a recent study [PET/ALE 2001]. A large number of metal oxides were classified in three groups as increasing, decreasing or causing almost no difference in the radiolytic yield of hydrogen in comparison with that measured in water. Several lanthanide oxides as well as ZrO_2 were found to belong in the first group. It was noted that oxides which have a band gap around 5 eV cause a remarkable increase in hydrogen production. Detailed mechanistic studies show that the increased hydrogen production is caused by excitons produced by the absorption of the radiation energy, which migrate to the surface of the oxide and cause the dissociation of adsorbed water molecules (H-O-H bond energy 5.1 eV, [CRC 1995]) to $\text{H}\cdot$ and $\text{OH}\cdot$ radicals. No study of the effect of any added hydrogen was carried out, but the kinetics of the reaction:



is well known and in hydrogen saturated solutions this would cause the production of a second atomic hydrogen from the dissociated water molecule. This potential mechanism indicates the importance of water molecules and their interactions with both the oxide surfaces and radiation, mediating through a photocatalytic-like dissociation process the overall reaction:



Uranium oxide was not included in the group of oxides studied in [PET/ALE 2001], but in another recent study of γ - and α -radiolysis of water sorbed on $\text{UO}_2(\text{s})$ surfaces [LAV/TAN 2003], much higher radiolytic yields (~ 10 fold) of hydrogen in sorbed water as compared to pure water were reported, while the yields of O_2 were at least an order of magnitude lower for water sorbed on UO_2 or ZrO_2 surfaces.

Much of the hydrogen production is initiated by the electronic excitations induced by the radiation, since the radiation produces little damage in the near surface region. For α -emitting materials such as U or Pu, significant lattice damage results from the recoil atom and the defects produced may alter the surface chemistry, leading to additional mechanistic participation in gas generation. In a study of the effect of the anionic defects created on the surface of $\text{UO}_2(\text{s})$ by sputtering with heavy ions on the production of hydrogen [STU/PAF 2004], it is reported that surface defects such as oxygen vacancies and Frenkel pairs lead to hydrogen evolution following water adsorption. Similar oxygen vacancies created on the surface of $\text{UO}_2(\text{s})$ by the α -recoil atom, likely contribute to the release of atomic hydrogen through the dissociative adsorption of a water molecule.

A quantitative estimation of such an effect on the neutralization of the radiolytic oxidants produced near the oxide surface by α -radiolysis in our tests may show that the effect is not significant, but one can not exclude that this or other surface processes contribute to the orders of magnitude lower effective radiolytic yields of α -particles emitted by $\text{UO}_2(\text{s})$ surfaces as compared to the yields measured with He^{2+} ions accelerated at similar energies in homogeneous solutions [LIU/NER 1995, CHR/SUN 1998, JOH/SMI 2000].

It is then possible that such combined effects of radiation and surfaces contribute to the observed effects under the experimental studies reported here. The formation of atomic hydrogen is a step in the mechanism of hydrogen production [KIN/SHO 2004] and deserves to be considered in the modeling of these systems.

Spent fuel leaching experiments carried out in Studsvik in dilute carbonate containing solutions flushed with low concentrations of hydrogen (Ar+10% H_2) show that the matrix continues to dissolve with almost constant rate, while a decrease of concentrations of U to levels of $\sim 10^{-7}$ M is observed [CUI/NIL 2004]. At the same time gas analysis measurements in closed vessels with similar solutions and spent fuel samples show that the concentrations of U start to decrease, even though the production of oxidants continues, as indicated by measurable levels of O_2 and H_2O_2 . At a certain level of the dissolved hydrogen concentration in the solution, which depends on the type of the radiation, its dose rate as well as the solution composition, it seems that the production of molecular radiolytic oxidants decreases to extremely low levels. Further experimental work is needed to determine this minimum hydrogen concentration for different systems and radiation types and to confirm the observations obtained under this project.

3.2.5 Summary and conclusions

Below a summary of the main results obtained during this project and some general conclusions based on our experimental data as well as literature studies discussed here are presented.

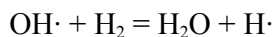
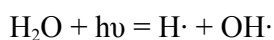
- In general, tests of a relatively high degree of complexity, mainly due to the extremely low oxygen concentrations realized in some of the systems and the need to avoid air contamination during sampling and other operations, were completed with good reproducibility and with a large number of test parameters varied and properties measured.

- In connection with the studies on the dissolution of radioactive materials in the presence of hydrogen, the most important parameter affecting the dissolution process is the concentration of dissolved H₂ and it should be preferably reported, instead of the H₂ partial pressure.
- A clear α -radiolysis enhancement of uranium dissolution was observed under anoxic conditions for 10% doped UO₂, while no such enhancement was observed for UO₂ containing 1% ²³³U. This may indicate that a possible threshold for observing radiolytic enhancement of dissolution lies between 1% and 10% ²³³U under our experimental conditions and timeframes considered.
- Under Ar/6% H₂, no further dissolution was observed in the static tests after the initial release, up to an activity level corresponding to 10% ²³³U.
- No oxidation of the 10% ²³³U doped UO₂ pellet surface occurred during the autoclave leaching, as shown by the XPS results, despite the low final hydrogen concentration and a leaching time of 2.2 years.
- The calculated radiolytic oxygen produced during the autoclave test is much higher than the measured oxygen concentrations indicating a consumption of oxygen through a UO₂ surface catalyzed reaction between O₂ and H₂.
- Background levels of U were measured on TiO₂(s) surfaces by SIMS, indicating no extensive sorption on autoclave walls.
- In electrochemical tests with ²³³U doped UO₂, by using the Tafel slopes measured under N₂/8% H₂, corrosion rates 3 orders of magnitude lower than those measured under oxidizing conditions could be determined. The 10% doped electrode had a corrosion rate about 10 times higher than the 1% doped one and a reduction of an order of magnitude or even more of the corrosion rate was observed under 8% hydrogen for the 1% doped material.
- The effect of relatively low concentrations of dissolved hydrogen in successfully hindering the oxidative dissolution of α -doped UO₂(s), is one of the major outcomes of the SFS project. In contrast, the expectations of this were low, based on the data from homogeneous radiolysis of hydrogen-saturated solutions.
- The release rates of several spent fuel components in concentrated NaCl solutions decrease almost linearly with the partial pressure of hydrogen in the system, reaching release rates of the order of 10⁻⁹/day at relatively low partial pressures of hydrogen (between 0.1 and 1 bar). Considering the low solubility of hydrogen in such concentrated solutions, the impact of hydrogen concentrations in the range 2.7×10⁻⁵–2.7×10⁻⁴ M is really large. These data indicate that molecular hydrogen is activated and participates in reactions with radiolytic oxidants.
- In all existing radiolytic modeling studies of fuel dissolution in the presence of H₂, even when an extra reaction of the reduction/precipitation of a part of dissolved U(VI) is considered, the concentrations of uranium in solution are predicted to increase with time. Our experimental data as well as all published studies indicate that above a certain concentration of dissolved hydrogen, which depends on various factors, among which the type and the intensity of the radiation field, the concentrations of molecular products of water radiolysis in the bulk solution reach likely extremely low values since the concentrations of U decrease to very low values.
- Contrary to the expectations from the influence of dissolved hydrogen in the homogeneous radiolysis of water, it seems that this limit is much lower for pure α -radiolysis than for the mixed α -, β -, γ -radiation of the spent fuel.

- The homogeneous β - and γ - radiolysis of hydrogen saturated solutions can lower considerably the steady state concentrations of the radical and molecular oxidants produced by radiolysis itself, but can not cause a the reduction of stable oxidized species such as U(VI) in solution. Published experimental data show that this decrease of oxidant levels during homogeneous α - radiolysis of hydrogen containing solutions is very small.
- From the long term U concentrations measured in all studied systems, the presence of U(VI) solid phases can be excluded. Post leaching characterization confirms their absence. The solid state chemistry of U(IV) is relatively simple: $\text{UO}_2(\text{s})$ in its microcrystalline (amorphous) form or $\text{UO}_2(\text{cr})$ are the only known solid phases (attempts to synthesize coffinite, $\text{USiO}_4(\text{s})$, have shown that it is a difficult task even under hydrothermal conditions favoring its formation). Uranium concentrations in all tests were similar to the lowest reported from solubility measurements of depleted crystalline $\text{UO}_2(\text{s})$ in the presence of very active reducing agents and systematically lower than those measured with microcrystalline $\text{UO}_2(\text{s})$, even though in all spent fuel tests precipitation of uranium in near neutral solutions is observed. The potential formation of U(VI) phases during spent fuel leaching carried out under oxidizing or anoxic conditions has made impossible the use of U releases in evaluating dissolution rates of spent fuel.
- The presence of 43 mM dissolved hydrogen in bicarbonate containing solutions inhibited the oxidation and dissolution of MOX fuel, as indicated by the uranium concentrations which decreased to about 3×10^{-10} M after almost 500 days. The concentrations of Cs reached a constant plateau after about 200 days, strongly implying the absence of U oxidation. The similar behavior of Tc, Mo, U, Np and Pu indicates that these elements were released congruently during the initial fuel loading and were thereafter most probably reduced to tetravalent state and precipitated as oxides.
- Practically no increases of the U concentrations with time were observed during the static or autoclave leaching of α -doped pellets and during the electrochemical tests. At the highest hydrogen concentrations tested (~ 40 mM) it is also not possible to determine any LWR or MOX fuel dissolution rate, either from the releases of U, Cs or any other radionuclide. For $[\text{H}_2] \sim 4$ mM, the fractional release rates of Cs or Sr decrease steadily with time until no release of Cs was observed after about one year. Measurable rates could be determined at the lowest hydrogen concentrations (~ 0.85 mM) used with spent fuel or at much lower ones with α -doped material in electrochemical tests. The relatively high Sr releases measured for the HBU fuel in 5 M NaCl solutions may be due to releases from Sr co-precipitated with U(VI) phases during the extensive washing cycles. The possibility that this concentration of hydrogen is not sufficient to completely hinder the oxidative dissolution of the fuel matrix can not be ruled out, even though another test under similar conditions, but with a non oxidized pellet and in the presence of actively corroding iron, shows very low releases of Sr.
- Based on all the experimental results obtained in this project with α -doped materials, high burn-up spent fuel and MOX fuel as well as literature data, for concentrations of hydrogen of greater than 1 mM and Fe(II) levels typical for European repository concepts, conservative fractional dissolution rates of spent fuel are of the order of $10^{-6}/\text{yr}$ – $10^{-8}/\text{yr}$, with a recommended value of $4 \times 10^{-7}/\text{yr}$.
- During the leaching of spent fuel in hydrogen-saturated solutions several factors contribute to the activation of hydrogen. Besides well known processes such as homogeneous solution activation of hydrogen by radical-rich β - and γ -radiation, the experimental data also indicate some effects of dissolved hydrogen that can not be explained with only a decrease of the levels of radiolytic oxidants in the bulk solution.

These include the very low levels of molecular radiolytic products after long leaching periods, the decrease of concentrations of uranium and other redox sensitive elements to very low levels corresponding to the solubilities of their reduced forms, the systematic decrease of the fractional release rates of Cs and Sr with time as well as the reported reduction of the $\text{UO}_2(\text{s})$ surfaces after tests with γ -radiation or α -radiation.

- The very low long-term concentrations of uranium, measured in all systems studied make it possible to exclude the presence of U(VI) solid phases, which in general have solubilities higher than 10^{-8} M. The evolution of U concentrations indicates in all cases no increase caused by the radiolytic oxidation of uranium from the $\text{UO}_2(\text{s})$ matrix. Since radiolysis continues to produce molecular oxidants in such systems, it follows that if they do not oxidize U(IV) to U(VI), then the only remaining pathway for their consumption is their reaction with dissolved hydrogen to produce water.
- The exact mechanism of this reaction in the case of depleted $\text{UO}_2(\text{s})$ surfaces would imply an activation of any of the reactants (H_2O_2 , O_2 or H_2) on the surface of $\text{UO}_2(\text{s})$. Experimental evidence on the ability of $\text{UO}_2(\text{s})$ surfaces to activate hydrogen and cause the reduction of U(VI) carbonate species has been presented, while no such evidence for the combination of H_2 with O_2 could be obtained on depleted $\text{UO}_2(\text{s})$.
- All experimental data indicate that this activation is more pronounced in the presence of different radiations. In our project no dedicated mechanistic studies were carried out, but based on recent literature data, a mechanism similar to photo-catalysis can be envisaged. The excitons produced by the absorption of radiation energy in uranium oxide dissociate water molecules adsorbed on the surface to $\text{H}\cdot$ and $\text{OH}\cdot$ radicals (dissociation energy 5.1 eV). In H_2 – saturated solutions the $\text{OH}\cdot$ radicals may then be consumed through reaction with dissolved H_2 :



Literature data show also that in the case of α -radiation, the oxygen vacancies produced by the recoil atoms may be an extra-pathway for the production of atomic hydrogen by the dissociative adsorption of water molecules. Further mechanistic studies are however necessary to understand and quantify such interfacial radiolytic effects.

- In the case of spent fuel, the presence of ϵ -metallic particles, shown in recent studies to be efficient hydrogen catalysts, is at present the only verified mechanism for the observed effect of dissolved hydrogen.
- The field of studies of α -doped $\text{UO}_2(\text{s})$ and spent fuel in hydrogen saturated solutions is relatively new and further studies are required to completely understand and quantify the various contributions to hydrogen activation, as well as to confirm the obtained results.

Acknowledgements

The authors of the HBU study in 5 M NaCl solutions like to express their thanks to the colleagues from FZK/INE involved to realize the study of spent fuel corrosion behavior under external hydrogen overpressure. These are in particular Mr N Müller for extensive careful hot cell and glove box laboratory work, Mrs E Bohnert and Dr M Kelm for analyzing the gas samples, Mrs A Görtzen, Mrs C Walschburger, Dr H Geckeis, Mr F Geyer and Mr A Seither for analysis of various leach solutions. The authors of the MOX fuel study would like to express their gratitude to P Peerani for his ORIGEN code calculations, S van Winckel, S Birck, G Rasmusson and A Nicholl for ICP-MS analysis, H Panissie for autoclave construction and V Ernst for help with CAD drawing. H-M Stutz and F Blattmann performed an excellent work in the workshop while manufacturing the MOX autoclave. The strength tests performed by J McGinley were of utmost importance [MCG/STU 2002]. Additionally, the excellent analysis made made by S Heatman (micro-XRD), G Tamborini (SIMS) T. Gouder and F Huber (XPS), H Thiele and B Cremer (SEM-EDX) are thankfully acknowledged. D. Solatie performed an excellent and important radiochemical analysis of the leachates. The assistance in the hot cells given by K Römer is greatly appreciated. The manuscript improved a lot after the corrections made by D Bottomley. The rest of the staff at ITU is very much acknowledged for their help and support. K Spahiu wishes to thank Lawrence Johnson for being a constant source of relevant literature on the subject, interesting discussions and improvement of the manuscript; Frank Garisto, OPG, for manuscript improvement as well as Daqing Cui, Max Lundström, Leif Kjellberg and Jeanett Low of Studsvik Nuclear for their contribution to the experimental work.

Literature

- [ALB/JEN 2003] Albinsson Y, Jensen A Ö, Oversby V M, Werme L. Leaching of spent fuel under anaerobic and reducing conditions. In: Scientific Basis for Nuclear waste management XXVI, Mat Res Soc Symp Series vol 757, (Finch, R. J. and Bullen, D.B. eds.), pp 407–413, 2003.
- [ALT/MET 2003] Altmaier M, Metz V, Neck V, Müller R, Fanghänel T. Solid-liquid equilibria of $\text{Mg}(\text{OH})_2(\text{cr})$ and $\text{Mg}(\text{OH})_3\text{Cl}\cdot 4\text{H}_2\text{O}(\text{cr})$ in the system Mg-Na-OH-Cl- H_2O at 25°C. *Geochimica et Cosmochimica Acta* 67, 3595–3601, 2003.
- [AST 1980] ASTM C698-80. Standard methods for chemical, mass spectrometric and spectro-chemical analysis of nuclear-grade Uranium dioxide powders and pellets, pp 54–85 (1980).
- [BAE/MES 1976] The hydrolysis of cations. C.F. Baes and R.E. Mesmer, John Wiley & Sons, New York, USA (1976).
- [BAK/LES 1966] Baker McD M, Less L N, Orman S: Uranium + water reaction. Part 2.- Effect of oxygen and other gases, *Trans. Faraday Soc.* 62, 2525–2530, 1966.
- [BON/COL 2000] Bonin B, Colin A, Dufloy A. Pressure building during early stages of gas production in a radioactive waste repository, *J. Nucl. Materials* 281, 1–14 2000.
- [BRO/NOE 2004] Broczkowski M E, Noël J J, Shoesmith D W. The inhibiting effects of hydrogen on the corrosion of uranium dioxide under nuclear waste disposal conditions. *In* International Youth Nuclear Congress, Canadian Nuclear Society, Toronto, Ontario, May 9-13, 2004.
- [BUN/ZOG 1958] Bunji B, Zogovic B. Reduction of uranium from carbonate solutions with hydrogen using UO_2 as catalyst. *Proceedings of the International Symposium on Peaceful Uses of Atomic Energy*, pp 350–355, Stockholm 1958.
- [CAR/COB 2003] P. Carbol, J. Cobos-Sabate, D. Solatie, D. Wegen, T. Wiss, S. van Winckel, R. Nasyrow, S. Birck. Characterisation of ^{233}U doped UO_2 pellet. Report JRC-ITU-TPW-2003/16. European Commission, DG JRC, Institute for Transuranium Elements, Karlsruhe, Germany. In print.
- [CAR/ENG 1997] Carbol P, Engkvist I. Compilation of radionuclide sorption coefficients for performance assessment. Swedish Nuclear Fuel and Waste Management Co, Stockholm, Sweden, SKB TR 97-13, 1997.
- [CAR/SOL 2000] Carbol P, Solatie D, Betti M. Analysis of $^{233}\text{U}_3\text{O}_8$ powder by radiometric methods. Report JRC-ITU-TN-2000/01. European Commission, DG JRC, Institute for Transuranium Elements, Karlsruhe, Germany. Released 12.05.2000.

- [CHR 1998] Christensen H. Calculations simulating spent fuel leaching experiments. Nuclear Technology. 124, pp 165–174, 1998.
- [CHR/FOR 1990] Christensen H, Forsyth R, Lundquist R, Werme L O, Radiation induced dissolution of UO₂, Studsvik Energiteknik Report NS-90/85, 1990.
- [CHR/SUN 1998] Christensen H, Sunder S. Current state of knowledge in radiolysis effects on spent fuel corrosion, Studsvik Report STUDESVIK/M-98/ 71, 1998.
- [COB/HAV 2002] Cobos J, Havela L, Rondinella V V, de Pablo J, Gouder T, Glatz J-P, Carbol P, Matzke H. Corrosion and dissolution studies of UO₂ containing α -emitters. Radiochim. Acta 90, 597–602, 2002.
- [COL 1984] Colmenares C A. Oxidation mechanisms and catalytic properties of the actinides, Prog. Solid State Chem, Vol 15 pp 257–364, 1984.
- [CRC 1995] CRC Handbook of Chemistry and Physics; D. R. Lide, H. P. R. Frederikse Eds.; CRC: Boca Raton-New York- London-Tokyo, 1995.
- [CRO 2002] Crocombete J-P Ab initio energetics of some fission products (Kr, I, Cs, Sr, and He) in uranium dioxide, J. Nucl. Mater, 305, 29-36, 2002.
- [CUI/ERI 1996] Cui D, Eriksen T. Reduction of Tc(VII) and Np(V) in solution by ferrous iron. A laboratory study of homogeneous and heterogeneous redox processes. SKB TR 96-03, Stockholm, March 1996.
- [CUI/LOW 2004] Cui D, Low J, Sjöstedt C J, Spahiu K. On Mo-Ru-Tc-Pd-Rh alloy particles extracted from spent fuel and their leaching behaviour under repository conditions, Radiochim. Acta, 92, pp 551–555, 2004.
- [CUI/NIL 2004] Cui D, Nilsson P, Spahiu K. The influence of hydrogen on spent fuel leaching and possible mechanisms, presented at MRS Spring meeting 2004, 12–15 April 2004, San Francisco, USA.
- [CUI/SPA 2002] Cui D, Spahiu K. The reduction of U(VI) on corroded iron under anoxic groundwater conditions, Radiochim. Acta, 90, pp 1–6, 2002.
- [DEV/HAS 2003] Devoy J, Haschke J, Cui D, Spahiu K. Behaviour of spent fuel: chemistry and catalysis in the UO₂-water system, Mat. Res. Soc. Symp. Series, 807 pp 41–46, 2003.
- [DEP/CAS 1996] de Pablo J, Casas I, Gimenez J, Marti E, Torrero M E. Solid surface evolution model to predict uranium release from unirradiated UO₂ and nuclear spent fuel dissolution under oxidizing conditions, J. Nucl. Mater, 232, 138, 1996.
- [EKE/JON 2004] Ekeröth E, Jonsson M, Eriksen T E, Ljungqvist K, Kovacs S, Puigdomenech I. Reduction of UO₂²⁺ by H₂, J. Nucl. Material. 334, pp 35–39, 2004.
- [ENG/MAR 1999] Engelhardt J, Marx G. Contact corrosion measurements on the pair UO_{2+x} and carbon steel 1.0330 in brines and bentonite pore water with respect to direct waste disposal, J. Nucl. Mat. 264, 161–168, 1999.

- [ERI 1996] Eriksen T. Radiolysis of water within a ruptured fuel element, SKB Progress Report U-96-29, Svensk Kärnbränslehantering AB, 1996.
- [FAN/NEC 2002] Fanghänel Th, Neck V: Aquatic chemistry and solubility phenomena of actinide oxides/hydroxides, *Pure and Appl. Chemistry*, 74 1895–1907, 2002.
- [FER/RIC 1999] Fernandez A, Richter K, Fourcaudot S, Closset J C, Fuchs C, Babelot J F, Voet R, Somers J. Fabrication of targets for the transmutation and incineration of actinides, *Adv. in Science and Technology*, 24 539–546, 1999.
- [FIS/WIE1983] Fischer U, Wiese H W. Verbesserte konsistente Berechnung des nuklearen Inventars abgebrannter DWR- Brennstoffe auf der Basis von Zell-Abbrand-Verfahren mit KORIGEN. KfK-3014, January 1983.
- [FOR/MAT 1988] Forsyth R S, Mattsson O, Schrire D, Fission product concentration profiles (Sr, Xe, Cs and Nd) at the individual grain level in power-ramped LWR fuel, SKB TR 88-24, Stockholm 1988.
- [FOR/WER 1992] Forsyth R S, Werme L O. Spent fuel corrosion and dissolution, *J. Nucl. Mater.*, 190, 3–19, 1992.
- [FUG 1993] Fuger J. Problems in the thermodynamics of the actinides in relation with the back-end of the nuclear cycle, *J. Nucl. Materials*, 201, 3–14, 1993.
- [GAR/CHR 1965] Garrels R M, Christ C L. “Solutions, Minerals, and Equilibria”, Harper & Row, New York, 450 p, 1965.
- [GIM/BAR 1996] Gimenez J, Baraj E, Torrero M E, Casas I, de Pablo J. Effect of H₂O₂, NaClO and Fe on the dissolution of unirradiated UO₂ in NaCl 5 molkg⁻¹, *J. Nucl. Materials*, 238, 64–69, 1996.
- [GRA/CAC 2005] B. Grambow, C. Cachoir, J-P Glatz, K. Lemmens, A. Martinez-Esparza, T. Mennecart, V. Rondinella, K. Spahiu, D. Wegen, Effect of alpha irradiation field on long term corrosion of spent fuel, Deliverable D9 of SFS project, ITU Report, 2005. In print
- [GRA/FOR 1990] Grambow B, Forsyth R S, Werme L O, Bruno J. Fission product release from spent UO₂ fuel under uranium saturated oxidic conditions, *Nuclear Technology*, 92, 202–213, 1990.
- [GRA/LOI 1996] Grambow B, Loida A, Dressler P, Geckeis H, Gago J, Casas I, de Pablo J, Gimenez J, Torrero M E. Long-term safety of radioactive waste disposal: Chemical reaction of fabricated and high burn-up spent fuel with saline brines, Forschungszentrum Karlsruhe, Wissenschaftliche Berichte FZKA 5702, 1996.
- [GRA/LOI 2000] Grambow B, Loida A, Martinez-Esparza A, Diaz-Arcoas P, De Pablo J, Paul J-L, Marx G, Glatz J-P, Lemmens K, Ollila K, Christensen H. Source term for performance assessment of spent fuel as a waste form, European Commission, Nuclear Science and Technology, EUR 19140 EN, 2000.

- [GRA/MEN 2004] Grambow B, Mennecart T, Fattahi M, Blondinaux G. Electrochemical aspects of radiolytically enhanced UO_2 dissolution, *Rdiochim. Acta*, 92, pp 603–609, 2004.
- [GRA/MUL 1990] Grambow, Müller R. Chemistry of glass corrosion in high saline brines *Mater. Res. Soc. Symp.Proc.* 176 229–241, 1990.
- [GRA/STR 1992] Gray W J, Strachan D M, Wilson C N. Gap and grain boundary inventories of Cs, Tc and Sr in spent LWR fuel, *Mat. Res. Soc. Symp. Proc.* Vol. 257, 353–360, 1992.
- [GOL/WEG 2003] Goll W, Wegen D. Personal communication, 2003.
- [GUI/FAN 2003] Guillamont R, Fanghänel T, Grenthe I, Neck V, Palmer D, Rand M H, Update on the chemical thermodynamics of uranium, neptunium, plutonium americium and technetium, OECD-NEA, *Chemical Thermodynamics Vol. 5*, pp 182–187, Elsevier 2003.
- [GUP/ATK 1989] Guppy R M, Atkinson A, Valentine T M. Studies of the solubility of technetium under a range of redox conditions HARWELL ARE-R 13467, DOE/RW/89/102, 1989.
- [HAN 2002] Hansen H C B. Environmental chemistry of iron(II)-iron(III) LDHs (green rusts). Chapter 13 in Rives, V. (Ed.) *Layered double hydroxides: Present and Future*, pp 413 – 434, Nova Sci. Publ, NY, 2002.
- [HAS/ALL 1996] Haschke J M, Allen T H, Stakebake J L. Reaction kinetics of plutonium with oxygen, water and humid air, *J. Alloys and Compounds*, 243, pp 23–35, 1996.
- [ICE/TOT 2004] Icenhour A S, Toth L M, Wham R M, Brunson R R. A simple kinetic model for the α -radiolysis of water, *Nuclear Technology*, 146, pp 206–209, 2004.
- [IMI/TAN 1979] Imizu Y, Tanabe K, Hattori H. Selective formation of trans-butene and methyl-butene in deuteration of butadiene derivatives over thorium oxide catalyst, *Journal of Catalysis*, 56, pp 303–314, 1979.
- [IMO 1986] Imoto S. Chemical state of fission products in irradiated UO_2 , *J. Nucl. Materials* 140, pp 19–27, 1986.
- [JEF 1967] Jeffrey B M. Microanalysis of inclusions in irradiated UO_2 , *J. Nucl. Mater.*, 22, p. 33–40, 1967
- [JEG 2004] Jegou C. Personal communication to ITU, 2004.
- [JEN/ALB 2004] Jensen A Ö, Albinsson Y. Preliminary results on oxygen production from α -radiolysis (^{238}Pu) under Ar/H_2 -pressure without any solid phase in high-pressure vessels. NR-PRO progress meeting, Gothenburg, May 2004.
- [JOH/SHO 1988] Johnson L H, Shoesmith D W. Spent fuel. In: *Radioactive Waste Forms for the Future*, Eds.: Lutze, W and Ewing, R. C, North-Holland Physics Publishing, The Netherlands, 1988.

- [JOH/SMI 2000] Johnson L H, Smith P A. The interaction of radiolysis products and canister corrosion products and the implications for spent fuel dissolution and radionuclide transport in a repository for spent fuel. NAGRA Technical Report 00-04, 2000.
- [JOH/POI 2005] Johnson ed LH, Poinssot C, Ferry C, Lovera P, Cavedon J M, Miserque F, Corbel C, Andriambololona Z, Wegen D, Carbol P, Glatz J.P, Cobos J, Rondinella V, Grambow B, Spahiu K, Kelm M, Metz V, Loida A, Kienzler B, Lundström T, Christensen H, Jonsson M, de Pablo J, Rovira M, Casas I, Martinez-Esparza A, Bruno J, Cera E, Clarens F, Gonzalez de la Huebra A, Iglesias E, Merino J, Quinones J, Serrano D, Gago J, Cachoir C, Lemmens K, Meyer G. Spent fuel evolution under disposal conditions – Synthesis of results from the EU Spent Fuel Stability (SFS) Project, NAGRA Technical Report NTB 04-09, Nagra, Wettingen, Switzerland, 2005.
- [JON 2004] Jonsson M. On the possible causes of the discrepancies between experimental results and radiolytic modelling of α -radiolysis of H_2 saturated solutions, SKB-SF meeting, Stockholm, May 2004.
- [JON/NIE 2003] Jonsson M, Nielsen F, Ekeroth E, Eriksen T. Modeling of the effects of radiolysis on UO_2 dissolution employing recent experimental data, Mat. Res. Soc. Symp. Series, vol. 807 (Oversby, V. M. and Werme, L.O. eds.), pp 385–390, 2003.
- [KEL/BOH 2002] Kelm M, Bohnert E. Radiolysis and corrosion of ^{238}Pu doped UO_2 pellets in chloride brine, Proc. Indian Acad. Sci.(Chem. Sci.) 114 (6), pp 697–704, 2002.
- [KEL/BOH 2004] Kelm M, Bohnert E. A kinetic model for the radiolysis of chloride brine, its sensitivity against model parameters and a comparison with experiments, FZKA 6977 Report, Forschungszentrum Karlsruhe, April 2004.
- [KIN/QUI 1999] King F, Quinn M J, Miller H H. The effect of hydrogen and gamma radiation on the oxidation of UO_2 in $0.1 \text{ mol} \times \text{dm}^{-3}$ NaCl solution, SKB Technical Report TR-99-27, 1999.
- [KIN/SHO 2004] King F, Shoesmith D. Electrochemical studies of the effect of H_2 on UO_2 dissolution, SKB Technical Report TR-04-20, 2004.
- [KLE 1985] Kleykamp H. The chemical state of the fission products in oxide fuels, J. Nucl. Mater. 131, pp 221–246, 1985.
- [KLE 1988] Kleykamp H. The chemical state of fission products in oxide fuels at different stages of the nuclear fuel cycle. Nuclear Technology, 80,412–422, 1988.
- [KLE/PAS 1985] Kleykamp H, Paschoal J O, Pejasa R, Thümmeler F. Composition and structure of fission product precipitates in irradiated fuels: correlation with phase studies in the Mo-Ru-Rh-Pd and BaO- UO_2 - ZrO_2 - MoO_3 systems, J. Nucl. Materials 130, pp 426–433, 1985.
- [LAV/TAN 2003] LaVerne J A, Tandon L. H_2 production in the radiolysis of water on UO_2 and other oxides, J. Phys. Chem. B, 107, pp 13623–13628, 2003.

- [LIU/NER 1995] Liu L, Neretnieks I. Some evidence of radiolysis in a uranium ore body –quantification and interpretation. MRS Symposium Proceedings, Vol. 353, pp 1179–1186, 1995.
- [LIU/NER 2002] Liu L, Neretnieks I. The effect of hydrogen on the oxidative dissolution of spent fuel, *Nuclear Technology*, 138, pp 69–77, 2002.
- [LOI/GRA 2001] Loida A, Grambow B, Geckeis H. Spent fuel corrosion behavior in salt solution in the presence of hydrogen overpressure, Proc. of ICEM'01: The 8th Internat. Conf. on Radioactive Waste Management and Environmental Remediation, Bruges, B, September 30–October 4, 2001 (CD-ROM).
- [LOI/GRA1 2001] Loida A, Grambow B, Geckeis H. Congruent and incongruent releases during matrix dissolution of partly oxidized high burn-up spent fuel, MRS Symp. Proc. 663, pp 417–426, 2001.
- [LOI/KIE 2002] Loida A, Kienzler B, Geckeis H. Mobilization/retention of radionuclides during co-dissolution of high burn-up spent fuel and near field materials in salt brines. MRS Symp. Proc. 757, pp 433–439, 2002.
- [LUN 2002] Lundström T. UO₂ dissolution and the effect of radiolysis, In Proc. Spent Fuel Workshop 2002, 23–25 September 2002, Avignon, France.
- [LUN/CHR 2002] Lundström T, Christensen H. Calculations of the effect of hydrogen on water-radiolysis induced oxidation of UO₂, In Proc. Spent Fuel Workshop 2002, 13–14 September 2001, Helsinki, Finland.
- [MAR 2000] Marx G, in Grambow B et al. EUR 19140- Source term for performance assessment of spent fuel as a waste form, Luxembourg 2000.
- [MCG/STU 2002] McGinley J, Stutz H-M. Titanium-2 weld-joint tests for a leaching autoclave. Report JRC-ITU-TPW-2002/31. European Commission, DG JRC, Institute for Transuranium Elements, Karlsruhe, Germany.
- [NEC/ALT 2003] Neck V, Altmaier M, Müller R, Schlieker M, Fanghänel T. Solubility of U(VI) in NaCl and MgCl₂ solutions. 9th International Conference on Chemistry and Migration Behaviour of Actinides and Fission Products in the Geosphere, Migration '03, 47, 2003.
- [NEC/KIM 2001] Neck V, Kim J I. (2001) Solubility and hydrolysis of tetravalent actinides. *Radiochimica Acta* 89, 1–16, 2001.
- [NEW 1975] Newton T W. The kinetics of oxidation-reduction reactions of uranium, neptunium, plutonium and americium in aqueous solutions, ERDA Critical Review Series; National Technical Information Service, Springfield VA, 1975.
- [OLL/ALB 2003] Ollila K, Albinsson Y, Oversby V, Cowper M. Dissolution rates of unirradiated UO₂, UO₂ doped with ²³³U, and spent fuel under normal atmospheric conditions and under reducing conditions using an isotope dilution method, SKB Technical Report TR-03-13, October 2003.
- [PAR/POH 1988] Parks G A, Pohl D C. Hydrothermal solubility of uraninite, *Geochim. Cosmochim. Acta* 52, 863–875, 1988.

- [PAS/ISA 1999] Pastina B, Isabey J, Hickel B. The influence of water chemistry on the radiolysis of primary coolant water in pressurized water reactors, *J. Nucl. Mat*, 264, pp 309–318, 1999.
- [PAS/LAV 2001] Pastina B, LaVerne J A. Effect of molecular hydrogen on hydrogen peroxide in water radiolysis, *J. Phys. Chem. A*, 105, pp 9316–9322, 2001.
- [PER/GRE 1997] Perry R H, Green D W. *Perry's Chemical Engineers Handbook*, 7th ed. McGraw-Hill Company Inc, New York, ISBN 0-07-049841-5, pp 2–126, 1997.
- [PET/ALE 2001] Petrik N G, Alexandrov A B, Vall A I. Interfacial energy transfer during gamma radiolysis of water on the surface of ZrO₂ and some other oxides, *J. Phys. Chem. B*, 105, pp 5935–5944, 2001.
- [QUI/COB 2004] Quinones J, Cobos J M, Gonzales de la Huebra A, Martinez Esparza A: An experimental study on the influence of gamma radiation on spent fuel dissolution in the presence of H₂ atmosphere, *Mat. Res. Soc. Symp. Proc*, 824, pp 153–158, 2004.
- [RAI/FEL 1990] Rai D, Felmy A R, Ryan J L. Uranium(IV) hydrolysis constants and solubility product of UO₂·xH₂O(am), *Inorg. Chem.* 29, 260–264, 1990.
- [RAI/YUI 2003] Rai D, Yui M, Moore D A. Solubility and solubility product at 22°C of UO₂(c) precipitated from aqueous U(IV) solutions, *J. Solution Chem.* 32, 1–17, 2003.
- [RON/COB 2001] Rondinella V V, Cobos J, Matzke HJ, Wiss T, Carbol P, Solatie D. Leaching behaviour and α -decay damage accumulation of UO₂ containing short-lived actinides, *Mat. Res. Soc. Symp. Proc*, 663 pp 392–399, 2001.
- [RON/COB 2003] Rondinella V V, Cobos J, Wiss T, Hiernaut J-P. Studies on spent fuel alterations during storage and radiolysis effects on corrosion behaviour using α -doped UO₂, *proc. ICEM '03*, Oxford, UK, Sept 21–25, 2003, ASME 2003, (CD-ROM).
- [RON/MAT 2000] Rondinella V V, Matzke HJ, Cobos J, Wiss T. Leaching behaviour of UO₂ containing α -emitting actinides, *Radiochim. Acta*, 88 pp 527–531 2000.
- [RÖL/SPA 2001] Röllin S, Spahiu K, Eklund U-B. Determination of dissolution rates of spent fuel in carbonate solutions under different redox conditions with a flow-through experiment, *J. Nucl. Mater*, 297, pp 231–243, 2001.
- [SEL 2001] Sellin P. P, SR 97: Hydromechanical evolution in a defective canister, In: *Scientific Basis for Nuclear waste management XXVI*, *Mat. Res. Soc. Symp. Series*, 663, pp 755–763, 2001.
- [SKI 1996] SKI Site-94, Deep Repository Performance Assessment Project, Volume II, Swedish Nuclear Power Inspectorate, Stockholm, Sweden, SKI Report 96:36, 1996.

- [SHO 2000] Shoesmith D W. Fuel corrosion processes under waste disposal conditions, *J. Nucl. Mater.* 282, 1–31, 2000.
- [SHO/SUN 1988] Shoesmith D W, Sunder S, Bailey M G, Wallace G J. Anodic oxidation of UO_2 . V. Electrochemical and x-ray photoelectron spectroscopic studies of film growth and dissolution in phosphate-containing solutions, *Can. J. Chem.* 66 p. 259–265, 1988.
- [SHO/SUN 1991] Shoesmith D W, Sunder S. An electrochemical model for the dissolution of UO_2 , Atomic energy of Canada Ltd Report, AECL-10488, 1991.
- [SOM/VOE 2002] Somers J, Voet R, Fuchs C, Hein H, Boshoven C, Fourcaudot S, Modery N, Murray-Farthing M. Fabrication of UO_2 pellets doped with ^{233}U for α -radiolysis investigations. Report JRC-ITU-TPW-2002/12. European Commission, DG JRC, Institute for Transuranium Elements, Karlsruhe, Germany.
- [SPA/CUI 2004] Spahiu K, Cui D, Lundström M. The fate of radiolytic oxidants during spent fuel leaching in the presence of dissolved near field hydrogen, *Radiochim. Acta*, 92, pp 625–629, 2004.
- [SPA/DEV 2004] Spahiu K, Devoy J, Cui D, Lundström M. The reduction of U(VI) by near field hydrogen in the presence of $\text{UO}_2(\text{s})$, *Radiochim Acta* 92, pp 597–601, 2004.
- [SPA/EKL 2002] Spahiu K, Eklund U-B, Cui D, Lundström M. The influence of near field redox conditions on spent fuel leaching, In: *Scientific Basis for Nuclear waste management XXV*, Mat. Res. Soc. Symp. Series, 713, pp 633–638, 2002.
- [SPA/WER 2000] Spahiu K, Werme L, Eklund U-B. The influence of near field hydrogen on actinide solubilities and spent fuel leaching, *Radiochim Acta*, 88 pp 507–511, 2000.
- [SPA/WER 2001] Spahiu K, Werme L, Low J, Eklund U-B. In - situ long term measurements of pH and redox potential during spent fuel leaching under stationary conditions – the method and some preliminary results. *Mat. Res. Soc. Symp. Series*, 608, pp 55–60, 2001.
- [STU/PAF 2004] Stultz J, Paffet M T, Joyce S A. Thermal evolution of hydrogen following water adsorption on $\text{UO}_2(100)$, *J. Phys. Chem. B*, 108, 2362–2364, 2004.
- [SUN/BOY 1990] Sunder S, Boyer G D, Miller N H, 1990. XPS studies of UO_2 oxidation by α -radiolysis of water at 100°C , *J. Nucl. Mater*, 175, p. 163–169, 1990.
- [TAM/BET 1998] Tamborini G, Betti M, Forcina V, Hiernaut T, Koch L. Secondary Ion Mass Spectrometry (SIMS) Analysis for the Identification of single Particles of Uranium and their Isotopic Measurement, *Spectrochimica Acta Part B*, 53(9), 1289–1302 (1998).
- [TAM/BET 2000] Tamborini G, Betti M. Characterisation of Radioactive Particles by SIMS, *Mikrochim. Acta*, 132, pp 411–417 (2000).

- [TAM/WAL 2001] Tamborini G, Wallenius M, Bildstein O, Pajo L, Betti M. Development of a SIMS method for isotopic measurements in nuclear forensic applications, *Mikrochimica Acta* 139, pp 185–188 (2001).
- [TOR/BAR 1997] Torrero M E, Baraj E, De Pablo J, Gimenez J, Casas I. Kinetics of corrosion and dissolution of uranium dioxide as a function of pH, *Int. J. Chem. Kinet*, 29, 261, 1997.
- [WEG/BOT 2001] Wegen D H, Bottomley P D W, Glatz J-P. The electrochemical modelling of irradiated UO₂ surface reactions in groundwater solution, ICEM 2001-8th International Conference on Radioactive Waste Management and Environmental Remediation, Sept 30th –Oct 4th 2001, Brugges, Belgium.
- [WOL 1992] Wolery T J. EQ3/6, a software package for geochemical modeling of aqueous systems: package overview and installation guide. UCRL-MA-110662 PT I, 1992.
- [YAJ/KAW 1995] Yajima T, Kawamura Y, Ueta S. Uranium (IV) solubility and hydrolysis constants under reducing conditions. *MRS Symp. Proc*, 353, pp 1137–1142, 1995.